Dissecting Pluripotency and Mammalian Embryonic Development via Droplet Microfluidics

Timo Nicolas Kohler

Department of Biochemistry

University of Cambridge

This dissertation is submitted for the degree of

Doctor of Philosophy

Hughes Hall, Cambridge

November 2019

Statement of authorship

This dissertation is my own work and contains nothing which is the outcome of work done in collaboration with others, except as specified in the text and acknowledgements.

This dissertation is not substantially the same as any that I have submitted, or, is being concurrently submitted for a degree or diploma or other qualification at the University of Cambridge or any other University or similar institution except as declared in the Preface and specified in the text. I further state that no substantial part of my dissertation has already been submitted, or, is being concurrently submitted for any such degree, diploma or other qualification at the University of Cambridge or any other university of similar institution.

This dissertation does not exceed the prescribed word limit for the relevant degree committee.

Timo N. Kohler, November 2019

Summary

Pluripotency, the ability of a cell to differentiate towards any type of somatic cell is a transient feature of the developing embryo. In vitro, pluripotency can be captured in the form of embryonic stem cells (ESCs). In this study, I developed a microfluidic-based system to encapsulate ESCs into agarose microgels, three-dimensional scaffolds that are in terms of their mechanical and biochemical properties fundamentally different from conventional tissue culture in plastic dishes. Subsequently, I investigated how these microenvironmental changes influence pluripotency. Interestingly, microgel culture of ESCs was not just accompanied by drastic changes in morphology, but also a promotion in naïve pluripotency. RNA-sequencing of microgel cultured ESCs elucidated global transcriptional changes of which many affected members of the pluripotency network. I then identified plakoglobin, a homologue of β-catenin, as one of the strongest upregulated proteins upon microgel encapsulation. However, molecular functions of plakoglobin in embryonic stem cells remain largely elusive. To investigate plakoglobin's potential role during naïve pluripotency, I created several ESC lines that constitutively expressed plakoglobin at varying levels. Cells expressing high amounts of plakoglobin, portrayed a distinct naïve phenotype with homogeneous transcription factor expression even under serum-based conditions. Single cell RNA-seq and the formation of blastocyst chimaeras were then used to confirm the re-establishment of the complete naïve network. In contrast, plakoglobin is absent or greatly reduced during primed pluripotency in epiblast-derived stem cells and conventional primate pluripotent stem cells. A finding that was further confirmed in the corresponding pre- and post-implantation embryo and naïve and primed marmoset and human pluripotent stem cells. Remarkably, forced expression of plakoglobin during primed pluripotency, unlike β-catenin, leads to stabilisation of the pluripotency network rather than differentiation. Finally, after having extensively elucidated plakoglobin's role within the continuum of pluripotency I used the microgel system to co-encapsulate ESCs with extraembryonic endoderm (XEN) cells. Co-encapsulation of these cell types led to the formation of self-organising aggregates in which the XEN cells surrounded an inner core of ES cells. These aggregates, termed EX-structures, exhibited deposition of a basal lamina, acquired apical-basal polarity, and initiated lumen formation with subsequent lineage-specific differentiation. Taken together, I have developed a cross-species compatible, compartmentalised system, for the suspension-culture of microgel-encapsulated embryonic stem cells that is generated in microfluidic devices. This interdisciplinary approach led to the identification of plakoglobin as a hitherto unknown, evolutionary conserved, regulator of naïve pluripotency. Furthermore, I have shown that co-culture of ES and XEN in microgels can mimic spatiotemporal events reminiscent to the peri-implantation embryo.

External contributions

- Joachim De Jonghe (Prof. Florian Hollfelder's lab, Department of Biochemistry, University of Cambridge) performed all bulk and inDrop single-cell sequencing, quality control and pre-processing in sections 3.2.3, 4.2.3 and 5.2.2.
- Dr Ayaka Yanagida (Prof. Jennifer Nichols' lab, Wellcome – MRC Cambridge Stem Cell Institute, University of Cambridge) performed the blastocyst injections in sections 3.2.3 and 4.2.3.
- Prof. Jennifer Nichols (Wellcome – MRC Cambridge Stem Cell Institute, University of Cambridge) thawed, fixed and stained all human embryos in section 4.2.9.1.
- Erin Slatery and Clara Munger were maintaining the cmESCs in section 4.2.9

Acknowledgements

First and foremost, I would like to thank my supervisor Prof. Florian Hollfelder for having offered me the opportunity of pursuing my doctoral research in his laboratory. Thank you for giving me the freedom and encouragement to push this project to the next level. All your trust and support into our exploration of the world of cell biology mean a lot to me. I will also be eternally grateful for the endless hours of work and effort by my student, sidekick and protégé Anna Lena. Thank you for your daily reminders to drink more water and less coffee, without you I would probably have died of dehydration. I am excited to see where you will take our work (I am obviously talking about the Jungle Office) over the next years during your doctoral studies. This project would have not been possible without the help of my friend and colleague Joachim and his impressive ability to solve any scientific challenge presented to him. Jo, thank you for your all your help with the sequencing and bioinformatic analysis – you are also a better ski instructor than Florian. I am grateful for Michael and his cloning expertise and willingness to listen to my never-ending questions. Miguelito, you have become a great friend and I am looking forward to go on more kayaking expeditions with you. Thank you, Eleanor, you are one precious, ginger Australian and definitely worth more than 800 camels! Furthermore, I am thanking Tomasz for several iterations of chip design, optimisation and production. I also owe a big thanks to everyone, past and present members of the Hollfelder group, for accepting me as the odd one out biologist into their circle of protein evolving and metagenomically analysing biochemists. There is certainly no better lab to be with, when drinking chai in India, surfing in Portugal or skiing in Austria!

I would also like to thank my co-supervisor Kevin Chalut and Carla Mulas for sharing their knowledge in embryonic stem cell biology and relentless feedback, discussions and suggestions. Thank you Ayaka, without you none of the chimera studies would have been possible, since my fine motor skills would have certainly not been sufficient. I am especially thankful to Prof. Jennifer Nichols. Jenny, your constant support, ideas and motivation were of great value to me. I am looking forward to our hike in the highlands! Kate and Lawrence thank you for being as crazy as you are. Without you my time at the Stem Cell Institute would have been a lot less fun! It is due to Thorsten Boroviak that I have learned a lot about pluripotency in primates – a field I could have not seen myself exploring at the beginning of my studies. Thorsten, thanks for sharing your exceptional scientific knowledge with me and always being ready for a pint. On that note, when are we getting those Yeti stem cells? I would also like to thank Erin (aka The Bioinformatician) and Clara (aka The Data Machine), working with the both of you has been a real joy and I am very much looking forward to continue our collaboration!

None of this work would have been possible without the love and support of my friends and family. Chibeza, your enthusiasm, Sarra, your kindness, and Jürgen, your efficiency, have always motivated me to go that one step further. I have learned a lot from all of you and I am indefinitely proud of what you have achieved! Special thanks to my two favourite North Pole explorers, Phyllis and Diane. Both of you do so much good for our planet and your positivity and energy is truly inspirational. Also, there's not a single day I do not dream about jalapeño-creamed-cheese bagels. Alan, expedition partner, drinking buddy and friend. You might not want to admit it, but you have the biggest heart, and I do not know many people as great as you. Thank you for treating me like being a part of your family. I am excited for our future expeditions and adventures! Christian, despite seeing you only once every couple of years in person, you have become a valued friend from across the ocean. I think now I am ready to open that bar with you. Heaven is indeed for real when having submitted a PhD thesis. Katerina, thank you for being great and such a weirdo! Special thanks to Gianmarco, I do not really know how we became friends, but I am glad we did! I hope, that now there will be more time for brunch again. Lucía, you are one of the most wonderfully awkward human beings on this planet. Thank you for our friendship, and needless to say, you and your family will always have a special place in my heart. Ole, you are a piece of gold. Thank you for sticking around throughout all these years, I hope that we will go on adventures together until we are old, stale and grey (or bald). Hannes, friends since primary school, that is an achievement! You would probably put it eloquently into one word: Danke. I am especially thankful for the support by my family. Mama und Hanna, ich habe euch unendlich lieb! And finally, Sylwia, you are the most gentle, kind and caring soul. Thank you for everything!

To Cristina Mittermeier and Paul Nicklen – the world needs more of your kind.

Table of content

Statement of authorship ..... **ii**

External contributions ..... **iv**

Acknowledgements ..... **v**

Summary ..... Error! Bookmark not defined.

Table of content ..... **viii**

1 General introduction **1**

1.1 Early embryonic development 2

1.1.1 Pre-implantation embryo 2

1.1.2 The peri- and post-implantation embryo 10

1.2 Embryonic mouse cell lines – pluripotency in vitro 14

1.2.1 Embryonic stem cells (ES cells) 14

1.2.2 Epiblast stem cells (EpiSCs) 16

1.3 Aims of this study 22

2 Experimental procedures **23**

2.1 Microfluidic chip fabrication 24

2.2 Microgel production 24

2.2.1 Demulsification of microgels 25

2.3 Cell culture 25

2.3.1 Mouse embryonic stem cells (mESCs) 25

2.3.2 Hanging drop culture 27

2.3.3 Mouse epiblast derived stem cells (EpiSC) 27

2.3.4 Extraembryonic endoderm cells (XEN cells) 27

2.3.5 Marmoset embryonic stem cells 27

2.3.6 Human embryonic stem cell 28

2.3.7 Cryopreservation of cell stock 28

2.4 Cell encapsulation in microgels 28

2.4.1 Preparation of cell suspension for subsequent cell encapsulation 28

2.4.2 Cell and colony recovery from microgels 28
2.5 Cell analysis 29
2.5.1 Flow cytometry and cell sorting 29
2.5.2 Immunocytochemistry 29
2.6 Molecular biology 29
2.6.1 Cloning 29
2.6.2 Piggy-Bacc Transfection 30
2.6.3 Gene knock-out via CRISPR Cas9 30
2.6.4 RNA-sequencing 31
2.7 Image acquisition, processing and quantification 32
2.8 Embryo work 32
2.8.1 Mouse embryo collection and culture 32
2.8.2 Human embryo collection and culture 33
3 Characterisation of a microgel culture system for embryonic stem cells 34
3.1 Introduction 35
3.2 Results 36
3.2.1 Microfluidic encapsulation of mouse embryonic stem cells 36
3.2.2 Microgel suspension culture of mouse embryonic stem cells promote ground state pluripotency 38
3.2.3 Systemic changes across the transcriptome stabilise the pluripotency network in microgel cultured embryonic stem cells 40
3.2.4 Microgel adjusted LIF and WNT signalling delays the exit from naïve pluripotency 44
3.2.5 Microgel culture leads to structural rearrangement of adherens junctions 47
3.3 Conclusions 49
4 The role of plakoglobin in regulating pluripotency 51
4.1 Introduction 52
4.2 Results 55
4.2.1 Generation and characterisation of a plakoglobin overexpressing mouse embryonic stem cell line 55

4.2.2 A certain plakoglobin threshold needs to be passed before re-establishment of ground state pluripotency 58
4.2.3 Single-cell sequencing confirms re-establishment of naïve state-like pluripotency in plakoglobin overexpressing cells 60
4.2.4 Plakoglobin expression impedes the exit from pluripotency 66
4.2.5 Plakoglobin overexpression allows maintenance of naïve pluripotency in the presence of just LIF or PD but not CH 70
4.2.6 Plakoglobin does not inhibit the exit from naïve pluripotency in serum-free conditions but blocks neuroectodermal differentiation. 73
4.2.7 Plakoglobin and β-catenin expression diverge upon implantation 77
4.2.8 Overexpression of plakoglobin does not revert epiblast stem cells to a naïve-pluripotent state 79
4.2.9 Plakoglobin in primates 86
4.3 Conclusions 92
5 Microgel co-culture of embryonic and extraembryonic cell lines 96
5.1 Introduction 97
5.2 Results 99
5.2.1 Microgel co-culture of ES and XEN cells 99
5.2.2 XEN cells support transition from naïve pluripotency to lineage specification of microgel cultured ESCs 102
5.3 Conclusions 106
6 General discussion and outlook 108
6.1 Advantages and drawbacks of microgels for the culture of embryonic stem cells .. 109
6.2 Plakoglobin, a previously unknown member of the naïve gene regulatory network? 111
6.3 Microgel co-culture of embryonic and extraembryonic cell lines 116
7 Conclusion and working hypothesis 119
8 References 121
9 List of abbreviation 152
10 List of figures 154

11 Appendix 156

11.1 List of antibodies 156

1 General introduction

1.1 Early embryonic development

The eukaryotic zygote, formed after a sperm entered the oocyte, is the one truly totipotent cell. It contains the complete blue print to form a new organism and is able to develop into all embryonic and extra-embryonic lineages. Embryogenesis is a tremendously complex interplay between internal and external signals controlling spatiotemporal localization as well as gene expression of all embryonic and extraembryonic cells. Generally speaking, embryogenesis can be separated into pre- and post-implantation development. Over the course of development, the single cell embryo develops into a complex structure with distinct morphological features and a multiplicity of cell types. When focusing on mammalian development, the developing pre-implantation embryo shows a surprisingly high degree of conservation across different species. The pre-implantation mouse embryo, looks in design and shape very similar to the human or any other mammal. A trait which is abruptly lost upon implantation of the embryo into the maternal uterus (or at time of gastrulation, which in some species happens before implantation). At this point, one must mention, that even though the embryos look similar, the underlying biological pathways are not always the same. For the purpose of clarity, in the following paragraphs, I shall only be describing the development of the early mouse embryo and merely mention other species when needed.

1.1.1 Pre-implantation embryo

After fertilization, the zygote immediately starts with the degradation of maternally stored RNA and initiates transcription of the zygotic genome, a process known as zygotic genome activation (ZGA). In the mouse, ZGA is initiated at the 2-cell stage, but protracted in primates, including the human (Boroviak et al., 2018). Initially, the zygote undergoes several cleavage divisions, in which the total cytoplasmic volume of the embryo remains the same (Aiken et al., 2004), to generate blastomeres. At this stage the embryo is still surrounded by the zona pellucida (ZP) (Dumont and Brummett, 1985), a glycoprotein layer surrounding the mammalian oocyte. Hence, the embryo can be seen as a self-contained system that is able to develop in the absence of maternal tissue, extracellular matrix or even be cultured *in vitro* without any developmental consequences (Whitten and Biggers, 1968). After three divisions the eight blastomeres are morphologically indistinguishable, almost spherical non-adherent cells. However, over the last several years a variety of studies have shown that, even though morphologically indistinguishable, heterogeneity can be detected as early as the 2-cell stage. Indeed, when separated, often only one of the blastomeres maintains the ability to form an embryo, suggesting unequal distribution of developmental potential (Casser et al., 2017; Katayama et al., 2010). This finding has been further supported by single-cell RNA sequencing of individual blastomeres, revealing small, but significant differences (Biase et al., 2014). These inhomogeneities might

firstly appear too small to affect cell behaviour, but when amplified could steer cells towards a specific fate. Timing and origin of heterogeneity still remain heavily debated questions. The latest perspectives and hypotheses have been thoroughly reviewed by Chen and colleagues (Chen et al., 2018). At the 8-cell stage, the embryo undergoes its first fundamental change in morphology (**Figure 1.1**). The so far loosely attached blastomeres compact to a point where they become visually indistinguishable, a state referred to as the compacted morula (Johnson et al., 1986; Johnson and Ziomek, 1981). The process of compaction is heavily based on the increase of

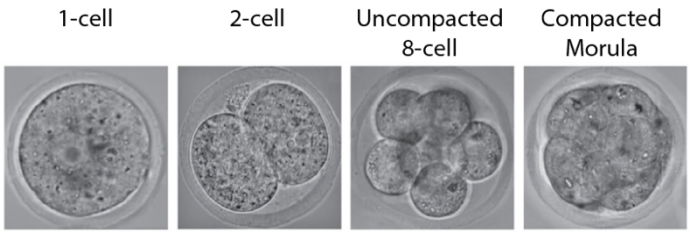

Figure 1.1 | Development from zygote to the compacted morula. Initially, the zygote undergoes several cleavage divisions until the 8-cell stage. At this point, the 8 blastomeres compact, a process in which individual cells become a visually indistinguishable and form the 'compacted morula'. Modified from White and Plachta, 2015

cell-cell adhesion, a phenomenon that can be observed across different mammalian species during pre-implantation development and seems to be of utmost importance for healthy embryonic development (White and Plachta, 2015). Already in the 1970's, it was shown that compaction can be impaired when chelating metal ions during embryogenesis (Wales, 1970). Yet, it took another decade before this observation could be linked to a specific protein: Uvomorulin (Hyafil et al., 1981; Hyafil et al., 1980). The group of François Jacob managed to raise a monoclonal antibody against this protein, which when applied before blastomere compaction, would hinder the former. Nowadays, Uvomorulin is commonly known under the name epithelial cadherin (E-cadherin), encoded by the *Cdh1* gene, and has been studied extensively and described in a variety of functions. E-cadherin, amongst other cadherins, is a major component of cell-cell adherens junctions (Takeichi, 1991), which I will designate the following paragraph as they (and their individual components) played such crucial role throughout this work. Recently live-imaging of 8-cell stage embryos has shown, that besides being the major constituent of adherens junctions, which hold cells together, E-cadherin is also found to great extend in blastomere membrane protrusions (Fierro-Gonzalez et al., 2013). These protrusions, recognized as filopodia, extend and retract several times during the course of compaction and are thought to help enabling initial membrane contact between the blastomeres (**Figure 1.2**). However, Maître and colleagues argue that E-cadherin alone is unable to generate the forces needed to initiate compaction (Maitre et al., 2012), an argument which has been further supported by the absence of changes in E-cadherin expression and motility during compaction (Samarage et al., 2015). Micropipette aspiration, to investigate tension amongst the blastomeres of the 8-cell stage

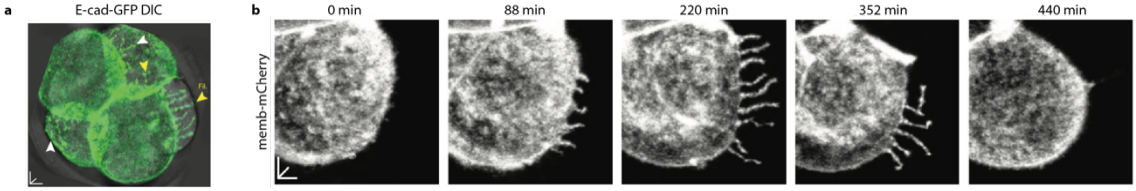

Figure 1.2 | E-cadherin dependent filopodia formation during blastomere compaction. a, 8-cell stage chimeric embryo of wild type and E-cadherin-GFP expressing blastomeres. **b**, Extension and retraction of the E-cadherin rich filopodia in the blastomeres before compaction. Scale bar: 5 µm. Modified from Fierro-Gonzalez et al., 2013

embryo, has shown an increase of cortical tension over the course of compaction. A phenomenon believed to be driven via pulsed contractions of the actomyosin cortex (Maitre et al., 2015). Concomitant with the compaction event is the appearance of distinct apical-basal polarity (White et al., 2018; Zhu et al., 2017; Ziomek and Johnson, 1980) (**Figure 1.3**). The outwards facing side of the blastomeres become enriched with ezrin and the PAR-aPKC complex (Louvet et al., 1996; Vinot et al., 2005) whilst the inner and contacting areas of the blastomeres display expression of E-cadherin, Jam-1 and Par-1 (Thomas et al., 2004; Vestweber et al., 1987; Vinot et al., 2005), thereby defining the emerge of basolateral cell-cell contacts. Interestingly, apical-basal polarity can be established in the absence of E-cadherin (Ziomek and Johnson, 1980). However, laser ablation of cadherin-depended filopodia (Fierro-Gonzalez et al., 2013) or knocking out E-cadherin all together cause embryos to fail compaction and are therefore unable to establish an epithelial structure (Larue et al., 1994; Ohsugi et al., 1997; Riethmacher et al., 1995; Stephenson et al., 2010). Taken together, compaction of the 8-cell embryo appears to be orchestrated by a combination of cadherin-mediated adhesion and pulsatile actomyosin contractility

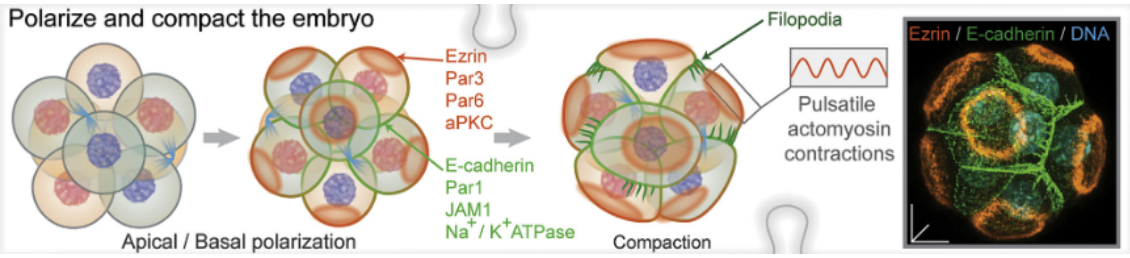

Figure 1.3 | Compaction via cadherin-mediated adhesion and pulsatile actomyosin contractility. At the 8-cell stage, blastomeres acquire apical-basal polarity. Apical domain markers such as ezrin, PAR3, PAR6 and aPKC are localized at the contact-free surface whereas the inner sides are enriched in E-cadherin, PAR1, JAM1 and Na^+/K^+ ATPase. Upon establishment of polarity, blastomeres compact via a combination of cadherin-mediated filopodia formation and pulsatile actomyosin contractility. Modified from White et al., 2018.

1.1.1.1.1 Adherens junctions

Due to their importance in following chapters, I'll insert an interlude regarding adherens junctions at this point, before continuing with early embryonic development and the first cell fate decision of the now compacted morula. Adhesion, whether it is cell-cell or

cell-matrix interactions, is one of the key components for morphogenesis, the association of individual cells into complex and highly ordered tissues in any multicellular life. Even though it is easy to imagine adhesion as a static property, it actually needs to be a dynamic process. One the one hand, cells must adhere to one another, whilst on the other hand, need to maintain the ability to constantly adjust their morphology. These properties can be achieved by the continuous formation, degradation and rearrangement of adherens junctions (AJ). AJs are multi-protein complexes in which cadherins and catenins play the central role (**Figure 1.4**). During early embryonic development, E-cadherin is the most prominent cadherin (Kemler, 1993). E-cadherin is a transmembrane protein with five (EC1-5), repeating, calcium dependent extracellular and several cytoplasmic domains (Hyafil et al., 1981). The extracellular domains interact solely with E-cadherin molecules from juxta-positioned cells (Gumbiner et al., 1988) through a *trans*-interaction of the EC1 domains and with E-cadherin molecules on the same cell through *cis*-interactions of the EC2 domains (Harrison et al., 2011). The cytoplasmic fraction of E-cadherin contains two catenin binding domains (CBD) including the juxta-membrane domain (JMD), which bind a whole array of proteins, collectively also known as the 'cadhesome'(Zaidel-Bar, 2013). The main group of binding proteins are called catenins (α-, β-, γ- and δ-catenin). p120-catenin (also known as δ-catenin) binds to E-cadherin's JMD (Jou et al., 1995; Ohkubo and Ozawa, 1999) and is crucial in the remodelling of AJs. When bound, p120 inhibits endocytosis and degradation of E-cadherin (Davis et al., 2003; Fujita et al., 2002; Ishiyama et al., 2010; Xiao et al., 2003) by blocking an, in cadherins conserved, peptide sequence (DEEGGGE) (Nanes et al., 2012). Over the last several years, additional functions regarding p120 were identified that differ from its classical role in cadherin trafficking and elucidate its role in stem cell differentiation (Lee et al., 2014a) and proper lineage specification of the primitive endoderm (Pieters et al., 2016). Unlike p120, β-catenin and plakoglobin (also known as γ-catenin) bind to the C-terminal CBD (instead of the JMD) of E-cadherin, connecting it to the actomyosin-cytoskeleton via α-catenin (Herrenknecht et al., 1991) and vinculin (Bertocchi et al., 2017). Binding of β-catenin/plakoglobin is indispensable for functioning adherens junctions mediated cell-cell adhesion (Fukunaga et al., 2005; Ozawa, 2002). β-catenin and plakoglobin are structurally similar proteins (Butz et al., 1992a; Mccrea et al., 1991a), and represent the vertebrate homologues of the *Drosophila* protein armadillo (Peifer et al., 1992b). Both proteins are involved in cell adhesion and several signalling cascades regarding embryonic development, in particular canonical WNT signalling (reviewed in (Aktary et al., 2017; MacDonald et al., 2009)). It is this similarity between these proteins and their dual functions in cell-cell adhesion and signal transduction that I shall devote more detailed description. However, at this point I postpone further discussion and will return to it in chapter 4 where I will have a closer look at the similarities and differences between β-catenin and plakoglobin. Finally, there is α-catenin.

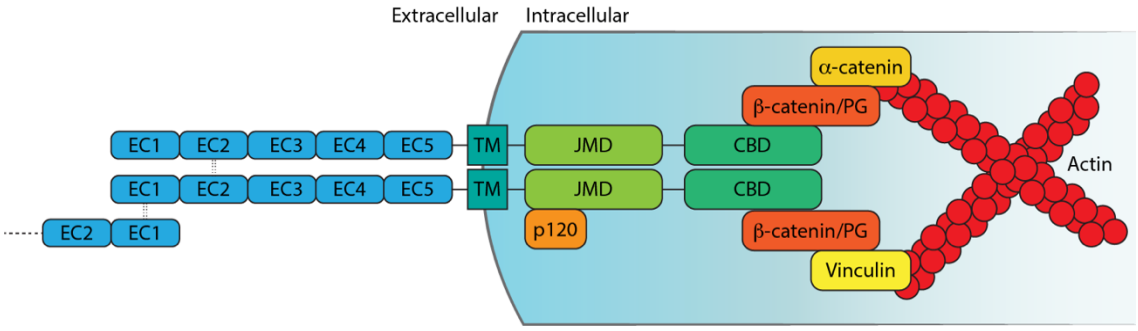

Figure 1.4 | Schematic illustration of the composition of adherens junctions. The main component of adherens junctions are the cadherins. E-cadherin consists of 5 extracellular domains (EC1-5), a transmembrane domain (TM) and the intracellular juxtamembrane (JDM) and the catenin binding domain (CBD). Cadherins interact in a homophilic fashion with cadherins of surrounding cells via trans interactions of their EC1 domains. They also bind to cadherins on the same cell via trans-interactions of the EC2 domains. p120 (also known as δ-catenin) binds to the JMD of E-cadherin and is heavily involved in its trafficking and recycling. b-catenin and its structurally similar plakoglobin (also known as γ-catenin) link E-cadherin to the actomyosin cytoskeleton via interaction with α-catenin or vinculin.

Whereas β-catenin, plakoglobin and p120 share considerable amount sequence identity, α-catenin differs significantly in its structural organization from the aforementioned proteins, but is similar to vinculin (Pokutta et al., 2008). α-catenin has generally been described as the link between adherens junctions and the cytoskeleton due to its ability to simultaneously bind to β-catenin and F-actin (Pokutta et al., 2002; Pokutta and Weis, 2000). Conclusively, cadherins and catenins play a vital role in the formation of adherens junctions at the plasma membrane and furthermore occupy roles in signal transduction in the nucleus.

1.1.1.2 First cell fate decision

I have now arrived back at the point where I left at the end of paragraph 1.1.1. After compaction, the individual blastomeres have become visually indistinguishable. At this stage, the embryo consists out of the newly formed, outer and polar trophectoderm (TE) and the apolar, inner cell mass (ICM). Both cell types display distinct expression of transcription factors such as OCT4, NANOG and SOX2 (Avilion et al., 2003; Mitsui et al., 2003; Nichols et al., 1998) in the ICM and CDX2 and EOMES in the TE (Niwa et al., 2005; Russ et al., 2000; Strumpf et al., 2005). The underlaying transcriptional programs of TE and ICM are reciprocally inhibitory and therefore mutually exclusive (Niwa et al., 2005). Initially it was unclear if and how the polarity differences between the inner and the outer cells were orchestrating differentiation towards trophectoderm. Eventually, the Hippo-signalling component angiomotin (AMOT), and its homologue angiomotin-like 2 (AMOTL2) had been identified as the missing link (Hirate et al., 2013; Leung and Zernicka-Goetz, 2013). Apolar ICM cells show homogeneous distribution of membrane associated AMOT which can directly tether the transcription factor YAP or cause its phosphorylation by Lats1/2, preventing it in both cases from entering the nucleus (Leung and Zernicka-Goetz, 2013; Nishioka et al., 2009; Paramasivam et al., 2011) (**Figure 1.5**). In contrast,

the outer cells (which eventually form the TE) show polarised AMOT localisation to their apical domain (Leung and Zernicka-Goetz, 2013). It is believed that components of the apical polarity complex, such as PAR6 and aPKC, deactivate AMOT as they are required for its apical localisation (Hirate et al., 2013). Due to inactive AMOT in the outer cells, YAP localises to the nucleus where it then binds to TEAD4 (Hirate et al., 2012; Nishioka et al., 2009). Subsequently, TEAD4 activates expression of CDX2 and EOMES, kickstarting the trophectodermal differentiation program through suppression of OCT4 and NANOG (Nishioka et al., 2008; Yagi et al., 2007). Consequently, knockout of AMOT or TEAD4 leads to TE gene expression within the ICM and failure to initiate the trophectodermal differentiation program in the outer cells (Leung and Zernicka-Goetz, 2013; Nishioka et al., 2008; Yagi et al., 2007). At this point, the first cell fate decision has been made and the hitherto equal blastomeres have differentiated towards TE, which forms the placenta, and ICM, which subsequently separates during the second cell fate decision into primitive endoderm and epiblast.

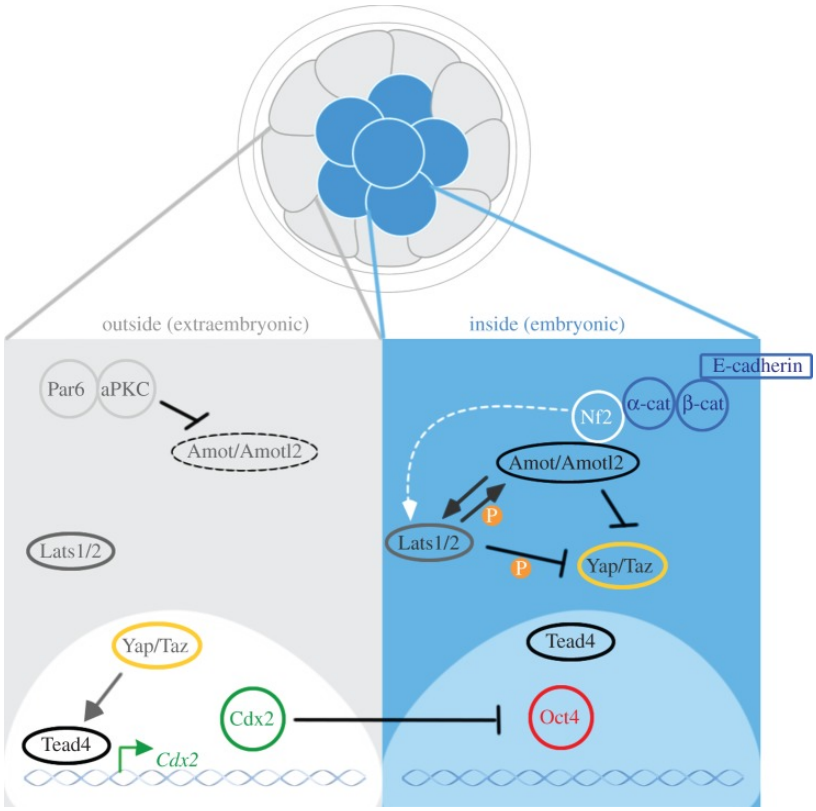

Figure 1.5 | Polarity-mediated localisation of YAP to the nucleus initiates trophectodermal differentiation. In the outer cells of the compacted morula, apical domain proteins such as PAR6 and aPKC inhibit AMOT/AMOTL2. Consequently, YAP can translocate to the nucleus where, in combination with TEAD4, it activates CDX2 expression. Subsequently, CDX2 kickstarts the trophectodermal differentiation program via downregulation of OCT4. In contrast, the inner cells of the compacted morula inhibit nuclear translocation of YAP via sequestration by AMOT/AMOTL2 and YAP's phosphorylation by LATS1/2. Modified from Bedzhov et al., 2014.

1.1.1.3 Second cell fate decision and the establishment of pluripotency

Simultaneously with the establishment of the trophectodermal epithelium around the apolar ICM, the embryo keeps proliferating and transitions from the compacted morula to the blastocyst stage (**Figure 1.6**). The formation of the blastocyst is coined by the expansion of a fluid-filled cavity, the blastocoel, and the second cell fate decision: the segregation of the ICM into epiblast (EPI) and primitive endoderm (PrE), respectively. Initially, the newly formed and polar TE cells 'seals' the embryo via extensive formation of desmosomes and ZO-1 enriched tight junctions (Fleming et al., 1991; Wang et al., 2008) (**Figure 1.6 a**). Subsequently, a multiplicity of intercellular micro lumens, originating from vesicles that had been secreted by the basal membrane of the trophectoderm, merge to form one central cavity: the blastocoel (Aziz and Alexandre, 1991). Active pumping of sodium ions into the blastocoel creates an osmotic gradient, which is then neutralised by the influx of fluid into the cavity, creating an 'inside pressure' within the sealed embryo (Barcroft et al., 2003; Benos et al., 1985) (**Figure 1.6 b**). In a recent set of elegant experiments, Chan and colleagues have demonstrated that the formation of the blastocoel is a highly dynamic process (Chan et al., 2019). Upon reaching a critical pressure threshold, tight junctions rupture and pressure is released. These oscillations are detected by the mechanosensitive adherens junction protein vinculin, which in turn activates a positive feedback loop strengthening the tight junctions (Chan et al., 2019). Taken together, this study nicely elucidated the relationship between embryonic morphology, tissue mechanics and luminal pressure. Concomitant with the expansion of the blastocysts, is the development of the PrE and EPI with mutually exclusive transcriptional programs (Chazaud et al., 2006) (**Figure 1.6 c**). Initially ICM cells are transcriptionally indistinguishable and co-express genes such as *Pou5f1*, *Nanog* and *Gata6* (Ohnishi et al., 2014). Yet, as development continues NANOG becomes restricted to the EPI precursors whereas GATA6 marks the PrE (Chazaud et al., 2006). EPI and PrE cells are further defined by the expression of Nanog (Chambers et al., 2003; Mitsui et al., 2003), Sox2 (Avilion et al., 2003) and Gata4/6 (Koutsourakis et al., 1999), platelet-derived growth factor receptor α (PDGFRα) (Plusa et al., 2008), Sox17 (Niakan et al., 2010), respectively. This lineage segregation has been shown to be driven by FGF4 signalling, such that cells receiving FGF4 signals will become PrE cells, whereas cells secreting FGF4 become the EPI (Guo et al., 2010; Krawchuk et al., 2013). How the decision between FGF4 secreting and receiving cells is made remains debated. Yet, it appears to be partially due to differential expression of FGFR1 and FGFR2 (Kang et al., 2017; Molotkov et al., 2017), a bias of early internalised cells to display higher FGF4 expression than cells that are internalised later (Morris et al., 2013), and variations in FGF4 expression caused by fluctuations in SOX2 levels (Mistri et al., 2018). Upon lineage allocation, EPI and PrE cells are randomly distributed within the ICM, however, by E4.5 have sorted into two spatially segregated compartments, with the PrE cells

having formed an epithelium lining the outside of the epiblast (Meilhac et al., 2009; Plusa et al., 2008). Simultaneously, EPI cells acquire naïve pluripotency and have the capacity to readily differentiate to all germ layers and the germline but have lost the ability to contribute to extraembryonic lineages (Boroviak et al., 2014). The transcription factors *Pou5f1* (OCT4) and *Sox2* have been identified as the master regulators of the pluripotency gene regulatory network, yet very little is known about how the network is initiated (Avilion et al., 2003; Nichols et al.,

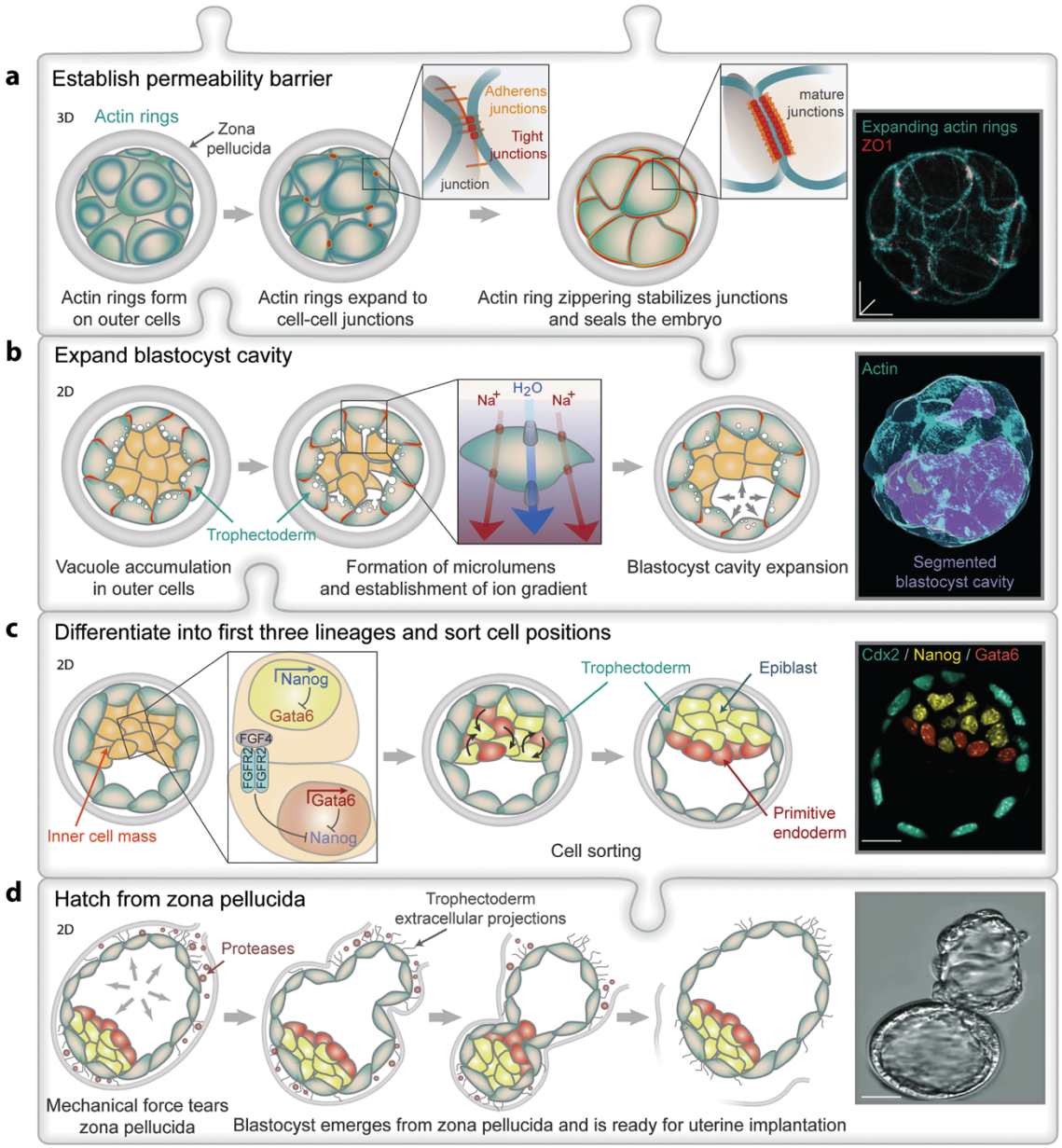

Figure 1.6 | Hallmark events during blastocyst formation. a, Establishment of a permeability barrier that 'seals' the embryo, a prerequisite for subsequent cavity formation. **b**, The cavity (blastocoel) is formed by the merging of several microlumens originating from the outer trophectodermal cells. Active pumping of sodium ions into the cavity results in osmotic pressure that is then equalised via influx of water, causing the cavity to expand. **c**, Concomitantly to blastocyst expansion, the ICM separates via an FGF4 driven process into the pluripotent epiblast and the primitive endoderm, expressing NANOG and GATA6, respectively. **d**, In the final step during pre-implantation development, the blastocyst hatches from its surrounding zona pelucida via proteolytic degradation and mechanical pressure. Modified from White et al., 2018

1998). The final steps of pre-implantation development is the hatching of the embryo from its surrounding zona pelucida, a process driven by proteolytic lysis originating from the mural trophectoderm (Perona and Wassarman, 1986) (**Figure 1.6 d**). With this last step, pre-implantation development is complete and the embryo begins its complex interaction with the maternal tissue in the form of implanting into the uterus.

1.1.2 The peri- and post-implantation embryo

At time of implantation, the embryo consists of three cell types: the two extraembryonic epithelia, the trophectoderm (TE) and the primitive endoderm (PrE) as well as the apolar aggregate of epiblast (EPI) cells, eventually forming the somatic lineages and the germ cells of the embryo proper. The TE mediates the initial interaction between embryo and uterus and subsequently proliferates and forms the extraembryonic ectoderm (ExE) and the ectoplacental cone, both progenitors of the placenta, whilst the PrE segregates into parietal and the visceral endoderm (VE). Simultaneously, the EPI cells undergo a radical change in their morphology, they become, an along the proximal-distal axis elongated, columnar epithelium which surrounds the pro-amniotic cavity. A process initiated by the actomyosin-driven polarisation of the epiblast into a rosette-like structure with a central apical domain (Bedzhov and Zernicka-Goetz, 2014) (**Figure 1.7**). As the embryo continues its development, the epiblast opens a lumen in the centre

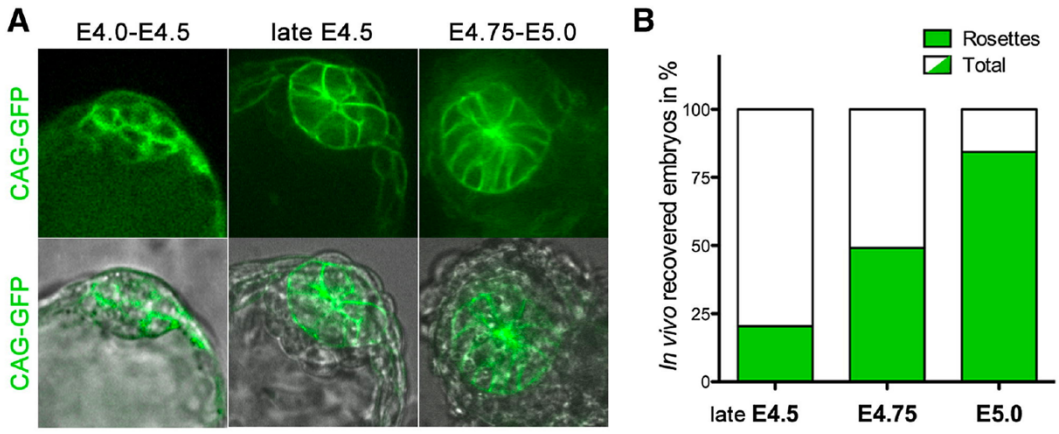

Figure 1.7 | Polarised rosette formation of the epiblast during implantation. a, Membrane-bound CAG-GFP in the epiblast reveals polarisation into a rosette-like structure during implantation. **b**, Percentage of rosette-like epiblast structures in embryos recovered at different stages during implantation. Modified from Bedzhov and Zernicka-Goetz, 2014.

of the rosette-like structure, eventually forming the pro-amniotic cavity. Remarkably, the process of cavity formation does not depend on apoptosis but appears to be orchestrated by membrane separation due to charge repulsion by apical secretion of the sialomucin podocalyxin (PODXL) (Bedzhov and Zernicka-Goetz, 2014). However, two question remained: what signals initially induce the polarisation of the epiblast and why only at the stage of implantation? It is very likely,

that EPI polarisation is induced by extracellular matrix (ECM) components, in particular laminin, and its interactions with β1-integrins. This assumption is based on the observation that Matrigel embedded embryonic stem cells (ESCs) undergo polarisation similar to the EPI, whereas ESCs in agarose, devoid of ECM components, or ESCs without β1-inegrins fail to polarise (Bedzhov and Zernicka-Goetz, 2014). This hypothesis is further supported by the evidence, that homozygous knockout of laminin in the embryo leads to peri-implantation lethality (Coucouvanis and Martin, 1995; Smyth et al., 1999). To answer the questing concerning the 'when', one has to look into the deposition of ECM by the different lineages. Albeit, the early ICM does express ECM genes such as *Fn1*, *Lama5*, *Lamb1* and *Lamc1*, formation of a basal membrane is not observed (Boroviak et al., 2014). In contrast, due to their epithelial character, PrE and TE deposit high amounts of basal membranes (Li et al., 2004; Murray and Edgar, 2000). Therefore, it is possible, that the extraembryonic lineages have to develop and establish a proper basal lamina before polarisation of the EPI can be achieved. Taken together, polarisation and lumen formation of the peri-implantation EPI are prerequisites for subsequent formation of the egg cylinder and symmetry breaking of the embryo.

1.1.2.1 Formation of the body axis

At around E5.0, as the EPI becomes a polarised epithelium with a central lumen, it starts to elongate along the proximal-distal (P-D) axis and forms a structure termed the 'egg cylinder' (**Figure 1.8**). On its proximal end, the ExE simultaneously undergoes epithelialisation and rosette formation, similar to the epiblast, eventually leading to the formation of a single fused cavity between these two compartments (Christodoulou et al., 2018). On top of the ExE forms the ectoplacental cone whilst the VE monolayer epithelium envelops the complete EPI. A variety of signalling molecules, including the TGFβ-family members nodal and bone morphogenetic proteins (BMP), as well as WNT and FGF, are involved in establishing distinct gene-expression patters along the EPI, finally resulting in is symmetry breaking. Initially, differential gene expression becomes apparent along the P-D axis. Reciprocal nodal signalling between EPI and ExE cells leads to the activation of BMP4 in the ExE, which in turn activates WNT3 in the EPI (Brennan et al., 2001; Guzman-Ayala et al., 2004; Norris and Robertson, 1999). Remarkably, it is in the distal part of the embryo, that nodal activates intracellular SMADs in the visceral endoderm and thereby creating a new signalling centre: the distal visceral endoderm (DVE) (Brennan et al., 2001). The DVE acts as a WNT and nodal signalling antagonist via the secretion of DKK1, CER1 and LEFTY1 (Perea-Gomez et al., 1999). Consistent with these findings, loss of SMAD2 or constitutive activation of the WNT/β-catenin pathway disrupt DVE formation and consequently cause upregulation of proximal-posterior markers such as brachyury and WNT (Chazaud and Rossant, 2006; Perea-Gomez et al., 2002; Waldrip et al., 1998). In contrast,

physical removal of ExE and ectoplacental cone leads to the acquisition of a DVE-like phenotype in the entity of VE cells and the absence of proximal-posterior markers within the EPI (Rodriguez et al., 2005). Therefore, the proximal extraembryonic tissue prevents the majority of the VE from transitioning into DVE-like state by hitherto unidentified signals. At around E6.0, the newly formed DVE migrates 'up' along the prospective anterior side of the epiblast, becoming the anterior visceral endoderm (AVE) and thereby defining the anterior-posterior (A-P) axis of the embryo (Beddington and Robertson, 1999; Lu et al., 2001; Thomas and Beddington, 1996). The underlaying mechanisms of AVE formation are still debated (Rodriguez et al., 2005; Srinivas et al., 2004; Takaoka et al., 2011; Yamamoto et al., 2004). Once study hypothesised, that enhanced

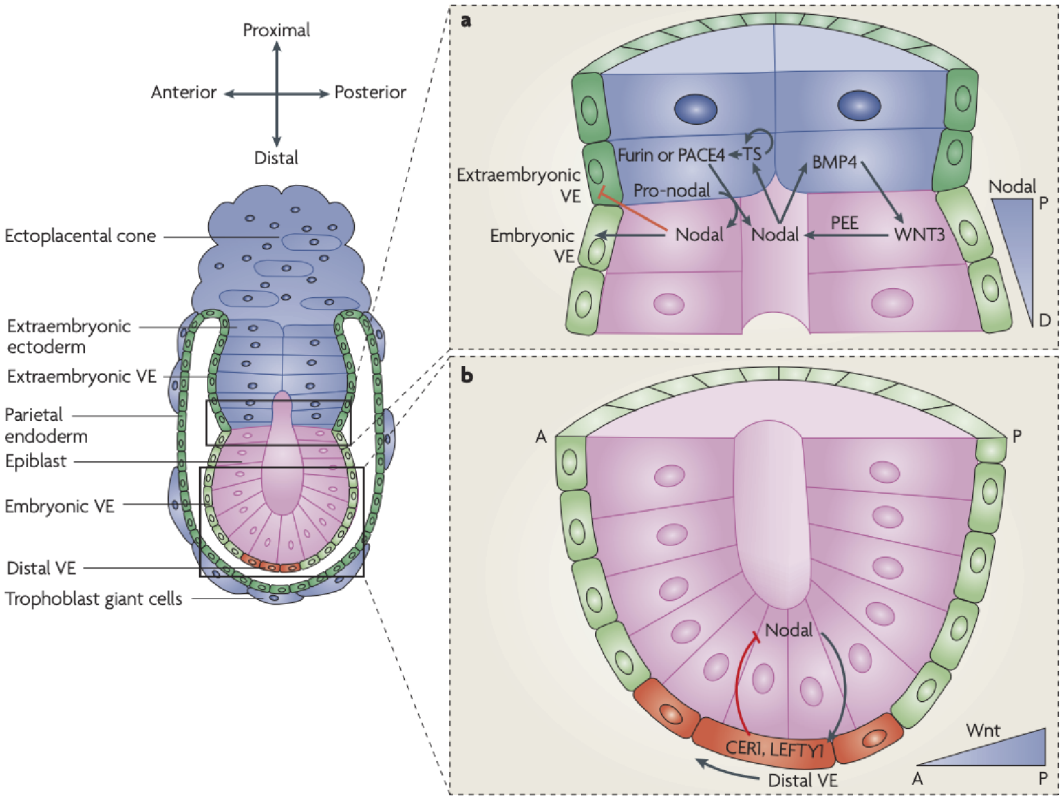

Figure 1.8 | Signalling in the pre-gastrulating embryo. At E5.0 the embryo is in the process of implanting into the uterus and has transitions from the blastocyst to the 'egg cylinder' stage. The proximal end of the embryo is defined by the ectoplacental cone which sits on the epithelial extraembryonic ectoderm (ExE). The epiblast (EPI) has become a polarised and columnar epithelium, surrounding the pro-amniotic cavity. The primitive endoderm has developed into embryonic and extraembryonic visceral endoderm (VE) as well as parietal endoderm. (**a**) Reciprocal nodal, BMP and WNT signalling between ExE and EPI initiate proximal-distal axis formation and establish a new signalling centre, the distal visceral endoderm (DVE) (**b**). The DVE subsequently secretes WNT and nodal antagonists and thereby creates discrete signalling gradients across the embryo. Modified from Arnold and Robertson, 2009.

cell proliferation at the distal tip of the embryo and subsequent, passive shifting of the DVE towards the anterior side is the origin of the AVE (Yamamoto et al., 2004) whereas Takaoka and colleagues claim that DVE and AVE are actually two different and non-overlapping cell populations (Takaoka et al., 2011). In contrast, lineage-tracing via fluorescent real-time imaging has shown that DVE cells actively migrate via filopodia formation towards the anterior side of

the embryo (Srinivas et al., 2004), an observation further supported by the evidence that loss of NAP1, a protein important for cytoskeletal rearrangement, impairs DVE migration (Rakeman and Anderson, 2006). Additionally, expression of nodal and its co-receptor cripto (gene: *Tdgf1*) have been shown to be crucial for DVE migration (Ding et al., 1998; Lowe et al., 2001; Norris and Robertson, 1999), however, the exact signals controlling DVE and AVE formation remain to be fully understood. Taken together, these studies elucidate how reciprocal signalling between the ExE and EPI establish firstly the P-D axis and how subsequently DVE and AVE formation prepare the embryo for gastrulation.

1.1.2.2 Gastrulation

Once the P-D and A-P axis have been defined, the embryo is forming the primitive streak and subsequently initiates gastrulation at around E6.5 (**Figure 1.9**). Gastrulation is the process in which the hitherto pluripotent EPI continues its development by establishing the three germ layers: ecto-, meso-, and endoderm. At the anterior side, the newly formed AVE shields the EPI from WNT and nodal signals via the expression of antagonists (Perea-Gomez et al., 1999). In turn, anterior EPI cells give rise to the neuroectodermal lineage (Lawson, 1999). Since no additional activating signals are required for neuroectoderm induction, and the absence of nodal or BMP signalling results in upregulation of neuroectodermal markers in the complete EPI, it is often considered the 'default' path of differentiation (Camus et al., 2006; Di-Gregorio et al.,

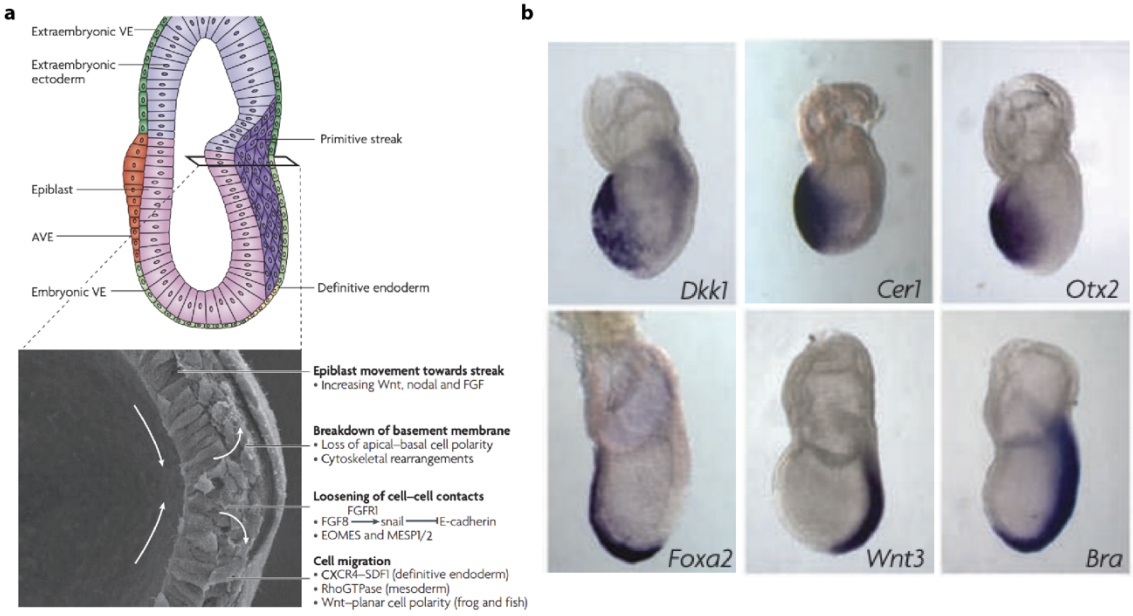

Figure 1.9 | The gastrulating embryo. a, Around E6.0 the P-D and A-P axis have been established. On the posterior side, a combination of nodal, WNT and FGF signalling induce the formation of the primitive streak in which EPI cells undergo an epithelial-to-mesenchymal transition and subsequently migrate out of the epithelium and form the mesendoderm between EPI and VE. Antagonistic WNT and nodal signals secreted by the AVE prevent formation of an anterior primitive streak and enable neuroectodermal differentiation. **b**, In-situ hybridization show anterior localisation of Dkk1, Cer1, Otx2 and Foxa2 whereas Wnt3 and Bra are mostly localised to the posterior side. Modified from Arnold and Robertson, 2009.

2007). In contrast, primitive streak and subsequent mesendoderm (general precursors of meso- and endoderm) differentiation requires BMP signals from the ExE and nodal signals from the EPI (Conlon et al., 1994; Dunn et al., 2004; Mishina et al., 1995). Furthermore, WNT3 and its surface receptors, LRP5 and LRP6, as well as its intracellular signal transducer β-catenin, are crucial for successful gastrulation (Haegel et al., 1995; Huelsken et al., 2000b; Kelly et al., 2004; Liu et al., 1999). Albeit there is no known signalling function of β-catenin in the pre-implantation embryo, stabilisation of β-catenin signalling or the absence of its antagonists CER1 and LEFTY1 at this stage, results in posterior gene activation and formation of multiple primitive streaks throughout the embryo (Kemler et al., 2004; Perea-Gomez et al., 2002; Zeng et al., 1997). Interestingly, gastrulation is not affected by the deletion of plakoglobin, a vertebrate homologue of β-catenin, however, its overexpression in *Xenopus* embryos leads to axis duplication similar to the phenotype of stabilised β-catenin in the mouse (Bierkamp et al., 1996; Karnovsky and Klymkowsky, 1995; Ruiz et al., 1996). During the formation of the primitive streak, EPI cells leave the monolayer epithelium via an epithelial-to-mesenchymal transition orchestrated by the upregulation of snail, a direct transcriptional repressor of the cell-cell adhesion molecule E-cadherin (Cano et al., 2000; Carver et al., 2001), and the progressive breakdown of the basal lamina (Williams et al., 2012). As the primitive streak elongates from its proximal-posterior origin to the distal-anterior endpoint, EPI cells become primed to different meso- and endoderm lineages depending on their time and location of egression within the streak (Lawson, 1999). EPI cell migrating through the more proximal primitive streak give rise to the paraxial and cardiac mesoderm, whereas cells leaving the primitive streak at its most anterior part become axial mesoderm and definite endoderm (Lawson, 1999). All things considered, it has been extensively demonstrated, that changes in embryonic morphology, symmetry breaking of the EPI and new signalling environments are of utmost importance for the initiation of gastrulation and the subsequent establishment of the three germ layers.

1.2 Embryonic mouse cell lines – pluripotency in vitro

In vivo, pluripotency is a transient feature of the developing embryo that arises in the ICM and quickly disappears after implantation. Embryonic stem cells, the in vitro counterpart of the pre-implantation epiblast, artificially keeping cells in a pluripotent and self-renewing time, hypothetically for indefinite time. In the next few paragraphs I will be briefly describing capturing the continuum of pluripotency in vitro.

1.2.1 Embryonic stem cells (ES cells)

The history of embryonic stem (ES) cells dates back to the early 50's and their discovery was based on the rather curious observation, that the mouse strain 129 would occasionally

develop testicular teratocarcinomas (Stevens and Little, 1954). Teratocarcinomas are a type of tumour consisting of a mixture of fully differentiated cells as well as highly proliferative and undifferentiated cells, termed embryonic carcinoma (EC) cells. Shortly after, it was shown that when injecting individual of these undifferentiated cells into adult mouse brains, they would go on and differentiate again to form multilineage tumours (Kleinsmith and Pierce, 1964). Therefore, these cells have a multipotent differentiation potential, a state similar to what has been previous described in the embryonic epiblast. Furthermore, it was possible to expand clonal EC cells in culture when supplemented with serum and grown on inactivated mouse embryonic fibroblasts (iMEF) (Kahan and Ephrussi, 1970). Remarkably, upon removal of iMEFs, EC cells could also be maintained on gelatin coated dishes, however, a part of the cell population would in this case differentiate to a feeder-like state and support the remaining EC cells in an undifferentiated state. However, albeit showing a multipotent differentiation potential, chimera contribution of EC cells remained poor. This challenge was finally overcome by the establishment of pluripotent cells directly from the epiblast of the pre-implantation embryo, termed embryonic stem cells (ESC) (Evans and Kaufman, 1981; Martin, 1981). Initially ESCs were also cultured under the same serum and feeder conditions, but in comparison to EC cells, ESCs showed higher chimeric contribution potential and their genetic material could be passed on through germline transmission (Bradley et al., 1984). Although gene regulatory networks of pluripotency in ESCs are now well established, the first in vitro cultures exhibited great heterogeneity across their phenotype, transcription and developmental potential (Chambers et al., 2007; Kolodziejczyk et al., 2015; Marks et al., 2012; Toyooka et al., 2008; Wray et al., 2010). However, culture conditions were far from ideal, serum batch variability and the unknown contribution of feeder cells appeared to be the main cause behind this metastability in ESC cultures (Robertson, 1997). In an effort to move towards more defined culture conditions, serum and feeder cells needed to be replaced. In this regard, one of the breakthrough discoveries was the identification of the protein ‘leukaemia inhibitory factor’ (LIF) which can substitute for the use of feeder cells in ESC cultures, a condition termed hereafter S+LIF (Smith et al., 1988; Williams et al., 1988). LIF was subsequently shown to act via pSTAT3, which translocates to the nucleus where it promotes the expression of pluripotency associated genes such as TFCP2L1 and the KLFs (Martello et al., 2013; Niwa et al., 1998). With the identification of LIF, dependency on feeder cells had been eliminated, yet quality variations across batches of serum remained an issue. Over 15 years later, it was shown BMP signals from the serum were the major contributor in maintaining pluripotency (Ying et al., 2003a). Therefore, a combination of LIF and BMP enabled the first fully defined culture conditions for ESCs. Surprisingly, despite having eliminated the quality variations in serum and feeder cells, ESCs still exhibited heterogeneous expression of the transcription factors known to be associated with the pre-implantation epiblast (Boroviak et al., 2014; Wray et al., 2010). Consequently, the question was raised if ESCs actually do represent the true in vitro

counterpart of the pluripotent epiblast. In particular the observation that ESCs could only be derived from embryos of the inbred mouse strain 129, further fuelled the argument that ESCs are an in vitro artefact and different from the EPI cells. In vivo, pluripotency is a transient feature of the EPI which last not even 48 hours (Boroviak et al., 2014). LIF and BMP signalling act by promoting pluripotency but do not inhibit the intrinsic drive towards developmental progression and somatic lineage differentiation. In 2008, Ying and colleagues addressed this issue by culturing ESCs in the presence of two small molecules PD0325901 (PD) and CHIR99021 (CH) inhibiting ERK (an FGF pathway kinase) and GSK3 (a WNT/β-catenin pathway kinase), respectively (Ying et al., 2008). Both of these pathways have previously been indicated to play crucial roles in ESCs differentiation (Doble et al., 2007; Sato et al., 2004; Wilder et al., 1997). This double inhibition of ERK and GSK with the optional addition of LIF, from here on termed 2i+LIF, finally enabled ESC derivation from any mouse strain and even other rodents such as the rat (Buehr et al., 2008; Nichols et al., 2009a; Ying et al., 2008). Remarkably, unlike ESCs in S+LIF or BMP+LIF, 2i+LIF cultured ESCs show no heterogenous expression of genes known to be associated with the naïve EPI and are therefore considered to be anchored in a so called 'ground state' (Silva and Smith, 2008)

1.2.2 Epiblast stem cells (EpiSCs)

The ability of the epiblast to give rise to ESCs disappears with quickly with implantation (Boroviak et al., 2014). However, pluripotent cell lines can be also derived from the post-implantation epiblast between E5.5 and E7.5 (Brons et al., 2007; Tesar et al., 2007). These cell lines, referred to as epiblast-derived stem cells (EpiSCs), have a distinct transcriptional signature from ESCs, require FGF and activin/nodal signalling and cannot be maintained in 2i+LIF (Brons et al., 2007; Kojima et al., 2014; Tesar et al., 2007). Furthermore, EpiSCs do not readily contribute to the developing embryo, when injected into the blastocyst (Ohtsuka et al., 2012) and show weak and heterogeneous expression of lineage-specific marker (Tsakiridis et al., 2014). Hence, EpiSCs are considered to occupy the primed space of pluripotency (Nichols and Smith, 2009)

Conclusively, it can be said, that ESCs and EpiSCs have been successfully employed as in vitro models for their respective in vivo counterparts, the naïve pre-implantation and the primed post-implantation epiblast, respectively.

1.3 Pluripotency, a developmental continuum.

To this end, I have described two methods of capturing pluripotency in vitro – through the use of ESCs and EpiSCs. Both of these cell types are self-renewing and can contribute to all germ layers of the developing embryo, they are therefore pluripotent. However, these are two distinct states of pluripotency that we are able to keep artificially from progressing in their developmental timeline. In the developing embryo, pluripotency arises and disappears as a developmental continuum in which cells are not arrested at a particular time point – with the exception of embryonic diapause (Renfree and Fenelon, 2017). ESCs and EpiSCs represent the early and late stages of pluripotency, respectively. ESCs can be derived from the pre-implantation epiblast between E3.5 and E4.5, transcriptionally cluster with the E4.5 epiblast and readily form blastocyst chimaeras and contribute to all germ layers and the germ line, therefore they are considered naïve pluripotent (Boroviak et al., 2014; Evans and Kaufman, 1981; Martin, 1981). Naïve ESCs require MEK/ERK and GSK3 inhibition and express a set of distinct naïve transcription factors such as *Zfp42*, *Tfcp2l1*, *Esrrb*, *Klf2*, *Klf4* and *Klf5* (Boroviak et al., 2014; Ying et al., 2008). Unlike differentiated cells, ESCs also have two active X chromosomes just like the pluripotent cells of the pre-implantation epiblast (Silva et al., 2009). In contrast to ESCs, EpiSCs are derived from the post-implantation epiblast, transcriptionally represent cells of the anterior primitive streak (Brons et al., 2007; Kojima et al., 2014; Tesar et al., 2007; Tsakiridis et al., 2014). Furthermore, EpiSCs require FGF/activin signalling and do not revert spontaneously to the naïve state when cultured in 2i+LIF but undergo rapid cell death (Guo et al., 2009). Furthermore, they do not contribute to blastocyst chimaeras but do integrate into the post-implantation epiblast (Huang et al., 2012). EpiSCs express the core pluripotency factors *Pou5f1*, *Sox2* and *Nanog*, but do not express any members of the naïve transcription factor network. Interestingly, EpiSCs show heterogeneous expression of lineage priming markers such as *T* (Brachyury) and post-implantation markers including *Fgf5* and *Otx2*, therefore EpiSCs are considered primed pluripotent. Remarkably, EpiSCs are not capable of differentiating into primordial germ cells (PGCs) despite their parental tissue, the E5.5 epiblast, being the origin of PGCs in vivo (Hayashi et al., 2011; Murakami et al., 2016; Ohinata et al., 2009). Similarly, ESCs cannot be directly differentiated into PGCs as they have to initially downregulate the naïve transcription factor network before becoming responsive to lineage inducing signals (Hayashi et al., 2011; Nakaki et al., 2013). Interestingly, when ESCs are transferred into medium containing FGF, activin and KSR, they start differentiating and, after 48 hours, transition into epiblast-like cells (EpiLCs) (Hayashi et al., 2011). EpiLCs are transcriptionally distinct from EpiSCs, can give rise to PGCs, but only exist transiently. Hence, another distinct state – the formative state – has been proposed in which the naïve pluripotency network has been completely downregulated, cells are responsive for PGC induction, but do not express any lineage priming factors (Smith, 2017). Neagu and

colleagues found that when culturing naïve ESCs in the presence of LIF, the WNT inhibitor IWP2 and the MEK PD03, they upregulate the peri-implantation marker OTX2 (Neagu et al., 2020). However, these cells still express the naïve marker KLF4, readily revert back to the naïve state when exposed to WNT signals. Therefore, these cells are considered to correspond to the rosette stage but have not acquired the formative state. Subsequently, it was found that the culture of naïve ESCs in low levels of activin, with the WNT inhibitor XAV and retinoic acid receptor inhibitor BMS 493 or the direct derivation of cells from the E5.5 epiblast under these conditions, leads to cultures that have downregulated the naïve network and are responsive to PGC induction and are therefore bona fide formative cells (Kinoshita et al., 2020).

Table 1 | Properties of naïve and primed pluripotency (Modified from (Nichols and Smith, 2009))

	Naïve	Primed
Expression of Oct4	Yes	Yes
Expression of naïve pluripotency TFs	Yes	No
Expression of early post-implantation TFs	No	Yes
X inactivation	No	Yes
DNA methylation	Low	High
Apicobasal polarity	No	Yes
Homogeneity	Yes	No
Dependence on FGF/ERK signalling	No	Yes
Dependence on nodal/activin signalling	No	Yes
Formation of blastocyst chimaeras	Yes	No
Formation of post-implantation chimaeras	No	yes
In vitro stem cell derivation	Yes	Yes

Pluripotent cells have also been derived from human and non-human blastocysts (Sasaki et al., 2005a; Thomson et al., 1998; Thomson et al., 1995; Thomson et al., 1996). However, these cells are, unlike mouse ESCs, transcriptionally and epigenetically different from their derived tissue – the primate pre-implantation epiblast (Guo et al., 2014; Yan et al., 2013). Furthermore, primate ESCs consistently failed to form chimaeras when injected into the respective embryo (Okano et al., 2012). They also share several features with mouse post-implantation EpiSCs including the requirement for FGF and activin/nodal signalling and transcriptionally cluster with the late post-implantation epiblast (Brons et al., 2007; Nakamura et al., 2016; Tesar et al., 2007). Eventually, through the use of derivations of the original mouse naïve medium 2i+LIF, it was possible to reset primate ESCs to a naïve state and also enables the derivation of naïve human pluripotent stem cells directly from the blastocyst (Guo et al., 2016; Takashima et al., 2014;

Theunissen et al., 2014). Extensive single-cell sequencing studies have revealed that, although the majority of pluripotency-associated transcription factors match that of rodents, primate ESCs still differ in the expression of several distinct transcriptional regulators (e.g. the absence of KLF2 and the upregulation of KLF17) and have therefore a primate-specific pluripotency network (Boroviak and Nichols, 2017; Boroviak et al., 2018).

1.4 WNT/β-catenin signalling during pluripotency

WNT/β-catenin signalling during pluripotency is complex, controversial and its role in pluripotency establishment, maintenance and execution remains debated. The outcome of WNT/β-catenin signalling in the early embryo heavily depends on the context, developmental stage and cell type (Munoz-Descalzo et al., 2015). The sheer amount of WNTs (19) and respective Frizzled receptors (12), in combination with the dual function of β-catenin as a cell adhesion molecule and signal transducer makes the deciphering of specific signalling pathways a non-trivial endeavour (Kemp et al., 2005; McCrea et al., 2015; van Amerongen and Berns, 2006). Mouse and human pre-implantation express many signalling components of the WNT/β-catenin pathway including several members of the WNT protein family and β-catenin (Lloyd et al., 2003; Yan et al., 2013). Historically speaking, the consensus was that there is no, or only marginal, requirement for WNT/β-catenin for embryonic pre-implantation development and the establishment of pluripotency. This hypothesis was based on the observation that β-catenin knockout mice develop normally until gastrulation. At time of gastrulation β-catenin null embryos fail to establish the anterior-posterior axis, cells start to detach from the embryonic ectoderm layer and no mesoderm formation was observed (Haegel et al., 1995; Huelsken et al., 2000a). Similar observations were made when abrogating the secretion of all WNTs through the knockout the WNT chaperone Porcupine. Porcupine null embryos lack the formation of the primitive streak and do not develop an anterior-posterior axis (Biechele et al., 2013). These studies have established a strong base of evidence for the importance of WNT/β-catenin signalling during gastrulation. Indeed, when manually removing the in vivo source of WNT signalling, the extraembryonic ectoderm, the complete epiblast takes on an anterior fate without the formation of mesoderm and its associated markers such as T and AFP (Rodriguez et al., 2005). On the contrary, stabilisation of β-catenin leads to premature EMT and the expression of posterior markers throughout the complete epiblast (Chazaud and Rossant, 2006; Kemler et al., 2004). Interestingly, a recent study has found that, despite being dispensable for regular pre-implantation development, WNT/β-catenin is crucial for pluripotency maintenance during murine embryonic diapause (Fan et al., 2020). This finding and the evidence that WNT/β-catenin signalling prevents the transition into the rosette stage, might explain the beneficial effects of the WNT/β-catenin

signalling pathways on pluripotency in embryonic stem cells (Neagu et al., 2020). Unlike in the embryo, the benefits of WNT/β-catenin signalling on the pluripotency network in ESCs are undisputed. Initially, it was observed that modulation of the WNT/β-catenin pathway by the GSK3 inhibitor BIO promotes pluripotency (Sato et al., 2004; Umehara et al., 2007). Subsequently, the inhibition of GSK3 by Chiron (CH) in combination with MEK inhibition and the optional addition of LIF, enabled the derivation and long-term culture of mouse embryonic stem cells from mice with varying genetic backgrounds (Ying et al., 2008). ESCs can also be maintained when activating the WNT signalling pathway through exogenous addition of WNT3A (ten Berge et al., 2011). In either case, exogeneous WNT or inhibition of GSK3, β-catenin becomes stabilised which leads to its nuclear accumulation where it interacts with the TCF/LEF transcription factor family (Behrens et al., 1996; Molenaar et al., 1996; van de Wetering et al., 1997). The most dramatic effects on the pluripotency network appears to be β-catenin's function in abrogating the repressive function of TCF3 on the pluripotency network, in particular the naïve transcription factor ESRRB (Lyashenko et al., 2011; Martello et al., 2012; Wray et al., 2011). However, there is further evidence that β-catenin also promotes pluripotency through TCF-independent mechanisms (Faunes et al., 2013; Kelly et al., 2011; Zhang et al., 2020). These TCF-independent mechanism have been suggested to act through a direct interaction of β-catenin with OCT4 (Kelly et al., 2011). β-catenin can promote OCT4 activity and also sequester it to regulate its pro-differentiation properties (Faunes et al., 2013; Kelly et al., 2011; Munoz Descalzo et al., 2013). Additionally, β-catenin has the ability to supply transcriptional coregulators to pluripotency loci and thereby stabilising the complete pluripotency network (Zhang et al., 2020)

Remarkably, stabilisation of β-catenin in EpiSCs leads to rapid differentiation and loss of OCT4, rather than promotion of pluripotency like in ESCs (Kinoshita et al., 2020; Kurek et al., 2015; Sumi et al., 2013). On the contrary, inhibition of WNT/β-catenin signalling reduces spontaneous differentiation, promotes more homogeneous cultures and even improves reprogramming of EpiSCs back to the naïve state (Murayama et al., 2015; Sumi et al., 2013). Consistent with the WNT/β-catenin signalling response of mouse EpiSCs, human conventional stem cells also differentiate upon stabilisation of β-catenin (Davidson et al., 2012; Dravid et al., 2005; Kurek et al., 2015; Singh et al., 2012; Sun et al., 2017). However, some studies have also suggested beneficial effects of WNT/β-catenin signalling on the pluripotency network in conventional human ESCs and mouse EpiSCs (Cai et al., 2007; Kim et al., 2013; Sato et al., 2004). Interestingly, the signalling outcome, differentiation or maintenance of pluripotency, appears to depend on the localisation of β-catenin with nuclear accumulation causing differentiation (Kim et al., 2013). Extrapolating from the knowledge gained in mice, one might expect WNT/β-catenin signalling to support human naïve pluripotency as well. However, original resetting experiments

elucidated that a precise titration of GSK3 inhibition was necessary to establish human naïve cells (Theunissen et al., 2014). A recent study found that actually WNT/β-catenin inhibition via XAV939 treatment is beneficial for pluripotency, suggesting that active WNT/β-catenin signalling to maintain pluripotency might be rodent specific pathway (Zimmerlin et al., 2016). Yet, another contradicting study found WNT/β-catenin to support the naïve state in human ECS by inhibiting the transition into primed pluripotency (Xu et al., 2016). Conclusively, it can be safely said that WNT/β-catenin signalling, in particular in primates, remains elusive and will need further investigation.

1.5 Aims of this study

All higher organisms consist of a multiplicity of cell types with distinct functions and morphological features. Already during the first few days after the fertilization of the egg, the mammalian embryo undergoes complex morphological rearrangement, transcriptional rewiring and epigenetic changes. It has become eminent, that conventional two-dimensional tissue culture systems cannot fulfil the requirements to recapitulate all these processes *in vitro*. Therefore, the development of new technologies is crucial to complete our understanding of such events. Over the last decade the amount of publications regarding three-dimensional cell culture has undergone an exponential growth, thereby exposing benefits, and limitations of these systems. In particular, the advances in the derivation of tissue specific organoids and synthetic embryos have enabled us to ask (and answer) a complete new set of questions, that could have been only answered to a very limited extend by conventional tissue culture techniques. I have performed my doctoral studies in collaboration between the Department of Biochemistry and Cambridge Stem Cell Institute which reflects itself in the experimental set ups and techniques I have used throughout my research. Thus, over the last several years I have addressed the following questions and aims:

- Are microgels are suitable format for culturing embryonic stem cells and does this microgels suspension culture represent a physiologically more relevant environment compared to cells grown on flat plastic surfaces?

- How do such environmental changes (e.g. 2D vs 3D, adhesion, stiffness, pressure) affect cell morphology and behaviour? Can these biophysical properties modulate the pluripotency gene regulatory network? If yes, to which extend and what are the underlying mechanisms?

- Will the co-encapsulate of cells of multiple embryonic lineages allow the synthetic reconstruction of spatiotemporal events of embryogenesis in vitro?

- Finally, how versatile is the proposed system of microgel suspension culture? Can the set-up be adapted to suit cells of other species than rodents, e.g. human or non-human primate? Will this enable us to decipher novel evolutionary conserved master regulators of pluripotency?

2 Experimental procedures

2.1 Microfluidic chip fabrication

I used a variety of different microfluidics chips throughout this study of which all were designed with the CAD software (DraftSight, Dassault Systems). Chip production followed the well-established soft-lithography protocols (Xia and Whitesides, 1998). Briefly, chip designs were cut out on a photo mask which is then used for the fabrication of a silicon wafer master mould in a clean room. Once fabricated, the silicon mould can be theoretically reused indefinitely. For the actual chip production, the master mould was placed in a petri dish and covered with a 1:10 (w/w) ratio of curing reagent with a polydimethylsiloxane (PDMS) precursor. Subsequently, the PDMS covered petri dish was placed in a desiccator and degassed until no more air bubbles were visible. The PDMS was polymerized at 65 °C overnight. The next day, the cured PDMS was carefully cut out of the petri dish and the chip in- and outlets were punched with a 1 mm biopsy needle. The PDMS was then thoroughly washed with 2-propanol and dried with compressed air. At this point, the PDMS is ready to be bond to a microscopy slide to produce the final microfluidic chip. PDMS and microscopy slides were placed in a low-pressure oxygen plasma generator. The plasma chamber was evacuated of air (0 mbar) and refilled with pure oxygen. The plasma treatment lasted for 12 seconds, after which the PDMS was gently pressed onto the microscopy slide resulting in covalent binding of the two surfaces to each other. Immediately afterwards, the microfluidic channels were filled with 1% (v/v) Trichloro(1H,1H,2H,2H-perfluorooctyl)silane in HFE-7500 (**Figure 2.1**) and the chip was placed on a hot plate at 65 °C for 30 min. Subsequently, the chip was washed with filtered HFE-7500 and stored sterile until use.

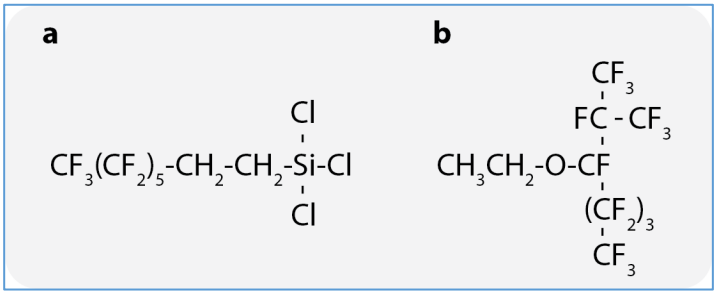

Figure 2.1 | Chemical structures of (**a**) Trichloro(1H,1H,2H,2H-perfluorooctyl)silane and (**b**) HFE-7500.

2.2 Microgel production

The in the literature previously described design (Anna et al., 2003) for a flow focusing device (FFD) was used for the production of microgels. The design contains two inlets, one for the HFE-7500 (oil phase) containing 0.3% PicoSurf-1 (Dolomite) surfactant and one for the agarose (aqueous phase). The channel intersection at which droplet formation (agarose in oil emulsion) occurs, has a width of 70 µm and a height of 75 µm unless stated otherwise. The

polydimethylsiloxane (PDMS) FFDs were prepared according to section 2.1. Due to its physical properties (low melting temperature and clearness) SeaPrep® agarose (Loza) was used for microgel production. The desired amount of agarose was dissolved in PBS at 70 °C for 20 min. Subsequently, the melted agarose was cooled down to 37 °C. To inject the liquid agarose into the chip, a syringe (SGE, 100 µL) was connected with a disposable needle (BD microlance 1 mm ID) to 80 cm of tubing (Smiths Medical fine-bore polyethylene tubing: ID: 0.38 mm, OD: 1.09 mm). The syringe and tubing were filled with HFE-7500 to remove all air, the syringe was then almost emptied and the tubing was filled backwards with the liquid agarose and connected to the FFD's aqueous inlet. A second syringe (SGE, 2.5 mL) was filled with HFE-7500 supplemented with 0.3% PicoSurf-1 and connected to the oil inlet. Syringe pumps (neMESYS and Harvard Apparatus) were used to control the flow rates. If not stated otherwise, the agarose flow was set to 6 µL/min and the oil flow to 30 µL/min. Finally, the agarose in oil emulsion was collected through the exit channel in an ice cooled test tube (Eppendorf, 1.5 mL) where microgel polymerization occurred.

2.2.1 Demulsification of microgels

For long term culture of cells, the microgels needed to be transferred from the emulsion into a corresponding cell culture medium. To break the emulsion, the excess of oil underlying the emulsion was carefully aspirated. The emulsion was then covered with 200 µL PBS (or appropriate cell culture medium). Afterwards, 45 µL PFO (Alfa Aesar) were pipetted under the emulsion and the mixture was immediately vortexed for 5 s and subsequently briefly centrifuged (small table centrifuge) until the phases were separated. The aqueous phase (on top) contains the microgels and was transferred by pipette into an uncoated tissue culture vessel filled with pre-warmed medium.

2.3 Cell culture

2.3.1 Mouse embryonic stem cells (mESCs)

The 129/Ola derived E14TG2a cells (Hooper et al., 1987) and Rex1:GFPd2 (Wray et al., 2011) were generally cultured under 2i+LIF (Ying et al., 2008) conditions. Briefly, N2B27 (1:1 DMEM/F-12 and Neurobasal media, N2 (Bottenstein and Harvey, 1985) [in-house] and B27 (Brewer et al., 1993) [GIBCO] additives, 2 mM L-glutamine, and 100 µM β-mercaptoethanol) was supplemented with 1 µM PD0325901 (MEK inhibitor), 3 µM CHIR99021 (GSK3 inhibitor), and 10 ng/mL leukaemia inhibitor factor (LIF) (in-house). For a certain set of experiments, ES cells were cultured under serum+LIF (S+LIF) conditions. Briefly, GMEM (Sigma-Aldrich) was supplemented with 10% foetal calf serum (FCS) (Sigma-Aldrich), 1x non-essential amino acids (NEAA) (Life Technologies), 1 mM sodium pyruvate (Life Technologies) and 1 mM

L-Glutamine (Life Technologies). Cells were maintained on gelatin-coated (0.1%) culture dishes in a 7% CO_2 humidified incubator at 37 °C and medium was replaced every other day. Cells were passaged every 2-3 days at a dilution of 1:10. Briefly, the medium was aspirated and cells were treated with accutase until cells detached from the dish. Colonies were dissociated into single cells by gentle pipetting the detached cells against the tissue culture dish. Afterwards, the accutase was diluted with 10x volume of wash medium (DMEM-F12 + BSA) and cell were centrifuged for 3 min. at 300 RCF. Finally, the supernatant was discarded, cells were resuspended and replated in the appropriate pre-warmed medium.

2.3.1.1 In vitro differentiation assays

2.3.1.1.1 EpiLC differentiation

EpiLC induction from ESCs was as described by Hayashi and colleagues (Hayashi et al., 2011). Briefly, 2i+LIF cultured ESCs were plated at a density of 200.000 cells/6-well on 10 µg/mL fibronectin coated 6-well plates. EpiLC induction medium consisted of N2B27 medium supplemented with 12 ng/mL bFGF, 20 ng/mL activin A and 1% KSR. Cells were analysed after 48 hours in culture. Alternatively, ESCs were plated on fibronectin coated plates, cultured in N2B27 supplemented with 12 ng/mL bFGF, 20 ng/mL activin A, 2 µM XAV and passaged every 48 hours.

2.3.1.1.2 Neuroectoderm differentiation

For monolayer neuroectodermal differentiation of ESCs I applied the protocol as described by Ying and colleagues (Ying et al., 2003b). Briefly, tissue culture dishes were coated with ~10 µg/mL laminin in PBS for a minimum of 3 hours. Subsequently, laminin was aspirated, replaced with N2B27 and stored in the incubator for equilibration. After passaging, ESCs were resuspended in N2B27 and plated at a density of $1.0x10^4$ cells/cm^2. Medium was replaced with fresh N2B27 after 48 hours and every day thereafter.

2.3.1.1.3 Mesendoderm differentiation

There are several different protocols for definite endoderm and mesoderm differentiation. However, initial ‘mesendoderm’ induction always rely on the stimulation of the WNT and activin/nodal pathways (Mulas et al., 2017; Thomson et al., 2011). For monolayer mesendoderm differentiation plates were coated for a minimum of 3 hours with 10 µg/mL fibronectin (Millipore, FC010) in PBS at 37 °C. Subsequently, fibronectin was aspirated and replaced with fresh N2B27. After passaging, ESCs were resuspended in N2B27 and plated at a density of $1.5x10^4$ cells/cm^2. After 48 hours in N2B27, medium was replaced with fresh N2B27 supplemented with 3 µM CH and 20 ng/mL activin A.

2.3.2 Hanging drop culture

For the aggregation of ESCs in suspension I utilized the hanging drops method. Briefly, after accutase treatment, ESCs were resuspended in 2i+LIF medium at a concentration of 10.000 cells/mL. Subsequently, 30 µL droplets (containing ~300 cells) were pipetted onto the inside lid of a 15 cm petri dish. Finally, the lid was placed on the petri dish, which was filled with PBS to mitigate evaporation.

2.3.3 Mouse epiblast derived stem cells (EpiSC)

Mouse epiblast-derived stem cells (EpiSCs) carrying the Oct4GiP transgene (Ying et al., 2002), were originally established from E5.75 embryos by Dr. Ge Guo (Austin Smith's lab, Cambridge Stem Cell Institute, University of Cambridge) (Guo et al., 2009). EpiSCs were cultured on 10 µg/ml fibronectin coated 6-well plates without feeder cells in serum-free N2B27 medium supplemented with 12 ng/mL bFGF, 20 ng/mL activin A and 2 µM XAV (Kim et al., 2013; Sumi et al., 2013). Cells were passaged every other day by accutase dissociation.

2.3.4 Extraembryonic endoderm cells (XEN cells)

XEN-EGFP cells were a gift from Magdalena Zernicka Goetz's lab (Department of Physiology, Development and Neuroscience, University of Cambridge) and originally derived in Peter Rugg-Gunn's lab (Babraham Institute) (Rugg-Gunn et al., 2010). XEN cells were routinely maintained in RPMI-1640, supplemented with 20% FBS, 1 mM sodium pyruvate, 50 U/mL penicillin, 50 µM 2-mercaptoethanol, 2 mM glutamine.

2.3.5 Marmoset embryonic stem cells

Common marmoset embryonic stem cells (cmESC) were established and maintained by Erin Slatery (Thorsten Boroviak's lab, Department of Physiology, Development and Neuroscience, University of Cambridge). Conventional cmESCs were cultured on inactivated mouse embryonic fibroblast (iMEF) feeder cells in KSR/bFGF medium. Briefly, DMEM/F-12 was supplemented with 20% KnockOut Serum Replacement (KSR), 10 ng/mL FGF2, 100 mM 2-mercaptoethanol, 1xNEAA and 2 mM L-glutamine. For the resetting to naïve-like pluripotency, conventional cmESCs were plated on iMEFs and cultured for at least 10 days in a resetting medium termed PLAXA. Briefly, this medium is based on N2B27 and additionally supplemented with 1 µM PD0325901, 10 ng/mL hLIF, 50 µg/mL ascorbic acid, 2 µM XAV939 and 20 ng/mL activin A. Optionally, PLAXA can be further supplemented with 5% chemically defined lipids. Conventional as well as reset naïve-like cmESCs were maintained at 37 °C, 5% CO_2, 5% O_2 and media were changed daily.

2.3.6 Human embryonic stem cell

The conventional human pluripotent cell line H9 (Thomson et al., 1998) was propagated on Geltrex coated 6-well dishes in Essential 8 (E8) medium (Chen et al., 2011) made in-house. Briefly, DMEM/F12 was supplemented with 64 mg/L L-ascorbic acid-2-phosphate magnesium, 100 µg/L FGF2, 19.4 mg/l insulin, 14 µg/L sodium selenium, 543 mg/L NaHCO3, 10.7 mg/L transferrin and 2 µg/L TGFβ1 or 100 µg/L Nodal. The human naïve derived ES cell line HNES1 (Guo et al., 2016) was routinely maintained on inactivated mouse embryonic fibroblast (iMEF) feeder cells in PXGL medium (Bredenkamp et al., 2019; Guo et al., 2017). Briefly, N2B27 was supplemented with 1 µM PD0325901, 2 µM XAV939, 2 µM Gö6983 and 10 ng/mL human LIF. For immunofluorescent staining, HNES1 cells were plated on laminin coated dishes to circumvent the use of MEFs. Naïve and conventional human ES cells were fed every day and passaged via accutase treatment every 3 to 5 days and cultured in 5% O_2 and 7% CO_2 in a humidified incubator at 37 °C. After passaging, 10 µM ROCK inhibitor (Y-27632, 688000, Millipore) were added to the culture for 24 hours.

2.3.7 Cryopreservation of cell stock

Cells were dissociated and washed as described in section 2.3.1. After the centrifugation, cells were resuspended in freezing medium (2i+LIF+20% FCS+10% DMSO). Cells were then transferred into 1 mL cryo vials and cooled at -1°C/minute with a Mr. Frosty™ freezing container (Thermo Fisher) overnight at -80 °C, before being transferred into liquid nitrogen for long term storage.

2.4 Cell encapsulation in microgels

2.4.1 Preparation of cell suspension for subsequent cell encapsulation

2i+LIF or S+LIF cultured ESCs were grown in 6-well plate and grown for two or three days. Medium was aspirated and cells were washed with 10 mL PBS. Afterwards, PBS was aspirated and cells were dissociated with 1.5 mL accutase for 3 min. at room temperature. Subsequently, 8.5 mL of BSA containing DMEM-F12 medium were added and cells were centrifuged for 3 min at 300 RCF. The supernatant was aspirated and cells were re-suspended in an appropriate amount of N2B27.

2.4.2 Cell and colony recovery from microgels

Cells can be recovered from the agarose microgels at any given time point by digestion of the hydrogel. For recovery, 0.3 U/mL agarase (Thermo Fisher) were added to the in-gel suspension culture, resulting in rapid digestion of the agarose. Cells were then transferred into a 15 mL tube and centrifuged at 300 RCF for 3 min. The supernatant was aspirated and cells were

resuspended in 1 mL accutase for 3 min. at room temperature. If additional dissociation was needed, cells were mixed gently with a 1 mL pipette. Afterwards, 9 mL of BSA containing DMEM/F-12 were added and centrifuged again at 300 RCF for 3 min. Cells were then resuspended in appropriate medium and replated or used for downstream analysis. Colonies were recovered as describe before, but accutase treatment was omitted.

2.5 Cell analysis

2.5.1 Flow cytometry and cell sorting

Flow cytometric analysis of the Rex1::GFPd2 and Jup-mCherry reporters were were analysed with the LSR Fortessa (BD Biosciences).

2.5.1.1 Fluorescence activated cell sorting

Fluorescence activated cell sorting (FACS) was performed at the Cambridge Stem Cell Institute Flow Facility on a MoFlow XDP cell sorter (Beckman Coulter) and the Gurdon Institute on a SH800S Cell Sorter (Sony). For single or bulk FACS, cells were accutase treated for 10 min. at 37 °C before resuspending in 10 ml washing buffer (DMEM/F-12 + 5% BSA). Cells were then centrifuged for 3 min. at 300 RCF. Subsequently, cells were resuspended in 500 µL wash buffer, filtered through a 100 µm cell strainer and stored on ice until sorting. Single cells were directly sorted into 96-well plates, whereas bulk sorted cells were collected in a 1.5 mL test tube and centrifuged after collection. The wash medium was then replaced with the appropriate culture medium before plating the cells.

2.5.2 Immunocytochemistry

Cells were fixed for 10 min. with 4% PFA in PBS. After washing with PBS, cells were permeabilised for 15 min. with 0.5% Triton X-100 in PBS. Subsequently, cells were blocked for at least 2 hours with 3% BSA in PBS blocking solution. Primary antibody incubation was performed at desired concentration at 4 °C, overnight (Table 3). Cells were then washed with blocking buffer and incubated with the secondary antibody for 2 hours at room temperature. Afterwards cells were washed with blocking buffer and stained with 1 µg/mL Hoechst.

2.6 Molecular biology

2.6.1 Cloning

All polymerase chain reactions (PCR) were performed with the Q5 High-Fidelity 2x Master Mix (NEB) and, if necessary, purified from 1% agarose gels using the Zymoclean Gel DNA Recovery Kit (Zymo Research). The plakoglobin (Gene name: *Jup*) overexpression plasmid PB_CAG_Jup-T2A-mCherry was constructed from PB-CAG-hOct4 (Sanger Institute) by

restriction digest and subsequent Gibson assembly(Gibson et al., 2009) with the Jup and T2A-mCherry fragments. *Jup* was previously amplified from cDNA with the primers F_Jup_cDNA and R_Jup_cDNA (**Table 2.1**). The T2A-mCherry fragment was obtained by PCR amplification of pCSpyT_mCherry-HA plasmid (kindly provided by Dr. Laurens Lindenburg, Florian Hollfelder's lab, Department of Biochemistry, University of Cambridge) using the primers F_T2A-mCherry and R_T2A-mCherry (**Table 2.1**). Alpha-select chemically competent cells (Bioline) were transformed with the Gibson assembly reaction mix and plated on selective LB-agar. Plasmid DNA was extracted from monoclonal *E. coli* using the GeneJET Plasmid Miniprep Kit (Thermo Fisher Scientific) and subsequently sequence-verified by Sanger sequencing at the Department of Biochemistry (University of Cambridge).

Table 2.1 | *Jup* and T2A-mCherry primer sequences for Gibson assembly of the plakoglobin overexpression construct.

F_Jup_cDNA	gtctcatcattttggcaaagaattcccATGGAGGTGATGAACCTTATTGAGCAG
R_Jup_cDNA	agcagacttcctctgccctcGGCCAGCATGTGGTCTGC
F_T2A-mCherry	gagggcagaggaagtctgctaacatgcggtgacgtcgaggagaatcctggcccaATGAGTAAAGGAG AAGAGGA
R_T2A-mCherry	cagtcgaggctgatcagcgagctctagaacctcaTTTGTACAGTTCGTCCATG

2.6.2 Piggy-Bacc Transfection

To generate the *Jup* overexpressing cell line, I used the PiggyBac transposon system. Briefly, 10 µL Lipofectamine 2000 were mixed with 300 µL 2i+LIF medium. Separately, 1.2 µL PB_*Jup*-T2A-mCherry (700 ng/mL, 0.8 µg) with 1.6 µL PBase (500 ng/mL, 0.75 µg) and 150 µL 2i+LIF medium. Then, 150 µL diluted DNA were mixed with 300 µL diluted Lipofectamine 2000 and incubated for 5 min. at room temperature. Subsequently, ~$5x10^5$ cells were resuspended in 450 µL of DNA/Lipofectamine 2000 and incubated for 10 min. at 37 °C. Then, cells were plated and stably transfected cells FACS-sorted based on their mCherry signal.

2.6.3 Gene knock-out via CRISPR Cas9

β-catenin knockout cells were generated via transient transfection with a CRISPR/Cas9 *Ctnnb1* KO plasmid according to the manufacturer's instructions (Santa Cruz, sc-419477).
Ctnnb1 was targeted by a mixture of the following 3 gRNAs:
1: ATGAGCAGCGTCAAACTGCG
2: AGCTACTTGCTCTTGCGTGA
3: AAAATGGCAGTGCGCCTAGC

2.6.4 RNA-sequencing

All library preparations, sequencing and bioinformatic pre-processing were performed by my collaborator Joachim de Jonghe (Florian Hollfelder's lab, Department of Biochemistry, University of Cambridge).

2.6.4.1 Smart-Seq2 (Bulk)

For 'bulk' RNA sequencing of ESCs in 2i+LIF cultured on tissue culture plastic or encapsulated in microgels, cDNA sequencing libraries were generated according to the Smart-seq2 protocol (Picelli et al., 2014). The amount of PCR cycles for the initial enrichment was set 12 for bulk samples. Subsequently, libraries were quantified using a Qubit HS (Invitrogen) kit and size distribution was assessed on a Bioanalyzer 2100 DNA HS kit. Libraries were then pooled at equimolar ratios and final molarity was obtained using both the Qubit HS and the Bioanalyzer 2100 HS kits.

For next-generation sequencing (NGS) reads processing, read quality was analysed via the fastQC tool. Low-quality reads (Q<25) and Nextera adapters were removed using the trimmomatic tool. The STAR aligner was further used to index a mm10 reference genome (downloaded via the FTP module from the USCS Genome browser server) using a GTF annotation file downloaded in Gencode. Reads from each sample were the mapped to the indexed reference using the STAR aligner in paired-end sequencing mode. FeatureCounts from the package subread was then used to count the mapped reads and multi-mapped reads were discarded. FeatureCounts were then imported as a matrix in DESeq2 for differential expression analysis.

2.6.4.2 inDrop Single Cell Sequencing

For inDrop single-cell sequencing (Klein et al., 2015), cells were diluted to a concentration of 120,000 cells/mL in PBS containing 15% (v/v) Optiprep® and processed according to the inDrop protocol (Zilionis et al., 2017) with the v3 barcoding design (Briggs et al., 2018). Diversity of barcodes for these experiments was 147,456, and polyacrylamide barcoded-bead batches were quality controlled using FISH on the extended primers. Additionally, species mixing experiments were carried out to measure cross-contamination levels and capture efficienc. Each of the collected fractions aimed to contain 2,949 cells, resulting in a theoretical barcode collision rate of 1%. Cell co-encapsulation with reverse transcription mix and barcoded beads and library preparation were carried out following published protocols (Zilionis et al., 2017). Limited-cycle PCR was employed to amplify and barcode the libraries and the quality of the latter was inspected using a BioAnalyzer HS kit. Samples were pooled at equimolar ratios using both the BioAnalyzer HS and Qubit HS metrics for size distribution and DNA

concentration. The final library was purified using AmpureXP beads (1.5x volumetric ratio) and molarity was measured using a BioAnalyzer HS kit and a Kapq NGS library quantification kit.

The libraries were sequenced using a 75 bp Illumina Nextseq 400M High output kit. In addition, 5% PhiX were used as a spike-in control. Illumina's bcl2fastq script was used to generate the fastq files, which were subsequently quality controlled using FastQC .

2.7 Image acquisition, processing and quantification

Imaging was performed with inverted Leica TCS SP5 and SP8 confocal microscopes using 40x and 20x objectives. Fluorophores were excited with a 405 nm diode laser (DAPI), a 488 nm argon laser (GFP), a 543 nm HeNe laser (Alexa Fluor 543/555) and a 633 nm HeNe laser (Alexa Fluor 633/647). Images were acquired with 1 µm z-steps at 400 Hz and a resolution of 1024x1024. Raw data were analysed with the open source software Fiji (Schindelin et al., 2012) and subsequently assembled in Illustrator CC (Adobe)

2.8 Embryo work

2.8.1 Mouse embryo collection and culture

All mice used in this dissertation were intercrosses of strain CD1 and obtained through natural mating. Embryonic staging was based on the assumption, that mating occurred at midnight. Hence, embryos were staged at E0.5 and noon of the following day. For analysis, pre-implantation embryos were flushed with M2 medium (Sigma) from the oviducts (8-cell stage embryos) or the uterine horns (blastocysts), respectively. Post-implantation E5.5 embryos were carefully dissected from the implantation sites within the uterus. This research has been regulated under the Animals (Scientific Procedures) Act 1986 Amendment Regulations 2012 following ethical review by the University of Cambridge Animal Welfare and Ethical Review Body (AWERB). Use of animals in this project was approved by the ethical review committee for the University of Cambridge, and relevant Home Office licenses (Project license No. 80/2597 and No. P76777883) are in place.

2.8.1.1 Embryo immunofluorescence staining

Mouse embryos were fixed, permeabilized and stained according to Prof. Jenny Nichols' protocol (Nichols et al., 2009b). Initially, the zona pellucida was removed using acid acid tyrode's (TA) to avoid incompatibilities with the immunostaining protocol. In summary, embryos were then fixed with 4% PFA for 20 min. at room temperature. After one wash in PBS supplemented with 3 mg/mL polyvinylpyrolidone (PBS/PVP), embryos were permeabilised for ~30 min. in PBS/PVP with 0.25% Triton X-100. Afterwards, embryos were blocked in PBS

containing 0.1% BSA, 0.01% Tween 20 and 2% donkey serum (blocking buffer). Primary antibodies were appropriately diluted in blocking buffer and incubated at 4 °C overnight (Table 3). Subsequently, embryos were washed 3x in blocking buffer for at least 15 min. each time before incubation with the secondary antibodies for 2 hours at room temperature and in the dark. All secondary antibodies were labelled with Alexa fluorophores and diluted 1:500 in blocking buffer. Subsequently, embryos were then washed in blocking buffer. Imagining was performed by placing the embryos in 2 µL droplets of water in an microscopy dish covered with mineral oil or were incubated briefly in increasing concentrations of Vectashield (Vector Labs) before mounting on glass slides in a small drop of concentrated Vectashield.

2.8.1.2 Embryo microinjection

For (single) cell injections, ESCs grown in the appropriate conditions were dissociated by accutase (500 µL/6-well) treatment for 5 min. at 37 °C. Cells were the centrifuged for 3 min. at 300xg in washing buffer (9.5 mL). Then, cells were resuspended in their appropriate medium and stored on ice until injection. Embryos were injected at the 8-cell stage with single (or multiple) ES cells via laser-generated perforation of the zona pellucida using the XYClone® (Hamilton Thorne Biosciences). Subsequently, injected embryos were cultured in Blast medium at 37 °C and 5% CO_2 for 48 hours, the equivalent of the E4.5 blastocysts.

2.8.2 Human embryo collection and culture

All human embryos were handled and processed by Prof. Jennifer Nichols (Wellcome – MRC Cambridge Stem Cell Institute). The human embryo research was licensed by the UK Human Fertilization and Embryology Authority under research licence RO178. Supernumerary embryos were donated from in vitro fertilization programs with informed consent. Liquid nitrogen stored embryos were thawed at day 6 post fertilisation and cultured for 24 hours in N2B27. Embryos were then fixed in 4% PFA and stained as described in section 2.8.1.1.

2.9 Statistical analysis

All experiments were performed with at least three biological or technical replicates unless otherwise stated. Samples were compared with individual or multiple T-test with the GraphPad PRISM software (v8.4.4). Error bars represent the standard deviations.
Asterisks legend: * $P \leq 0.05$, ** $P \leq 0.01$, *** $P \leq 0.001$.

3 Characterisation of a microgel culture system for embryonic stem cells

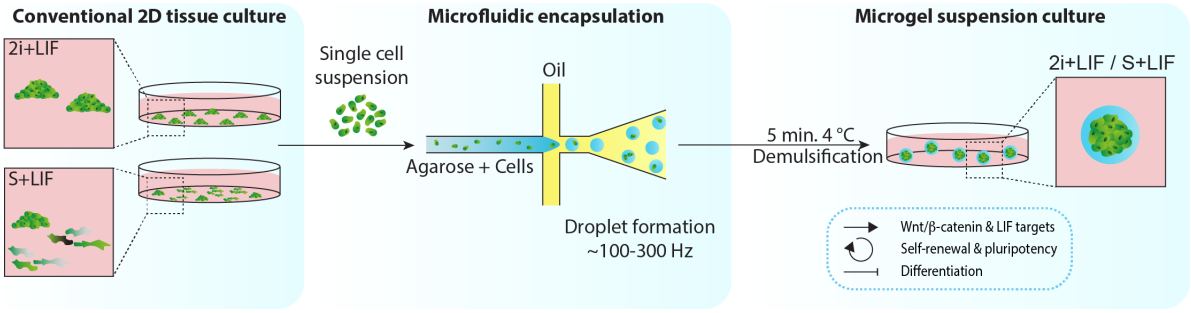

3.1 Introduction

Droplet microfluidics allows the high-throughput and precisely controllable generation of monodisperse microcompartments – droplets. Microdroplets have been used for several decades across different disciplines and functions (Huebner et al., 2008; Theberge et al., 2010). Recently in cell biology, droplets microfluidics emerged as a valuable tool for single-cell sequencing (Klein et al., 2015; Macosko et al., 2015), or when turned into microgels, as a novel culturing method and an alternative to conventional tissue culture plastic. Cells encapsulated in microgels, are surrounded by a three-dimensional (3D) scaffold that, depending on the chosen gel, comes with a variety of properties mimicking the in vivo microenvironment – often better than plastic can. 3D polymers allow to control parameters such as stiffness, extracellular matrix components, degradability, nanotopography and cell adhesivity. Consequently, with the use of gels, 2D and 3D, arises a complex toolbox to regulate cell fate and behaviour (Murphy et al., 2014). Microgels, compared to regular bulk gels, have the advantage of being scalable through high-throughput generation (Headen et al., 2018) and expansion in bioreactors (Tabata et al., 2014), and they are compatible with other microfluidics platforms (Kleine-Bruggeney et al., 2019; Shi et al., 2013). In stem cell biology these features become relevant, as it has been known for several years, that adult stem cells reside in tissue specific microenvironments, called "niches", that regulate self-renewal and differentiation (Morrison and Spradling, 2008). In a ground breaking study, Engler and colleagues elucidated the capabilities of directing mesenchymal stem cells towards different fates by adjusting the stiffness of the substrate they were grown on (Engler et al., 2006). Shortly after, it was also shown, that mouse embryonic stem cells (ESCs) appear to be substrate sensitive, with softer substrates promoting pluripotency (Chowdhury et al., 2010a). Recently, Lutolf and colleagues used soft and defined 3D gels to improve the generation of induced pluripotent stem cells (iPSC) by accelerating the mesenchymal to epithelial transition and enhancing epigenetic plasticity (Caiazzo et al., 2016). Mouse ESCs are in a way special, as they can grow matrix-independent in suspension, allowing their culture in a variety of different hydrogels, even when biologically inert and not supplying any extracellular matrix (Allazetta et al., 2015; Kumachev et al., 2011; Siltanen et al., 2016; Wilson et al., 2014). Recently, our group has demonstrated the successful micro-encapsulation and several day long culture of naïve mouse embryonic stem cells in ultra-low melting agarose (Kleine-Bruggeney et al., 2019). However, microgel culture drastically changes the cells microenvironment and thus far little is known about any downstream signalling events and changes in cell behaviour. In this chapter, I will be characterising the effects of microgel culture on mouse embryonic stem cells, its implications on pluripotency, self-renewal and differentiation.

3.2 Results

3.2.1 Microfluidic encapsulation of mouse embryonic stem cells

At the beginning of this project, the first critical step was to establish a reliable and reproducible protocol for the microfluidic encapsulation of mouse embryonic stem cells (ESCs). All microfluidic cell encapsulations throughout this study were performed with so called flow-focussing devices (FFD). The simplest microfluidic FFDs have one inlet for the aqueous phase and the another one for the non-miscible continuous oil phase (**Figure 3.1 a&b**). At the cross section of these channels, droplet formation occurs due to the non-miscibility of the two phases. The operation of such FFDs is relatively simple, briefly, inlet flows were controlled via precision pumps and droplet formation was observed by placing the chip on a microscope connected to a high-speed camera. In case of mammalian cell encapsulation, sterility was one of the greatest concerns. Initially, contaminations were circumvented by strict standard operating procedures and the use of antibiotics during encapsulation. Later on, I installed a microfluidic encapsulation rig under completely sterile conditions within a laminar flow hood. Droplets exit the chip via an exit channel and can then be handled and analysed off-chip. When introducing a hydrogel precursor as aqueous phase, droplets can be turned into microgels upon polymerisation. Our group has previously shown the use of ultra-low melting agarose for microgel production (Kleine-Bruggeney et al., 2019). Ultra-low melting agarose stays liquid at 37 °C (after initial melting at 50 °C) and polymerises quickly upon cooling through physical cross-linking (Lahaye and Rochas, 1991). Additional advantages are that agarose is biologically inert, chemically defined, visually clear, compatible with most molecular biology techniques and if needed can be degraded via agarase treatment. For all my experiments I exclusively used LONZA's SeaPrep® agarose in which hydroxyethylation reduced the melting and gelling temperature as well as gel strength. To keep the microgels as soft as possible I had to use the lowest agarose percentage possible. According to the manufacturer's data, SeaPrep® agarose melts at temperatures below 37 °C when at a lower percentage than 1.5% (**Figure 3.1 c**). Hence, to ensure stable hydrogels at 37 °C in the incubator, all encapsulations were performed with 1.5% SeaPrep® agarose unless stated otherwise. According to the product information sheet, at a concentration of 1.5%, gel strength lays around 100 g/cm^2 (~10 kPa) and is therefore several magnitudes softer than conventional tissue culture plastic which is in the range of GPa (Saruwatari et al., 2005) (**Figure 3.1 d**). Besides changing the substrate stiffness, microgels also suddenly offer a 3D scaffold to the cells, rather than a flat 2D surface. Depending on the experiments, cells needed to be cultured for different lengths. Therefore, microgel volumes would need to be changed as well. This was achieved by adjusting the channel diameter of the cross section at which droplet formation occurs. The most commonly used FFDs had channel widths of 75, 100 and 200 µm. Also, as the encapsulation

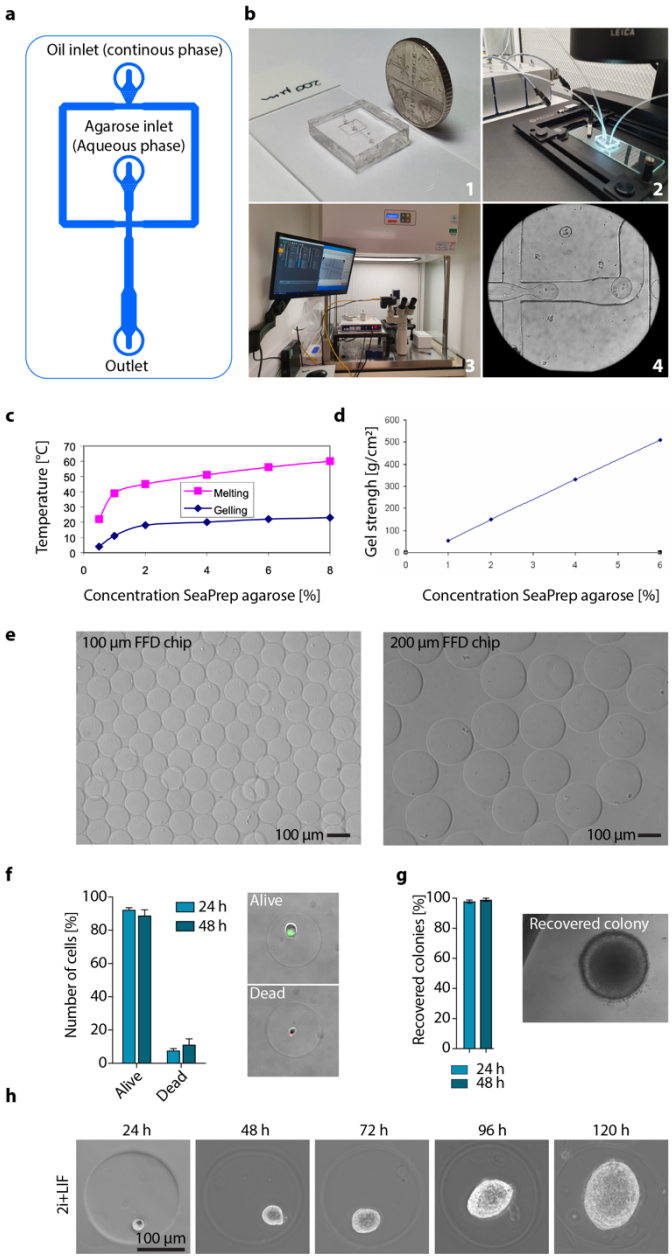

Figure 3.1 | Microfluidic encapsulation of mouse embryonic stem cells into agarose micro gels with subsequent in-gel suspension culture.

a, Schematic illustration of a microfluidic flow focussing device (FFD). **b**, Microfluidic chip (1 &2), sterile microfluidic control module (3) cells being encapsulated into microdroplets at cross-section of FFD (4). **c&d**, SeaPrep® ultra-low meting agarose melting/gelling points and gel strength as supplied by manufacturer (LONZA). **e**, representative images of agarose microgels produced with 100 µm and 200 µm FFDs, respectively. **f**, Viability analysis of cells 24 hours and 48 hours after encapsulation. **g**, Efficiency of colony recovery from microgels after 24 hours and 48 hours in culture. **h**, Representative images of microgel cultured ESCs cultured in 2i+LIF for up to 120 hours.

procedure, normally taking between 20 and 30 minutes, was assumed to be harsher on the cells than regular cell maintenance, I had to ensure good cell viability past encapsulation. However, 2i+LIF cultured ESCs survived the micro-encapsulation surprisingly well. At 24 hours past encapsulation, ~90% of encapsulated cells were alive as determined by calcein-AM assay (**Figure 3.1 f**). As no further increase in cell death was observed after 48 hours in culture, I considered the effects of the microgel encapsulation procedure on the overall cell viability as negligible. Besides showing no cell-toxicity, another of the advantages of low-melting agarose is its simple enzymatic degradability via agarase treatment, allowing cell retrieval at any given timepoint which is, for example, necessary for single cell sequencing or blastocyst injections. To determine the effects of agarase treatment on cell viability, I dissolved individual microgels and re-plated

the previously encapsulated colonies back onto tissue culture plastic. When recovered 24- or 48-hours past encapsulation, >90% of the released colonies attached and continued to proliferate (**Figure 3.1 g**). I therefore concluded, that agarase treatment had no measurable negative effects on cell viability. At this point, I have demonstrated that ESCs can be successfully encapsulated into microgels and even when using a rather unsophisticated material such as agarose, there is no appearance of negative effects on cell viability. Therefore, microfluidic-based encapsulation is a suitable tool for the culture and expansion of ESCs and offers the opportunity to ask questions regarding the impact of microenvironmental changes on e.g. pluripotency, self-renewal and differentiation.

3.2.2 Microgel suspension culture of mouse embryonic stem cells promote ground state pluripotency

Little is known about the influence of the microenvironment on embryonic stem cells, however, some studies claim that softer materials and three-dimensional culture environments support the pluripotency network (Caiazzo et al., 2016; Chowdhury et al., 2010a). Yet, the underlaying mechanisms of how microenvironmental changes might influence gene regulatory networks, and overall cell behaviour, remain poorly understood. In this paragraph I will be describing how I have made use of the previously described REX1::GFPd2 (RGd2) reporter cell line to investigate pluripotency in microgel encapsulated ESCs (Kalkan et al., 2017; Wray et al., 2011). REX1, encoded by the gene *Zfp42*, is known to be expressed in the epiblast of the pre-implantation embryo but sharply downregulated upon implantation into the uterus (Boroviak et al., 2014; Pelton et al., 2002). REX1 is also expressed in undifferentiated ESCs and has been associated with naïve state pluripotency (Toyooka et al., 2008; Wray et al., 2010). Therefore, tracking expression levels of REX1 via the destabilised GFP (GFPd2) enables a near real-time readout for naïve pluripotency in ESCs (Kalkan et al., 2017) (**Figure 3.2 a**). In vitro, ES cells can be maintained in an undifferentiated and self-renewing, pluripotent state in 2i+LIF medium. Under these conditions, ESCs grew as tightly packed colonies with individually indistinguishable cells (**Figure 3.2 b**). In 2i+LIF, ESCs show homogeneous naïve-state associated gene expression as measured by single-cell RNA-seq (Kolodziejczyk et al., 2015). This trait reflects in the homogeneous single-peak Rex1::GFPd2 reporter signal when analysed via flow cytometry (**Figure 3.2 c**). Upon transfer to N2B27 medium ESCs exited pluripotency and started to differentiate, individual cells became visible as they morphologically changed to form a flat monolayer of spread out cells (**Figure 3.2 b**). Within the first 24 hours after 2i+LIF removal, cell shape changed but most cells remained GFP positive (**Figure 3.2 c**). However, after 48 hours the majority of cells had lost the GFP signal and successfully exited naïve pluripotency (**Figure 3.2 c**). In contrast, cells cultured under S+LIF

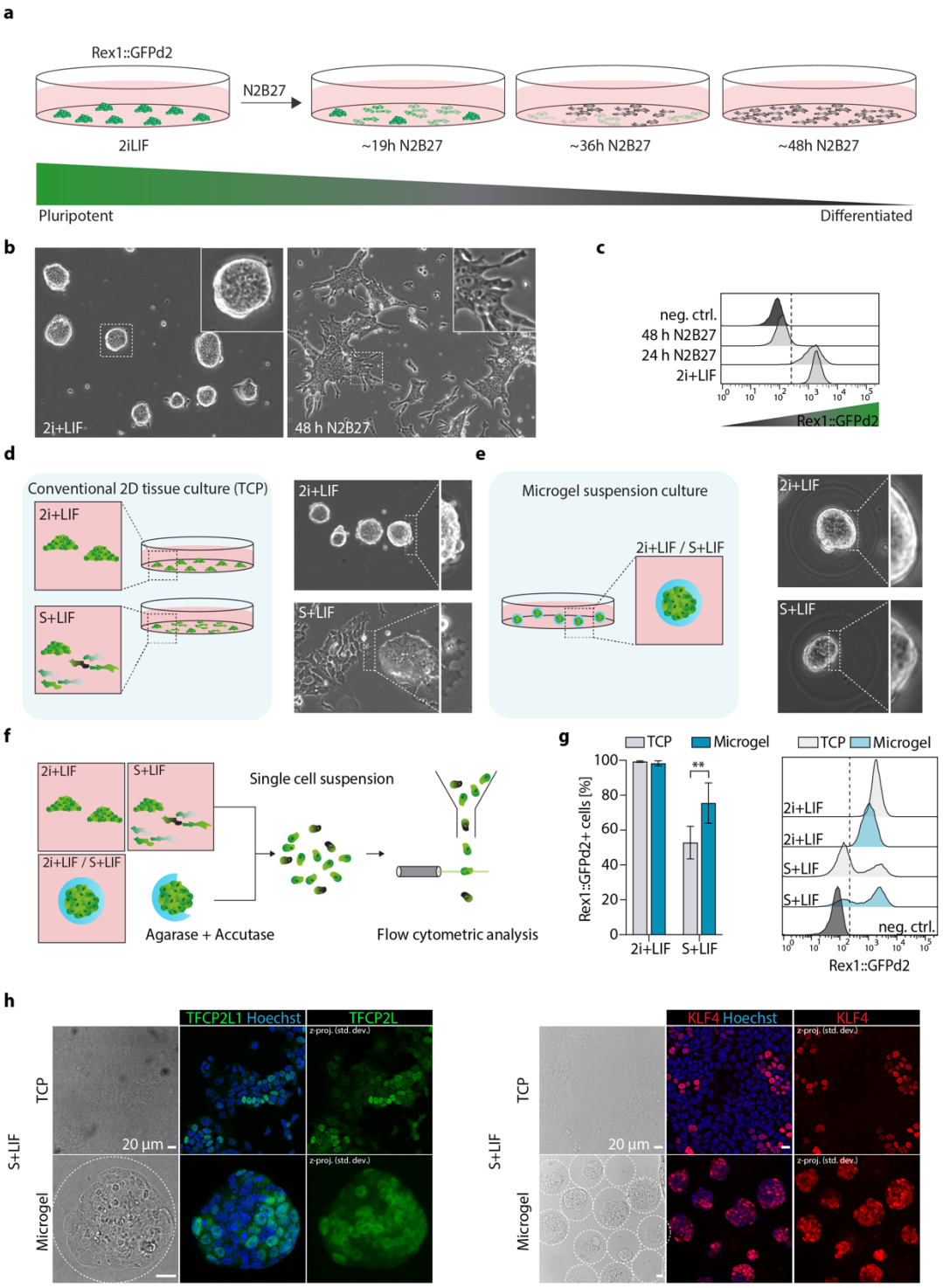

Figure 3.2 | The Rex1::GFPd2 reporter system. **a**, Schematic illustration of the Rex1::GFPd2 reporter system in mouse embryonic stem cells (ESC). REX1 is expressed during naive pluripotency and abruptly downregulated upon differentiation. Within 48 hours of culture in N2B27 medium, all cells have differentiated and lost the Rex1::GFPd2 reporter signal. **b**, Representative images of ESC cultured in 2i+LIF (pluripotent and self-renewal conditions) or in N2B27 (differentiation conditions). Pluripotent ESC form tight dome-shaped colonies in which individual cells are indistinguishable. Upon differentiation, cells start to spread and form a flat monolayer. **c**, Flow cytometric analysis of Rex1::GFPd2 ESC in 2i+LIF or after 24 hours and 48 hours differentiation in N2B27. **d&e**, representative images of 2i+LIF and S+LIF cultured ESCs on conventional tissue culture plastic (TCP) and after being microgel encapsulated. **f**, Schematic illustration of the dissociation of microgels and cells for subsequent flow-cytometric analysis. **g**, Flow-cytometric analysis of Rex1::GFPd2 cells in 2i+LIF and S+LIF on TCP and in microgels (N=3). **h,** Representative confocal images of S+LIF cultured ESCs on TCP and in microgels stained for the naïve transcription factors TFCP2L1 and KLF4.

conditions are morphologically and transcriptionally distinct from 2i+LIF cells (Kolodziejczyk et al., 2015). The attribute of homogeneity, transcriptionally as well as morphologically, is lost under S+LIF conditions (Chambers et al., 2007; Toyooka et al., 2008). ESCs in S+LIF are still pluripotent and self-renewing but show great heterogeneity across these properties, manifesting in a bimodal GFP distribution (Toyooka et al., 2008). Morphological heterogeneity became apparent as some cells still grew in the typical dome-shaped structure, whereas predominantly cells started to flatten out (**Figure 3.2 d**). In contrast to conventional tissue culture plastic, once microgel encapsulated, ESCs grew as morphologically homogeneous colonies regardless of their media conditions (**Figure 3.2 e**). I next investigated, whether this shift towards homogeneity also happened on transcriptional level and not just morphologically. Therefore, RGd2 cells were cultured in 2i+LIF and S+LIF medium, subsequently the GFP signal was analysed via flow cytometry to assess the level of pluripotency (**Figure 3.2 f&g**). As expected, all cells in 2i+LIF, whether cultured on plastic or microgel encapsulated, were GFP positive. Also, cells cultured in S+LIF exhibited the above described heterogeneity with about ~50% of cells being GFP positive when cultured on plastic. However, when these cells were transferred to S+LIF and their pluripotency was assessed after 48 hours of in-gel culture, I was surprised to see that this number had risen to ~70% of cells expressing GFP. As this 20% increase indicated a shift of the cell population towards naïve pluripotency I next investigated the expression levels of TFCP2L1 and KLF4, additional members of the naïve gene regulatory network (Boroviak et al., 2014; Martello et al., 2013), via immunofluorescence staining (**Figure 3.2 h&i**). Notably, TFCP2L1 displayed a heterogeneous expression pattern with only a fraction of the cells (~36%, n=478) being positive for TFCP2L1 when cultured on plastic in S+LIF medium (**Figure 3.2 h**). KLF4 positive cells appeared rarely (~26%, n=320) and as small clusters surrounded by KLF4 negative cells (**Figure 3.2 h**). Consistent with the increased Rex1::GFP signal, I also observed the majority of cells being positive for TFCP2L1 and KLF4 when cultured in microgels (**Figure 3.2 h**). Taken together, these data show that microgel culture of ESCs in S+LIF medium leads to a higher degree of morphological and transcriptional homogeneity compared to regular tissue culture plastic. Finally, these effects appear to be converging on promoting the naïve pluripotency gene regulatory network, however, extensive single-cell RNA-seq analysis will be necessary to validate this claim.

3.2.3 Systemic changes across the transcriptome stabilise the pluripotency network in microgel cultured embryonic stem cells

The previously described observations regarding microgel induced promotion of ground state pluripotency, the increase in the expression of naïve transcription factors like TFCP2L1 and KLF4, led us to ask the question whether just a few individual (pluripotency) genes were affected

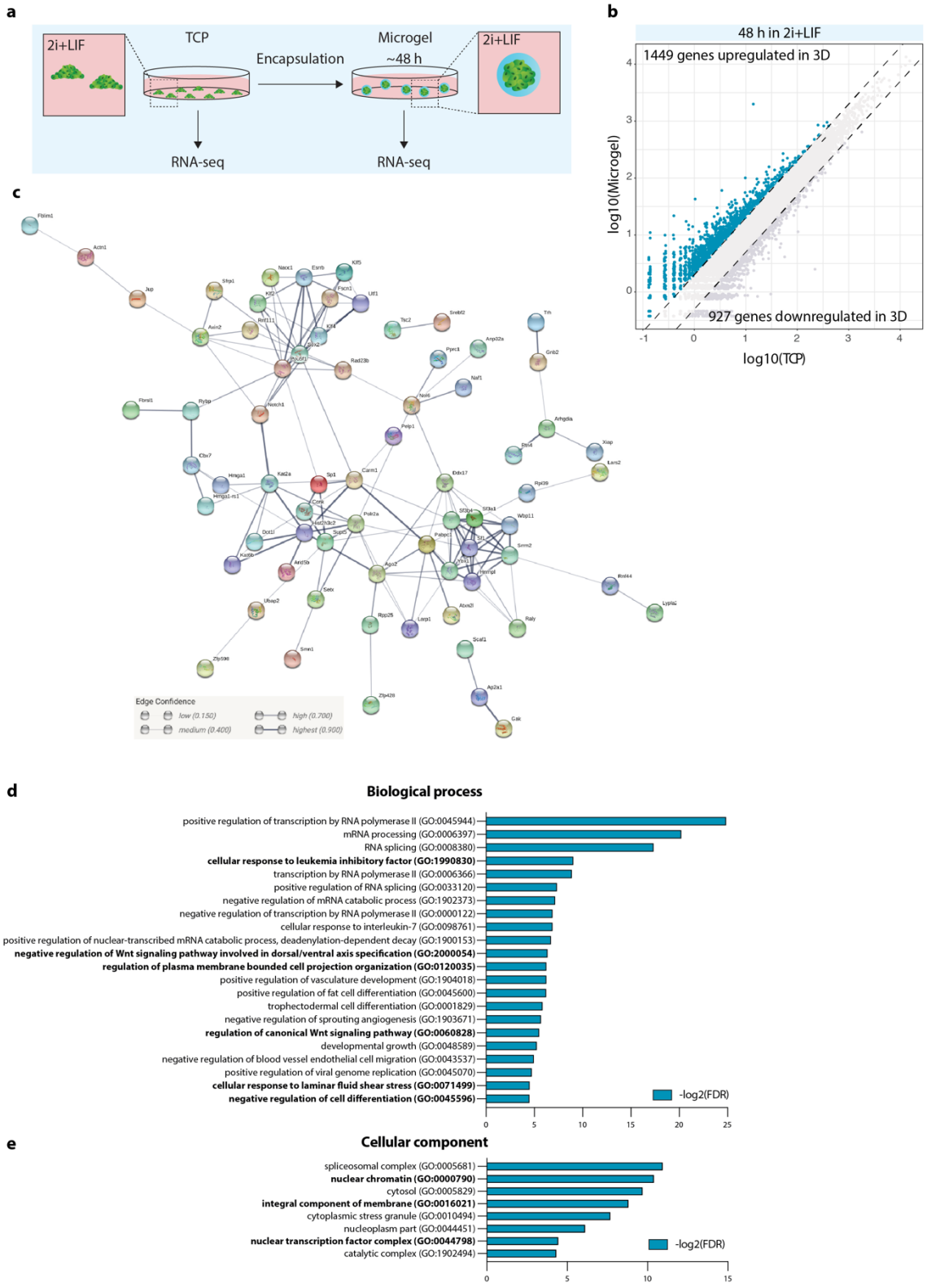

Figure 3.3 | RNA-seq analysis of microgel encapsulated ESC vs conventionally cultured ESC in 2i+LIF. **a**, Experimental set-up for whole genome RNA-seq analysis. Embryonic stem cells were cultured under 2i+LIF conditions and sequenced either directly from conventional tissue culture plastic or after 48 h of in-gel suspension culture. **b**, Scatterplot of log2-fold differentially regulated genes **c**, STRING protein-protein interaction network analysis. After top 200 upregulated genes (according to log2(normalised counts)) were then sorted by significance (padj) and plotted with STRING. Each node represents a protein (splice isoforms and post-translational modifications collapsed). The network edges represent protein interactions based on text mining, experiments, databases, co-expression, neighbourhood, gene fusion and co-occurrence (line thickness indicates the strength of data support). Hence, edges represent but do not ineluctably mean that these proteins physically bind to each other. **d&e**, Gene ontology analysis for biological processes and cellular components. | All RNA-seq was performed in collaboration with Joachim de Jonghe, Department of Biochemistry, University of Cambridge.

or if there was a more global change in transcription. However, due to the inherent heterogeneity of S+LIF cultured cells (Kolodziejczyk et al., 2015), they were unsuitable for bulk RNA sequencing (RNA-seq) analysis as I would be averaging transcripts across different cells. I hypothesized, that microgel culture would affect cells cultured in 2i+LIF, which are more homogeneous in gene expression and therefore suitable for bulk RNA-seq, in a similar fashion as it does in S+LIF cultured cells – by promoting pluripotency. Consequently, I decided to perform RNA sequencing on ESCs cultured in 2i+LIF from regular tissue culture plastic (TCP) and 48 hours past encapsulation (**Figure 3.3 a**). Indeed, on global level I have observed a >log2-fold change in 1449 up- and 927 downregulated genes when cultured in microgels compared to TCP (**Figure 3.3 b**). I then took the top 200 (by log2-fold change) upregulated genes and sorted them by their significance (adjusted p-value). Subsequently, I used the STRING software (von Mering et al., 2005) to analyse potential protein-protein interactions networks amongst the 100 most differentially regulated genes (**Figure 3.3 c**). I then used gene ontology (GO) analysis (Ashburner et al., 2000) to further investigate the protein functions and localisations of the upregulated genes (**Figure 3.3 d&e**). Upregulated genes were predominantly be clustered into pluripotency, chromatin structure/modifications and RNA metabolism associated groups. GO terms for biological processes include "negative regulation of WNT signalling pathway involved in dorsal/ventral axis specification", "regulation of the canonical WNT signalling pathway" and "cellular response to leukaemia inhibitory factor" based on the upregulation of *Sfrp1*, *Axin2* and the *Klfs* (**Figure 3.3 d**). GO terms for cellular components include the "spliceosomal complex", "nuclear chromatin", "integral components of membrane" and "nuclear transcription factor complex" (**Figure 3.3 e**). I also utilized the KEGG pathway enrichment tool (Kanehisa and Goto, 2000), which highlighted the "Signalling pathways regulating pluripotency of stem cells" pathway, based on the upregulation of *Axin2*, *Esrrb*, *Pou5f1*, *Sox2* and *Klf4*. Taken together, these data show transcriptomic adjustments on a global level. These adjustments originated from an accumulation of several small changes rather than a few individual genes that were drastically differentially regulated. Due to the extent of changes in gene expression I had to ensure next, that microgel cultured cells did not transit into an artificial state or have lost any of their original function. Therefore, I encapsulated H2B-turquoise (H2B-tq) tagged ESCs and cultured them for 48 hours in 2i+LIF medium (**Figure 3.4 a**). Subsequently to in-gel culture, I released the colonies from the microgels and dissociated the colonies into single-cell suspension. I then injected several cells (~5 cells/embryo) into the developing 8-cell stage embryos (n=11) and cultured them in vitro until the blastocysts stage. Embryos were then fixed and immunostained for Lamin B1 (nuclear envelop protein) and SOX2 (epiblast marker) (**Figure 3.4 b**). The injected cells integrated into the embryos, with about 70% of them being positive for H2B-tq signal within the epiblast (**Figure 3.4 c**). None of the chimeric embryos showed extraembryonic potential of the

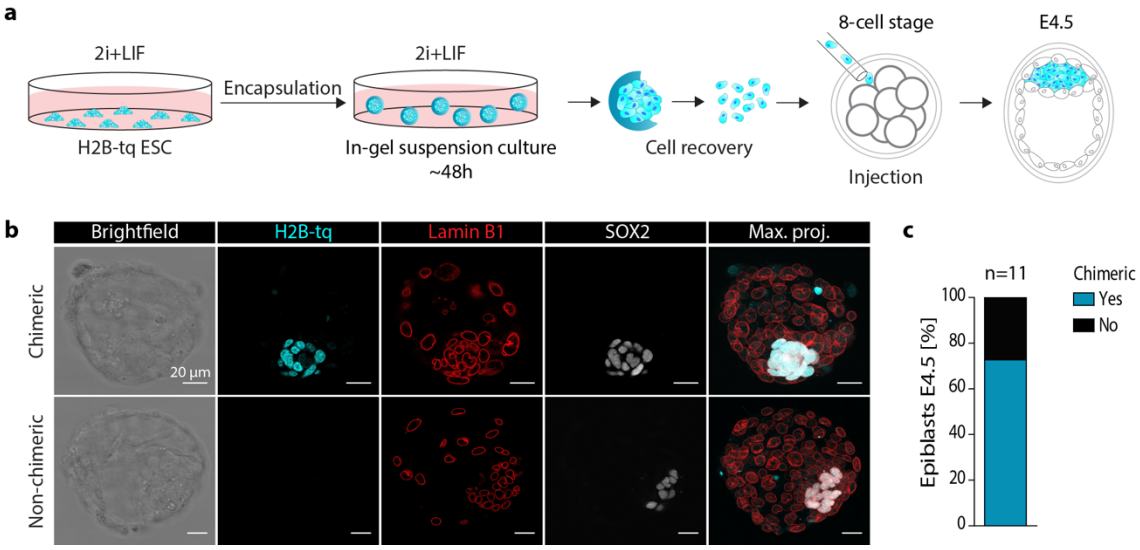

Figure 3.4 | In-gel cultured embryonic stem cells readily integrate into the developing epiblast after injection into 8-cell embryos. a, Schematic illustration of the injection preparation and procedure. Several cells were injected per embryo. **b**, Confocal images of chimeric and non-chimeric blastocysts after cell injection and in vitro culture. Injected cells had a nuclear H2B-turquoise (H2B-tq) reporter and the embryos were additionally stained for Lamin B1 and SOX2. **c**, Chimera contribution efficiency of cells injected during the 8-cell stage (n=11). | Injections were performed by Dr Ayaka Yanagida, Cambridge Stem Cell Institute.

microgel cultured ES cells. Now, after having confirmed that microgel encapsulated cells have not lost their potential to contribute to the developing embryo, even though they show a distinct gene expression pattern compared to TCP cultured cells, I had a closer look at the expression

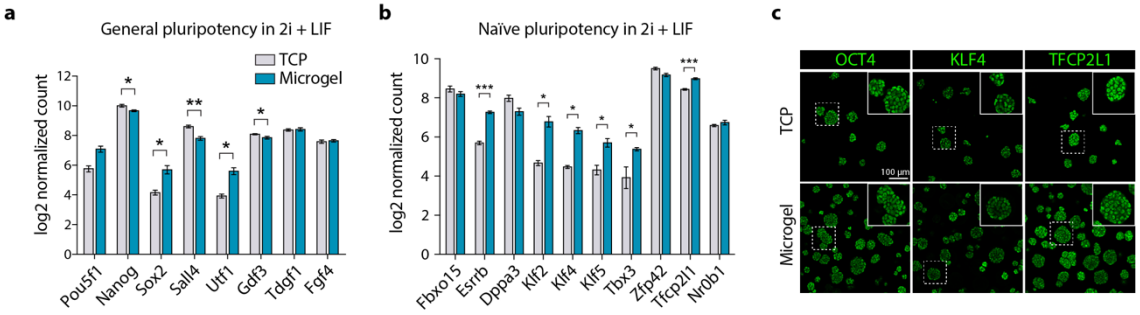

Figure 3.5 Microgel cultured embryonic stem cells display adjustments across their pluripotency gene regulatory network. a, Log2 normalised counts of general pluripotency transcription factors (N=3). **b**, Log2 normalised counts of naïve pluripotency transcription factors. **c**, Confocal z-slice images of TCP and microgel cultured ESCs stained for OCT4, KLF4 and TFCP2L1.

levels of general and naïve state associated transcription factors (**Figure 3.5 a&b**) as described by Boroviak and colleagues (Boroviak et al., 2014). Surprisingly, even amongst the core pluripotency genes *Pou5f1* (OCT4), *Nanog* and *Sox2* I detected changes. *Pou5f1* and *Sox2* were significantly upregulated whereas *Nanog* was slightly downregulated. Within the group of naïve transcription factors, *Esrrb*, *Tbx3*, *Tfcp2l1* and the *Klfs* were upregulated, all of which are downstream targets of the LIF and WNT signalling pathways (Hall et al., 2009; Martello et al.,

2013; Martello et al., 2012; Qiu et al., 2015; Renard et al., 2007). One may note that *Zfp42* (REX1) expression levels slightly dropped, coinciding with the reduced GFP signal when analysed by flow cytometry (**Figure 3.6 a&b**). Taken together, these data show a global transcriptomic change that facilitated through cumulative changes across several groups of genes regulating chromatin structure, RNA metabolism and pluripotency. In particular, pluripotency appears to be re-wired to as genes changes across the general and naïve gene regulatory networks. Nevertheless, microgel cultured cells can readily incorporate into the developing embryo where they contribute exclusively to the epiblast.

3.2.4 Microgel adjusted LIF and WNT signalling delays the exit from naïve pluripotency

The upregulation of LIF and WNT signalling targets within the pluripotency network prompted us to investigate if encapsulated cells can readily exit the naïve state or if the exit is delayed. Therefore, I transferred microgel encapsulated and TCP cultured RGd2 cells from 2i+LIF medium into differentiation permissive N2B27 medium and measured the GFP signal via flow cytometry at several time points over the course of 48 hours (**Figure 3.6 a&b**). The GFP signal consistently diminished at equal rates in encapsulated and TCP cultured cells. Consistent with previous studies (Kalkan et al., 2017), after 48 hours almost all cells (>99%) had lost their GFP signal and had therefore successfully exited the state of naïve pluripotency. Downregulation of the naïve network was additionally confirmed via immunostaining for OCT4, KLF4 and β-catenin (**Figure 3.6 c**) . In contrast to conventional culture on TCP, differentiating cells in agarose microgels did not change their morphology as seen by the b-catenin distribution. However, after 48 hours in N2B27 the naïve marker KLF4 was completely absent from these cells while OCT4 levels were only slightly decreased (**Figure 3.6c&d**). As any dual combination of the components of 2i+LIF is able to maintain naïve pluripotency (Wray et al., 2010; Ying et al., 2008), I tested the differentiation capacities of RGd2 cells in the presence of either just LIF, PD or CH. As expected, in all three conditions maintenance of the pluripotency network was prevented and cells initiated the exit from naïve pluripotency, however differentiation kinetics were delayed compared to differentiation in N2B27 (**Figure 3.7 a-c**). LIF and CH appeared to be the more potent signals to maintain the naïve state as ~80% and ~70% respectively were still GFP positive 48 hours after removal of 2i. Initially, there was no change between TCP and microgel cultured cells after 48 hours of LIF only, however, after 72 hours microgel cultured cells were still ~60% GFP-positive whereas TCP cultured cells were reduced to ~23%. This finding indicates, that indeed the WNT signalling pathways appeared to be partially activated by microgel culture even in the absence of CH. The differences between TCP and microgel culture were less striking in the case of CH only culture. This might be due to the effect, that CH alone is already

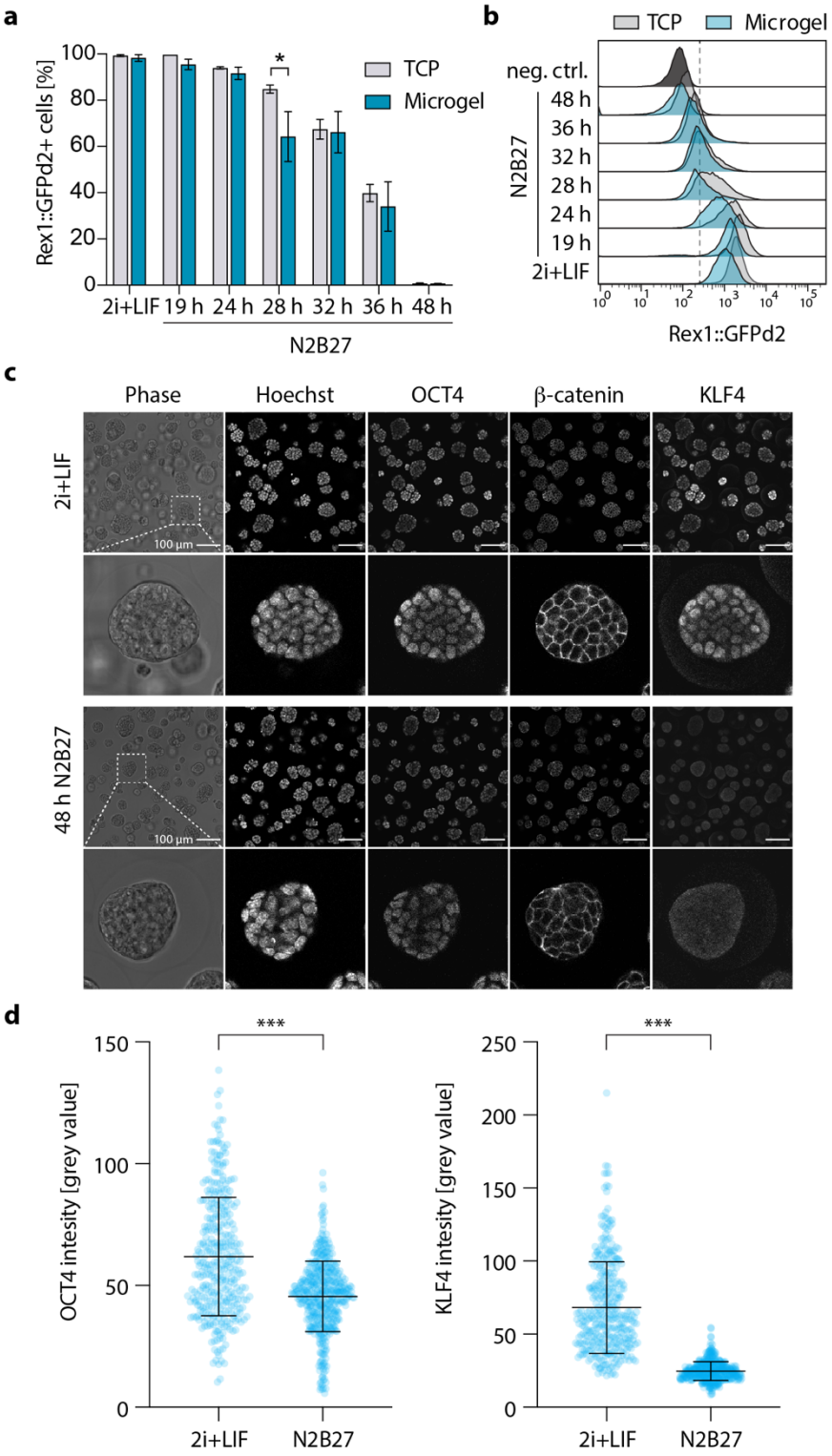

Figure 3.6 | Microgel culture does not inhibit the exit from naive pluripotency. a&b, Flow cytometric analysis of the Rex1::GFP reporter as cells exit naive pluripotency in differentiation permissive N2B27 medium. **c**, Confocal images (single z-slice) of microgel encapsulated embryonic stem cells in 2i+LIF medium and after 48 h in N2B27. Cells were stained for OCT4 (general pluripotency), KLF4 (naïve pluripotency) and β-catenin. **d**, Fluorescence intensity measurements of OCT4 and KLF4 in 2i+LIF (n=359) and N2B27 (n=458) medium.

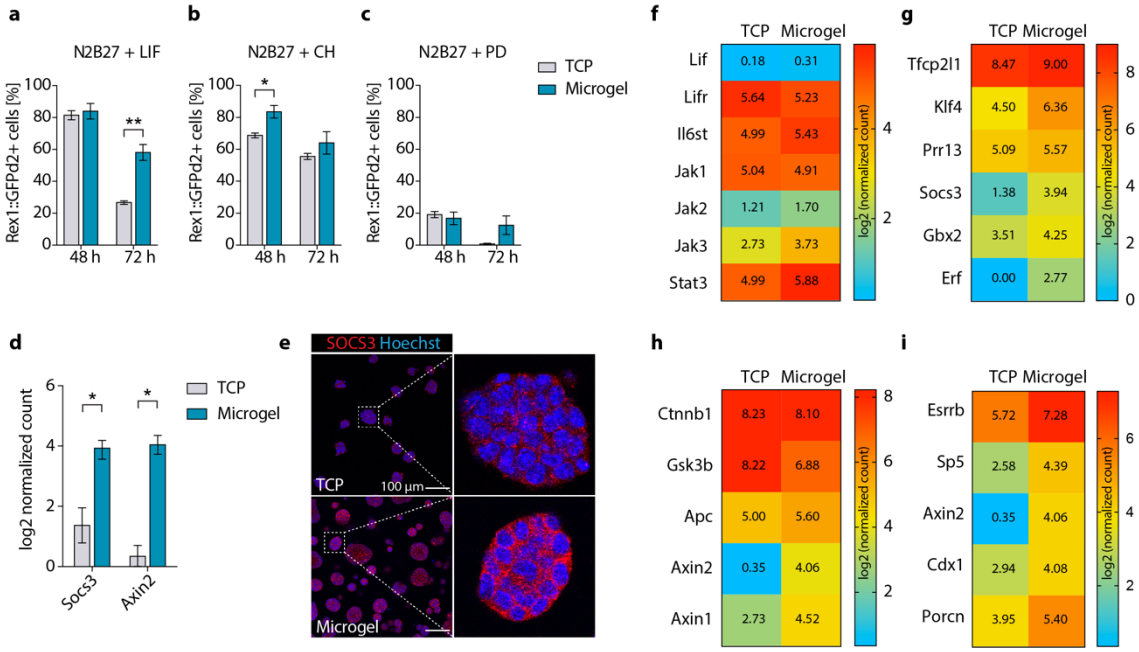

Figure 3.7 | Microgel encapsulated ESCs display enhanced activation of WNT/β-catenin and LIF/STAT3 targets under naïve culture conditions. a, b & c, Rex1::GFPd2 positive cells as measured by flow cytometry after 48 and 72 hours of culture in N2B27 with either LIF, CH or PD (N=3). **d**, Log2 normalised count for the LIF/STAT3 signalling target Socs3 and the WNT/β-catenin signalling target Axin2 under naïve conditions (N=3). **e**, Confocal z-slice images of TCP and microgel cultured ESC stained for SOCS3. **f&g**, Log2 normalised counts for LIF/STAT3 signalling members and targets. **h&i**, Log2 normalised counts for WNT/β-catenin signalling members and targets.

a strong signal and maintains half of the cell population in a GFP-positive state when cultured on TCP. However, I still detected a ~15% increased GFP signal in the microgel cultured cells compared to TCP after 48 hours. Hence, microgels appears to be supporting the LIF signalling pathway even though not to the extend as they do support the WNT signalling pathway. I did not further focus on PD only, as the majority of cells had exited naïve pluripotency after 48 hours. Due to these findings and our earlier GO-term analysis (**Figure 3.3 d**) that highlighted the responsiveness of the LIF and the WNT signalling pathways to microgel culture, I further scrutinised the expression of their signalling components and targets (**Figure 3.7 d-i**). Indeed both, the target and negative feedback regulator of LIF signalling *Socs3* (Nicholson et al., 1999) and of WNT signalling *Axin2* (Jho et al., 2002) were significantly upregulated in 2i+LIF cultured cells when encapsulated in microgels (**Figure 3.7 d**). Interestingly, I did not observe any drastic transcriptional changes in the components of the LIF and WNT signalling pathways (**Figure 3.7 f&h**). However, exclusively all LIF signalling targets as defined by Martello and colleagues (Martello et al., 2013) as well as the known WNT targets *Esrrb*, *Sp5*, *Tbx3* and *Cdx1* (Boroviak et al., 2014; Renard et al., 2007; Wray et al., 2011; Ye et al., 2016) were upregulated (**Figure 3.7 g&i**). Concluding, these data show that microgel encapsulated ESCs can readily exit naïve state pluripotency with similar kinetics as TCP cultured cells. However, slowed differentiation kinetics became apparent in response to single activation of the LIF or WNT signalling pathways,

potentially explained by a partial compensatory activation of the pluripotency network by the microgel culture.

3.2.5 Microgel culture leads to structural rearrangement of adherens junctions

Intrigued by the enhanced activity of the WNT and LIF signalling pathways, I was wondering if these observations were independent events or have been potentially co-activated by an upstream regulator. β-catenin (*Ctnnb1*) is an integral component of the canonical WNT signalling pathway (Rudloff and Kemler, 2012) and E-cadherin (*Cdh1*) is crucial for the proper activation of the LIF signalling cascade (del Valle et al., 2013). Both proteins are also core components of the membrane localised adherens junctions (Harris and Tepass, 2010). Therefore, I went back to our RNA-seq data set and had a closer look at the expression levels of the individual components of adherens junctions. To our surprise, neither *Cdh1* or *Ctnnb1* were differentially expressed (**Figure 3.8 a**). α-catenin, which acts as the linker protein between adherens junctions and the cytoskeleton, appeared to be slightly reduced in its expression when cultured in microgels. However, I then found the β-catenin homologue plakoglobin (*Jup* [Junctional plakoglobin]) and another armadillo protein, p120-catenin (*Ctnnd1*), to be significantly upregulated. Interestingly, plakoglobin was overall one of the most differentially regulated proteins between plastic and microgel culture. To confirm that the transcriptional

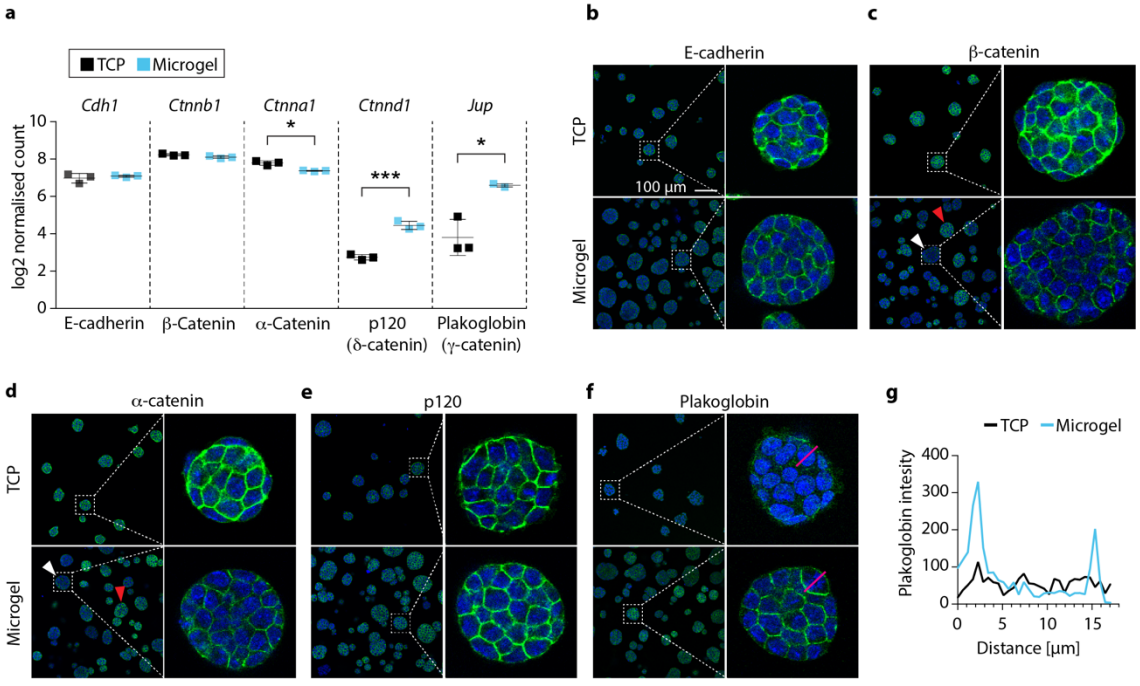

Figure 3.8 | Microgel encapsulated embryonic stem cells upregulate plakoglobin under naïve culture conditions. **a**, Log2 normalised expression levels as measured by RNA-seq for the adherens junction components E-cadherin (*Cdh1*), β-catenin (*Ctnnb1*), α-catenin (*Ctnna1*), p120 (*Ctnnd1*) and plakoglobin (*Jup*) (N=3). **b-f**, confocal images of TCP and microgel cultured cells immunostained for (b) E-cadherin, (c) β-catenin, (d) α-catenin, (e) p120 and (f) plakoglobin. Nuclei were stained with Hoechst. **g**, Plakoglobin staining intensity measured across a single cell as indicated in (f) with a red line.

changes actually had influence on the protein level, I immunostained RGd2 cells in 2i+LIF medium, cultured on TCP or in microgels, for the different adherens junction proteins – E-cadherin, α-catenin, β-catenin, p120 and plakoglobin (**Figure 3.8 b-f**). In general, protein levels were corresponding precisely to the measured transcript levels, however on a closer look some deviation became apparent. E-cadherin levels remained stable in both conditions whereas β-catenin, even though no differences were detectable on transcriptional level, showed heterogeneity in its protein level. This heterogeneity was obvious between different colonies, but not within the same colony. Equally, α-catenin displayed a similar heterogeneity across different colonies with some being high and other low in expression. Now, for p120, which showed a clear increase on transcriptional level, I could not detect a clearly quantifiable increase in protein via immunofluorescence. Yet, all the previously mentioned fluctuations become negligible when considering the dramatic changes of plakoglobin. On conventional TCP, embryonic stem cells exhibited extremely low levels of plakoglobin, whereas encapsulated cells showed strong plakoglobin signal (>2-fold increase intensity compared to TCP), mostly in association with the cell membrane (**Figure 3.8 f&g**). As I had observed drastic morphological changes of S+LIF ESCs when cultured in microgels, I was wondering if these changes were concomitant with adjustments in the adherens junction's structure, similar to the upregulation of plakoglobin under

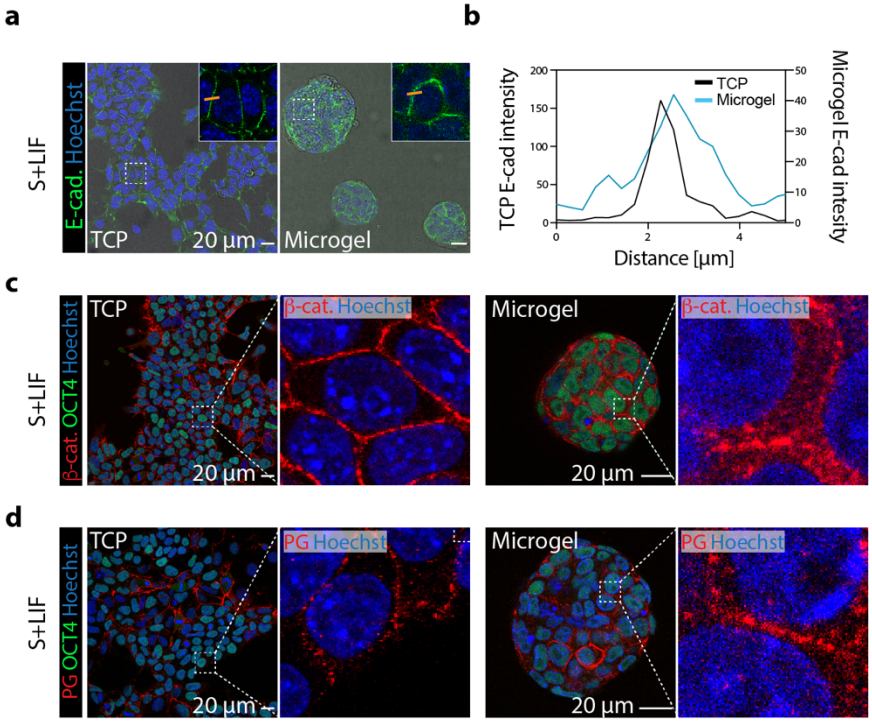

Figure 3.9 | Microgel suspension culture of embryonic stem cells leads to structural reorganisation of adherens junctions in S+LIF medium. a, S+LIF cultured cells on TCP or microgel encapsulated were stained for E-cadherin. b, E-cadherin immunostaining intensity and diameter at the cell membrane. d&d, S+LIF cultured cells on TCP or microgel encapsulated were stained for β-catenin or plakoglobin and OCT4.

2i+LIF conditions. Therefore, I immunostained RGd2 cells cultured in S+LIF for E-cadherin, β-catenin and plakoglobin (**Figure 3.9 a-d**). The previously observed changes in the cells' phenotype indeed coincided with a rearrangement of adherens junction components. ESCs in S+LIF show E-cadherin along their membrane but not in their cytoplasm (**Figure 3.9 a**). In contrast, upon encapsulation E-cadherin signal became increasingly diffuse, instead of detecting a clear membrane localisation, now E-cadherin was also located in the cytoplasm (**Figure 3.9 a&b**). If E-cadherin can be found in the cytoplasm in encapsulated cells, the E-cadherin associated protein β-catenin and plakoglobin should display a similar distribution. Indeed, both proteins were found to have dissociated from the membrane as shown by strong cytoplasmic signal (**Figure 3.9 c&d**). Conclusively, microgel culture of ESCs triggered an upregulation of plakoglobin in 2i+LIF, and a general compositional re-organisation of the adherens junctions in S+LIF.

3.3 Conclusions

In this chapter I have introduced and explained the microfluidic-based encapsulation of mouse embryonic stem cells (ESCs) into microgels. The relatively humble needs of ESCs on their microenvironment, when maintained as self-renewing and pluripotent cells, enabled the use of such a simple hydrogel as agarose for the scaffold material. Agarose is perfectly compatible with microfluidics and most techniques used in molecular biology, it is also chemically defined, biologically inert and easy to work with. These are all clear advantages of agarose. On the other hand, because biologically inert, agarose does not supply any extra cellular matrix and is also not degradable by the cells on their own. Nonetheless, it appears to be a suitable material for the culture of ESCs under pluripotent conditions, as they can proliferate over several days without any observable negative implications. Yet, initially we knew very little about the effects of microgel culture on pluripotency and these cells in general. When culturing heterogeneous S+LIF ESCs in microgels, the most prominent change was their adjusted morphology. Suddenly these cells had lost the typical, spread out morphology and turned into something, resembling what we normally associate with the dome-shaped colonies in 2i+LIF medium. I then confirmed this observation of morphological homogeneity on transcriptional and protein level via the Rex1::GFP transcriptional reporter and immunostainings. The naïve-state associated transcription factors REX1, TFCP2L1 and KLF4 (Boroviak et al., 2014; Martello et al., 2013), all appeared to be upregulated when S+LIF cells were cultured in microgels. Postulating that this 'boost' towards naïve pluripotency was inherent to microgel culture, and should therefore also act on 2i+LIF cultured cells, I performed RNA-seq analysis of these cells and compared them to cell grown on conventional tissue culture plastic. This approach allowed me to elucidate changes on a global level – because so far, I had little knowledge of what could potentially regulate

pluripotency upstream when cells were microencapsulated. Indeed, even in 2i+LIF I was able to detect the hypothesised microgel induced 'boost' of pluripotency. Most naïve state associated transcription factors, including *Tfcp2l1*, *Esrrb*, *Klf2*, *Klf4* and *Klf5*, were expressed at higher levels than on plastic whilst simultaneously detecting differential regulation of the core pluripotency genes *Pou5f1*, *Sox2* and *Nanog*. Unbiased gene ontology analysis of the top 100 differentially regulated genes elucidated the microgels influence on the regulation of the WNT and LIF signalling pathways as well as spliceosomal regulation and chromatin modifications. Because ESCs in 2i+LIF are considered to be naïve and closely resemble the E4.5 epiblast (Boroviak et al., 2014; Plusa and Hadjantonakis, 2014), I was concerned that the extend of transcriptional changes would be an artificial state with unwanted cell properties – e.g. losing the ability to integrate into the developing embryo. However, when injecting microgel cultured ESCs into the 8-cell embryo, no integration disabilities were observed. Pleased to see that microgel cultured cells did not display any obvious disadvantages in chimera contribution in comparison to the wild type cells, I was then investigating the encapsulated cells ability to exit naïve pluripotency. When microgel cultured cells were transferred to differentiation permissive N2B27 medium, the Rex1::GFP reporter was downregulated at similar kinetics as in the conventionally cultured cells. This finding and the absence of the naïve transcription factor KLF4, as confirmed via immunostaining, indicated the cells ability to exit the naïve state despite the differentially regulated pluripotency network. However, when N2B27 was supplemented with LIF or CH, the exit from pluripotency was significantly prolonged in microgel cultured cells, suggesting a partial activation of the pluripotency maintenance pathways by the microgel. The LIF and WNT signalling pathways converge at the adherens junctions. E-cadherin, crucial for LIF signalling (del Valle et al., 2013), and β-catenin, an essential component of canonical WNT signalling, both are key components of the adherens junction complex. The enhanced activation of both of these signalling pathways prompted me to further investigate the adherens junction complex. In S+LIF conditions, microgels cultured cells underwent a structural reorganization of their adherens junctions, with E-cadherin and β-catenin being found not just at the membrane, but also in the cytoplasm. Interestingly, in 2i+LIF the reorganisation of adherens junctions was mainly due to the dramatic upregulation of plakoglobin. Plakoglobin is a homologue of β-catenin and has been implicated to be potentially involved in WNT signalling. However, it's signalling functions and how they differ from β-catenin remain elusive. In the next chapter I will be investigating plakoglobin's role in mouse embryonic stem cells, its potential role in pluripotency and how it might differ from the known β-catenin signalling cascade.

4 The role of plakoglobin in regulating pluripotency

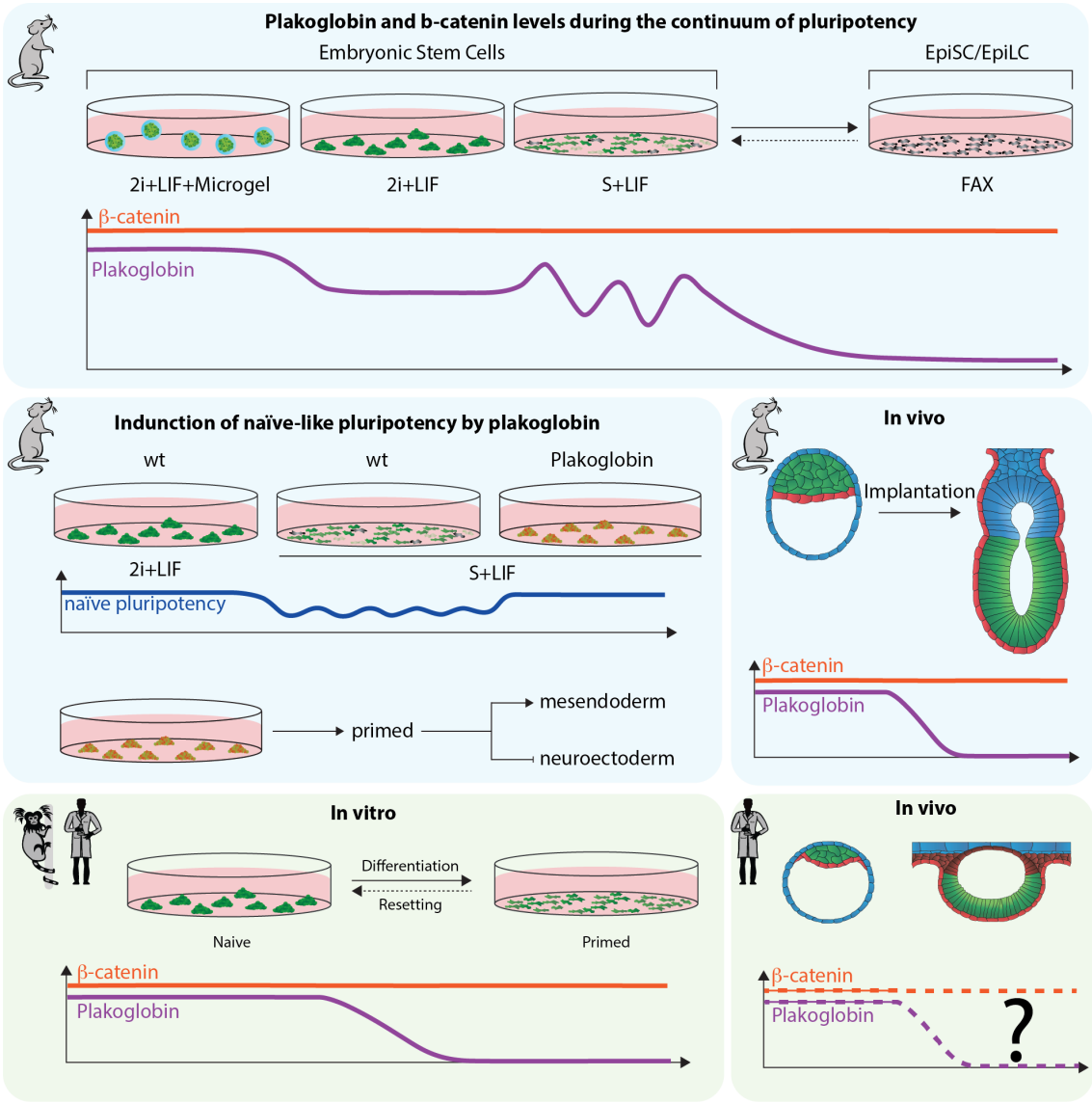

4.1 Introduction

In the last chapter I have introduced a microgel culture system for mouse embryonic stem cells and elucidated the microenvironmentally induced changes in cell morphology, pluripotency and transcription. Amongst the differentially regulated genes between conventional 2D tissue culture and 3D microgel culture, I identified *Jup*, a gene encoding a protein named 'junctional plakoglobin', as one of the most upregulated genes upon cell encapsulation. Plakoglobin (also known as γ-catenin) is a ~82 kDa protein, that has originally been identified in desmosomes (Cowin et al., 1986; Franke et al., 1983), where it connects the cell membrane to intermediate filaments via linkage of desmocollin and desmoglein to desmoplakin (Kowalczyk et al., 1997; Troyanovsky et al., 1994a; Troyanovsky et al., 1994b). Plakoglobin, like most catenins, belongs to the group of armadillo proteins and is a closely related homologue of β-catenin, the mammalian homologue of armadillo in *Drosophila* (Butz et al., 1992b; McCrea et al., 1991b; Peifer et al., 1992a). Plakoglobin and β-catenin have an overall high sequence similarity (~69%), especially their central regions, which in both proteins consist of 13 armadillo repeats (Butz et al., 1992b; Hatzfeld, 1999). Albeit preferentially localised at desmosomal plaques, plakoglobin, just like β-catenin, can also bind to E-cadherin and be incorporated into cell-cell adherens junctions (Butz and Kemler, 1994; Knudsen and Wheelock, 1992). The formation of this cadherin-catenin-complex (CCC) is facilitated through the cytoplasmic catenin-binding domain (CBD) encompassing amino acid positions 832-862 (Ozawa et al., 1990). Interestingly, interaction between the CBD acts in a mutually exclusive fashion, resulting in either E-cadherin/β-catenin or E-cadherin/plakoglobin CCC formation (Butz and Kemler, 1994; Hinck et al., 1994; Nathke et al., 1994). In addition to their interaction with E-cadherin, plakoglobin and β-catenin also bind directly to α-catenin and vinculin, which in turn bind to α-actinin and thereby connect the cell membrane with the cytoskeleton (Huber et al., 1997). So far, no differential function has been observed between these different types of CCCs, suggesting that plakoglobin and β-catenin have similar or identical function in the formation of adherens junctions. All the above studies have focussed on adhesion properties but largely omitted signalling functions of catenins. Yet, just like β–catenin, plakoglobin has a dual functionality in cell-cell adhesion whilst simultaneously acting as a signalling molecule. Especially in cancer biology, β-catenin and plakoglobin have gained special interest since both proteins, despite their structural similarity, have opposing signalling functions. On the one site, hyperactive β-catenin signalling has been shown to have powerful oncogenic potential (Korinek et al., 1997), whereas plakoglobin has been implicated in functioning as a tumour suppressor (Alaee et al., 2018; Charpentier et al., 2000; Sechler et al., 2015; Simcha et al., 1996). During embryonic development, formation of the CCCs is of crucial importance for maintaining structural integrity of the embryo. Any single homozygous knockout of the components of the CCCs is embryonically lethal. Whilst E-cadherin and α-catenin

knockout embryos fail to undergo compaction (Larue et al., 1994; Riethmacher et al., 1995; Torres et al., 1997), p120 (δ-catenin) knockout embryos arrest only around E8.5 showing distinct abnormalities in axis formation (Hernandez-Martinez et al., 2019). Both, plakoglobin and β-catenin null embryos, show no defects during pre-implantation development but die at different stages post-implantation. β-catenin null embryo development arrests ~E7.0 due to the lack of mesodermal differentiation whilst plakoglobin null embryos develop until ~E10.5 at which they die due to severe failure in heart and skin formation (Bierkamp et al., 1996; Haegel et al., 1995; Huelsken et al., 2000b; Ruiz et al., 1996). Consequently, plakoglobin and β-catenin can substitute for one another in the adherens junctions during compaction, but fail to take on more specific roles during gastrulation and desmosome formation, respectively. When inducing hyperactive β-catenin mediated transcription via its stabilisation, embryos undergo premature epithelial-to-mesenchymal transition and display T(Bra)-positive cells in their anterior site (Kemler et al., 2004). To my knowledge, there are no studies investigating the overexpression of plakoglobin in mammalian embryos, however, injection of plakoglobin mRNA into fertilized Xenopus eggs leads to axis duplication reminiscent to ectopic expression of int-1 (WNT1), β-catenin or treatment with an antibody against β-catenin antibody (Karnovsky and Klymkowsky, 1995; McCrea et al., 1993; McMahon and Moon, 1989). These were some of the first experiments indicating plakoglobin's potential involvement during developmental signalling, however, no follow-up studies have been performed regarding mammalian embryogenesis. Despite the embryos ability to develop without β-catenin until implantation, WNT/β-catenin signalling has been shown to be extremely beneficial for the maintenance of mouse embryonic stem cells during naïve pluripotency (Ying et al., 2008). An observation that can be mostly attributed to the alleviating effect of β-catenin on the repressive function of TCF3 (*Tcf7l1*) on the pluripotency network (Lyashenko et al., 2011; Wray et al., 2011). Interestingly, Mahendram and colleagues have shown that plakoglobin can, albeit at lower efficiency, rescue TCF/LEF mediated transcription in β-catenin knockout cells (Mahendram et al., 2013). However, plakoglobin's contribution to WNT induced signalling has still to be fully deciphered. Remarkably, upon transition from naïve ESCs to primed pluripotency in EpiSCs, the role of β-catenin mediated transcription switches from maintaining pluripotency to induce differentiation (Kim et al., 2013; Sumi et al., 2013). Consistent with these findings, overexpression of β-catenin in conventional hPSCs, also leads to differentiation (Sun et al., 2017). However, contrary to naïve mouse ESCs, β-catenin signalling does not show naïve pluripotency promoting effects when reset to naïve-like pluripotency. Hence, its inhibition rather than its activation supports the naïve pluripotency network (Zimmerlin et al., 2016). Neither β-catenin nor plakoglobin are necessary for self-renewal in conventional hPSCs, however, plakoglobin's effects on pluripotency have not yet been studied (Sun et al., 2017). Generally speaking, due to

the complex interactions between plakoglobin and β-catenin, and their dual functionality as adhesion-mediating and signal-transducing proteins, the underlaying mechanisms remain largely unclear. In this chapter I will be elucidating plakoglobin's role in the establishment of naïve pluripotency in mouse embryonic stem cells and embryonic development. Further, I will be investigating plakoglobin in human pluripotent stem cells, naïve and primed, as well as during embryonic pre-implantation development. Finally, I shall explore plakoglobin expression in a new model system, the common marmoset.

4.2 Results

4.2.1 Generation and characterisation of a plakoglobin overexpressing mouse embryonic stem cell line

Due to the microgel induced upregulation of plakoglobin and its accompanied upregulation of pluripotency transcription factors, I hypothesised that plakoglobin might play a role in the maintenance and establishment of naïve state pluripotency. Therefore, I used the RGd2 cell line as my starting material to generate a plakoglobin (Gene name: *Jup*) overexpressing cell line (PG OE). I assembled a plasmid containing mouse *Jup* under the control of the CAG promotor (Niwa et al., 1991). The *Jup* gene was followed by a T2A self-cleaving peptide (Ahier and Jarriault, 2014; Daniels et al., 2014) which itself was followed by an mCherry reporter (**Figure 4.1 a**). With this construct, I was able to have a fluorescent readout of the transcriptional level of the *Jup* transgene in addition to the Rex1::GFPd2 reporter for naïve state pluripotency. I used the PiggyBac transposon system (Li et al., 2013) for stable cell line generation. After transfecting the RGd2 cells with the Jup-T2A-mCherry and the PiggyBac plasmid, I expanded the cells for several days before than sorting the mCherry-GFP double positive cells via FACS (**Figure 4.1 b**). To ensure that mCherry positive cells overexpress plakoglobin, I then confirmed the actual plakoglobin protein levels by immunofluorescence staining (**Figure 4.1 c**). The "wt" RGd2 cells showed very little plakoglobin, irrespectively of their media conditions (S+LIF or 2i+LIF). In contrast, the PG OE cells displayed a tremendous increase of plakoglobin protein level, and as expected, the mCherry reporter signal positively correlated with the amount of plakoglobin. As I did not start from a single clone, but sorted a bulk population of mCherry/GFP double positive cells, I was not surprised to find a heterogeneous mixture of mCherry, and therefore plakoglobin expression (**Figure 4.1 c**). However, I did not expect its differential cellular localisation, depending on the plakoglobin expression level. Plakoglobin seems to initially saturate the cell membrane, and only when passing a certain threshold, it started to accumulate in the cytoplasm and the nucleus (**Figure 4.1 c**). This phenomenon was observed in S+LIF and 2i+LIF. When investigating cell morphology, RGd2 and PG OE cells were indistinguishable when cultured in 2i+LIF (**Figure 4.1 d**). Yet, when cultured under S+LIF conditions, PG OE cells acquired a tighter and dome-shape appearance, normally associated with naïve pluripotency in 2i+LIF medium. I then quantified this change in cell shape by measuring the aspect ratio of individual cells (**Figure 4.1 e**). RGd2 cells in 2i+LIF showed a mean aspect ratio of 1.4 (n=15) and of 2.8 (n=17) S+LIF, reflecting the previously described differences in morphology. Interestingly, PG OE cells in S+LIF exhibited a mean aspect ratio of 1.2 (n=17) confirming our observation of being more similar to 2i+LIF associated morphology (**Figure 4.1 d&e**). It has previously been shown, that the knockout of β-catenin (*Ctnnb1*) leads to a compensatory upregulation of plakoglobin (Sun et al., 2017). In return, I was intrigued if the upregulation of

plakoglobin leads to a decrease in β–catenin levels. Thus, I also immunostained the RGd2 and PG OE cells for β-catenin, and additionally p120 (δ-catenin) (**Figure 4.1 f&h**). In 2i+LIF medium, RGd2 and PG OE cells both show similar levels of β-catenin with a slight reduction in the PG OE cells (**Figure 4.1 f**). However, under S+LIF conditions, in which GSK3 is not inhibited by CH, β-catenin levels drop to almost undetectable levels in the PG OE cells, whereas the RGd2 cells show strong expression of β-catenin. PG OE cell behaviour was therefore consistent with the previous studies showing a reciprocal protein level between β-catenin and plakoglobin (Sun et al., 2017) (**Figure 4.1 g**). One may note that p120 (δ-catenin) remained largely unaffected by plakoglobin overexpression (**Figure 4.1 h**), most likely due to an E-cadherin binding epitope

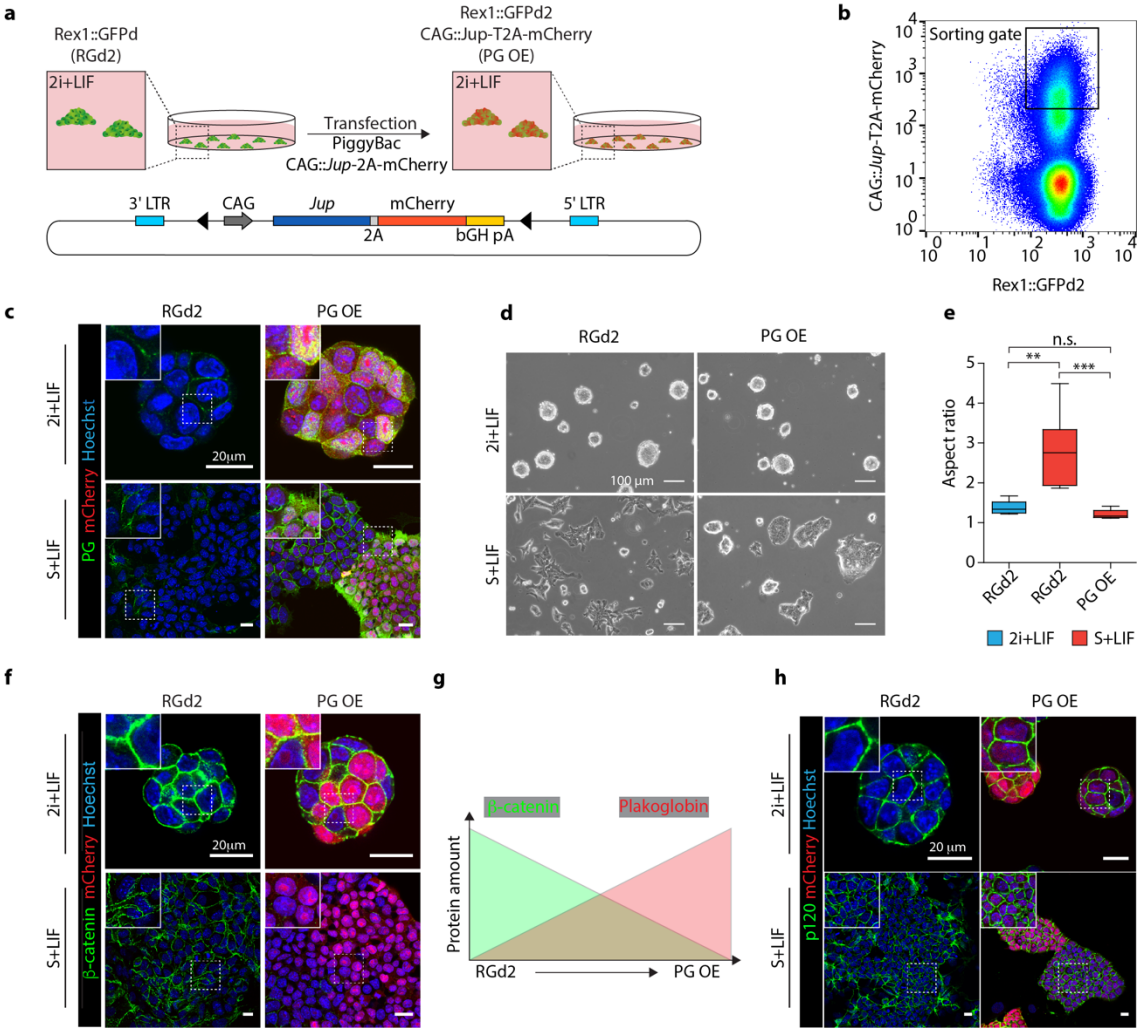

Figure 4.1| Generation and characterisation of a mouse embryonic stem cell line overexpressing plakoglobin. **a**, Schematic illustration of the PiggyBac transfection of the RGd2 (Rex1::GFPd2 reporter) cell line with the plakoglobin overexpression construct (Jup-T2A-mCherry). **b**, Subsequently to PiggyBac transfection, cells were sorting according to their GFP and mCherry signals. Double positive cells were bulk sorted (sorting gate as indicated) and were expanded in 2i+LIF medium to generate the PG OE cell line. **c**, Confocal images of RGd2 and PG OE cells stained for Plakoglobin in 2i+LIF and S+LIF medium. **d**, Phase contrast images of RGd2 and PG OE cells in 2i+LIF and S+LIF. **e**, Aspect ratio measurements of RGd2 and PG OE cells. **f**, Confocal images of RGd2 and PG OE cells stained for β-catenin in 2i+LIF and S+LIF medium. **g**, Schematic illustration of plakoglobin and β-catenin protein levels in the RGd2 and PG OE cells. **h**, Confocal images of RGd2 and PG OE cells stained for p120 in 2i+LIF and S+LIF medium.

separate of β-catenin and plakoglobin (Daniel and Reynolds, 1995; Shibamoto et al., 1995). Once I had confirmed the successful generation of a plakoglobin overexpressing ES cell line, I next had to investigate if there were any downstream effects regarding the state of pluripotency. As I had previously observed an upregulation of the REX1::GFPd2 reporter when S+LIF cultured cells were microgel encapsulated, I was wondering if the forced expression of plakoglobin also facilitated a shift towards naïve state pluripotency. Under 2i+LIF conditions, no differences were

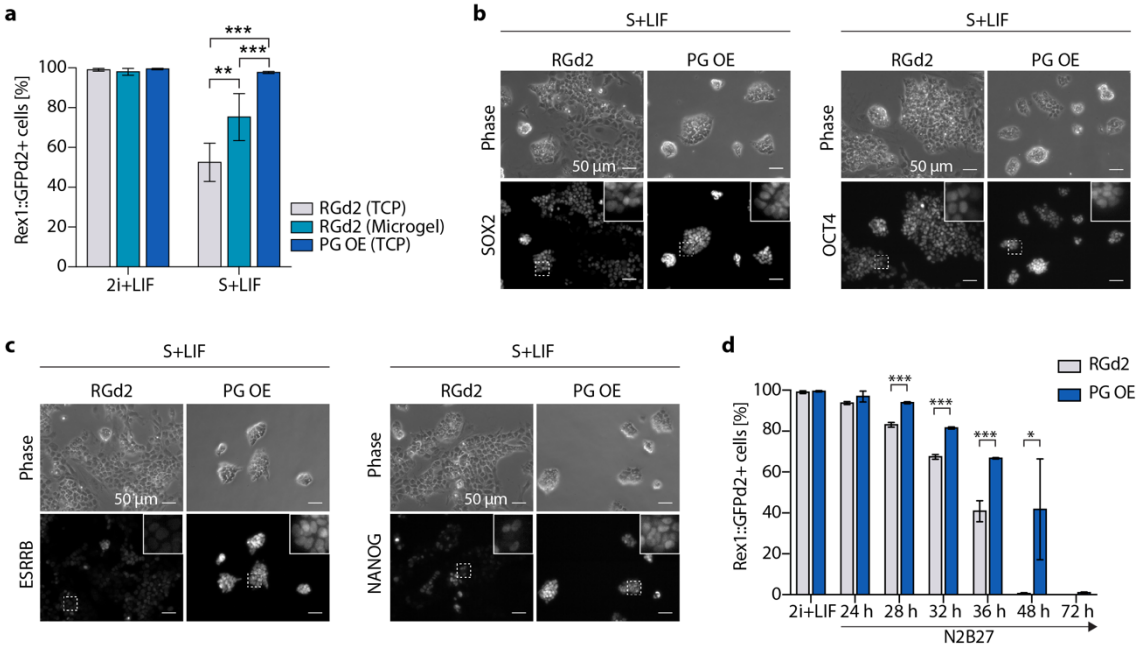

Figure 4.2 | Plakoglobin overexpression promotes naïve pluripotency and slows differentiation kinetics of embryonic stem cells. a, Rex1::GFPd2 reporter analysis via flow cytometry of RGd2 and PG OE cells in 2i+LIF and S+LIF conditions (N=3). **b**, Epifluorescence images of RGd2 and PG OE cells stained for the general pluripotency makers SOX2 and OCT4. **c**, Epifluorescence images of RGd2 and PG OE cells stained for the naive pluripotency makers ESRRB and NANOG. **d**, Flow cytometric analysis of the differentiation kinetics of RGd2 and PG OE cells as measured by Rex1::GFPd2 signal in 2i+LIF and several time points in N2B27 medium (N=3).

detectable between RGd2 and PG OE cells with ~100% of the cells being GFP positive (**Figure 4.2 a**). Surprisingly, I also found that in S+LIF almost all cells of the PG OE cell line were GFP positive, indicating a re-establishment of ground state pluripotency (**Figure 4.2 a**). I therefore immunostained for the general pluripotency markers OCT4 and SOX2 as well as the naïve pluripotency markers NANOG and ESRRB (**Figure 4.2 b&c**). SOX2 and OCT4 were homogeneously expressed across all cells with PG OE cells showing slightly elevated protein levels. However, NANOG and ESRRB showed low and heterogeneous expression in the RGd2 cells, but in PG OE cells homogeneity was regained and all cells showed strong signals for both transcription factors (**Figure 4.2 c**). Morphology and homogeneous expression of naïve pluripotency transcription factors in the PG OE cells supported the hypothesis of plakoglobin being involved in the establishment of naïve pluripotency. Since PG OE cells constitutively express plakoglobin, I was wondering if these cells still have the ability to exit pluripotency.

When PG OE cells were transferred into N2B27 medium they readily exited the naïve state, however, with slowed kinetics compared to RGd2 cell (**Figure 4.2 d**). In summary, I have generated a plakoglobin overexpression cell line. These cells were morphologically distinct from wild type cells in S+LIF and displayed homogeneous expression of the transcription factors SOX2, OCT4, ESSRB and NANOG. Taken together, these data support my hypothesis of plakoglobin being involved in the establishment of naïve pluripotency. However, one main drawback was the heterogeneity of plakoglobin expression across the PG OE cells. In the next paragraph, I will be addressing this issue and proposed solutions.

4.2.2 A certain plakoglobin threshold needs to be passed before re-establishment of ground state pluripotency

The initial PG OE cell line displayed a great degree of plakoglobin heterogeneity, making it hard to draw conclusive results on its influence on pluripotency. To elucidate the effect of different levels of plakoglobin, I used the parental PG OE cell line to sub-clone cells expressing high and low levels of plakoglobin, respectively. Therefore, single PG OE cells were FACS sorted into 96-well plates based on their mCherry reporter signal (**Figure 4.3 a**). After several days of growth, I chose three plakoglobin high (PG^{HIGH} [2, 4 and 5]) and three plakoglobin low (PG^{LOW} [1, 2 and 4]) clones for further expansion (**Figure 4.3 b&c**). All PG^{HIGH} clones displayed the same mCherry intensity, the PG^{LOW} clones were about one magnitude lower in mCherry intensity and also showed a greater variance between the three clones. PG^{LOW}#1 showed the strongest mCherry signal and PG^{LOW}#2 the weakest of the three PG^{LOW} clones. Nevertheless, in 2i+LIF medium all clones, regardless of their mCherry intensity, displayed homogeneous Rex1::GFPd2 expression across all cells (**Figure 4.3 b**). Therefore, high and low PG overexpression do not inhibit naïve state pluripotency. Furthermore, all clones were morphologically indistinguishable, exhibiting the tight, dome-shaped colonies associated with 2i+LIF conditions. When transferred into S+LIF medium, the PG^{LOW} clones reverted to a flat, spread out monolayer of cells, whereas the PG^{HIGH} clones retained the dome-shape morphology (**Figure 4.3 c**). When analysing the GFP signal, one may note that the PG^{LOW} clones re-acquired a bimodal REX1 distribution, while exclusively all PG^{HIGH} clones maintained their unimodal, positive GFP signal. Now, after having established several PG^{HIGH} and PG^{LOW} clones, I was wondering if I could detect differences between the clones on protein level. All further experiments were done with the PG^{LOW} clone #2 (PG^{LOW}#2) and PG^{HIGH} clone #5 (PG^{HIGH}#5), as representatives for the two different plakoglobin expression levels. I therefore immunostained RGd2, PG^{LOW}#2 and PG^{HIGH}#5 in S+LIF for plakoglobin. Consistent with our previous observations (see 4.2.1), RGd2 cells showed minimal levels of plakoglobin, all of which was associated to the membrane (**Figure 4.3 d**). The PG^{LOW}#2 cells

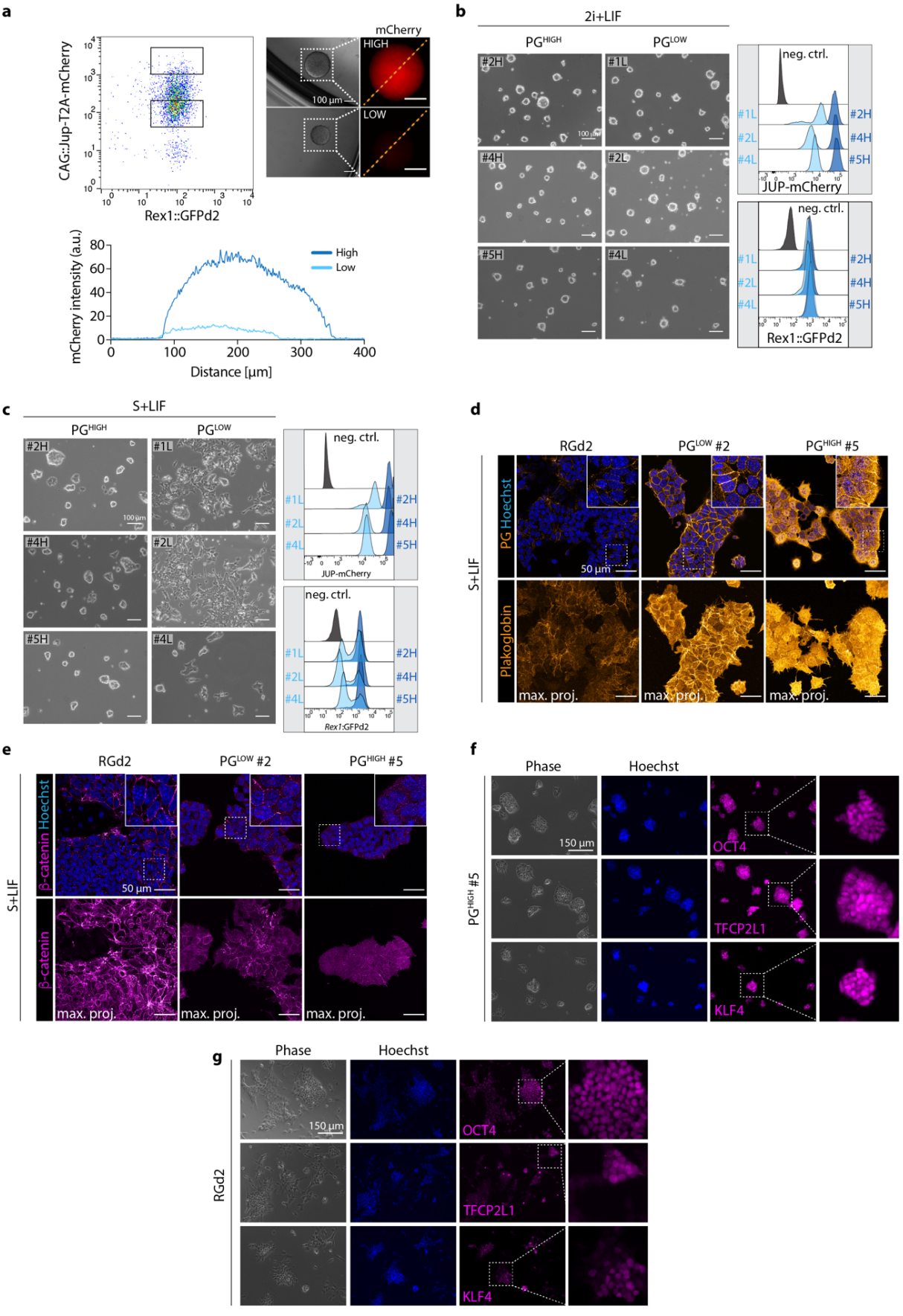

Figure caption on the next page.

Figure 4.3| Plakoglobin acts in a concentration-dependent manner to promote naïve pluripotency. **a**, FACS profile of the parental plakoglobin (PG) overexpression cells. Sorting gates for high and low expression are indicated with rectangles. **b**, Images of clonal PG cell lines in 2i+LIF and corresponding flow cytometry profiles for Rex1::GFP and JUP-mCherry. **c**, Images of clonal PG cell lines in S+LIF and corresponding flow cytometry profiles for Rex1::GFP and JUP-mCherry. **d**, Confocal z-slice and maximum projection images of RGd2, PG^{LOW}#2 and PG^{HIGH}#2 cells in S+LIF stained for plakoglobin. **e**, Confocal z-slice and maximum projection images of RGd2, PG^{LOW}#2 and PG^{HIGH}#2 cells in S+LIF stained for β-catenin. **f**, Epifluorescence images of PG^{HIGH}#5 cells stained for OCT4, TFCP2L1 and KLF4. **g**, Epifluorescence images of RGd2 cells stained for OCT4, TFCP2L1 and KLF4.

exhibited a substantial increase in plakoglobin levels over the RGd2 cells. However, plakoglobin was again mostly found attached to the membrane and only negligible cytoplasmic levels were observed. In contrast, PG^{HIGH}#5 cells still exhibited plakoglobin signal at the membrane, but additionally also showed abundant cytoplasmic and nuclear localisation (**Figure 4.3 d**). As I had already observed a negative correlation between plakoglobin and β-catenin in the parental PG OE cell line, I next stained the clonal lines for β-catenin (**Figure 4.3 e**). Indeed, I was able to confirm the previous findings, increased levels of plakoglobin caused degradation of β-catenin in S+LIF. Notably, the PG^{HIGH}#5 cells appeared to have lost completely all β-catenin, potentially having been made redundant by abundant amounts of plakoglobin. As I had already observed the homogeneous expression of NANOG and ESRRB in the parental PG OE cells, I also wanted to confirm naïve transcription factor expression under S+LIF conditions in the PG^{HIGH}#5 clone. Indeed, all PG^{HIGH}#5 cells were positive for KLF4, TFCP2L1 and OCT4 whereas RGd2 cells showed homogeneous, even though weaker, OCT4 expression but heterogeneous expression for KLF4 and TFCP2L1 (**Figure 4.3 f&g**).

4.2.3 Single-cell sequencing confirms re-establishment of naïve state-like pluripotency in plakoglobin overexpressing cells

To confirm the existence of bona fide naïve state pluripotency upon expression of plakoglobin and to fully capture the inherent transcriptional heterogeneity in serum-based media, I used the inDrop (Klein et al., 2015) technology to single-cell sequence ESCs from five different conditions: RGd2 cells cultured on tissue culture plastic (TCP) in 2i+LIF (**1**) and S+LIF (**2**), microgel encapsulated RGd2 cells in S+LIF (**3**), and PG^{HIGH}#5 (**4**) and PG^{LOW}#2 (**5**) cells on TCP in S+LIF. After quality-control I obtained in total 4154 transcriptomes across the five different conditions. I then used principal component analysis to investigate relationship between populations and heterogeneity across the different samples (**Figure 4.4 a**). The RGd2 cells in 2i+LIF and PG^{HIGH}5 in S+LIF displayed a smaller degree of gene expression heterogeneity compared to all other S+LIF cultured. Furthermore, PG^{HIGH}#5 cells clustered between the naïve RGd2 cells in 2i+LIF and the remaining S+LIF sample, further supporting the shift towards naïve pluripotency. I then used the nonlinear dimensionality reduction technique T-distributed stochastic neighbour embedding (t-SNE) (van der Maaten and Hinton, 2008), to visualise gene

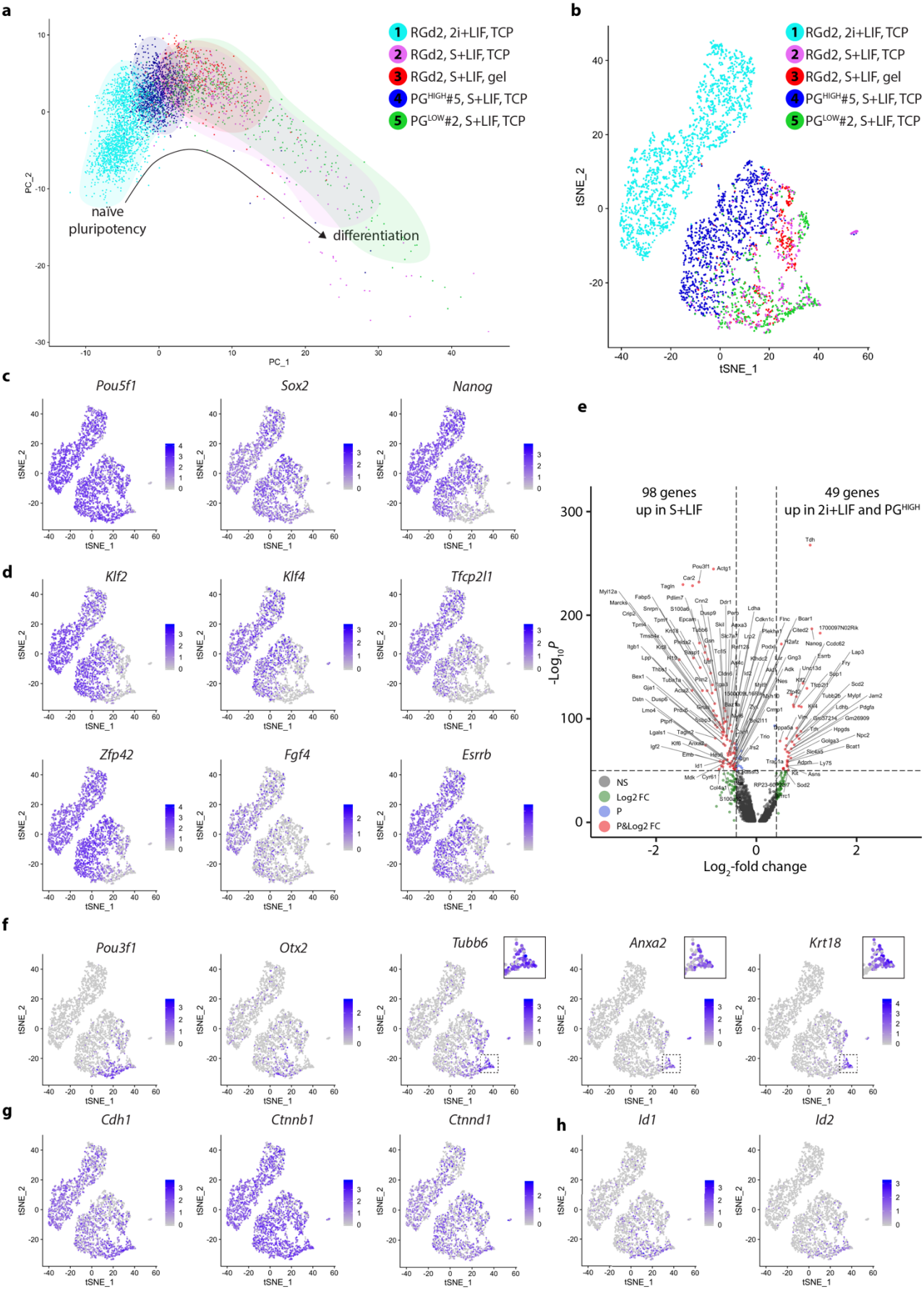

Figure caption on the next page.

Figure 4.4 | Single-cell sequencing confirms re-establishment of naïve pluripotency. **a**, Principal component analysis including all samples. **b**, t-SNE non-linear dimensionality reduction visualisation of all sequenced samples. **c**, t-SNE visualisation of the core pluripotency factors *Pou5f1*, *Sox2* and *Nanog*. **d**, t-SNE visualisation of naïve state associated transcription factors. **e**, Scatter plot of genes with $\log_2$-fold change > 0.4 and $-\log_{10}P > 50$, comparing 2i+LIF control and PG^{HIGH}#5 cells against all other serum-based culture conditions. **f**, t-SNE visualisation of genes associated with early post-implantation (*Pou3f1* and *Otx2*) or background differentiation in serum-based ESCs (*Tubb6*, *Anxa2* and *Krt18*). **g**, t-SNE visualisation of genes associated with formation of adherens junctions. **h**, t-SNE visualisation the BMP signalling targets *Id1* and *Id2*. | All single cell RNA-seq was performed in collaboration with Joachim de Jonghe, Department of Biochemistry, University of Cambridge.

expression amongst individual cells (**Figure 4.4 b**). As expected, the core pluripotency genes *Pouf51* and *Sox2* were homogeneously expressed across all cells in all samples. However, naïve transcription factors are known to be heterogeneously and lower expressed in serum-based medium (Chambers et al., 2007; Kolodziejczyk et al., 2015; Toyooka et al., 2008; Wray et al., 2010). Yet, I had previously observed the homogeneous expression of KLF4 and TFCP2L1 in PG^{HIGH}#5 cells despite being cultured in S+LIF. Hence, I asked how these, and other naïve transcription factors, would appear on transcriptional level. Remarkably, I found that the complete naïve gene regulatory network, including *Klf2*, *Klf4*, *Tfcp2l1*, *Zfp42*, *Esrrb* and *Fgf4*, was homogeneously upregulated in PG^{HIGH}#5 cells (**Figure 4.4 c-e**). When comparing the 2i+LIF control and PG^{HIGH}#5 cells against all other serum-based culture conditions, I found 49 upregulated genes ($\log_2$-fold change > 0.4 and $-\log_{10}P > 50$) including the above-mentioned naïve transcription factors. In contrast, I found 98 upregulated genes in serum-based conditions, mostly connected to differentiation and the cytoskeleton (**Figure 4.4 e**). When applying KEGG pathway analysis on these genes, pathways regarding focal adhesion and tight junction as well as the regulation of actin cytoskeleton were detected. Interestingly, early post-implantation associated genes such as *Pou3f1* and *Otx2* as well as genes marking background differentiation of cells in S+LIF (Kolodziejczyk et al., 2015), such as *Tubb6*, *Anxa2* and *Krt19,* were completely absent from 2i+LIF RGd2 and PG^{HIGH}#5 cells in S+LIF (**Figure 4.4 f**). Furthermore, I did not see any changes in transcription concerning the adherens junction proteins *Cdh1*, and *Ctnnb1* (β-catenin) and *Ctnnd1* (**Figure 4.4 g**). Interestingly, despite cultured in serum containing BMPs, downstream signalling targets such as *Id1* and *Id2* normally involved in maintaining pluripotency in S+LIF (Ying et al., 2003a) were not expressed in PG^{HIGH}#5 cells, indicating changes in the maintenance of pluripotency in these cells (**Figure 4.4 h**). To decipher in detail how PG^{HIGH}#5 cells differed from the other populations, I then compared them against all other S+LIF samples and subsequently against the 2i+LIF control cells (**Figure 4.5**). In comparison to the other serum-based samples, PG^{HIGH}#5 cells are distinct in their upregulation of the naïve transcription factors and the threonine dehydrogenase (*Tdh*), a metabolic enzyme converting threonine into acetyl co-A and glycine as part of a unique threonine-depended catabolism during pluripotency and known to be downregulated upon differentiation (Kalkan et al., 2017; Wang et al., 2009) (**Figure 4.5 a,b &d**). When performing gene ontology (GO) analysis on this subset of genes, GO

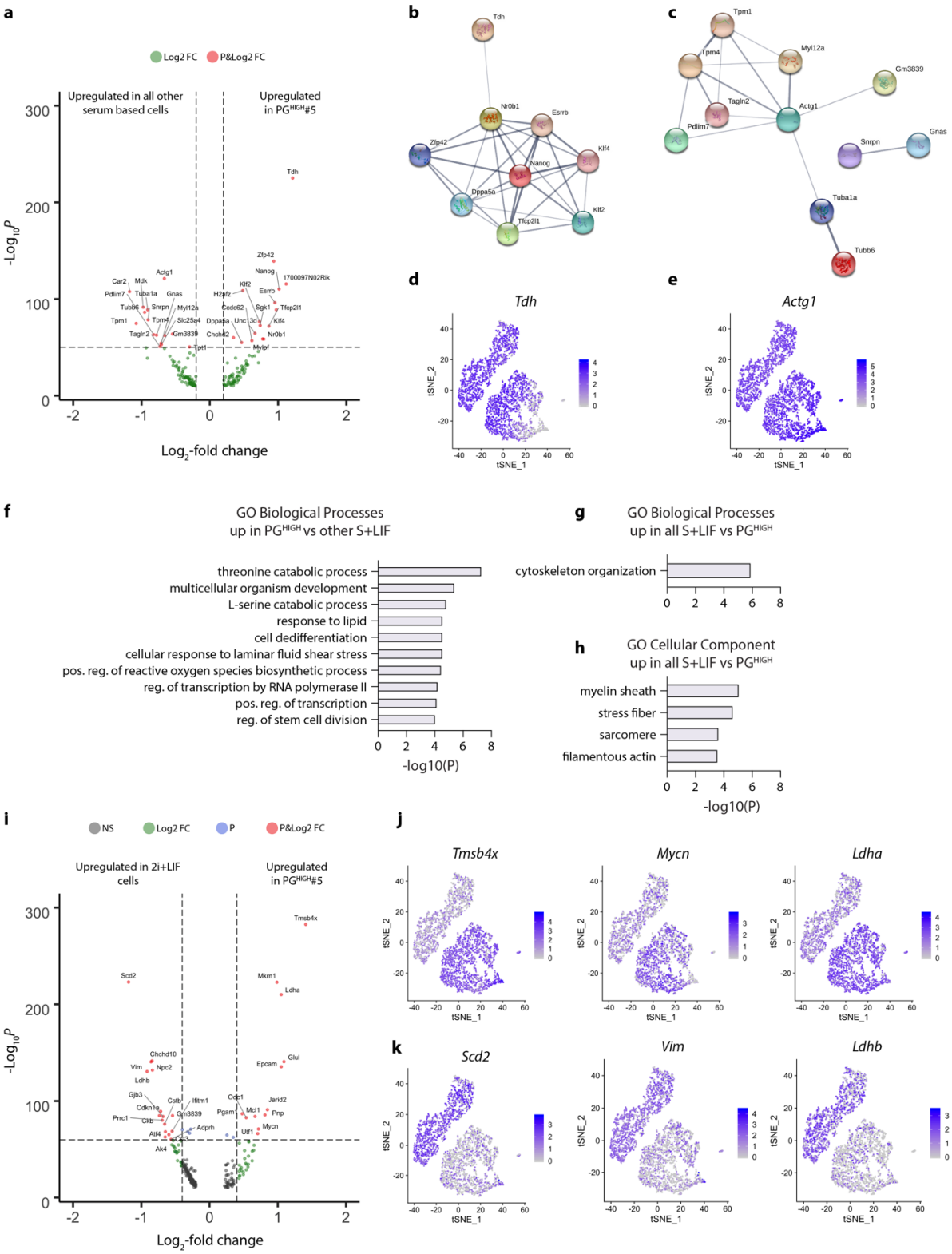

Figure 4.5 | Strong plakoglobin expression is concomitant with a distinct transcriptomic signature. a, Scatter plot of genes with log_2-fold change > 0.4 and $-log_{10}P$ > 50, comparing PG^{HIGH}#5 cells against all other serum-based culture conditions. **b**, STRING protein network analysis including genes upregulated in PG^{HIGH}#5 cells. **c**, STRING protein network analysis including genes upregulated in all serum-based samples (except PG^{HIGH}#5 cells). **d**, t-SNE plot for *Tdh*. **e**, t-SNE plot for *Actg1*. **f-h**, Gene Ontology (GO) analysis concerning biological processes and cellular components. **i**, Scatter plot of genes with log_2-fold change > 0.4 and $-log_{10}P$ > 60, comparing 2i+LIF cells against PG^{HIGH}#5 cells in S+LIF. j, t-SNE plots for *Tms4bx*, *Mycn* and *Ldha*. k, t-SNE plots for *Scd2*, *Vim* and *Ldhb*.

terms for biological processes such as "threonine catabolic process", "multicellular organism development", "cell dedifferentiation", "positive regulation of transcription" and "regulation of stem cell division" were detected (**Figure 4.5 f-h**). In contrast, all other S+LIF samples were defined by a distinct upregulation of cytoskeletal genes such as *Actg1*, *Myl12a*, *Tuba1a* and *Tubb6* which also reflected in the associated GO biological processes including "cytoskeleton organization" and GO cellular components "stress fibres" and "filamentous actin" (**Figure 4.5 a, c, e, g&h**). When comparing PG^{HIGH}#5 cells with the 2i+LIF control, no such clustered gene regulatory networks were immediately obvious and differences were defined by a few and distinct genes (**Figure 4.5 i-k**). The 2i+LIF control cells were defined by expression of *Vim* (Vimentin), a component of intermediate filaments, and *Scd2*, a stearoyl-CoA desaturase connected to lipid metabolism and has been implied to play a role in regulating pluripotency (Hailesellasse Sene et al., 2007; Kaestner et al., 1989). On the other side, PG^{HIGH}#5 cells were defined by the upregulation of *Tmsb4x*, encoding β_4-thymosin, a protein with the ability of sequestering actin monomers and that has been shown to improve reprogramming cardiac fibroblasts to iPSCs (Qian et al., 2012; Safer et al., 1990). Furthermore, I detected the expression of *Mycn*, consistent with higher expression of Myc proteins in serum-based media compared to 2i+LIF (Scognamiglio et al., 2016). Additionally, PG^{HIGH}#5 cells were defined by *Mkrn1* expression, a gene encoding Makorin-1 which is part of the pluripotency gene regulatory network in S+LIF cultured ESCs (Cassar et al., 2015; Walker et al., 2007). Pluripotency is further denoted by a distinct metabolism – where somatic cells mainly use oxidative phosphorylation for energy production, pluripotent cells rely heavily on a glycolytic metabolism (Zhang et al., 2012). Lactate dehydrogenase (LDH),

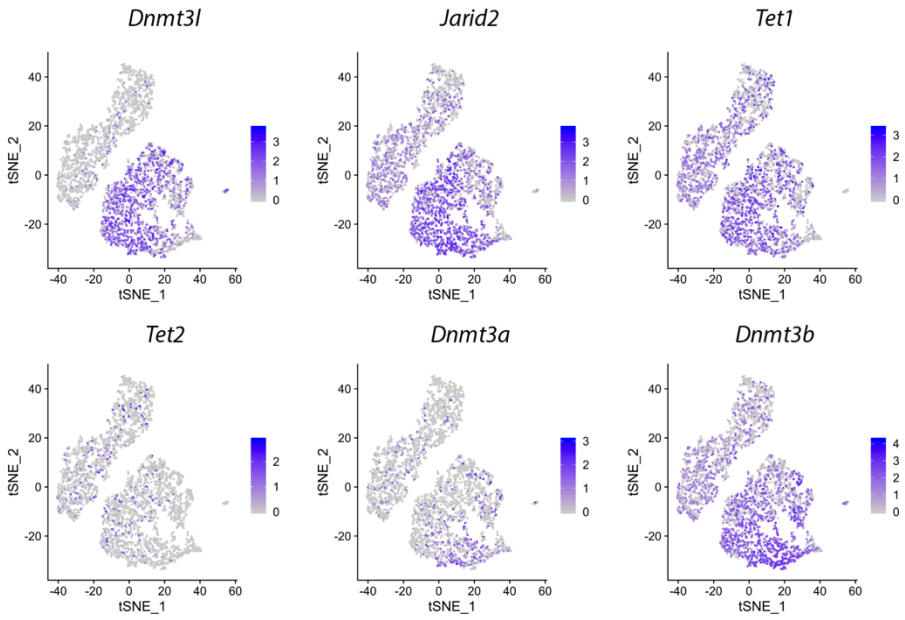

Figure 4.6 | Plakoglobin overexpressing cells display changes in the transcription of epigenetic regulators. t-SNE plots for the epigenetic regulator genes *Dnmt3l*, *Jarid2*, *Tet1*, *Tet2*, *Dnmt3a* and *Dnmt3b*.

a key component of glycolysis, was expressed in both cell populations, curiously, *Ldha* marking PG^{HIGH}#5 and *Ldhb* marking the 2i+LIF control cells. As the change in metabolism between S+LIF and 2i+LIF cultured ESCs contributes to the epigenetic state of the respective cells (Carey et al., 2015) and PG^{HIGH}#5 cells displayed upregulation of *Dnmt3l*, a catalytically inactive DNA methyltransferase that interacts with *Jarid2* (Neri et al., 2013), also upregulated and part of the Polycomb-Repressive Complex 2 (PRC2) (Li et al., 2010), I was prompted to also investigate *Tet* and *Dnmt* expression, regulating DNA methylation and demethylation, respectively (Lyko, 2018; Rasmussen and Helin, 2016). I found *Tet1* and *Tet2* to be upregulated in the 2i+LIF control and PG^{HIGH}#5 cells, whereas *Dnmt3a* and *Dnmt3b* were downregulated, suggesting changes in overall

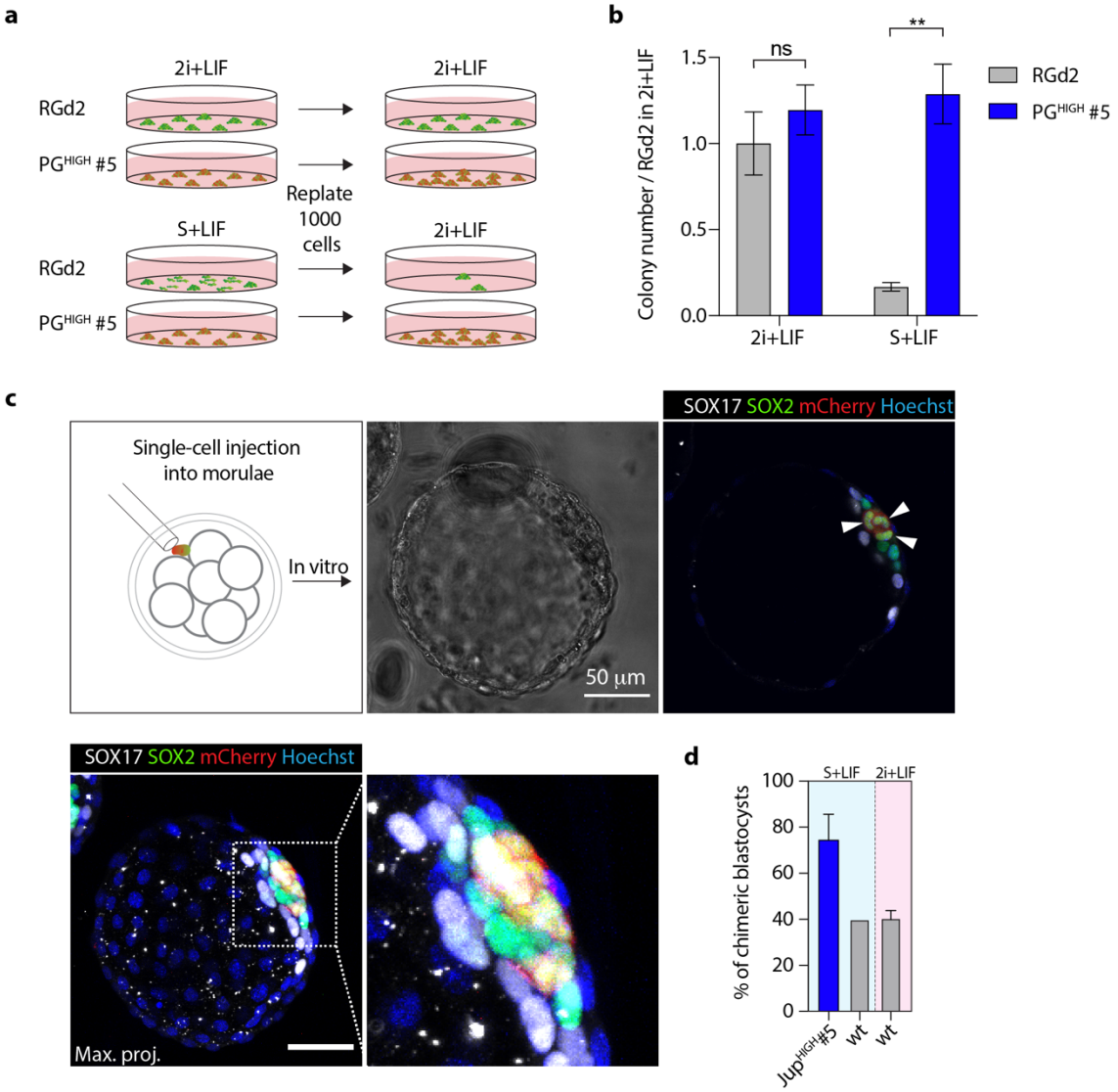

Figure 4.7 | Single plakoglobin overexpressing cells contribute twice as efficiently to the epiblast when injected into 8-cell embryos in comparison to wild type cells. a, Schematic illustration of the experimental set-up for a clonogenicity assay**. b,** Quantification of the clonogenicity assay 3 days after re-plating in 2i+LIF (N=3). **c**, Schematic illustration of single-cell injections into 8-cell stage embryos and representative confocal image of a blastocysts that had previously been injected with a single Jup^{HIGH}#5 cell. The cell had successfully integrated and proliferated within the developing epiblast of the embryo (mCherry-positive cells are indicated with a white arrow head). None of the contributing cells showed extraembryonic contribution potential (see max. proj. image). **d**, Quantification of chimera efficiency of injected single-cells from either wt (2i+LIF, n=15), wt (S+LIF, n=28) or Jup^{HIGH}#5 (S+LIF, n=26) cells. All single cell injections were performed by Dr Ayaka Yanagida, Cambridge Stem Cell Institute.

DNA methylation (**Figure 4.6**). However, additional experiments are required to fully decipher the epigenetic profile of the plakoglobin overexpressing cells. Now, after having elucidated the plakoglobin induced transcriptional re-establishment of naïve-like pluripotency in S+LIF cultured cells, I wanted to confirm this finding also on a functional level. Therefore, I determined the clonogenicity potential and chimera contribution efficiency of the PG^{HIGH}#5 cells in comparison to the RGd2 control cells (**Figure 4.7 a-d**). No significant differences between RGd2 and PG^{HIGH}#5 cells were detectable in 2i+LIF, however when previously cultured in S+LIF, RGd2 cells were greatly reduced in their clonogenicity potential whereas PG^{HIGH}#5 cells, in alignment with the upregulation of the naïve gene regulatory network, showed no difference to the 2i+LIF control cells (**Figure 4.7 b**). Finally, single S+LIF and 2i+LIF cultured RGd2 and S+LIF cultured PG^{HIGH}#5 cells were injected into 8-cell embryos to investigate their potential to integrate into the developing embryo (**Figure 4.7 c**). Chimera contribution efficiency was scored after in vitro culture of the embryos to the blastocyst state (~E4.5). Remarkably, PG^{HIGH}#5 (S+LIF) cells contributed about twice as efficiently (~70%) as RGd2 (S+LIF and 2i+LIF) cells to the contributing embryo (**Figure 4.7 d**). Collectively, the extensive single-cell transcriptional analysis in combination with functional studies have confirmed the original hypothesis of the re-establishment of naïve-like pluripotency in ESCs expressing high levels of plakoglobin, despite being cultured under serum-based conditions.

4.2.4 Plakoglobin expression impedes the exit from pluripotency

After having extensively elucidated plakoglobin's role in promoting naïve state pluripotency in mouse embryonic stem cells, I sought to investigate how constitutive plakoglobin expression effects their exit from pluripotency. Therefore, I initially differentiated the PG^{HIGH}#5 and PG^{LOW}#2 clonal cell lines in the presence of serum, after removal of LIF, and followed their REX1::GFP signal over time (**Figure 4.8 a**). In S+LIF, just below 80% of the PG^{LOW}#2 cells were GFP-positive. This number steadily declined upon removal of LIF to less than 5% GFP-positive cells after 96 hours of differentiation. The PG^{HIGH}#5 cells, previously shown to be in a naïve-like state, even in S+LIF conditions, presented a stark contrast to the PG^{LOW}#2 cells. All PG^{HIGH}#5 cells were GFP-positive in S+LIF. Remarkably, these cells were unable to properly exit pluripotency according to their GFP signal. After 48 hours of LIF removal, the number of GFP-positive cells had initially dropped to ~80%, yet, no further decline was observed over the next several days. Despite maintaining high levels of REX1, PG^{HIGH}#5 cells could not be kept in culture for extended amount of time without the support LIF, due to extensive cell death upon passaging (data not shown). Interestingly, even after LIF removal PG^{HIGH}#5 cells maintained the dome-shaped morphology caused by plakoglobin overexpression, whereas RGd2 cells displayed the flat monolayer structure, irrespectively of LIF (**Figure 4.8 b**). The unexpectedly high levels

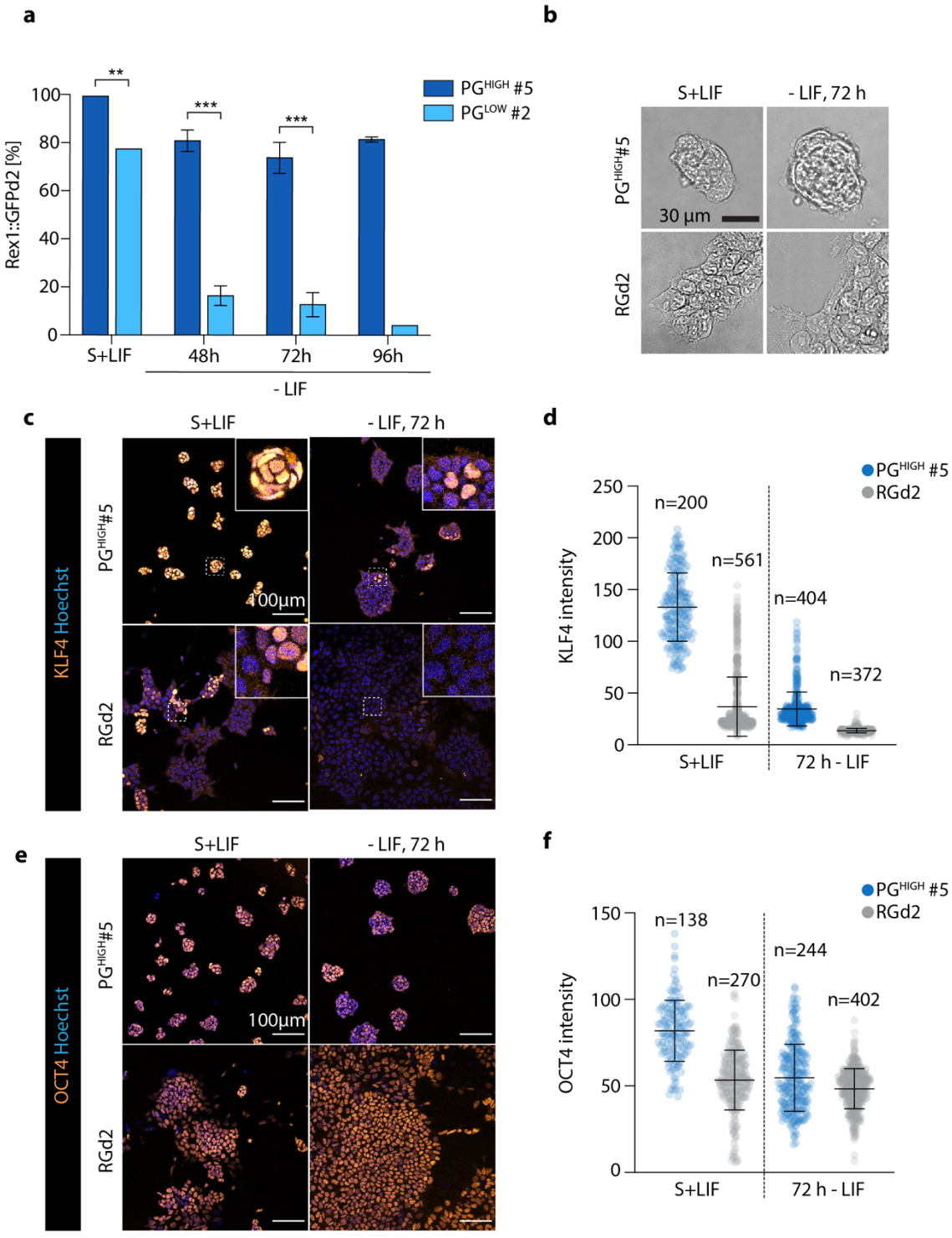

Figure 4.8 | Plakoglobin impedes the exit from pluripotency in the presence of serum. a, Flow-cytometric analysis of Rex1::GFPd2 in PG^{HIGH}#5 and PG^{LOW}#2 cells in S+LIF and after LIF removal (N=3). **b**, Brightfield images of PG^{HIGH}#5 and RGd2 cells in S+LIF and 72 hours after LIF removal. **c**, Confocal z-slice images of PG^{HIGH}#5 and RGd2 cells in S+LIF and 72 hours after LIF removal stained for KLF4. **d**, Nuclear KLF4 intensities of PG^{HIGH}#5 and RGd2 cells in S+LIF and 72 hours after LIF removal. **e**, Confocal z-slice images of PG^{HIGH}#5 and RGd2 cells in S+LIF and 72 hours after LIF removal stained for OCT4. **f**, Nuclear OCT4 intensities of PG^{HIGH}#5 and RGd2 cells in S+LIF and 72 hours after LIF removal.

of GFP-positive PG^{HIGH}#5 cells after LIF removal, prompted me to further investigate additional transcription factors of the pluripotency network. KLF4, downstream target of the LIF signalling pathway, naïve state transcription factor and enhanced by plakoglobin overexpression, was homogeneously expressed in all PG^{HIGH}#5 cells in S+LIF, whereas KLF4 expression was heterogeneous in the parental RGd2 cells (**Figure 4.8 c&d**). After 72 hours of LIF removal, none of the RGd2 cells were positive for KLF4, yet strikingly, individual PG^{HIGH}#5 cells maintained KLF4 expression despite the absence of LIF (**Figure 4.8 c**). Remarkably, PG^{HIGH}#5 cells displayed a similar KLF4 intensity distribution, without the support of LIF, as RGd2 cells exhibited in S+LIF (**Figure 4.8 d**). This observation supports the hypothesis of plakoglobin's role in the maintenance of naïve state pluripotency, especially because it has been shown that naïve-state pluripotency is normally disassembled within 48 hours, unless extrinsically stabilised (Kalkan et al., 2017). Since OCT4 belongs to the group of general pluripotency transcription factors, protein levels should not change dramatically throughout the initial stages of differentiation (Boroviak et al., 2014; Kalkan et al., 2017). Indeed, OCT4 was expressed in all cells regardless of their background or culture condition (**Figure 4.8 e**). Simultaneously, OCT4 displayed similar intensities in RGd2 and PG^{HIGH}#5 cells, only in S+LIF, PG^{HIGH}#5 showed slightly elevated OCT4 intensities, as would be expected with the naïve state-like transcriptional

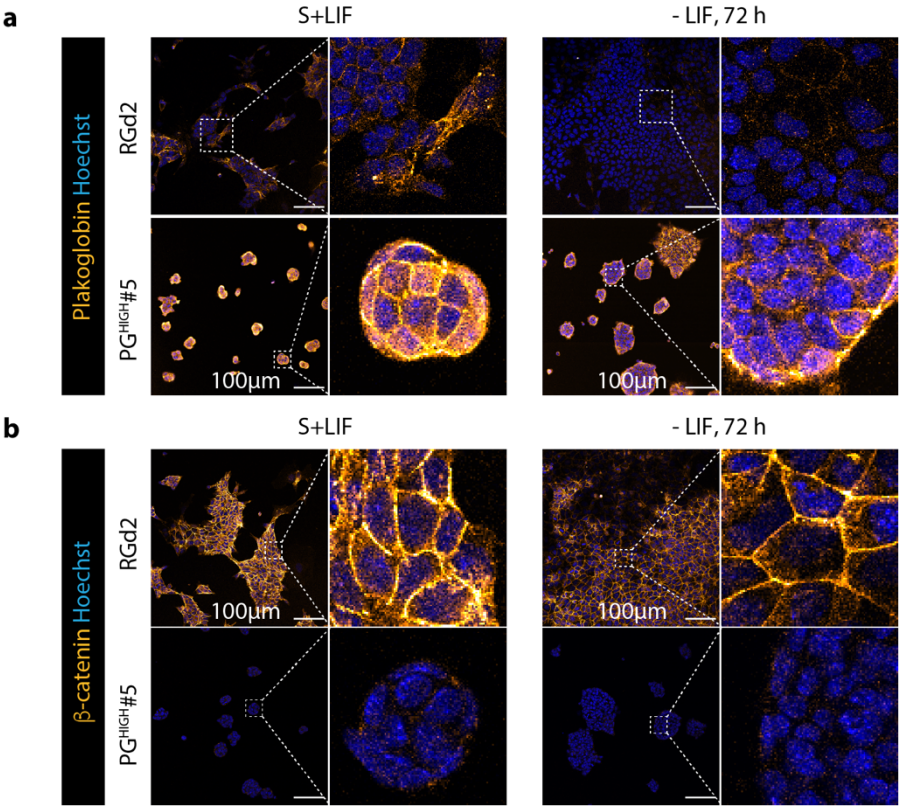

Figure 4.9 | Plakoglobin and β-catenin display differential protein levels upon differentiation. Confocal images of plakoglobin (**a**) and β-catenin (**b**) expression in PG^{HIGH}#5 and RGd2 cells in S+LIF and 72 hours after LIF removal.

profile of these cells (**Figure 4.8 f**). As plakoglobin overexpression severely impeded the exit from pluripotency when kept in serum, I next investigated how the removal of LIF would affect protein levels of plakoglobin and β-catenin in RGd2 and PG^{HIGH}#5 cells. Interestingly, immunostainings for both proteins elucidated a differential expression of plakoglobin and β-catenin upon the removal of LIF in the RGd2 cells. The low levels of plakoglobin under S+LIF conditions disappeared after dismantling the pluripotency network via removal of LIF, (**Figure 4.9 a**), whereas β-catenin expression remained stable even after the exit from pluripotency (**Figure 4.9 b**). Contrary, in PG^{HIGH}#5 cells, plakoglobin levels remained high, unaffected by the removal of LIF causing simultaneously the degradation of β-catenin. As I have observed an impeded exit from pluripotency when overexpressing plakoglobin, I was intrigued if these cells also have lost their ability to enter lineage specific differentiation. Therefore, RGd2 and PG^{HIGH}#5 cells were differentiated for 72 hours in the presence of serum and immunostained for the neuroectodermal precursor protein SOX1 and the mesendodermal protein T (Brachyury). PG^{HIGH}#5 cells failed to upregulate SOX1 and RGd2 cells exhibited only sparsely (<1%), very low levels of SOX1 (**Figure 4.10 a**). However, this was to be expected as BMP signals,

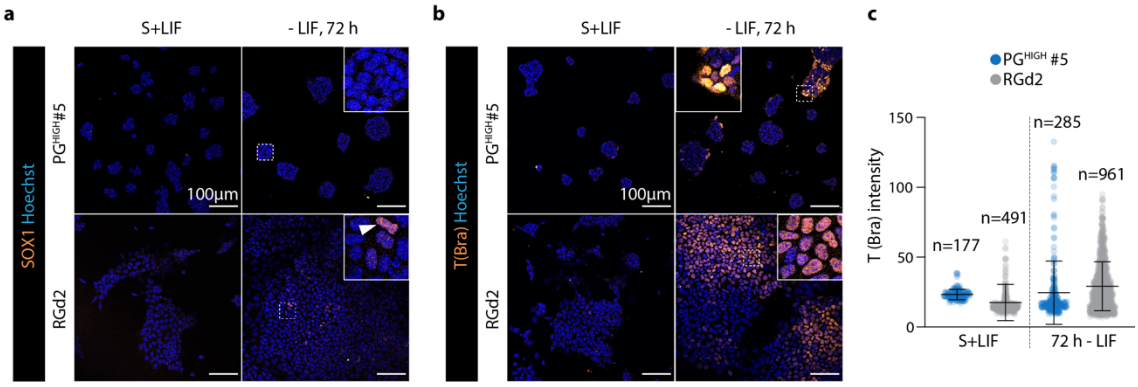

Figure 4.10 | Plakoglobin overexpressing cells display severe differentiation defects in the presence of serum. RGd2 and PG^{HIGH}#5 cells in S+LIF and 72 hours after LIF removal were immunostained for the neuroectodermal precursor protein SOX1 (**a**) and the mesendodermal precursor protein T (Brachyury) (**b**). **c**, Nuclear intensity distribution of T (Brachyury) as measured via confocal microscopy.

originating from the serum, are known to suppress neural differentiation. (Di-Gregorio et al., 2007; Finley et al., 1999). In contrast, both cell lines were able to enter mesendodermal lineage specification as determined by the upregulation of T (Brachyury). About 39% (n=961, T-positive when intensity >30 a.u.) of RGd2 cells showed T expression after 72 hours without LIF and T-intensity analysis showed a population wide trend in T upregulation (**Figure 4.10 b&c**). PG^{HIGH}#5 cells also upregulated T, but the efficiency had dropped to ~16% (n=285, T-positive when intensity >30 a.u.). Yet, one may note that, even though the overall percentage of T-positive PG^{HIGH}#5 was lower than in RGd2 cells, T-intensities of individual cells were often higher (**Figure 4.10 c**). Overall, plakoglobin expression suppressed the exit from pluripotency in the

presence of serum whilst simultaneously inhibiting the upregulation of lineage specific proteins such as SOX1 and T (Brachyury).

4.2.5 Plakoglobin overexpression allows maintenance of naïve pluripotency in the presence of just LIF or PD but not CH

As it has become evident, that plakoglobin expression impedes the disassembly of the pluripotency network when maintained in serum, I next investigated plakoglobins ability to sustain pluripotency in serum-free conditions. Therefore, I cultured RGd2, PG^{LOW}#2 and PG^{HIGH}#5 cells over several passages in N2B27 medium supplemented with the individual components of 2i+LIF — LIF for activating STAT3 mediated transcription, the ERK inhibitor PD to disable FGF signalling and the GSK3 inhibitor CH to activate β-catenin mediated transcription. The state of pluripotency was then assessed by flow cytometric analysis of the REX1::GFP reporter. Remarkably, when transferred into LIF alone, 100% of PG^{HIGH}#5 cells stayed GFP-positive, indicating that overexpression of plakoglobin with the only support of LIF is enough to sustain the naïve-pluripotency network (**Figure 4.11 a,d&e**). In contrast, RGd2 and PG^{LOW}#2 cells behaved similarly in a manner of GFP decrease to ~50% of the cells after 6 days of LIF alone treatment (**Figure 4.11 a,d&e**). However, PG^{LOW}#2 cells were able to be maintained in culture, albeit with the GFP signal fluctuating between 50% and 60%, for extended periods of time (over 20 days). This observation was not the case for the RGd2 cells, although GFP signals were similar to the PG^{LOW}#2 clone, RGd2 cells started to detach after 6 days. When culturing in the presence of the small molecule ERK inhibitor PD, PG^{HIGH}#5 cells initially dropped in GFP signal to ~70% after 3 days, however, quickly recovered to ~90% at day 6 (**Figure 4.11 b,d&e**).. Contrary, PG^{LOW}#2 and RGd2 cells quickly exited naïve pluripotency and were completely GFP-negative after 3 days (**Figure 4.11 b,d&e**). These cells could not be kept in culture due to extensive cell death after 4 days in PD alone (**Figure 4.11 e**). Intriguingly, when cultured in the presence of the small molecule GSK3 inhibitor CH, the previous observation of high plakoglobin levels coinciding with stable pluripotency were inverted. When supplemented with CH, PG^{HIGH}#5 cells dropped in GFP signal to ~50% and could not be kept in culture for more than 6 days (**Figure 4.11 c-e**). RGd2 cells, despite remaining to ~60% GFP-positive, were lost due to cell death on day 6. Remarkably, PG^{LOW}#2 cells survived when supplemented with CH with the GFP signal fluctuating between 80% and 90% (**Figure 4.11 c-e**). This observation was surprising as any one of the components of 2i+LIF is not alone to maintain naïve pluripotency on its own (Wray et al., 2010). Therefore, plakoglobin might promote pluripotency differently than β-catenin. Hypothetically, in PG^{LOW}#2 cells enough β-catenin remains to act in concert with plakoglobin, whereas the high levels of plakoglobin in the PG^{HIGH}#5 clone reduced β-catenin to an extend

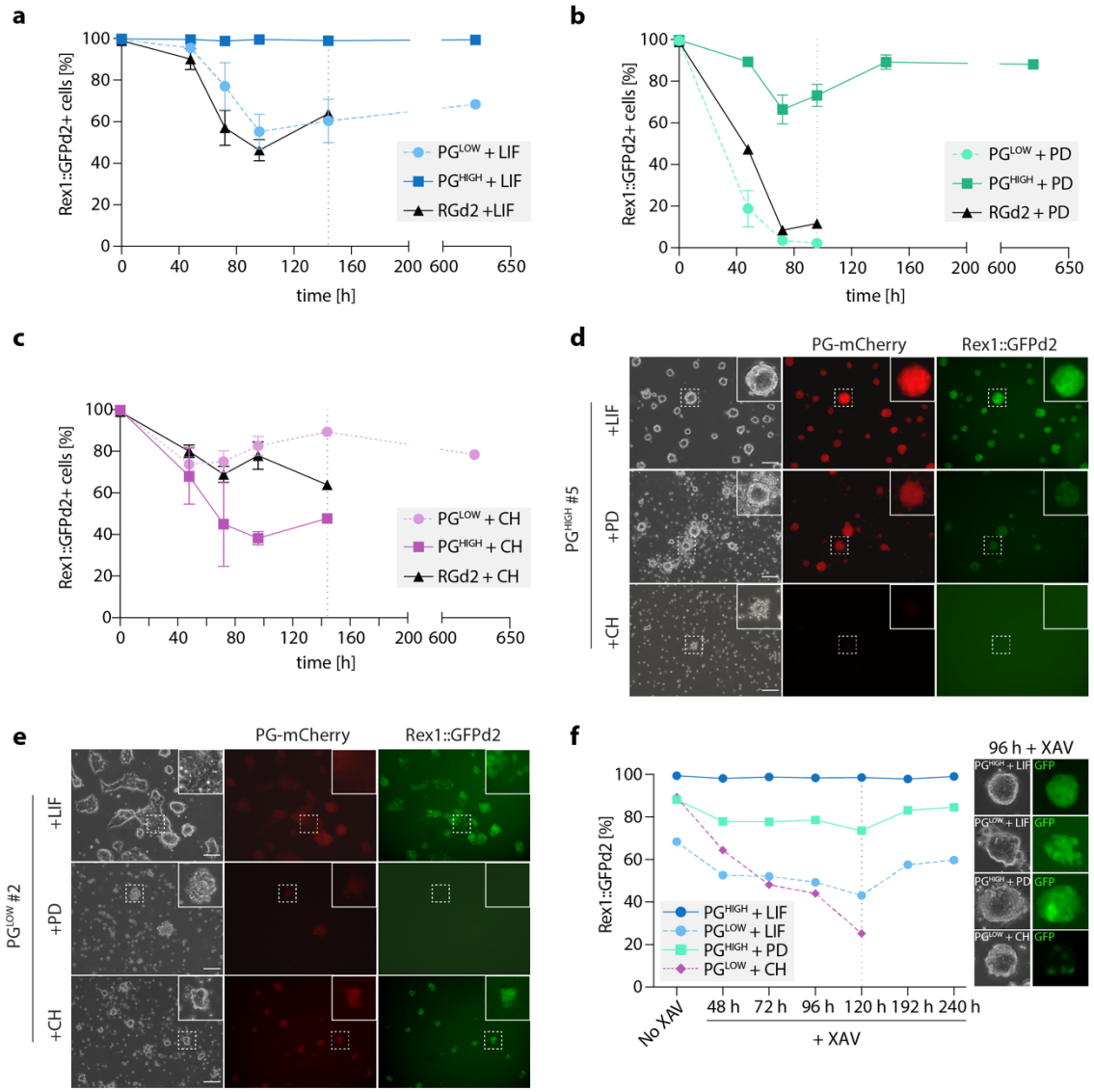

Figure 4.11 | Plakoglobin overexpressing cells maintain naïve pluripotency when supplemented with LIF or PD but not CH. **a-c**, Percentage of Rex1::GFPd2-positive RGd2, PG^{LOW}#2 and PG^{HIGH}#5 cells that were cultured for in N2B27 supplemented with just LIF (**a**), just PD (**b**) or just CH (**c**) (N=3). **d&e**, Phase contrast and epifluorescent images of PG^{HIGH}#5 and PG^{LOW}#2 cells after 96 hours in the aforementioned conditions. **f**, Percentage of Rex1::GFPd2-positive cells upon WNT signalling inhibition via XAV treatment (N=1).

where pluripotency cannot be maintained even with the addition of CH. To elucidate if plakoglobin acts independently of β-catenin, I supplemented all the above described surviving conditions with the tankyrase inhibitor XAV to (Huang et al., 2009) to abrogate β-catenin mediated transcription (**Figure 4.11 f**). Unexpectedly, neither PG^{HIGH}#5 cells supplemented with LIF or PD, nor PG^{LOW}#2 cells supplemented with LIF were affected by XAV treatment as their corresponding GFP signals remained largely constant (**Figure 4.11 f**). Contrary, PG^{LOW}#2 cells supplemented with CH were not able to maintain the naïve pluripotency network upon addition of XAV. After 5 days, the GFP signal had decreased from ~90% to ~30% and cells could not be kept in culture due to detachment from the surface. Taken together, these data suggest that plakoglobin acts independently of β-catenin in promoting naïve state pluripotency. To eliminate

any ambiguity over potential β-catenin signalling I used the CRISPR/Cas9 system to knockout β-catenin in the RGd2 and PG^{HIGH}#5 cells (**Figure 4.12 a**). The commercially available knockout plasmids contained three CRISPR gRNAs against *Ctnnb1* and additionally a GFP-transfection control. Since both, RGd2 and PG^{HIGH}#5 cells, already expressed GFP, I exclusively sorted cells they displayed GFP levels above the baseline expression (**Figure 4.12 b**). Subsequent immunostaining against β-catenin revealed that the CRISPR-mediated knockout resulted in a mixed population of hetero- and homozygous knockouts (**Figure 4.12 c**). Hence, in ongoing experiments I apply single-cell sorting to generate clonal homozygous knockouts.

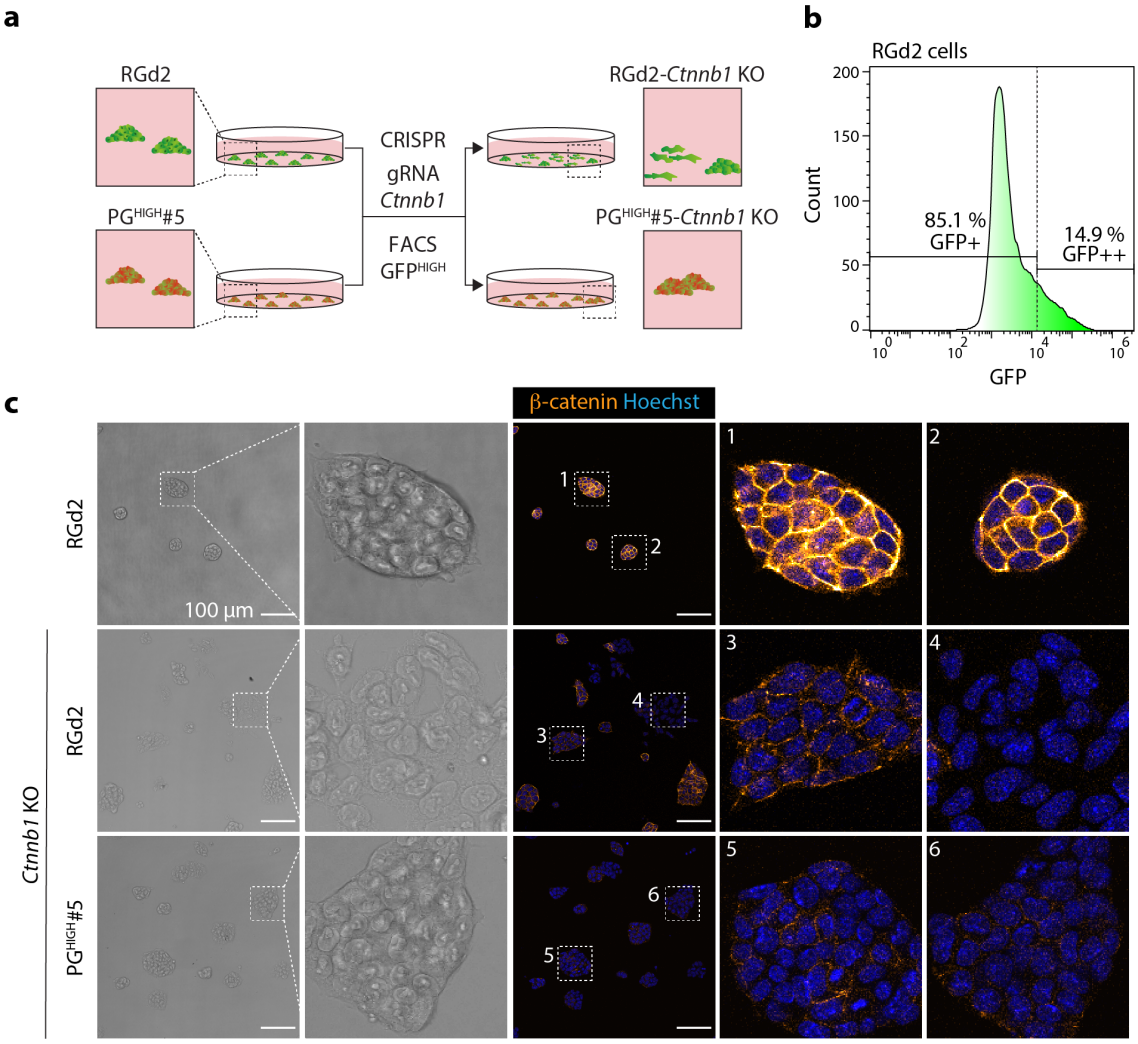

Figure 4.12 | CRISPR mediated knockout of Ctnnb1 (β-catenin) in RGd2 and PG^{HIGH}#5 cells. a, Schematic illustration of the CRISPR mediated knockout of *Ctnnb1* in RGd2 and PG^{HIGH}#5 cells. **b**, Histogram of FACS-sorted RGd2 cells based on high GFP expression. **c**, Representative confocal z-slice images of wt RGd2 and Ctnnb1-KO RGd2 and PG^{HIGH}#5 cells stained for β-catenin.

4.2.6 Plakoglobin does not inhibit the exit from naïve pluripotency in serum-free conditions but blocks neuroectodermal differentiation.

After having observed plakoglobin mediated maintenance of naïve pluripotency in serum-free conditions, I next asked if these cells could readily exit pluripotency and enter lineage specific differentiation. Upon release from 2i+LIF and culture in differentiation permissive N2B27 medium, ESCs enter neuroectodermal differentiation as measured by the upregulation of neuroectoderm associated gens such as *Sox1*, *Nestin* and *Tuj1* (Ying et al., 2003b). As no additional exogeneous signals are required for the neuroectodermal differentiation of ESCs, it has often been regarded as the "default" path of differentiation (Munoz-Sanjuan and Brivanlou, 2002). In contrast, to induce mesendodermal differentiation, WNT/β-catenin and activin signalling is required (Turner et al., 2014). To investigate lineage specific differentiation potential, neuroectodermal and mesendodermal, I exposed RGd2, PG^{LOW}#2 and PG^{HIGH}#5 cells to both respective culture conditions (**Figure 4.13 a&d**). Consistent, with the differentiation in serum-supplemented medium, PG^{HIGH}#5 cells also displayed delayed differentiation kinetics when cultured in serum-free N2B27 as measured by the REX1::GFP signal, whereas PG^{LOW}#2 cells behaved similar to the RGd2 wild type cells (**Figure 4.13 b**). To confirm neuroectodermal lineage specification, cells were stained for SOX1, a protein known to be associated with nascent neuroectoderm formation in the developing embryo (Pevny et al., 1998; Wood and Episkopou, 1999), after 72 hours in N2B27 (**Figure 4.13 c**). RGd2 and PG^{LOW}#2 cells efficiently upregulated SOX1, whereas its expression was complete disrupted in the PG^{HIGH}#5 clone, suggesting that strong plakoglobin expression inhibits neuroectodermal differentiation. In contrast, mesendodermal differentiation initially appeared to be unaffected by plakoglobin overexpression, as determined by the consistent expression of the primitive streak associated T-box transcription factor brachyury across all samples (Wilkinson et al., 1990) (**Figure 4.13 e**). However, on closer inspection morphological differences became visible between the different cell lines. It has been reported that mesendodermal differentiation of ESCs in activin and CH is accompanied by events resembling the epithelial to mesenchymal transition (EMT) in the primitive streak of the gastrulating embryo — e.g. upregulation of brachyury, downregulation of E-cadherin and an increase in cell motility (Turner et al., 2014). After the 24 hours pulse of activin and CH, RGd2 cells had started to detach from their originating colonies, however, freely moving cells were rare (**Figure 4.13 e**). This observation became more frequent with an increase in plakoglobin overexpression levels, suggesting a potential increase in EMT dynamics (**Figure 4.13 e**). Since the EMT precedes the differentiation between mesoderm and definite endoderm (DE), I was intrigued if the proposed acceleration in EMT kinetics biased the lineage between meso- and endoderm. Therefore, I extended the activin and CH pulse to 48 hours (48 h N2B27 + 48 h activin & CH) and immunostained for FOXA2, a member of the forkhead transcription factor family that

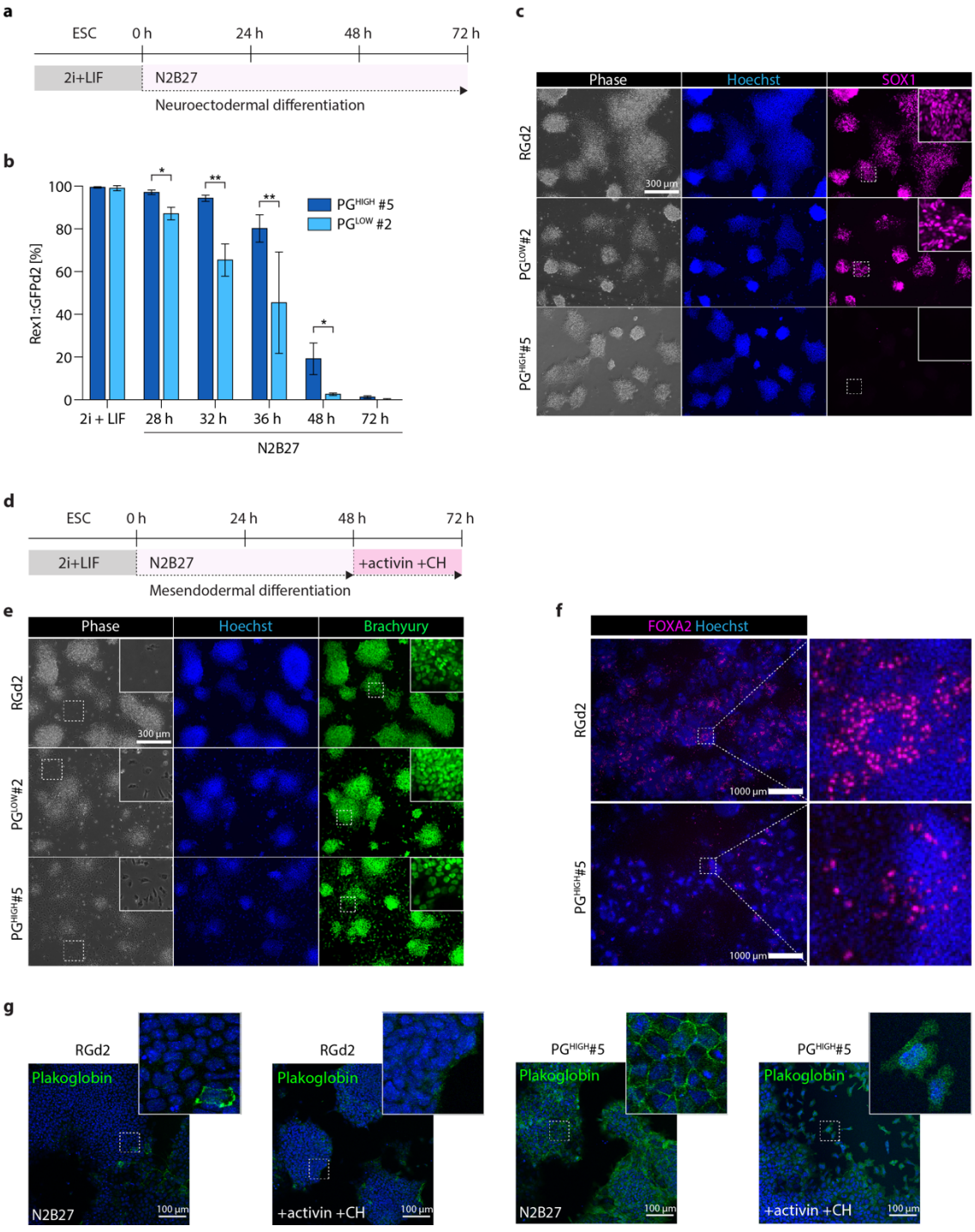

Figure 4.13 | Plakoglobin overexpression suppresses neuroectodermal but not mesendodermal differentiation of ESC. a, Neuroectodermal differentiation strategy. **b**, Flow cytometric analysis of Rex1::GFPd2 signal in PG^{LOW}# and PG^{HIGH}#5 cells upon transfer from 2i+LIF to N2B27 (N=3). **c**, Representative epifluorescence images of RGd2, PG^{LOW}#2 and PG^{HIGH}#5 cells after 72 hours of neuroectodermal differentiation. Cells were then stained for the neuroectoderm marker SOX1 and nuclei were stained with Hoechst. **d**, Mesendodermal differentiation strategy. **e**, Representative epifluorescence images of RGd2, PG^{LOW}#2 and PG^{HIGH}#5 cells after 72 hours of mesendodermal differentiation. Cells were then stained for the primitive streak marker T (Bra) and nuclei were stained with Hoechst. **f**, Epifluorescence images of RGd2 and PG^{HIGH}#5 cells in mesendodermal differentiation conditions stained for the definite endoderm marker FOXA2. **g**, Confocal z-slice images of RGd2 and PG^{HIGH}#5 cells after 48 hours in N2B27 or N2B27+activin+CH stained for plakoglobin.

is crucial for DE formation (Dufort et al., 1998). Consistent with published protocols for DE induction (Mfopou et al., 2014), treatment with activin and CH alone is inefficient in upregulating DE markers, such as FOXA2, in RGd2 cells (**Figure 4.13 f**). Competence for DE differentiation was further more reduced in PG^{HIGH}#5 clone as judged by the number of FOXA-positive cells. Due to the lack of FOXA2, it suggests a primarily mesodermal differentiation path, however, additional experiments are required to fully elucidate the lineage specific potential of plakoglobin overexpressing cells. As I have previously observed an increase in cell-cell adhesion upon overexpression of plakoglobin, under pluripotent conditions in S+LIF as well as in the absence of LIF, I was surprised to see the described increase in cell motility of the PG^{HIGH}#5 clone upon stimulation by activin and CH. To elucidate this phenomenon, I stained RGd2 and PG^{HIGH}#5 cells in N2B27, and N2B27 supplemented with activin and CH, for plakoglobin and analysed its expression and distribution via confocal microscopy. Consistent with my previous data of differentiation in the presence of serum, RGd2 cells also downregulated plakoglobin in serum-free medium, regardless of the supplementation with activin and CH (**Figure 4.13 g)**. In contrast, the PG^{HIGH}#5 cells maintained high levels plakoglobin in N2B27, however remarkably, when supplemented with activin and CH, plakoglobin was released from the membrane, potentially due to EMT induced rearrangement of cell-cell adhesion. Now, after having observed differentiation defects in plakoglobin overexpressing cells I was prompted to investigate if the downstream pathways would also affect the transition from naïve to primed pluripotency. Therefore, I applied the protocol by Hayashi and colleagues (Hayashi et al., 2011), that allows the transition of ESCs to epiblast-like cell (EpiLCs), which are remarkably similar to the post-implantation epiblast-derived stem cells and reconstitute the state of primed pluripotency (Brons et al., 2007; Tesar et al., 2007). Briefly, 2i+LIF cultured RGd2 and PG^{HIGH}#5 cells were transferred to N2B27 medium supplemented with FGF, activin and 1% KSR, termed FAK, and cultured for 48 hours before further analysis (**Figure 4.14 a**). Both, RGd2 and PG^{HIGH}#5 cells changed their morphology from tightly packed, round and dome-shaped colonies in 2i+LIF to a flat monolayer, reminiscent to EpiSCs (**Figure 4.14 b**). To assess pluripotency and transcriptional levels of plakoglobin overexpression, I measured the REX1::GFP and Jup-mCherry signals via flow cytometry. Both cell lines readily downregulated the naïve state pluripotency transcription factor REX1 as seen by decrease in GFP signal (**Figure 4.14 c**). As expected, overexpression of plakoglobin was not affected by the differentiation to EpiLCs, according to the mCherry signal (**Figure 4.14 c**). To confirm the transition from naïve to primed pluripotency, I analysed expression of the naïve pluripotency factor KLF4 and the general pluripotency factor OCT4 via immunostainings (**Figure 4.14 e-f**). After 48 hours of culture in FAK, all cells had successfully exited the naïve state of pluripotency, regardless of the expression of plakoglobin. OCT4 expression was maintained under naïve and primed conditions, though fluorescent intensities were reduced upon transfer to FAK (**Figure 4.14 e&f**). Next, I investigated the expression of

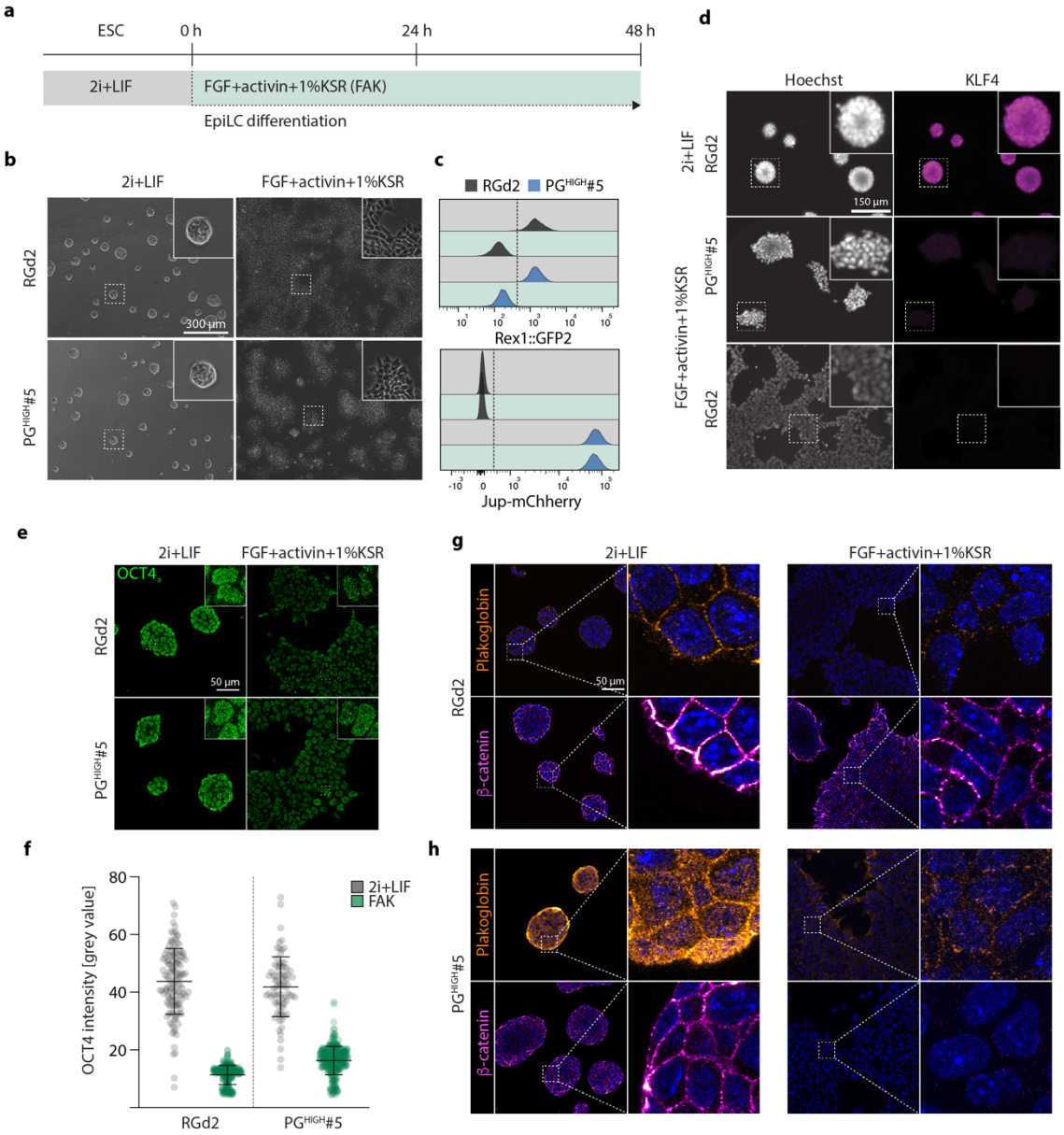

Figure 4.14 | EpiLC differentiation of ESC. a, Schematic illustration of the differentiation of ESC to EpiLC by transfer from 2i+LIF to FGF+activin+KSR. **b**, Representative images of RGd2, PG^{LOW}#2 and PG^{HIGH}#5 cells in 2i+LIF and after 48 hours of EpiLC differentiation. **c**, Flow cytometric analysis of the Rex1::GFPd2 and Jup-mCherry reporter signals. **d**, Epifluorescence images of RGd2 cells in 2i+LIF and RGd2 and PG^{HIGH}#5 cells in FAK stained for KLF4. **e**, Confocal z-slice images of RGd2 and PG^{HIGH}#5 cells in 2i+LIF or FAK, stained for OCT4. **f**, Nuclear OCT4 intensity distribution. **g&h**, Confocal z-slice images of RGd2 and PG^{HIGH}#5 cells in 2i+LIF or FAK, respectively. Cells were stained for plakoglobin and β-catenin.

β-catenin and plakoglobin in RGd2 and PG^{HIGH}#5 cells upon differentiation to EpiLCs. After 48 hours in FAK medium, RGd2 cells had lost plakoglobin expression, whereas β-catenin levels remained largely the same (**Figure 4.14 g**). Remarkably, even the plakoglobin overexpressing PG^{HIGH}#5 cells show a clear downregulation of plakoglobin protein despite transcription remained unchanged (**Figure 4.14 h**). In contrast to RGd2 cells, the PG^{HIGH}#5 clone also loses β-catenin when maintained under primed conditions.

4.2.7 Plakoglobin and β-catenin expression diverge upon implantation

Hitherto, I have shown that plakoglobin appears to have similar function to β-catenin in mouse ES cells. This shall not be surprising as plakoglobin and β-catenin are closely related homologues and several studies have shown their partially compensatory effects for one another. Depending on the cellular context, β-catenin takes on different signalling roles. Stabilisation of β-catenin is known to promote pluripotency through elevating the repressive effects to TCF3 (TCF7L1) in mouse ES cells (Wray et al., 2011), however, stabilisation of β-catenin in epiblast-derived stem cells (EpiSCs) leads to rapid differentiation (Kim et al., 2013; Sumi et al., 2013). These findings prompted me to investigate plakoglobin expression during these two respective stages of pluripotency – naïve and primed. Therefore, I used EpiSCs carrying the Oct4GiP transgene (Ying et al., 2002), that were originally established from E5.75 embryos by Dr. Ge Guo (Austin Smith's lab, Cambridge Stem Cell Institute, University of Cambridge) (Guo et al., 2009), as a model for the primed (post-implantation) stages of pluripotency. I cultivated EpiSCs in N2B27 supplemented with the originally described growth factors FGF and Activin A (Brons et al., 2007) and the addition of the small molecule tankyrase inhibitor XAV939 (Huang et al., 2009), which inhibits β-catenin facilitated transcription via stabilising axin. I then assessed β-catenin and plakoglobin levels via immunostainings (**Figure 4.15 a**). Under these conditions, the majority of cells displayed β-catenin either in their cytoplasm, or when in larger colonies, additionally in association with E-cadherin at the membrane. Surprisingly, I was not able to detect any plakoglobin, neither cytoplasmic nor, as observed before, in colocalization with E-cadherin. Next, I examined *Jup* (Plakoglobin) and *Ctnnb1* (β-catenin) transcript levels of EpiSCs, ES cells and reprogrammed EpiSCs (Single-cell RNA-seq data kindly provided by Hannah Stuart, Jose Silva's lab, Cambridge Stem Cell Institute, University of Cambridge). *Ctnnb1* showed homogeneous and equal expression levels across all samples. In contrast, *Jup* is also homogeneously expressed in all reprogrammed samples and the ES cells, but displayed great heterogeneity in EpiSCs (**Figure 4.15 b**). Notably, several EpiSCs still showed similar or even higher *Jup* transcript levels than the ES cells. Therefore, not detecting any plakoglobin via immunostaining suggests that regulation occurred on protein level rather than on transcriptional level. The unexpected degradation of plakoglobin in EpiSCs encouraged us to investigate β-catenin and plakoglobin throughout early embryonic development. Thus, I immunostained mouse embryos at E2.5, E3.5, E4.5 and post-implantation at E5.5 for β-catenin and plakoglobin

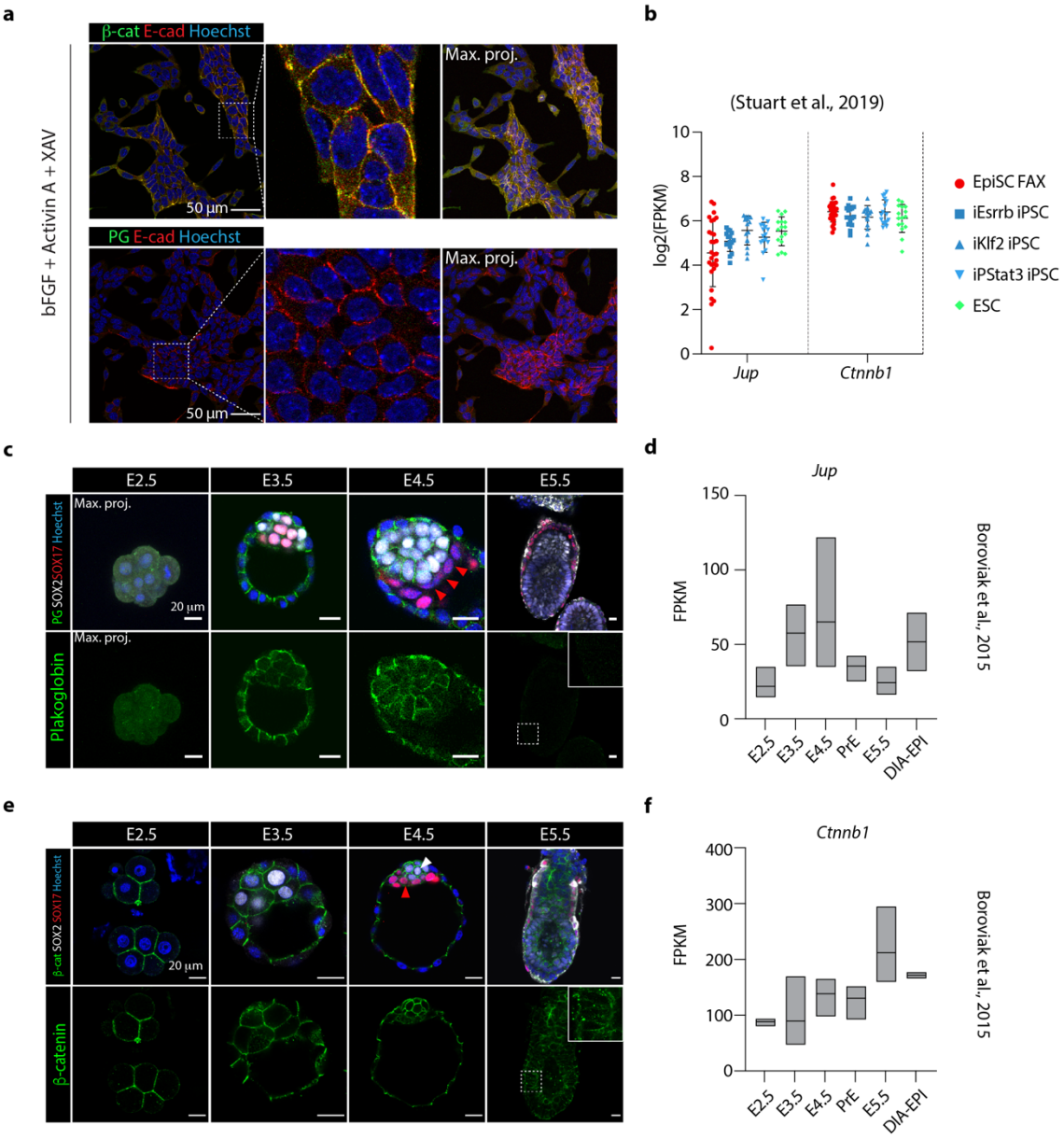

Figure 4.15 | Differential expression of β-catenin and plakoglobin during naïve and primed pluripotency. **a**, Confocal z-slice and maximum projection images of EpiSCs stained for β-catenin, plakoglobin and E-cadherin. **b**, *Jup* (plakoglobin) and *Ctnnb1* (β-catenin) transcripts as measured by single-cell RNAseq in EpiSCs, Epi-iPSCs and ESCs. RNAseq data sets were taken from Stuart et al., 2019. **c**, Representative confocal images of pre-implantation embryos (E2.5, E3.5 and E4.5) and post-implantation (E5.5) stained for plakoglobin, SOX2 and SOX17. Nuclei were stained with Hoechst. **d**, RNAseq data for *Jup* transcription in the epiblast and primitive endoderm during pre- and post-implantation embryos. Data taken from Boroviak et al., 2015. **e**, Representative confocal images of pre-implantation embryos (E2.5, E3.5 and E4.5) and post-implantation (E5.5) stained for β-catenin, SOX2 and SOX17. Nuclei were stained with Hoechst. **f**, RNAseq data for *Ctnnb1* transcription in the epiblast and primitive endoderm during pre- and post-implantation embryos. Data taken from Boroviak et al., 2015.

(**Figure 4.15 c&e**). To discern between the embryonic and extraembryonic lineages, I also stained for SOX2 (epiblast marker) and SOX17 (primitive endoderm marker). I found that β-catenin was expressed throughout all stages of early embryonic development as well as all lineages (**Figure 4.15 e**). At E2.5 most β-catenin appeared to have localized between adjacent blastomeres with only very little β-catenin protein on the side facing the exterior of the embryo. β-catenin was then also found throughout the inner cell mass and the trophectoderm, at E3.5. Upon formation of the

primitive endoderm at E4.5, β-catenin levels dropped in the SOX17-positve cells and was particularly strong in the SOX2-positive epiblast. Once the embryo had implanted into the uterus, β-catenin was found throughout the egg cylinder in all lineages. In contrast to β-catenin, plakoglobin expression varied greatly throughout the different developmental stages. At E2.5 none of the blastomeres displayed any plakoglobin expression. However, at E3.5 strong plakoglobin expression became apparent in the trophectoderm and lower levels were detectable within the inner cell mass (**Figure 4.15 c**). At 4.5, SOX2-positive epiblast cells, also showed strong expression of plakoglobin, whereas SOX17-positive primitive endoderm cells displayed a complete lack thereof. Astonishingly, upon implantation exclusively all cells of the embryo had rapidly downregulated plakoglobin which stands in stark contrast to the expression of β-catenin at this stage. Intrigued by this finding, I then analysed a previously published RNA-seq data set of pre- and post-implantation embryos, for the transcript levels of *Jup* and *Ctnnb1* (Boroviak et al., 2015) (**Figure 4.15 d&f**). Consistent with the observed protein level of β-catenin, *Ctnnb1* transcripts were relatively constant throughout pre-implantation development, whereas *Jup* transcripts clearly rose, peaking with the highest transcript levels at E4.5. Consistent with our observations, primitive endoderm cells showed decreased transcript levels of *Jup* but similar levels of *Ctnnb1* with the E4.5 epiblast cells. Substantiating our finding of diverging protein levels of plakoglobin and β-catenin, transcript levels of *Jup* dropped at implantation, whereas *Ctnnb1* transcript levels were even higher than at any stage during pre-implantation development.

4.2.8 Overexpression of plakoglobin does not revert epiblast stem cells to a naïve-pluripotent state

The abrupt disappearance of plakoglobin in the embryo upon implantation, the absence of it in post-implantation epiblast derived stem cells (EpiSCs) and its ability to stabilise the naïve pluripotency gene regulatory network in embryonic stem cells, encouraged me to ectopically express plakoglobin in EpiSCs. Could the forced expression of plakoglobin potentially revert EpiSCs back to a naïve-like state of pluripotency or will it facilitate differentiation in synergy with β-catenin? To elucidate this question this question, I used the previously described (see 4.2.1) Jup-T2A-mCherry plasmid in combination with the PiggyBac transposase system to generate an EpiSC line that was constitutively expressing plakoglobin (**Figure 4.16 a**). As the parental EpiSC line (Guo et al., 2009) was already carrying an OCT4-GFP reporter (Ying et al., 2002), I was able to simultaneously investigate plakoglobin transcription (mCherry) as well as having a fluorescent read-out pluripotency and differentiation (GFP). Several days after the transfection of the EpiSCs with the plakoglobin overexpression plasmid, double-positive (mCherry/GFP) cells were FACS-sorted and subsequently expanded to generate the EpiSC-PG

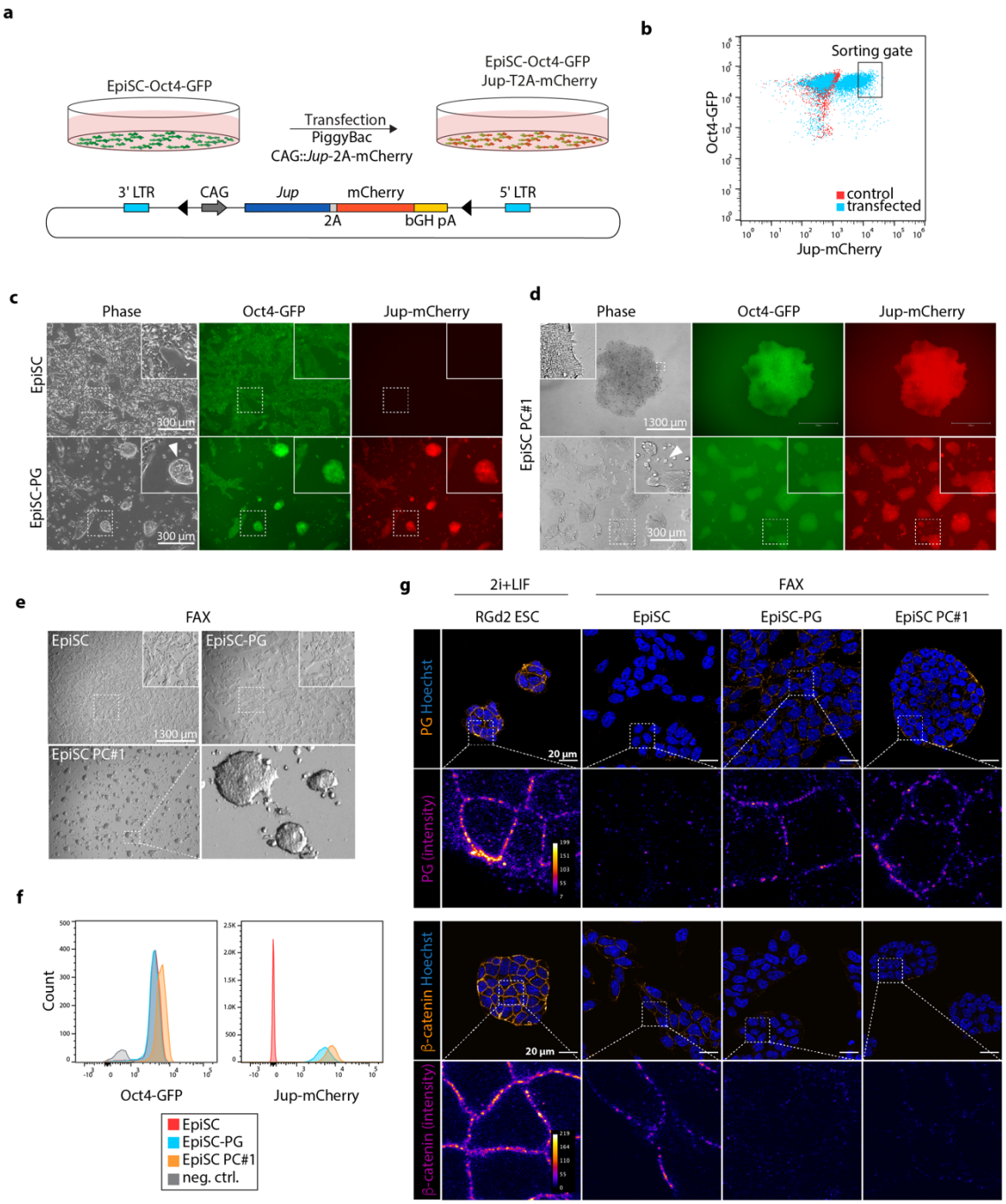

Figure 4.16 | Generation of plakoglobin overexpressing epiblast-derived stem cells (EpiSCs). a, Schematic illustration of the transfection procedure and design of the plakoglobin overexpression plasmid. EpiSCs carrying an Oct4-GFP reporter were transfected with the plakoglobin overexpression plasmid enabling simultaneous fluorescent read-out for pluripotency (GFP) and transcriptional levels of plakoglobin (mCherry). **b**, FACS plot of control and transfected EpiSCs. Sorted cell population as indicated. **c&d**, Phase contrast and epifluorescence images of EpiSC, EpiSC-PG and EpiSC-PC1. **e**, phase contrast images of EpiSC, EpiSC-PG and EpiSC-PC1 after several passages in culture. **f**, Oct4-GFP and Jup-mCherry histograms of EpiSC, EpiSC-PG and EpiSC-PC1 in FAX medium. **g**, Representative confocal z-slice images of ESCs in 2i+LIF and EpiSC, EpiSC-PG and EpiSC PC1 in FAX, stained for plakoglobin and β-catenin.

cell line (**Figure 4.16 b&c**). In FGF+Activin+XAV supplemented medium (FAX, the standard EpiSC maintenance medium), wild type EpiSC grew as a flat monolayer, whereas EpiSC-PG adopted a heterogeneous mixture of cell morphologies. The majority of cells maintained the flat

cell shape, however, scattered round and dome-shaped colonies, resembling the morphology of naïve ESCs, started to appear throughout the culture (**Figure 4.16 c**). As these colonies also displayed a stronger GFP and mCherry signal than the rest of the culture, implying a higher expression of plakoglobin and OCT4, I subsequently picked one of these colonies and further expanded it to generate a pseudo-clonal EpiSC-PG line with high plakoglobin expression, from here on called pseudo-clone #1 (PC#1) (**Figure 4.16 d**). Directly after picking, PC#1 grew as a flat colony, however, individual cell boundaries were already indistinguishable. Remarkably, within the next several passages the EpiSC-PG cells reacquired the typical flat monolayer morphology, whereas PC#1 cells started to round up and grow as tight, dome-shaped colonies, a feature associated with naïve-state pluripotency in ESCs (**Figure 4.16 e**). Next, I investigated the Oct4-GFP and Jup-mCherry reporters via flow cytometry. EpiSCs and EpiSC-PG cells did not differ in their Oct4-GFP signal, whereas the PC#1 cells displayed slightly elevated levels (**Figure 4.16 f**). This rise in GFP levels was simultaneously accompanied by an increase in mCherry, supporting the theory, that even in primed pluripotency and in contrast to β-catenin, plakoglobin promotes pluripotency (**Figure 4.16 f**). As EpiSC-PG and PC#1 cells both showed high mCherry signals as measured my flow cytometry fluorescence microscopy, I then confirmed plakoglobin overexpression levels, and corresponding β-catenin levels, via immunostainings (**Figure 4.16 g**). As observed before (see section **4.2.7**)**,** wild type EpiSC did not exhibit any plakoglobin expression, yet β-catenin was detected in association with the cell membrane. Surprisingly, even the plakoglobin overexpression cell lines, EpiSC-PG and PC#1, displayed low amount of plakoglobin, all of which was membrane-bound (**Figure 4.16 g**). When compared to RGd2 cells in 2i+LIF, plakoglobin levels in EpiSC-PG and PC#1 cells, seemed to be even lower than plakoglobin levels in wild type ESCs, suggesting the active degradation of plakoglobin protein, despite strong transcriptional expression. However, simultaneously these low expression levels of plakoglobin were enough to completely degrade β-catenin, which was not detectable anymore in EpiSC-PG and PC#1 cells. Furthermore, since the PC#1 cells had acquired a dome-shaped and tight colony morphology, similar to ESCs in 2i+LIF, despite the primed culture conditions (FAX medium), I immunostained the cells for the naïve pluripotency factors KLF4 and TFCP2L1 (**Figure 4.17**). As expected, 2i+LIF cultured ESCs showed homogeneous expression of both proteins, whereas none, neither the wild type EpiSCs nor the plakoglobin overexpressing EpiSCs, exhibited any fluorescent signal for these transcription factors. Hence, plakoglobin overexpression in EpiSCs caused a change in morphology resembling similarity to the naïve-state but cannot activate the naïve transcription factor network in primed culture conditions. Next, I investigated whether plakoglobin expression with simultaneous change in culture conditions could activate the naïve gene regulatory network and reprogram EpiSCs to an induced pluripotent state (Epi-iPSCs). Generally, EpiSCs do not spontaneously revert to an ESC-like state when

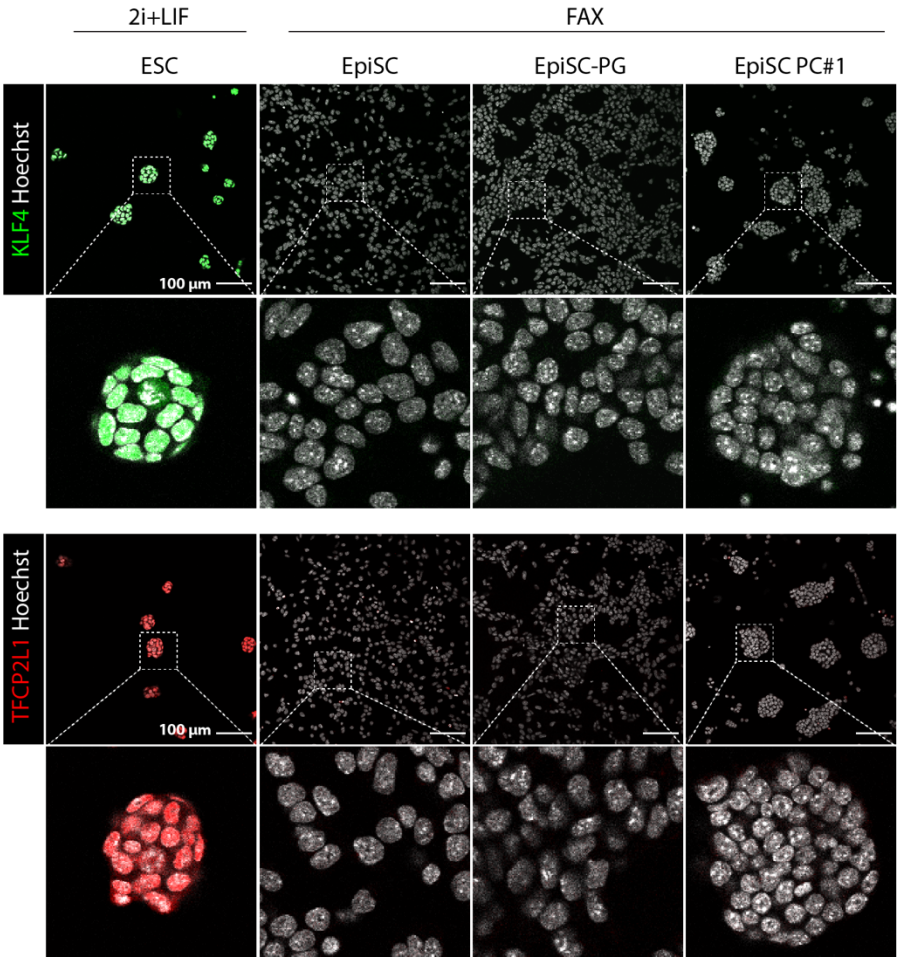

Figure 4.17 | Plakoglobin expression in EpiSCs does not upregulate the naïve-state associated transcription factors KLF4 and TFCP2L1. Confocal fluorescent images of embryonic stem cells (ESC) in 2i+LIF medium, epiblast-derived stem cells (EpiSC) and plakoglobin overexpressing EpiSCs (EpiSC-PG & PC#1) in FAX medium, immunostained for the naïve-state associated transcription factors KLF4 and TFCP2L1. Nuclei were stained with Hoechst.

transferred into 2i+LIF medium (Brons et al., 2007; Guo et al., 2009; Tesar et al., 2007). Yet, the ectopic expression of a single naïve-pluripotency factor (e.g. KLF4) is enough to overcome this reprogramming barrier and, even though at low efficiency (less than 1%), EpiSCs turn into Epi-iPSCs (Guo et al., 2009; Stuart et al., 2019). Therefore, I tried to reprogram wild type EpiSCs, EpiSC-PG and PC#1 cells in 2i+LIF. Since it has been shown, that the absence of β-catenin signalling is important for the maintenance of the EpiSCs (Sumi et al., 2013), and I have shown that plakoglobin can most likely substitute for β-catenin in ESCs, I have also tried reprogramming with the addition of the WNT signalling inhibitor XAV (2i+LIF+XAV). Furthermore, I tested the absence of CH in PD, LIF, XAV (PLX), and the addition of activin (PLAX). Due to the shift towards naïve pluripotency in ESCs under S+LIF conditions when overexpressing plakoglobin, we finally tried to reprogram EpiSCs in S+LIF. To initiate reprogramming, cells were plated in FAX medium and cultured for 24 hours before then switching to the corresponding media as described above (**Figure 4.18 a**). After four days exposure to reprogramming conditions, cells

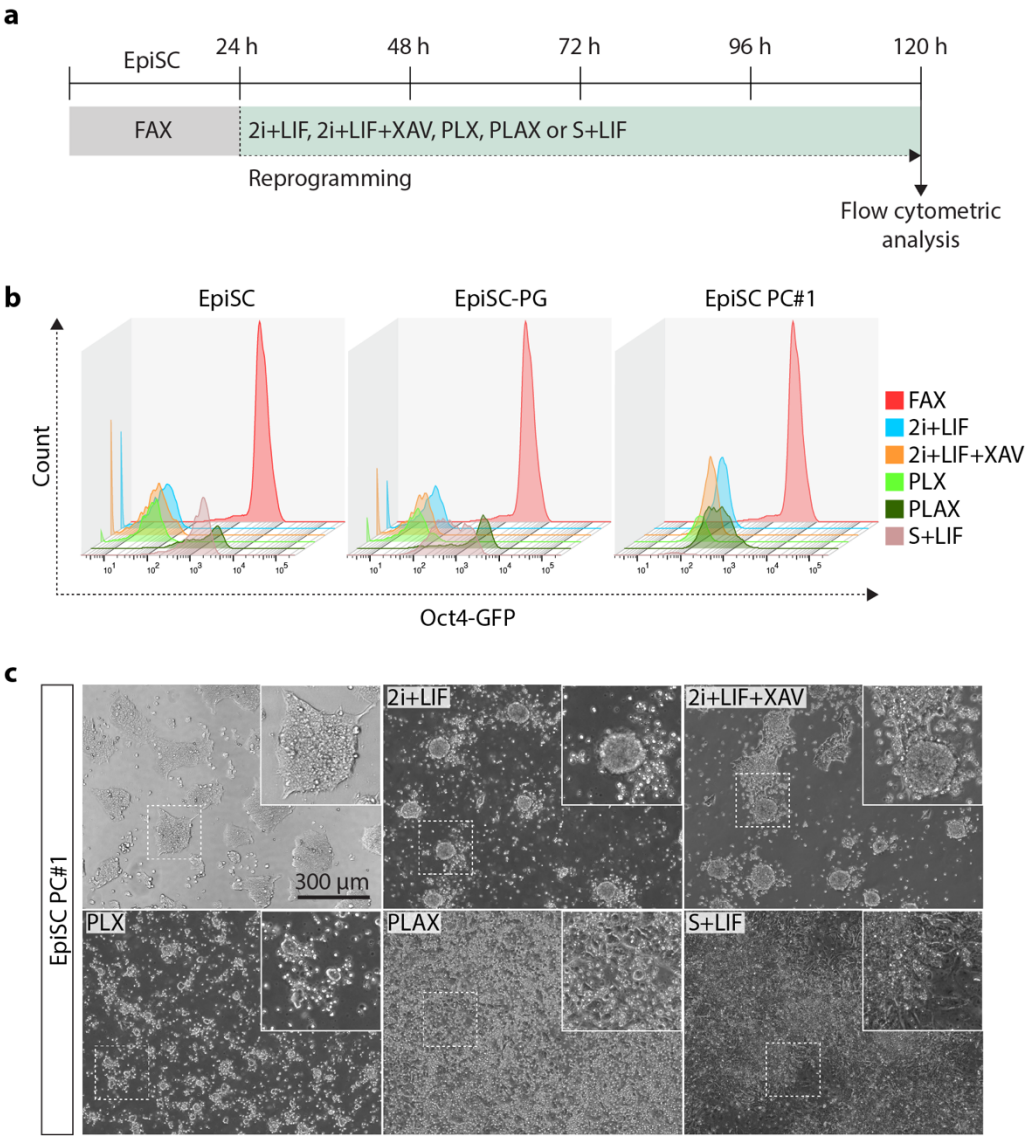

Figure 4.18 | Plakoglobin overexpression does not mitigate the reprogramming barrier from primed to naïve pluripotency. a, Schematic illustration of the reprogramming strategy for EpiSCs. **b**, Histograms of Oct4-GFP levels in EpiSC, EpiSC-PG and EpiSC PC#1 after four days in reprogramming conditions. **c**, Phase contrast images of EpiSC PC#1 after four days in reprogramming conditions.

were analysed for their Oct4-GFP signal via flow cytometry. Only when the primed pluripotent state of EpiSCs was maintained or when cells successfully reprogrammed to Epi-iPSCs, GFP signal was to be expected. Wild type EpiSCs, EpiSC-PG and PC#1 cells all lost their GFP signal upon the transfer to 2i+LIF, 2i+LIF+XAV and PLX, and have therefore differentiated or died (**Figure 4.18 b**). In both, PLAX and S+LIF, GFP signal was partially maintained. However, since the majority of the cells were still GFP-positive four days after change in media conditions, these cells most likely just slowly differentiated and did not reprogram. Remarkably, in 2i+LIF and also with the addition of XAV, PC#1 cells did expand as individual dome-shaped colonies as I would have expected when successfully reprogramed to Epi-iPSCs (**Figure 4.18 c**). However, the absence of Oct4-GFP and the inability to passage these cells indicates that these cells too have

differentiated. As β-catenin knockout embryos fail to successfully undergo gastrulation (Haegel et al., 1995) and β-catenin was shown to be pivotal for mesendodermal and neuroectodermal differentiation of EpiSCs (Sumi et al., 2013), I was curious to see if the plakoglobin induced reduction of β-catenin in EpiSC-PG and PC#1 cells would impede the exit from primed pluripotency. Therefore, wild type EpiSCs and the plakoglobin overexpressing EpiSC-PG and PC#1 cells were cultured for 48 hours in N2B27 and N2B27 + CH, respectively (**Figure 4.19 a**). In non-inductive N2B27, the majority of cells, regardless of plakoglobin overexpression, died. Yet, scattered and small GFP-negative colonies emerged across all cell lines, indicating a complete downregulation of the pluripotency network (**Figure 4.19 a&b**). When supplemented with CH, no widespread cell death was observed and EpiSCs as well as EpiSC-PG cell continued

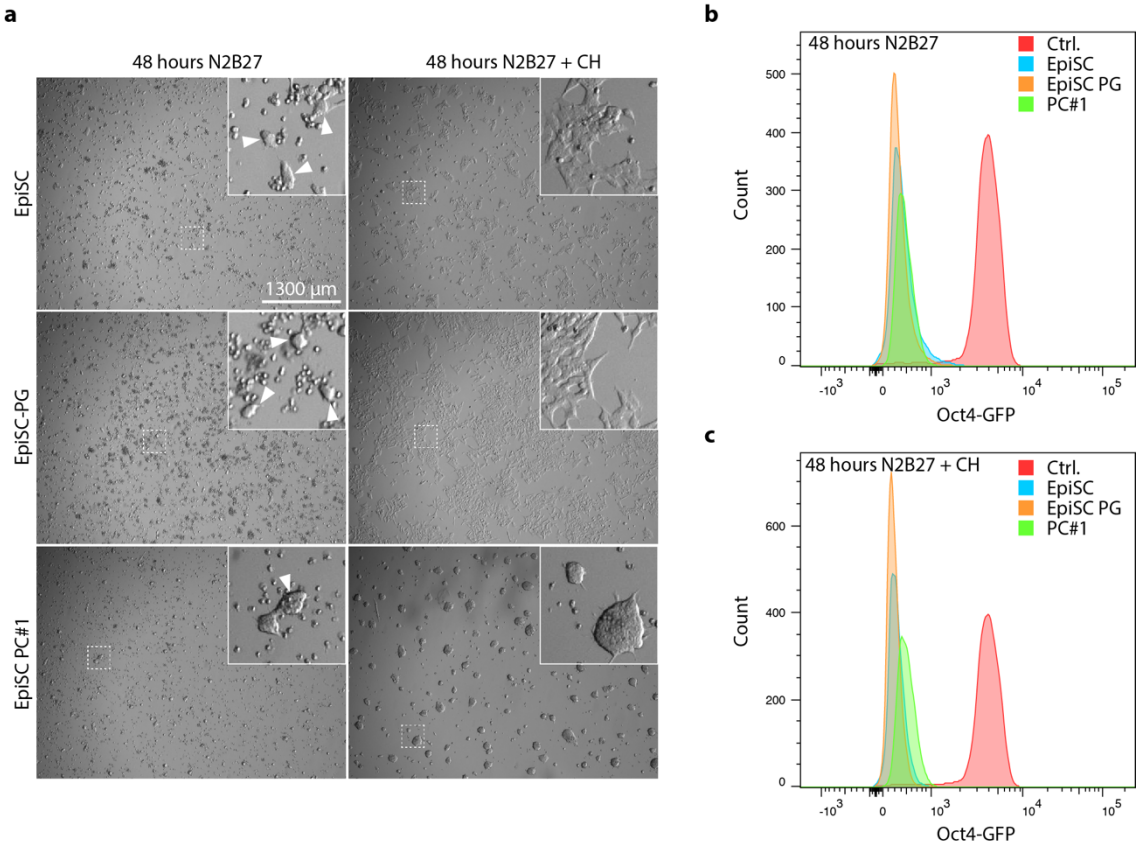

Figure 4.19 | Forced plakoglobin expression does not inhibit the exit from primed pluripotency in EpiSC. **a**, Phase contrast images of EpiSC, EpiSC-PG and EpiSC PC#1 after 48 hours in N2B27 or N2B27+CH, respectively. **b&c**, Oct4-GFP histograms of EpiSC, EpiSC-PG and EpiSC PC#1 after 48 hours in N2B27 or N2B27+CH, respectively.

to grow as a flat monolayer of cells. In contrast, PC#1 cells maintained the previously acquired dome-shaped structure. However, in all conditions, GFP signal was lost and therefore consistent with the assumption that plakoglobin overexpression alone does not hinder the exit from primed pluripotency (**Figure 4.19 c**). Still, additional experiments are required to confirm the complete downregulation of the pluripotency network the ability to upregulate lineage specific markers. As

I have previously shown a differential expression of plakoglobin and β-catenin in the post-implantation epiblast, in which plakoglobin was rapidly degraded, and because of β-catenin's dual function in promoting pluripotency and in mesendodermal differentiation, I asked if forced plakoglobin expression in EpiSC would activate β-catenin signalling targets and lead to differentiation. Therefore, wild type EpiSCs and PC#1 cells, normally maintained in FGF and activin supplemented with the WNT signalling antagonist XAV, were transferred for

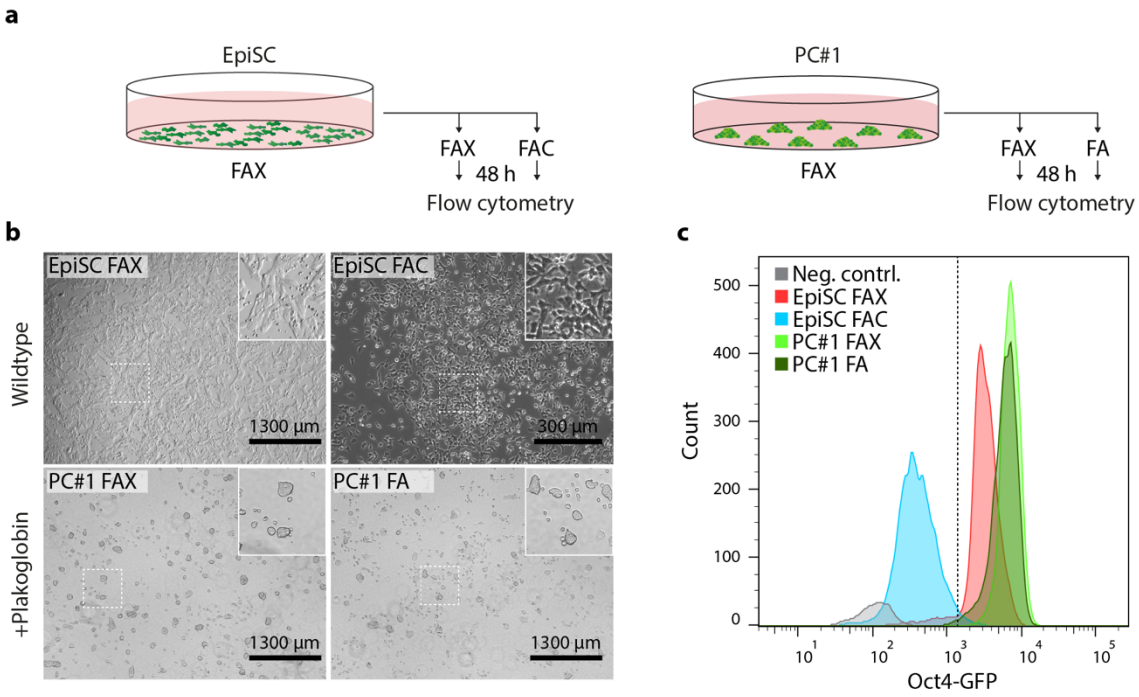

Figure 4.20 | Plakoglobin, unlike β-catenin, does not promote differentiation of EpiSCs. a, Schematic illustration of experimental set up. b, Phase contrast images of EpiSC and EpiSC PC#1 in FAX maintenance medium and after removal of the WNT signalling inhibitor XAV with the addition of CH to the wt EpiSCs. c, Oct4-GFP Histogram after 48 hours past change of medium.

48 hours into FGF+activin+CH and FGF+activin, respectively (**Figure 4.20 a**). Upon the removal of XAV and simultaneous stabilisation of β-catenin via CH treatment, EpiSCs quickly lost their Oct4-GFP signal which was accompanied by prominent morphological changes (**Figure 4.20 b&c**). EpiSCs downregulated cell-cell adhesion, whilst detaching from one another and simultaneous formation of membrane protrusions. Remarkably, PC#1 plakoglobin overexpressing EpiSCs retained their GFP signal after removing XAV and no change in morphology was observed. One may note, that regardless of the removal of XAV, plakoglobin overexpressing cells exhibit elevated levels of GFP in comparison to wild type EpiSCs (**Figure 4.20 c**). Concluding, in this paragraph I have described the generation of the plakoglobin overexpressing EpiSC lines EpiSC-PG and PC#1. Due to an unknown mechanism, specific to primed state pluripotency, resulting in the fast degradation of plakoglobin protein, overexpression levels as achieved in ESCs (see 4.2.1) were never reached. Nonetheless, even though only

marginally elevated, the rise of plakoglobin levels lead to the degradation of β-catenin whilst accompanied by morphological changes resulting in tightly packed and dome-shaped colonies, both traits which had been also observed in plakoglobin overexpressing ESCs (see 4.2.1). The low levels of plakoglobin expression did not yield in the expression of naïve pluripotency factors and EpiSC-PG and PC#1 cells stayed refractory to reprogramming towards naïve state pluripotency, a barrier that might be overcome once higher plakoglobin levels can be reached during primed pluripotency. Most importantly, these data elucidate not just transcriptional and post-transcriptional differences in regulation between β-catenin and plakoglobin during naïve and primed pluripotency, but moreover a differential signalling function — In the presence of stabilised β-catenin, EpiSCs rapidly differentiated whereas plakoglobin overexpression enhanced the Oct4-GFP reporter signal even in the absence of XAV.

4.2.9 Plakoglobin in primates

After having extensively elucidated the role of plakoglobin in mouse embryonic stem cells (see 4.2.1), epiblast-derived stem cells (see 4.2.8), the developing embryo (see 4.2.7) and due to the high degree of evolutionary conservation of the WNT/β-catenin signalling pathway, I was intrigued to investigate plakoglobin in other mammals. In the next several paragraphs, I will be describing plakoglobin expression and localisation during the different stages of pluripotency in human, and finally, give an outlook on the role of plakoglobin in the common marmoset, a model system located between human and mouse.

4.2.9.1 Naïve human embryonic stem cells and the pre-implantation embryos

In this paragraph, I will be elucidating plakoglobin expression and localisation during human embryonic development. Therefore, I utilized two previously established human pluripotent stem cell (hPSCs) lines – H9 (Thomson et al., 1998) and HNES1 (Guo et al., 2016) (**Figure 4.21 a**). The H9 hPSCs, one of the first hPSC lines, corresponds approximately to the stage of primitive streak in the post-implantation epiblast (Davidson et al., 2015; Nakamura et al., 2016; Wu et al., 2015) and mouse EpiSCs. Hence, these conventional hPSCs are generally considered to inhabit in the primed state of pluripotency. In contrast, HNES1 have been shown to resemble, transcriptionally and epigenetically, a more accurate representation of the pre-implantation epiblast and can therefore be considered naïve (Guo et al., 2016). Originally HNES1 cells were derived from the pre-implantation embryo in t2iLGö, including the small molecule GSK3 inhibitor CH, which enhances β-catenin mediated transcription. However, since it has been shown that WNT inhibition, via the small molecule tankyrase inhibitor XAV, improves resetting from primed to naïve pluripotency (Guo et al., 2017) as well as improving the maintenance of the naïve state (Zimmerlin et al., 2016), it has become common practice to culture

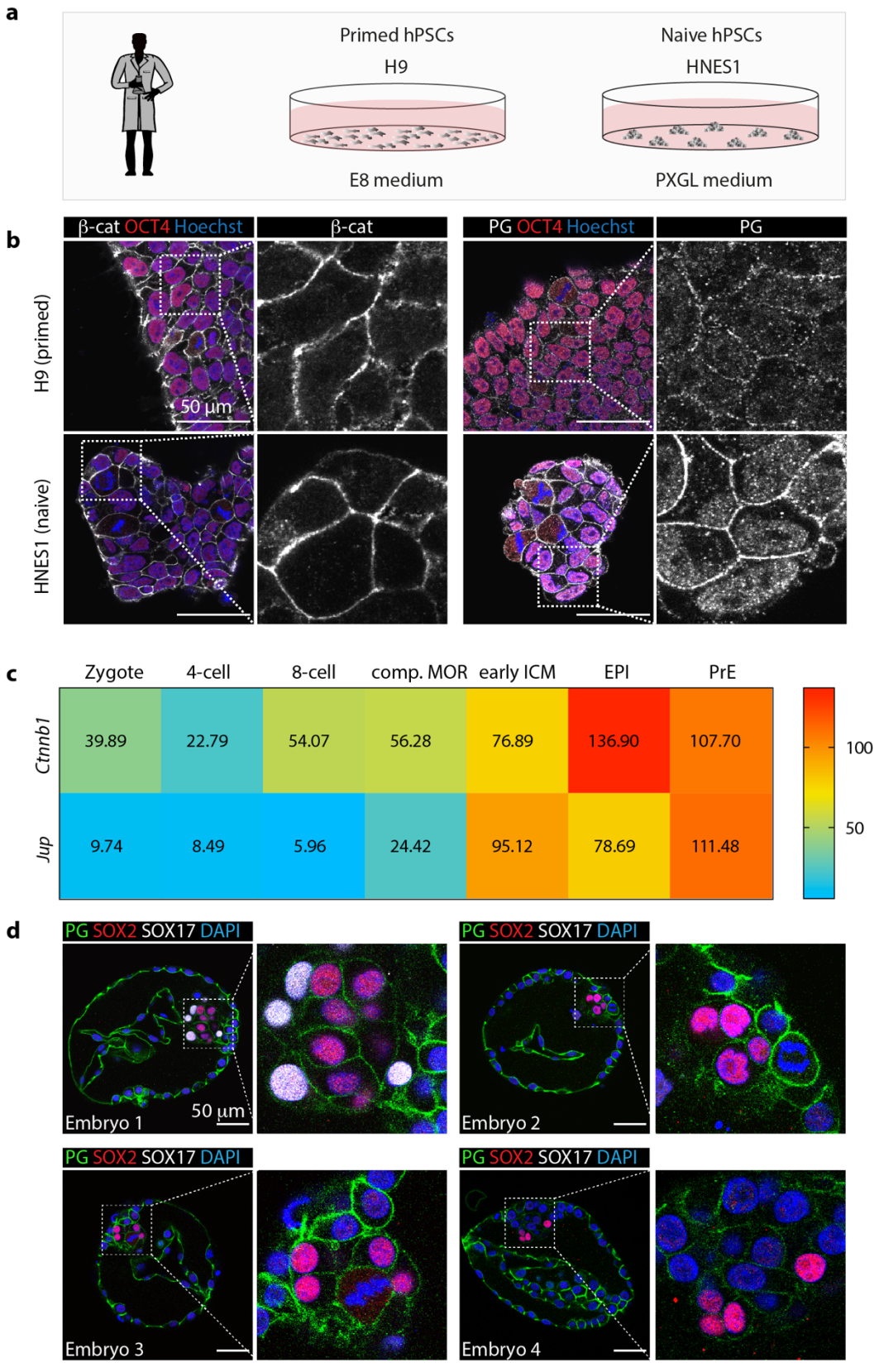
a
Primed hPSCs
H9
E8 medium
Naive hPSCs
HNES1
PXGL medium
b
β-cat OCT4 Hoechst
β-cat
PG OCT4 Hoechst
PG
H9 (primed)
HNES1 (naive)
50 µm
c
Zygote
4-cell
8-cell
comp. MOR
early ICM
EPI
PrE
Ctnnb1
Jup
39.89
22.79
54.07
56.28
76.89
136.90
107.70
9.74
8.49
5.96
24.42
95.12
78.69
111.48
100
50
d
PG SOX2 SOX17 DAPI
Embryo 1
50 µm
Embryo 2
Embryo 3
Embryo 4

Figure 4.21 | Human naïve embryonic stem cells as well as the pre-implantation epiblast express plakoglobin. **a**, Schematic illustration of human ESC lines and media conditions used in this chapter. The conventional human ESC line H9 was cultured in E8. The human naïve cell line HNES1 was cultured in N2B27 supplemented with PD, XAV, GÖ and LIF (PXGL). **b**, Confocal z-slice images of H9 and HNES1 cells stained for plakoglobin and β-catenin. c, Single-cell RNA-seq data for β-catenin (*Ctnnb1*) and plakoglobin (*Jup*) at different stages of pre-implantation embryonic human development. **d**, Confocal z-slice images of four human embryos collected from three different IVF patients. The embryos were stained for plakoglobin, SOX2 (epiblast marker), SOX17 (primitive endoderm marker) and nuclei were labelled with DAPI. | All human embryos were processed by Prof. Jennifer Nichols, Cambridge Stem Cell Institute.

naïve hPSCs in N2B27 supplemented with PD, XAV, GÖ, and LIF (PXGL) (Bredenkamp et al., 2019; Guo et al., 2017). Based on the observation of plakoglobin levels in mouse ESC, EpiSCs, primed and naïve-like marmoset ESCs, I hypothesized that plakoglobin should be expressed highly in naïve HNES1, but not in primed H9 cells, whereas β-catenin should be detectable in both cell lines. To test my hypothesis, primed H9 in E8 medium and naïve HNES1 hPSCs in PXGL medium were immunostained for β-catenin and plakoglobin (**Figure 4.21 b**). Consistent with my previous data, β-catenin was indeed equally expressed in both cell lines and always colocalised with the cell membrane. In contrast, H9 cells only displayed low amounts of plakoglobin whereas HNES1 cells exhibited a distinct upregulation. Interestingly, distinguishing from β-catenin, plakoglobin was also detected in the nucleus, indicating that XAV treatment cannot disrupt plakoglobin mediated transcription. I then used previously published single-cell RNA-seq data sets of human embryos (Blakeley et al., 2015; Petropoulos et al., 2016; Yan et al., 2013) that had been stage- and lineage-specifically aligned (Stirparo et al., 2018) to investigate *Ctnnb1* and *Jup* expression in vivo (**Figure 4.21 c**). Consistent with the RNA-seq data of the mouse embryo, *Jup* expression levels rise at a later point during embryonic development than *Ctnnb1*. The highest *Jup* levels were detected in the early inner cell mass (ICM) and, in contrast to mouse, also in the primitive endoderm (PrE). Ultimately, I questioned whether plakoglobin was also to be found in vivo. To answer this question, I collaborated with Prof. Jennifer Nichols (Wellcome MRC Cambridge Stem Cell Institute) to elucidate plakoglobin expression and localisation within the human embryo. We therefore thawed four supernumerary embryos that were donated from three different patients of in vitro fertilisation programs. Liquid nitrogen stored embryos were thawed at day 7 post fertilisation and subsequently prepared for immunofluorescent analysis. The embryos were then stained for plakoglobin as well as SOX2 and SOX17, markers for the epiblast and PrE, respectively (**Figure 4.21 d**). Since the human pre-implantation embryo contains a high degree of desmosomal intercellular junctions in its trophectoderm (Hardy et al., 1996), it was not surprising to find it enriched with plakoglobin. Yet, consistent with the mouse embryo, human embryos do not form desmosomes within the inner cell mass but plakoglobin, albeit to a lesser extent, was still found in all SOX2-positive epiblast cells. One may note, that only embryo 1 displayed SOX17-positive cells that had differentiated towards PrE, the remaining embryos had weak SOX17 signal within the ICM (in a different z-plane than displayed in the figure, data not shown), indicating a potentially earlier

developmental time point. However, consistent with the RNA-seq data, PrE cells of embryo 1 were positive for plakoglobin. Together, these data reveal an expression pattern of β-catenin and plakoglobin in primed and naïve hPSCs which corresponds to plakoglobin levels I have observed in mouse EpiSCs and ESCs. Additionally, the expression of plakoglobin in the human pre-implantation epiblast indicates also a high degree of conservation across mouse and human in vivo.

4.2.9.2 Marmoset stem cells show plakoglobin expression when reset to a naïve-like state

Over the last several years, in vitro models of human development have become increasingly sophisticated. The in vitro culture of human embryos mimicking peri-implantation stages (Shahbazi et al., 2016), the generation of endometrial and trophoblast organoids (Boretto et al., 2017; Turco et al., 2017; Turco et al., 2018), that have exhibit traits similar to their in vivo counter parts, the maternal endometrium and the placenta respectively, have allowed preliminary insights into human development. Yet, human research must succumb to strict ethical guidelines and can therefore not offer in vivo reference for post-implantation stages. Non-human primate model organisms have been shown to be a middle-ground, featuring many chracteristics of human development whilst simultaneously allowing the options for in vivo post-implantation reference material. Common marmoset (*Callithrix jacchus*) embryonic stem cells (cmESC) have been used as an in vitro model for primate development (Boroviak et al., 2018; Sasaki et al., 2005b; Thomson et al., 1996). Albeit derived from the pre-implantation epiblast, cmESCs have consistently failed to form chimeras (Okano et al., 2012) and resemble transcriptionally the post-implantation embryo. However, recent data from the Boroviak lab has indicated that conventional cmESCs can be reset to a naïve-like state of pluripotency (Personal communication with Erin Slatery, unpublished data), when transferring cells into medium supplemented with, PD, hLIF, activin XAV and ascorbic acid, termed PLAXA (**Figure 4.22 a**). These cells show a loss in polarity, upregulate primate-specific naïve pluripotency associated transcription factors and cluster transcriptionally with the pre-implantation epiblast (Nakamura et al., 2016). Upon resetting, cmESCs lose the clear colony outline by the apical polarity marker ezrin (Berryman et al., 1993) and upregulate the primate-specific naïve pluripotency transcription factor KLF17 (**Figure 4.22 b&c**). I next questioned if cmESCs expressed plakoglobin and if expression was consistent with my previous findings of its association with naïve pluripotency (**Figure 4.22 d**). In contrast to mouse EpiSCs, but consistent with primed human cells, conventional cmESCs show weak expression of plakoglobin (**Figure 4.22 d**). Yet, consistent with naïve-state pluripotency in mouse ESCs and human PSCs, upon resetting of cmESCs, plakoglobin levels dramatically increased (**Figure 4.22 d**). This differential expression was not observed for β-catenin, conventional and naïve-like cmESCs both exhibited similar amount of membrane associated

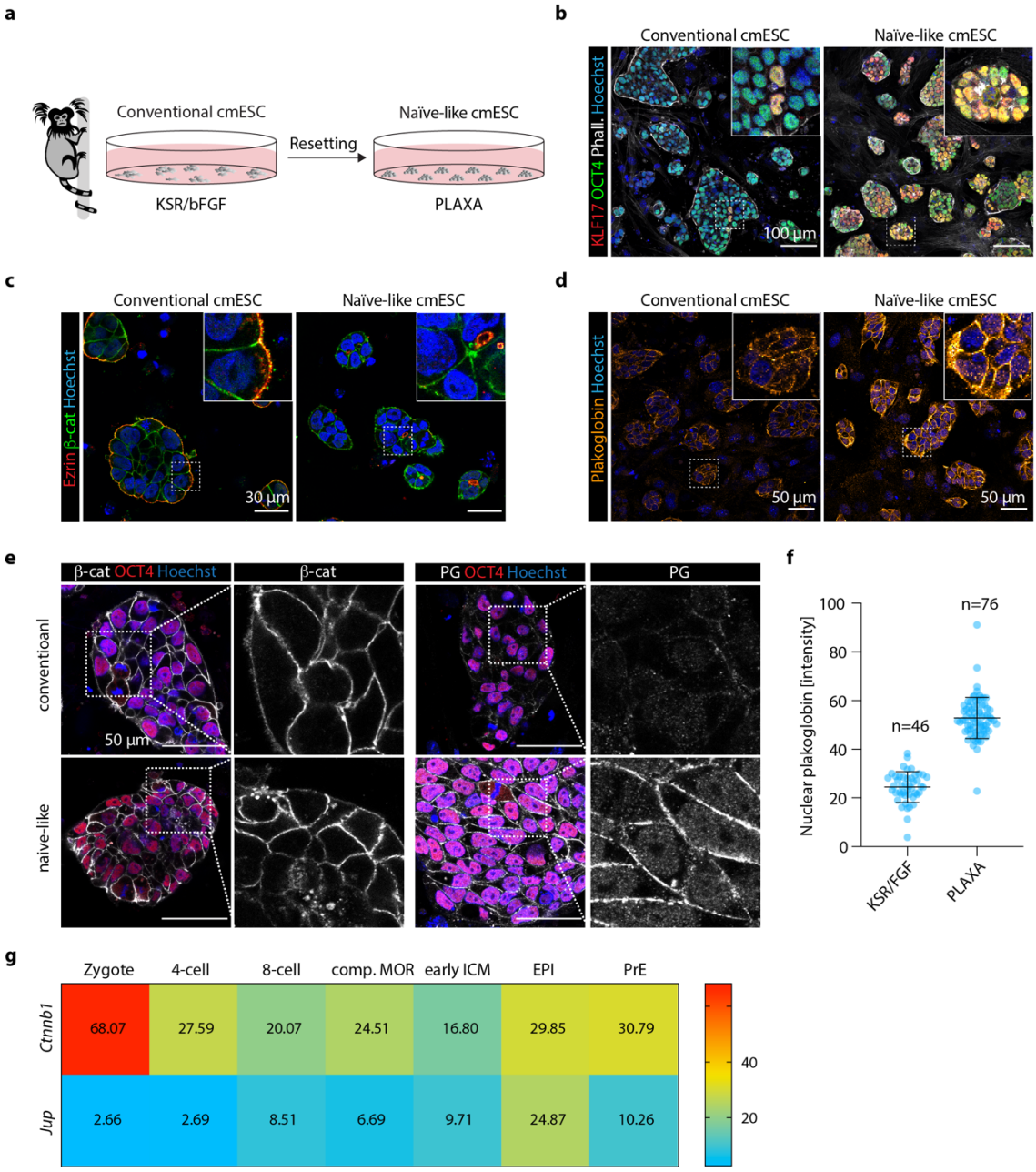

Figure 4.22 | Resetting of conventional cmESCs towards naïve-like pluripotency is accompanied by upregulation of plakoglobin. a, Schematic illustration of the resetting of conventional cmESCs towards naïve-like pluripotency. **b-d**, Confocal z-slice images of conventional and naïve-like cmESCs stained for (**b**) OCT4, KLF17, actin (phalloidin), (**c**) ezrin, β-catenin, and (**d**) plakoglobin. Nuclei were stained with Hoechst. **e**, Comparison and β-catenin and plakoglobin in primed and naïve-like cmESCs via confocal microscopy. **f**, Nuclear plakoglobin intensity distribution of conventional (KSR/bFGF) and naïve-like (PLAXA) cmESCs. **g**, Averaged single-cell transcript levels of *Ctnnb1* (β-catenin) and *Jup* (plakoglobin) during pre-implantation marmoset embryonic development. | cmESCs were cultured by Erin Slatery and Clara Munger, PDN, University of Cambridge.

β-catenin whereas nuclear β-catenin was not detectable regardless of the pluripotent state (**Figure 4.22 e**). Coherent with the data on hPSCs, cmESCs exhibit an ~2-fold increase of nuclear plakoglobin when maintained under naïve-like pluripotent conditions (**Figure 4.22 f**). Finally, when analysing single-cell transcripts (Single-cell RNAseq data of pre-implantation marmoset embryos taken from Boroviak et al., 2018) of *Ctnnb1* (β-catenin) and *Jup* (plakoglobin), I found

low expression levels of plakoglobin throughout pre-implantation development with a sudden spike during the formation of the pluripotent epiblast, whereas Ctnnb1 remained rather stable after initial reduction in comparison to the zygote (**Figure 4.22 g**). In an effort to further expand the previously described microgel culture system, I worked in collaboration with the Boroviak lab to adapt the encapsulation procedure and culture conditions to enable cmESCs to grow in agarose microgels. Due to the more complex needs of cmESCs on their media, we initially tested

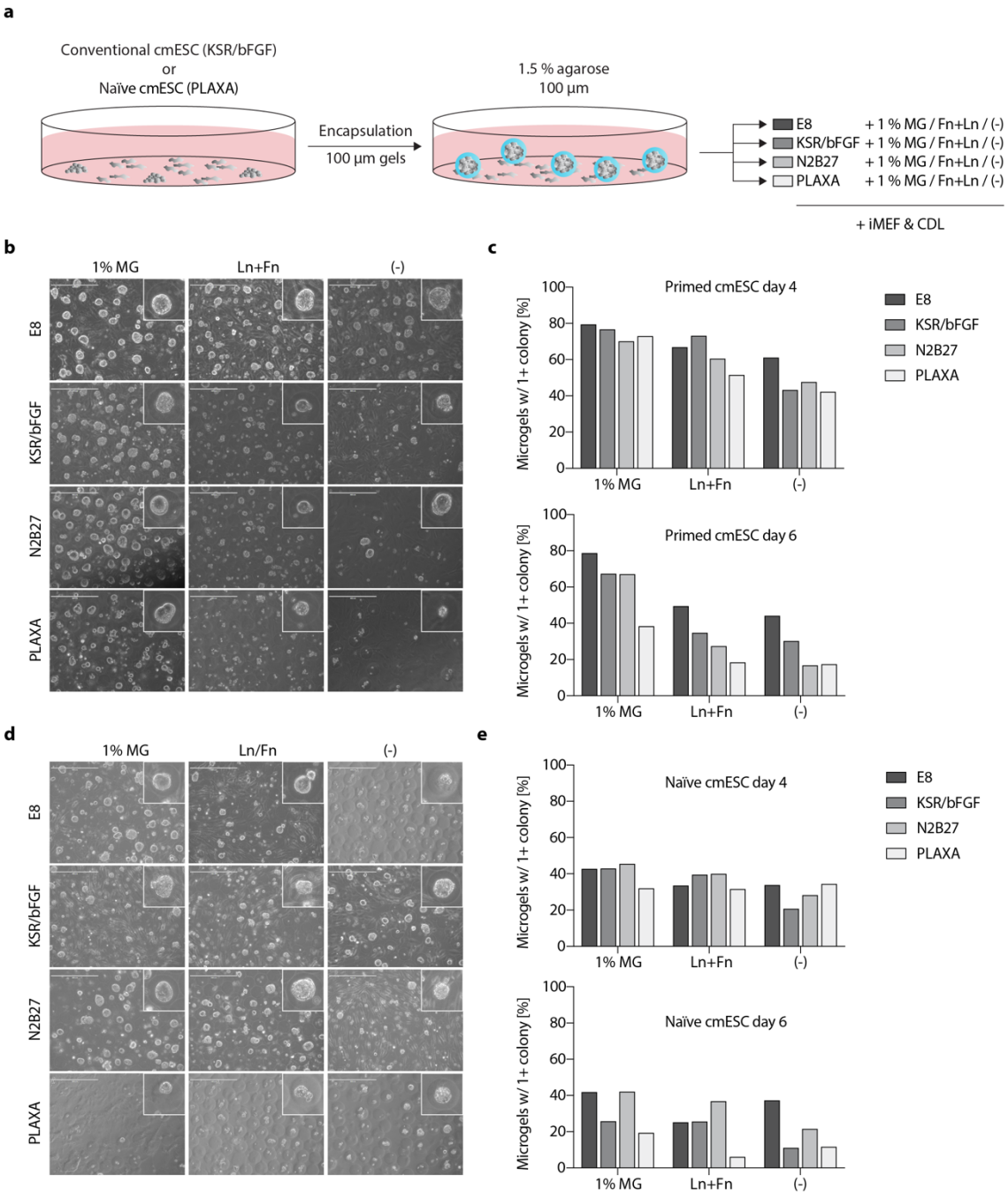

Figure 4.23 | Microgel culture of conventional and naïve-like cmESCs in different media conditions. a, Schematic illustration of the media screening for cmESCs in agarose microgels. **b&c**, Phase contrast images of encapsulated conventional cmESCs cultured for 6 days under different media conditions. Efficiency was determined by counting all gels containing at least 1 colony divided by the total number of gels after 4 and 6 days (N=1) . **d&e**, Phase contrast images of encapsulated naïve-like cmESCs cultured for 6 days under different media conditions. Efficiency was determined by counting all gels containing at least 1 colony divided by the total number of gels after 4 and 6 days (N=1).

12 different media compositions on conventional and naïve-like cmESCs (**Figure 4.23 a**) to ensure cell viability after encapsulation into the biologically inert agarose microgels. Briefly, we used E8, KSR/bFGF, N2B27 and PLAXA as starting media and supplemented them with extracellular matrix (ECM) components in the form of laminin and fibronectin (Ln+Fn) or 1% Matrigel (MG). Microgel encapsulated cmESCs were then cultured in-gel suspension, and all media conditions were further supplemented with 2.5% chemically defined lipids and the culture-wells were coated with mitomycin-c inactivated mouse embryonic fibroblasts. Subsequently, microgel encapsulated cells were cultured in a low-oxygen incubator and imaged after 4 and 6 days in culture. Efficiency was assayed by counting microgels containing at least one cell colony and dividing it by the total number of microgels. Concluding from this screen, we achieved cell proliferation and colony formation in all conditions, however, efficiency varied greatly with the state of pluripotency, the base medium and the amount of ECM (**Figure 4.23 b-e**). In summary, conventional cmESCs survived better than naïve-like cmESCs and the addition of ECM components increased the overall cell viability. Efficiencies ranged between ~40% (PLAXA, no ECM) to ~80 % (E8, 1% MG) on day 4 and ~20% (PLAXA, no ECM) to ~80% (E8, 1% MG) on day 6 for conventional EpiSCs (**Figure 4.23 b&c**). Whereas efficiencies for naïve-like cmESCs lay between ~20% (KSR/bFGF, no ECM) and ~40% (N2B27, 1%MG) on day 4 and ~5% (PLAXA, Ln+Fn) and ~40% (N2B27, 1%MG) on day 6 (**Figure 4.23 d&e**).

4.3 Conclusions

This chapter was devoted to elucidating plakoglobin's role in the establishment and maintenance of naïve pluripotency in embryonic stem cells and their in vivo counterparts, the epiblast. Therefore, I have generated an ESC line constitutively expressing plakoglobin-T2A-mCherry (termed PG-OE). The previously described REX1::GFPd2 reporter allowed the near real-time analysis of naïve pluripotency whilst the mCherry signal indicated plakoglobin transcript levels. Under naïve conditions, in 2i+LIF, no morphological differences were apparent, however, PG-OE cells in serum-supplemented medium acquired the round and dome-shaped morphology associated with naïve-state pluripotency. Consistent with other studies (Mahendram et al., 2013; Salomon et al., 1997), forced expression of plakoglobin was accompanied by the degradation of β-catenin, however, this effect was mitigated in the presence of the GSK3 inhibitor CH. Due to the morphological changes, I was encouraged to further investigate the state of pluripotency. Remarkably, PG-OE cells showed in S+LIF homogeneous REX1::GFP signal, indistinguishable from 2i+LIF. As this observation indicated naïve-state pluripotency in all cells, I also immunostained for the naïve pluripotency associated transcription factor ESRRB and NANOG. Consistent with the GFP signal, all PG-OE cells were positive for both proteins, whereas RGd2 cells showed heterogeneous expression in S+LIF. However, since

PG-OE cells were originally not established as a clonal cell line, plakoglobin overexpression levels varied. To completely understand how different levels of plakoglobin would influence pluripotency, I next generated clonal PG-OE cell lines. Therefore, the parental PG-OE cell line was single cell sorted based on the mCherry signal into PG^{HIGH} and PG^{LOW} cells that were subsequently expanded into several clonal cell lines. Interestingly, only PG^{HIGH} cells displayed the described changes in morphology, round and dome-shaped, whereas PG^{LOW} cells were mostly indistinguishable from the RGd2 'wild type' cells. Also, only PG^{HIGH} cells showed homogeneous REX1::GFP signal in S+LIF, in contrast to PG^{LOW} and RGd2 cells which had a bimodal GFP distribution. Taken together, these data indicated that a certain plakoglobin threshold had to be passed before being transcriptionally active. I then confirmed actual plakoglobin levels and distribution via fluorescent microscopy. Upon overexpression, plakoglobin was firstly localised to the cell membrane as seen in PG^{LOW} cells. Only when plakoglobin levels were further increased, it was found also cytoplasmic and nuclear, further consolidating the hypothesis that a plakoglobin acts in a dosage-depended manner. The homogeneous REX1::GFP signal as well as the homogeneous expression of a variety of naïve-state associated transcription factors (e.g. ESRRB, NANOG, TFCP2L1 and KLF4) in PG^{HIGH} cells prompted me to comprehensively compare the different cell lines transcriptionally via inDrop single-cell sequencing (Klein et al., 2015) to determine if plakoglobin overexpression indeed lead to the re-establishment of bona fide naïve pluripotency. Remarkably, PG^{HIGH} cells in S+LIF clustered separately from all other cells and have shifted towards the naïve control cells, RGd2 in 2i+LIF. This shift was mostly due to the re-establishment of the naïve gene regulatory network and the absence of any post-implantation and early differentiation genes (e.g. *Otx2*, *Pou3f1*, *Tubb6* and *Krt18*) known to be normally expressed in a subset of cells when cultured in S+LIF. If indeed bona fide naïve ESCs, these cells should functionally behave like RGd2 cells in 2i+LIF. Consistent with this hypothesis, PG^{HIGH} in S+LIF performed just as good as RGd2 cells in 2i+LIF during a clonogenicity assay and moreover, exhibited a 2-fold increase in chimera contribution efficiency when injected as single cells into 8-cell embryos. After having established that upregulation of plakoglobin leads to a state of naïve-like pluripotency, I next investigated how the forced expression affects the ability to exit pluripotency and enter lineage specific differentiation. When cultured in serum-based medium, PG^{HIGH} cells failed to properly exit naïve pluripotency as indicated by prolonged REX1::GFP and KLF4 signal in the absence of LIF. Having observed plakoglobin's abilities of promoting naïve-like pluripotency in serum-based medium, I next investigated its potential in sustaining naïve pluripotency in serum-free conditions. Remarkably, PG^{HIGH}, unlike RGd2 cells, were able to maintain a unimodal and positive REX1::GFP signal when solely supplemented with LIF or the ERK inhibitor PD but not with the GSK3 inhibitor CH. However, CH supplementation of the PG^{LOW} cells also resulted in stable maintenance of naïve pluripotency, suggesting that plakoglobin might act differently in promoting pluripotency

than β-catenin as normally a dual combination of LIF, PD or CH is necessary to maintain naïve pluripotency (Wray et al., 2010). This argument was further solidified with the observation that XAV treatment, a known inhibitor of β-catenin mediated transcription had no effect on plakoglobin mediated stabilisation of naïve pluripotency. To circumvent any ambiguity caused by residual β-catenin, I am in the process of using CRISPR technology to generate RGd2 and PG^{HIGH} β-catenin knockout cells, however, this project is still ongoing. After having elucidated plakoglobins ability to maintain naïve pluripotency in serum-free medium in the combination with LIF, PD or CH, I then asked how its forced expression would affect the exit from naïve pluripotency and differentiation in serum-free conditions. In contrast to serum-based medium, ectopic expression of plakoglobin did not impede the exit from naïve pluripotency but did disturb lineage specification. Thus far, these data support the hypothesis of plakoglobin's involvement in the regulation of naïve pluripotency. Yet hitherto, plakoglobin mostly appeared to be phenocopying the effects of stabilised β-catenin, despite the differences regarding its regulation (e.g. plakoglobin's unresponsiveness to XAV treatment). Of particular interest is, that β-catenin takes on different signalling functions in naïve ESCs and primed EpiSCs by promoting pluripotency and differentiation, respectively (Kim et al., 2013; Wray et al., 2011) . Hence, I was intrigued to investigate plakoglobin's role during primed pluripotency. Therefore, I initially converted RGd2 and PG^{HIGH} ESCs to EpiLCs via FGF and activin (Hayashi et al., 2011). The absence of REX1::GFP and KLF4, but expression of the core pluripotency factor OCT4 confirmed the transition into primed pluripotency. Unexpectedly, albeit being constitutively expressed, plakoglobin levels had dropped in the PG^{HIGH} cells suggesting the acute activation of its degradation mechanism. I then checked wild type post-implantation epiblast-derived stem cells, that are known to occupy the primed space of pluripotency (Brons et al., 2007; Tesar et al., 2007), for plakoglobin expression and found its complete absence in these cells. In contrast, β-catenin expression remained stable throughout naïve and primed pluripotency. The exclusive expression of plakoglobin during naïve pluripotency and its abrupt disappearance of upon transition into the primed state prompted me to examine plakoglobin during the respective states in vivo – the pre- and post-implantation embryo. Remarkably, β-catenin was found throughout all stages of development in embryonic and extraembryonic lineages whereas plakoglobin emerged only around E3.5, peaked at E4.5 and was absent from the implanted embryo at E5.5. This tight associated of plakoglobin with naïve pluripotency raised the question if forced expression of plakoglobin during primed state pluripotency would promote reprogramming to naïve pluripotency or act in synergy with β-catenin and support the regular developmental trajectory towards differentiation. To answer this question, I generated an EpiSC line exogenously expressing plakoglobin. Albeit having used the same overexpression construct as in the ESCs, EpiSC plakoglobin levels were more comparable to wild type ESCs, indicating an

intrinsically active degradation pathway of plakoglobin in EpiSCs. Nonetheless, the low levels of expressed plakoglobin were enough to cause the degradation of membrane associated β-catenin, change EpiSC morphology and increase OCT4 levels. However, I did not observe expression of naïve pluripotency associated transcription factors (e.g. KLF4 and TFCP2L1) and these cells were not able to survive under naïve culturing conditions. Finally, I investigated plakoglobin during pluripotency in human and marmoset using hPSCs, pre-implantation embryos and cmESCs, respectively. Remarkably, human and marmoset cells displayed similar expression pattern of plakoglobin as previously seen in the mouse – low levels of plakoglobin in primed cells and high levels during naïve pluripotency. In an ongoing project, I am now further expanding the microgel culture system to cmESCSs. How this culture format affects pluripotency in primate cells remains to be investigated. Taken together, these data elucidated an across different species highly conserved function of plakoglobin's role in the establishment and maintenance of naïve state pluripotency.

5 Microgel co-culture of embryonic and extraembryonic cell lines

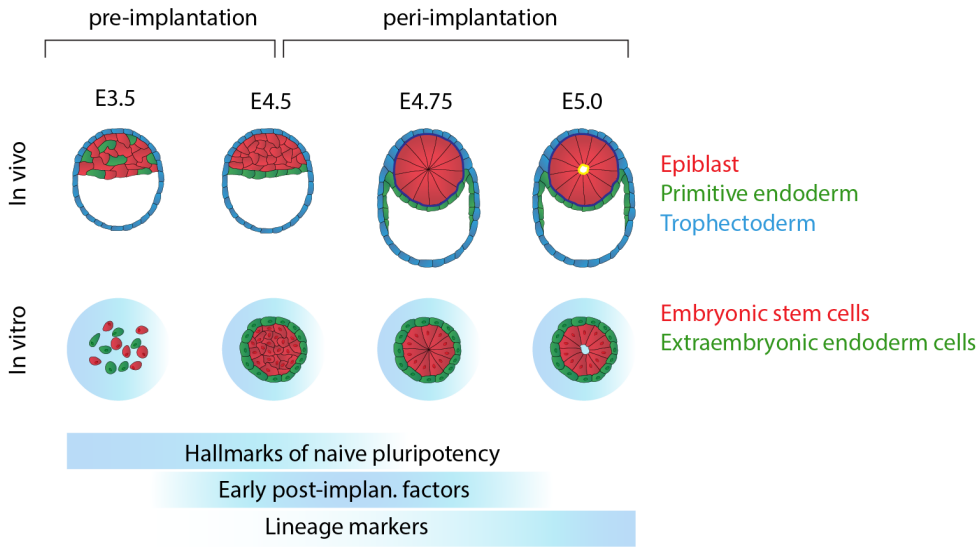

5.1 Introduction

Embryonic stem cells'(ESC) potential to indefinitely self-renew and to differentiate to all germ layers and the germ cells have been proven to be an excellent model for pluripotency and lineage specification (Thomson et al., 2011; Ying et al., 2003b). However, two-dimensional (2D), conventional tissue culture has come to its limits when, for example, trying to emulate the complex spatiotemporal events of in vivo embryogenesis. To tackle such challenges, the move towards three-dimensional (3D) culture system was just a matter of time. Some of the earliest studies date back to the early 20th century when Ross G. Harrison cultured fragments of embryonic nerve cord in hanging drops (Harrison, 1906). The same methodology was later used to aggregate ESCs into little structures, that in the absence of the pluripotency stabilising leukaemia inhibitory factor (LIF), spontaneously differentiated into the three germ layers when cultured in serum-based medium (Boxman et al., 2016). These aggregates, generally referred to as 'embryoid bodies', can be considered as some of the first attempts of modelling embryonic development in vitro as EBs show, albeit very poor, self-organisation, extracellular matrix deposition (Goh et al., 2013) and axis formation upon activation of the WNT/β-catenin pathway (ten Berge et al., 2008). Despite the possibility of manipulating EB composition, the ratio of endo-, meso- and ectoderm, via the use of different methodologies and media compositions, precise control over spatiotemporal events remains modest. EBs have been used for several decades, in more recent studies ESCs have been aggregated, in a similar fashion as EBs, but differentiated in chemically defined, serum-free medium (Baillie-Johnson et al., 2015; van den Brink et al., 2014). When mimicking extraembryonic WNT signals through the addition of the GSK3 inhibitor Chiron (CH), these aggregates displayed features of the developing embryo, including symmetry breaking, elongation and cell migration resembling the epithelial to mesenchymal transition during primitive streak formation (Baillie-Johnson et al., 2015; Turner et al., 2017). Hence, these structures have been termed 'gastruloids'. In their latest work, Beccari and colleagues have shown that, given enough time, gastruloids also display patterned *Hox* gene expression along their anterior-posterior axis, thereby acquiring another key hallmark of development (Beccari et al., 2018). Gastruloids show a major improvement in control over the spatiotemporal events compared to the mostly heterogeneous differentiation in EBs. Nonetheless, a major drawback remains the complete absence of the extraembryonic lineages – the primitive endoderm and trophectoderm, respectively. Recently, the laboratory of Magdalena Zernicka-Goetz has used the in vitro counterparts of these extraembryonic tissues, extraembryonic endoderm (XEN) cells (Kunath et al., 2005) and trophectoderm stem cells (TSC) (Tanaka et al., 1998), to generate composite cell aggregates containing embryonic and extraembryonic cells (Harrison et al., 2017; Sozen et al., 2018). In their first study, ESCs were aggregated with TSCs which subsequently self-organised into an embryonic and extraembryonic

compartment (Harrison et al., 2017). Furthermore, these aggregates which were then termed ETS-embryos, displayed the formation of polarised epithelia surrounding and inner cavity, reminiscent of the pro-amniotic cavity in the embryo. Based on the ETS-embryos, Sozen and colleagues advanced the approach by the addition of XEN cells during aggregate formation which led to self-organisation into two adjacent central compartments, an embryonic (ESC) and an extraembryonic (TSC) compartment, both of which were surrounded by a single layer of XEN cells (Sozen et al., 2018). These so called ETX-embryos indeed show many hallmarks of natural in vivo embryogenesis. In addition to closely rambling the natural embryo morphologically, ETX-embryos also undergo gastrulation-like events, show mesoderm as well as definite endoderm differentiation and display primordial germ cell-like specification (Sozen et al., 2018; Zhang et al., 2019). Although these model systems have increased in complexity and sophistication, EBs, gastruloids, ETS- and ETX-embryos all have one feature in common: they mimic peri/post-implantation development. In an attempt to model pre-implantation development, Rivron and colleagues co-cultured pre-aggregated ESCs with TSCs, which in combination with tankyrase and protein kinase A inhibition lead to the formation of structures resembling the pre-implantation blastocyst (Rivron et al., 2018). When injecting these ‘blastoids’ into the uterus, they induce decidualization but subsequently fail to develop into bona fide embryos (Li et al., 2019; Rivron et al., 2018). Finally, in one of the most recent studies, synthetic embryogenesis has been applied to model human embryonic development (Zheng et al., 2019). It was shown, that hPSCs exposed to signalling gradients within a microfluidic system can differentiate in a polarised fashion to form structures similar to the embryonic disc and the amniotic ectoderm, respectively. In this chapter, I will be describing the microfluidic-based co-encapsulation of ES and XEN cells to generate composite cell aggregates in high-throughput to model peri-implantation events of in vivo embryonic development.

5.2 Results

5.2.1 Microgel co-culture of ES and XEN cells

In the last two chapters I have described the microfluidic based culture of microgel encapsulated embryonic stem cells (ESC) and its effects on pluripotency and self-renewal. I found that biologically inert agarose microgels supported naïve pluripotency, however I hypothesised that the lack of extracellular matrix component would negatively affect cell viability as they differentiate towards somatic lineages. Indeed, when culturing encapsulated ESCs in differentiation permissive N2B27 medium, an increase in fragmented nuclei was detected in the periphery of cell colonies where cells interfaced with the agarose (**Figure 5.1 a&c**). This observation was absent when using Matrigel instead of agarose (**Figure 5.1 b&c**). Besides the lack of extensive peripheral cell death, Matrigel microencapsulated cells also acquired an apical-basal polarity, determined by the polarised expression of aPKC, as they exited pluripotency. An observation that has been previously linked to corresponding events of pro-amniotic lumen formation in the embryo (Bedzhov and Zernicka-Goetz, 2014). However, using Matrigel always comes with its inherent drawbacks – an undefined composition of ECM components and growth factors as well as variability across different batches. In vivo, basal membrane formation is mainly driven by primitive endoderm (Murray and Edgar, 2000; Salamat et al., 1995). Hence, I asked if the in vitro counterpart, extraembryonic endoderm (XEN) cells, could substitute the use of Matrigel and support ESCs differentiation in agarose microgels, thereby maintaining a fully defined culturing system (**Figure 5.1 d&e**). Therefore, I initially tested the XEN cells' ability to grow in agarose microgels and found that they grew and adopted a morphology dramatically different from their conventional culture on tissue culture plastic (**Figure 5.1 e**). Microgel encapsulated XEN cells that were in close proximity to each other, immediately started interacting via cell-cell adhesion. At 24 hours past encapsulation, XEN cells had started to arrange themselves into small colonies with a large central lumen. Over the next 24 hours this lumen would further expand and surrounding XEN cells appeared in different morphologies – from round and unpolarized to somewhat similar of a squamous epithelium. The phenomenon of lumen formation was observed in the serum-based XEN cell maintenance medium (RPMI) but also under fully defined conditions in N2B27. Next, I was intrigued to see how XEN and ES cells would interact when co-encapsulated into agarose microgels. Hence, I used a modified flow-focussing device that had two inlets, one for the XEN and another one for the ES cells (**Figure 5.1 f**). When encapsulating, I used an excess of XEN cells to ensure every ES cell would be paired with at least one XEN cell. In a typical experiment this would result in ~72% of microgels containing both cell types, ~23% only XEN cells, ~4 % only ES cells and ~1% empty gels (**Figure 5.1 g)**. Subsequently, cells were grown in N2B27 medium for up to 72 hours.

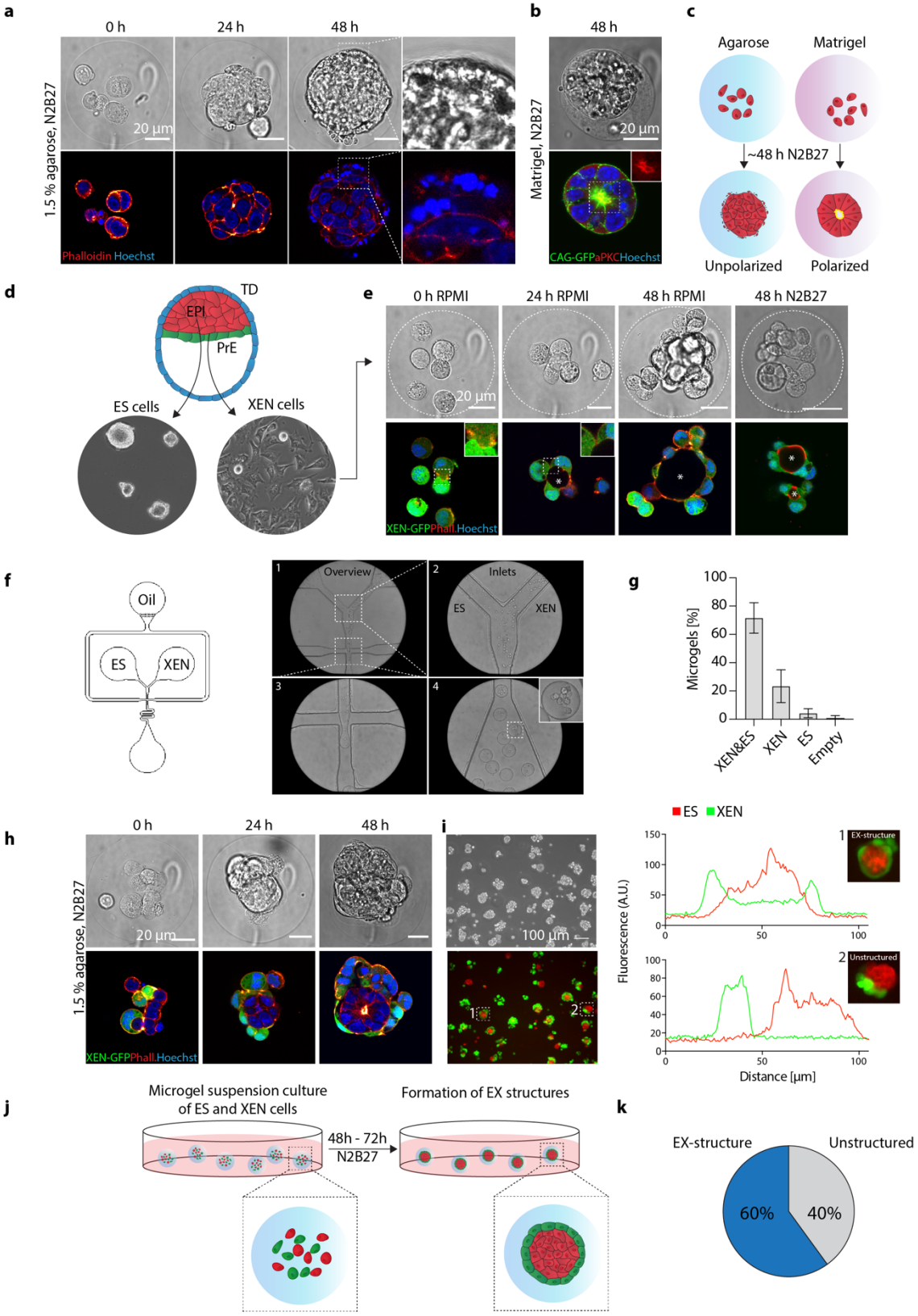

Figure caption on the next page.

Figure 5.1 | Microgel co culture of embryonic stem cells (ESC) and extraembryonic endoderm (XEN) cells. a, Representative confocal z-slice images of agarose microgel encapsulated ESCs cultured in N2B27. Filamentous actin was stained with phalloidin and nuclei were stained with Hoechst. **b**, ESCs in N2B27 medium in Matrigel microgels. ESCs were labelled with a membrane attached GFP and cells were further stained for aPKC. **c**, schematic illustration of polarised ESCs in Matrigel and unpolarised and dying cells in agarose under differentiation-permissive conditions. **d**, Illustration of the embryonic origin of ES and XEN cells. **e**, Confocal z-slice images of agarose microgel encapsulated XEN-GFP cells cultured in RPMI or N2B27. Cells were additionally stained with phalloidin and Hoechst. Lumen formation is indicated with white asterisks. **f**, Schematic illustration of a double-inlet FFD. Microscopic view of double-inlet FFD (1), cell mixing (2), droplet formation (3) and FFD outlet with droplets containing ES and XEN cells. **g**, Microgel occupancy after co-encapsulation of ES and XEN cells. **h**, Confocal z-slice images of co-encapsulated ES and XEN-GFP cells after 0 h, 24 h and 48 h in N2B27. Cells were additionally stained with phalloidin and Hoechst. **i**, EX-structures formed from ES-m-tdT and XEN-GFP cells and representative fluorescence intensity profiles of successful and unsuccessful EX-structure formation. n **j**, Schematic illustration of EX-structure formation. **k**, Efficiency of EX-structure formation.

Remarkably, despite being initially randomly distributed within the gel, after 24 hours structural reorganization became apparent, in which the XEN cells would end up on the outside of the nascent colony, surrounding an inner core of ES cells (**Figure 5.1 h-k**). When the inner ES cells were completely surrounded by XEN cells, these aggregates were then termed 'EX-structures'. To elucidate the formation of these EX-structures I used time-lapsed confocal imaging of co-encapsulated XEN-GFP and membrane-tdTomato (m-tdT) ESCs (**Figure 5.2 a&b**). Directly after encapsulation, XEN cells began to form cell-cell contacts with ESCs via highly dynamic membrane protrusions (**Figure 5.2 a**). These protrusions extended and retracted in rapid succession over the first 24 hours. Even after mitosis, XEN or ES, cells did not separate from

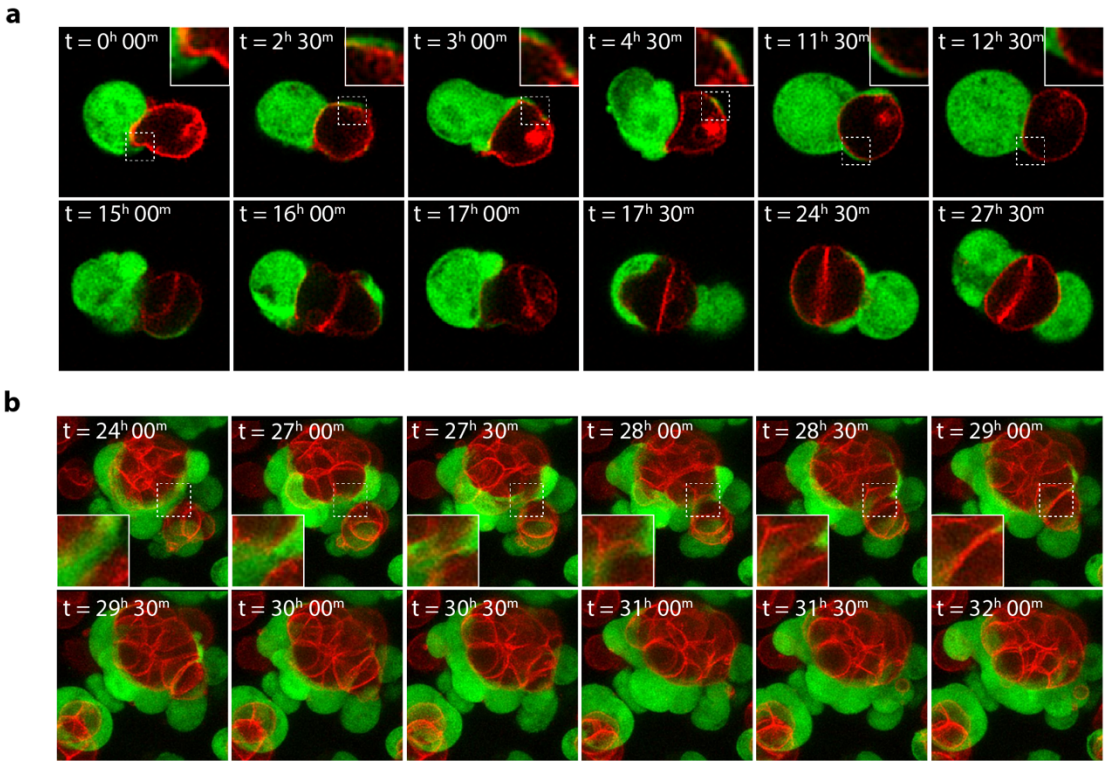

Figure 5.2 | EX-structure formation is orchestrated by highly dynamic XEN cell membrane protrusions. Time-lapsed confocal imaging of co-encapsulated XEN-GFP and m-tdT ES cells. **a**, Initial cell-cell contact between a single ES and single XEN cell. **b**, XEN cell coordinated re-arrangement of ES cells. Imaging was started after 24 hours of culture in N2B27 medium.

each other. Finally, ESCs would always end up in the centre whilst being surrounded by XEN cells. Besides probing and restraining ESCs, XEN cells additionally showed the ability to merge separate clusters of ESCs with one another (**Figure 5.2 b**). This was surprising as the agarose does not provide any extracellular matrix and adhesion sites. Consequently, ESCs grown in agarose were not able to actively migrate within the gel. Yet, XEN cells had the ability to hold on to separately growing ESC clusters and actively moving them together initiated

5.2.2 XEN cells support transition from naïve pluripotency to lineage specification of microgel cultured ESCs

To understand EX-structure formation and the underlaying mechanisms, I further scrutinized them via single-cell sequencing and immunostainings. For single-cell sequencing I used the commercially available 10x Genomics platform (**Figure 5.3 a**). EX-structures were cultured in chemically-defined N2B27 medium for ~50 hours before releasing them from the gels, disrupting to single-cell suspension and subsequent sequencing. In total, I obtained 1870 transcriptomes. To visualize gene expression across the different cell types I used T-distributed stochastic neighbour embedding (t-SNE) (van der Maaten and Hinton, 2008). Cell types were then assigned using the ESC-specific genes *Nanog* and *Pou5f1*, whereas XEN cells were defined by *Sox17*, *Gata4* and *Gata6* expression (**Figure 5.3 b**). Surprisingly, XEN cells appeared in two separate clusters indicating at least two different cell states. When investigating differential gene expression between these clusters, I found one subpopulation to be exclusively expressing *Peli2*, an ubiquitin ligase, whereas the other one displayed expression of *Srgn*, a proteoglycan first isolated from a rat yolk sac tumour cell line and also known to be expressed in the murine uterine decidua and the parietal endoderm (Keith Ho et al., 2001; Oldberg et al., 1981) (**Figure 5.3 c**). When immunostaining for Serglycin, XEN cells expressed cytoplasmic and membrane-bound protein, whereas it was not detectable in most XEN cells that had formed EX-structures in symbiosis with ES cells (**Figure 5.3 d)**. However, at this point I cannot say with certainty the origin of these distinct cell populations. Hence, additional experiments will be required to fully elucidate the origin of the different XEN cell subpopulations. When EX-structures formed, a single layer of squamous epithelial, FOXA2-positive XEN cells surrounded the ES cells which in turn also epithelised with columnar morphology (**Figure 5.3 e**). Contrary, ES cells on their own did not change their morphology upon differentiation in N2B27, failed to polarise and detected fragmented nuclei in the periphery of the majority of colonies. To confirm cell death I immunostained for the apoptosis marker cleaved caspase-3 (Porter and Janicke, 1999), and found that fragmented nuclei on the outside of the colonies were positive for cleaved caspase-3 (**Figure 5.3 f**), most likely due to the lack of extra cellular matrix in form of a basal membrane as it is known that the absence of basal membrane, in particular its laminin component, causes

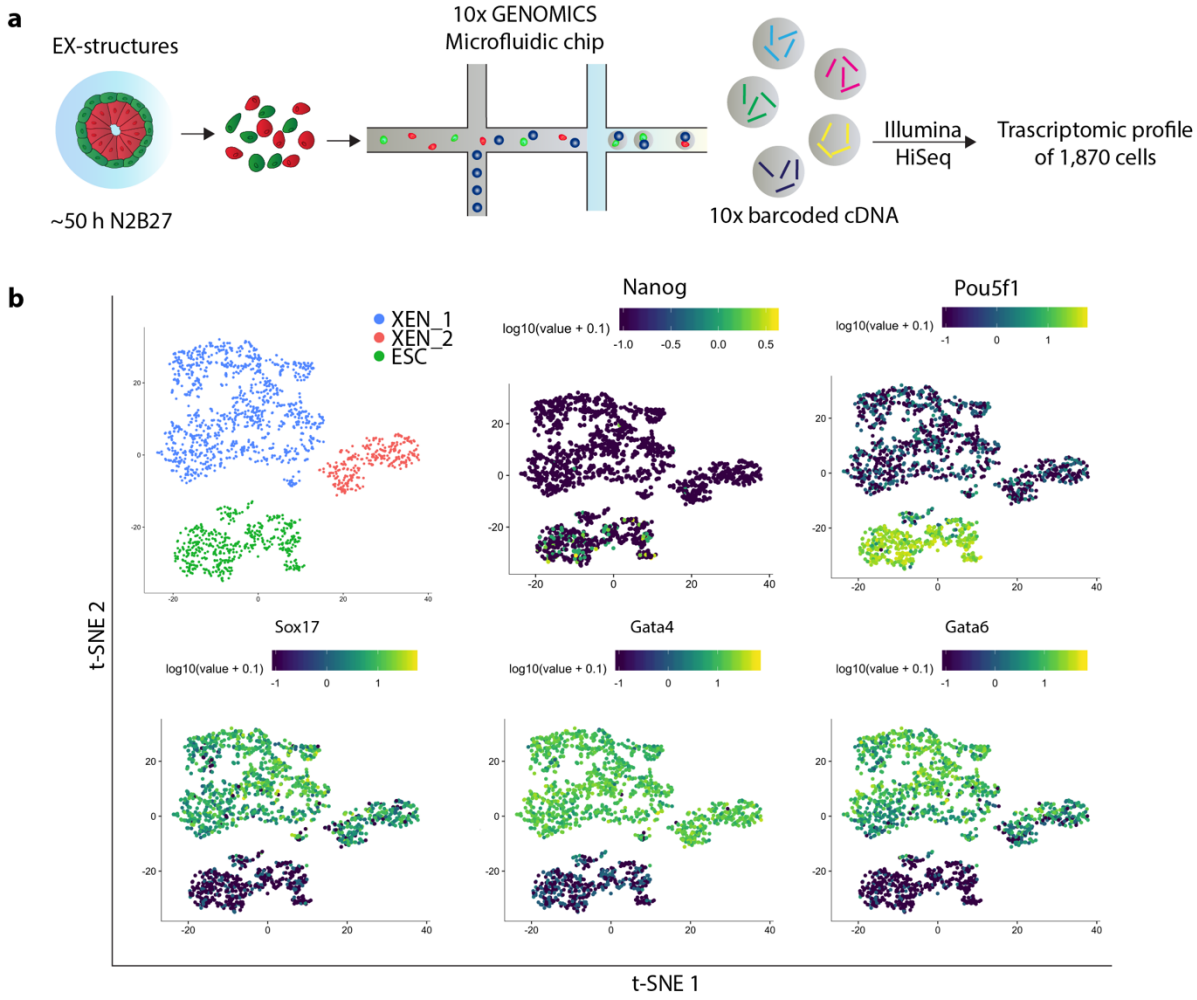

Figure caption on the next page.

Figure 5.3 | Characterisation of EX-structures via single-cell transcriptomics. a, Schematic illustration of transcriptional profiling of EX-structures via 10x GENOMICS. **b**, Lineage allocation was based on known marker expression. t-SNE plots *Nanog*, *Pou5f1* (ES cells) and *Sox17*, *Gata4* as well as *Gata6* (XEN cells). **c**, t-SNE plots for *Peli2* and *Srgn*. **d**, Confocal z-slice images of encapsulated XEN-GFP cells with or without contact to ESCs stained for Serglycin. **e&f**, Confocal z-slice images of EX-structures and encapsulated ESCs after 48 hours in N2B27 stained for OCT4/FOXA2 (**e**) and cleaved caspase-3 (**f**).

peri-implantation lethality (Coucouvanis and Martin, 1995; Smyth et al., 1999). Interestingly, in co-culture wit XEN cells, ESCs did not exhibit the previously observed systemic apoptosis and only few and scattered cells within the epithelium underwent cell death. In the developing embryo, basal membrane deposition is mainly driven by endodermal precursors (Li et al., 2004; Li et al., 2003; Li et al., 2002), hence I was intrigued to elucidate the XEN cells' ability to deposit a basal membrane. Therefore, I initially analysed on transcriptional level the expression of the core basal membrane component laminin and found that both XEN subpopulations displayed strong and homogeneous expression of *Lama1*, *Lamb1* and *Lamc1* (**Figure 5.4 a**). Subsequently, I immunostained EX-structures after 72 hours in N2B27 for laminin protein and found a distinct layer of laminin in between the two epithelia – the squamous XEN cells and the columnar ES cells (**Figure 5.4 b**). Furthermore, EX-structures were characterised by a central lumen, reminiscent of the pro-amniotic cavity in the embryo. Due to the deposition of the basal membrane component laminin and the cavity formation, I hypothesised, that the ESCs would

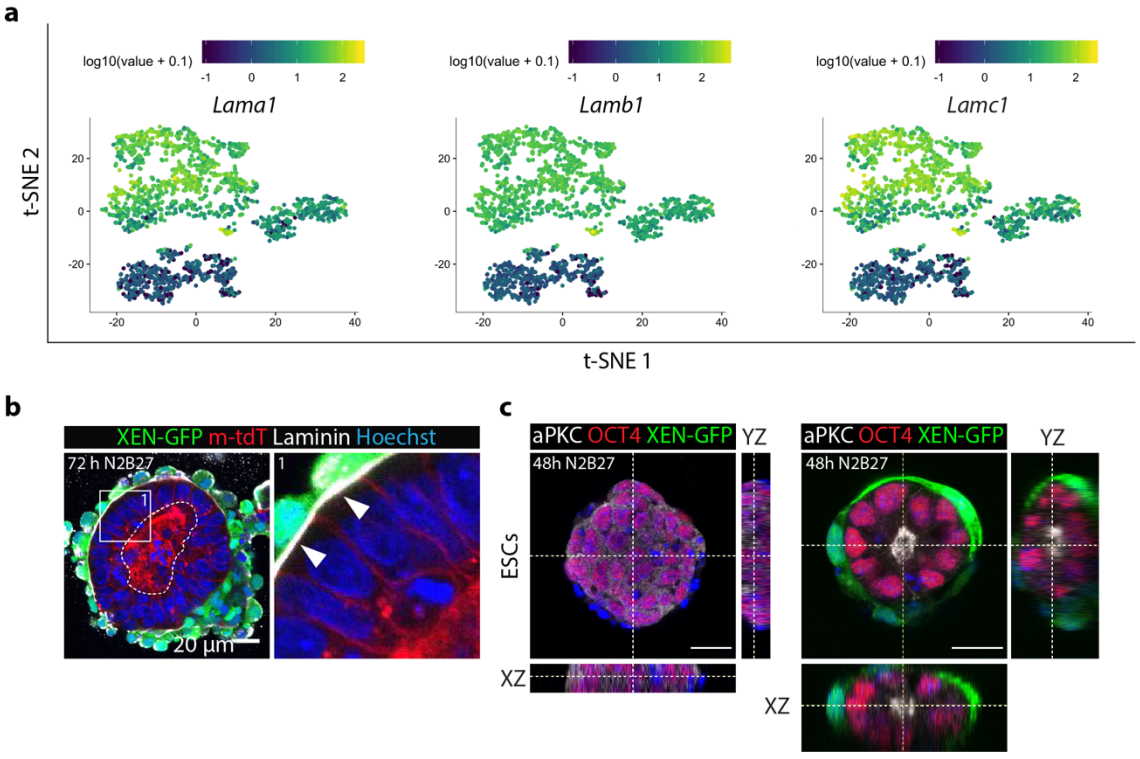

Figure 5.4 | XEN cells deposit the basal membrane component laminin, thereby supporting polarisation of ESCs. **a**, t-SNE plots for the laminin isoforms *Lama1*, *Lamb1* and *Lamc1*. **b**, Representative confocal z-slice image of an EX-structure after 72 hours of culture in N2B27 stained for laminin (basal lamina formation indicated by white arrow heads. Central lumen outlined by a white, dotted line). **c**, Confocal z-slice images of an encapsulated ESC colony and an EX-structure cultured for 48 hours in N2B27 stained for OCT4 and aPKC.

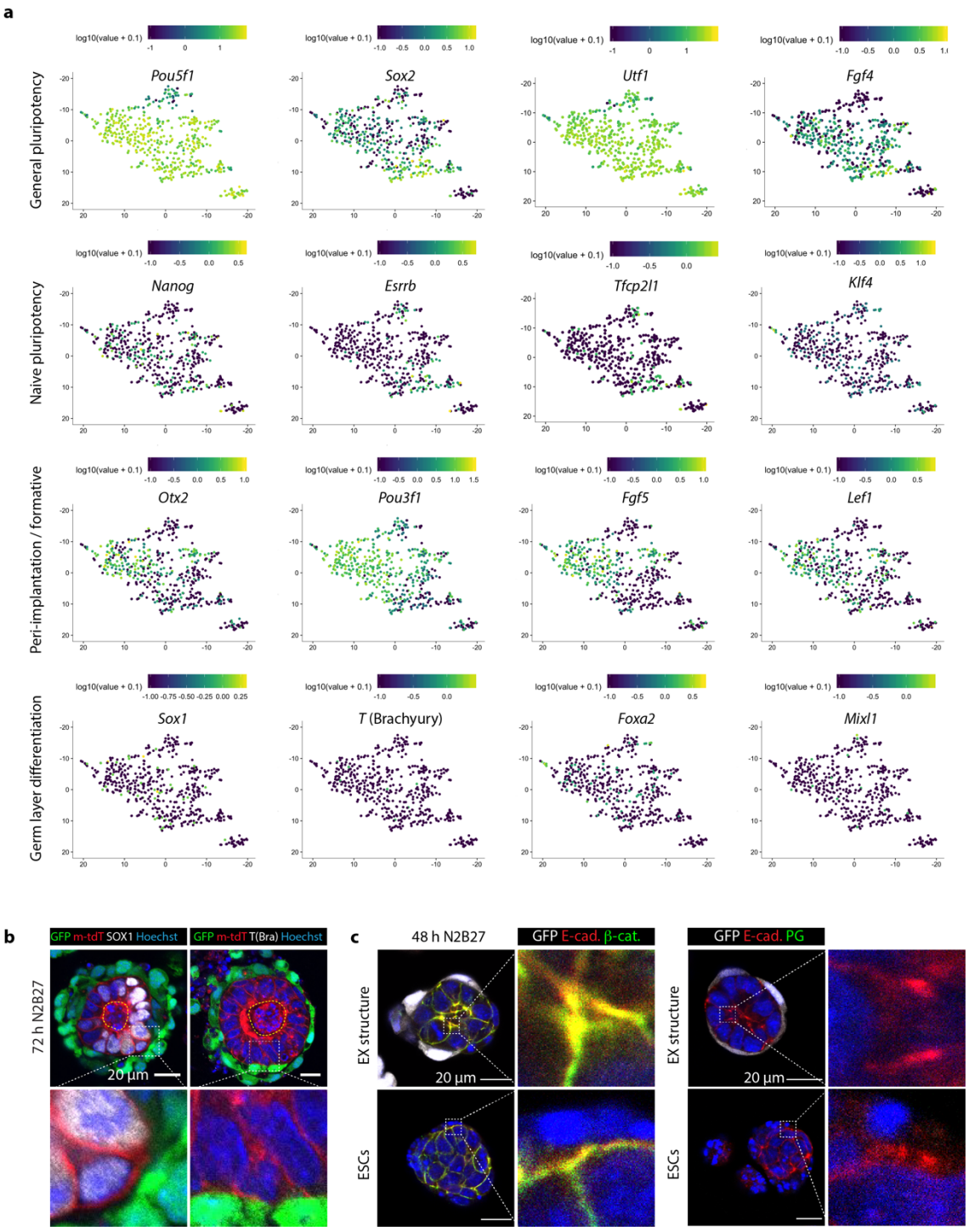

Figure 5.5 | XEN cells support the transition from naïve to primed pluripotency and subsequent lineage specification in EX-structures. a, t-SNE plots for general and naïve pluripotency associated genes as well as markers for peri-implantation and germ layer specification. **b**, Confocal z-slice images of EX-structures after 72 hours in N2B27 stained for the neuroectodermal precursor marker SOX1 and the mesendodermal precursor marker T (Brachyury). **c**, Confocal z-slice images of EX-structures and encapsulated ESCs after 48 hours in N2B27 stained for E-cadherin, β-catenin and plakoglobin.

display localised apical marker proteins towards the lumen. To confirm the acquisition of correct apical-basal polarity, I then stained for the polarity marker aPKC (Ohno, 2001) 48 hours past encapsulation. I found, that EX-structures would display clear localisation of aPKC towards the centre of the colony (**Figure 5.4 c**). Having shown, that the co-culture of XEN and ES cells

resulted in a fundamentally different morphology, basal membrane deposition, polarization and lumen formation, none of which can be detected in the absence of XEN cells, I next investigated the transcriptional state of ES cells in more detail (**Figure 5.5 a**). Two days into the differentiation process of EX-structures in N2B27, ESCs still homogeneously expressed the general pluripotency transcription factors *Pou5f1* and *Utf1* whereas *Sox2* and *Fgf4* already appeared heterogeneously. In contrast, the naïve pluripotency gene regulatory network had been completely downregulated. In the vast majority of cells, the naïve pluripotency associated transcription factors such as *Nanog*, *Esrrb*, *Tfcp2l1* or *Klf4* were detectable anymore. Simultaneously, peri-implantation markers, such as *Otx2*, *Pou3f1*, *Fgf5* and *Lef1* were upregulated, indicating the transition into primed pluripotency. Further evidence for the acquisition of primed pluripotency, was the complete absence of lineage specific marker genes including *Sox1*(neuroectoderm), *Mixl1* (mesoderm), *Foxa2* (endoderm) and primitive streak associated transcription factor *Brachyury*. To confirm the EX-structure's ability to enter lineage-specific differentiation, I extended the culture period to 72 hours in N2B27. At this point, EX-structures did not upregulate Brachyury (*T*) but consistently displayed expression of the neuroectodermal precursor marker SOX1(**Figure 5.5 b**). This result was expected, since N2B27 as a serum-free medium, and the absence trophectoderm did not supply any inductive cues such as BMPs or WNTs, which are known to be necessary for mesendoderm specification. Finally, with regard to the previous chapter, in which I investigated the functions and mechanisms of plakoglobin and β-catenin during different states of pluripotency, I was naturally also interested in analysing expression of these proteins in EX-structures. Consistent with my previous data, EX-structures but also ES cells encapsulated on their own, maintained expression of β-catenin and E-cadherin during differentiation towards primed pluripotency and subsequent lineage specification, whereas plakoglobin was not detectable anymore (**Figure 5.5 c**).

5.3 Conclusions

Biologically inert agarose microgels are a suitable culturing format for embryonic stem cells (ESCs) when kept under self-renewing and pluripotent conditions (see chapter 3). However, due to the lack of extracellular matrix components and their concomitant adhesion sites, agarose has a very limited ability to support the exit from pluripotency or promote lineage specification. Upon release from 2i+LIF (pluripotency) into N2B27 (differentiation), ESCs were able to exit from naïve pluripotency, but failed to enter proper lineage specific differentiation due to extensive apoptotic cell death. Previous studies have shown that differentiating ESCs can acquire morphological features, similar to the peri-implantation rosette structure of the embryo, when cultured in Matrigel (Bedzhov and Zernicka-Goetz, 2014). Yet, Matrigel is an undefined combination of extracellular matrix components and growth factors, making mechanistical

studies troublesome. To circumvent this issue, I made use of extraembryonic endoderm (XEN) cells that are known for their ability to deposit extracellular matrix components such as laminin. In this chapter I have used the previously described microgel culture system, to co-encapsulate XEN and ES cells. I hypothesised that matrix deposition by XEN cells would support the differentiation of ES cells in the otherwise biologically inert microgels. Microgel encapsulated XEN cells had a distinct phenotype from the conventional culture on plastic – in the gels, cells were perfectly spherical and, unlike on plastic, and interacted immediately via cell-cell contacts with one another. These interactions lead to the formation of a central lumen with the first 24 hours, a morphology that was observed in serum-based XEN cell maintenance medium (RMPI), but also in serum-free N2B27. Remarkably, when co-encapsulating both cells types, a morphological self-organisation was observed in which the XEN cells ended up in the periphery of the nascent colony, surrounding an inner core of ES cells. Upon complete enclosure of the ES cell by the XEN cells, these aggregates were termed EX-structures. Time-lapsed confocal imaging revealed that this sorting process into EX-structures was mostly orchestrated by the XEN cell, through highly dynamic membrane protrusions. I then used a combined approach of single cell sequencing with immunostainings to further investigate EX-structure formation and progression. Transcriptionally, ES and XEN cells were easily identified by lineage specific markers such as *Pou5f1* and *Gata4*, respectively. However, unexpectedly, XEN cells appeared with at least two distinct transcriptional signatures of hitherto unknown origin. However, differential gene expression analysis revealed specific genes for each XEN subpopulation, e.g. *Srgn* and *Peli2*. Subsequent immunofluorescent analyses suggested that physical contact with ESCs might be the cause for a distinct population of XEN cells. Nonetheless, additional experiments are required to fully elucidate the origin and function of the different type of XEN cells. Furthermore, XEN cells surrounding the ESCs took on a squamous epithelial morphology whereas ES cells appeared to have acquired a columnar epithelial shape. This change in morphology was accompanied by a reduction in apoptotic cell death which had been observed upon exit from pluripotency in the absence of XEN cells. Hypothesised due to the absence of any extracellular matrix. Indeed, XEN cell did express high levels of laminin transcripts and deposited it resembling the basal lamina in the embryo. Besides laminin deposition by the XEN cells, EX-structures had acquired an overall apical-basal polarity as seen by localised aPKC expression towards the centre of the colonies. Followed by lumen expansion and subsequent lineage specification. Taken together, these data elucidate that microgel co-culture of ES and XEN cells as EX-structures, enables the transit from naïve pluripotency into a state of primed pluripotency, similar to the peri-implantation embryo.

6 General discussion and outlook

Over the course of this dissertation, I have outlined the interdisciplinary approach of combining microfluidic technologies with traditional cell biology. In the first part, I have described the establishment of a microgel culture system for mouse embryonic stem cells (ESCs) and elucidated how such microenvironmental changes would affect general cell behaviour, but in particular, their pluripotent potential (Chapter 3). After identifying plakoglobin as one of the most differentially expressed proteins between conventional tissue culture plastic and microgel culture, I further investigated its role in ESC maintenance, pluripotency and differentiation (Chapter 4). In the final results chapter, I then explored how microgels could potentially be used as co-culture systems for different cell lines from the embryo (Chapter 5). Over the next several paragraphs I will be discuss the salient conclusions of the individual chapters in detail, and also give an outlook on what direction this research might take in the future.

6.1 Advantages and drawbacks of microgels for the culture of embryonic stem cells

Over the last several years, the trend towards sophisticated three-dimensional (3D) tissue culture and the use of synthetic bioengineering has allowed researchers to answer a multiplicity of question that could have not been elucidated solely by the use of conventional, two-dimensional (2D), tissue culture. New tissue-specific adult stem cells continue to be identified and are subsequently used to establish 3D ‘organoids’ in the hope to model diseases better and to understand how organs develop and gain function (Huch and Koo, 2015; Rossi et al., 2018). Similarly, ESCs, and more recently extraembryonic cell lines, have been utilised for ‘synthetic embryogenesis’, as such systems are much better at representing the complex developmental mechanisms of embryogenesis compared to 2D culture. Furthermore, they allow access to the otherwise in vivo inaccessible counterparts (Vianello and Lutolf, 2019). Simultaneously with the rise of 3D systems, physical properties of the culture environment, such as stiffness, adhesion, topography and degradability, shifted into focus as it became apparent that tissues and their occupying cells can mechano-sense their microenvironment and react correspondingly (Discher et al., 2005). To study such mechanical effects, a variety of natural and synthetic as well as 2D and 3D hydrogels have been used (Lutolf et al., 2009). In particular, microgels (instead of bulk gels) offer the advantage of large-scale production in bioreactors, better diffusion on nutrients and waste products, their compatibility with other microfluidics systems (e.g. droplet sorting and long-term perfusion culture) and they hold the possibility to evaluate matrix composition in a high-throughput fashion (Allazetta and Lutolf, 2015; Kleine-Bruggeney et al., 2019). As such, they have become a valuable tool for biology with a variety of applications (Allazetta and Lutolf, 2015; Orive et al., 2004; Theberge et al., 2010).

Our lab has previously shown, that agarose microgels are a suitable system for the culture of mouse ESCs, but how this culture method would affect cell behaviour remained to be investigated (Kleine-Bruggeney et al., 2019). Agarose is a naturally occurring thermosensitive polysaccharide and has the advantages of being cheap, optically transparent and well suited for the use in microfluidics. When using low-melting agarose, it can be kept liquid at 37 °C for cell encapsulation, but subsequently stays gellified at 37 °C after polymerisation by cooling on ice. Furthermore, agarose can be digested by the simple addition of the bacterial enzyme 'agarase' (Yaphe, 1957), allowing cell retrieval at any given time for down-stream analysis including FACS, RNA-seq and chimera injection studies. Consequently, agarose cannot be intrinsically degraded by mammalian cells, a property which effects remain to be investigated. Also, agarose is 'biologically inert' and does not provide ECM molecules and adhesion sites, which could potentially render it unsuitable for cell differentiation as integrin-ECM interactions are known to be of crucial importance (Hayashi et al., 2007). In return, this property could actually be beneficial for maintenance of the pluripotency network as differentiation inducing cues by the ECM are lacking. Additional support for the pluripotency network could be grounded in the relative softness of agarose microgels. For adult stem cells, it is widely accepted, that substrate stiffness can influence lineage choice (Engler et al., 2006), however, mechano-sensing in ESCs remains debated. Whilst some studies claim that ESCs only become mechanosensitive upon exit from pluripotency (Chowdhury et al., 2010b; Evans et al., 2009; Verstreken et al., 2019), others implicate maintenance of the pluripotency network to be directly affected by the stiffness/softness of the microenvironment (Chowdhury et al., 2010a; Lu et al., 2014). In a recent pre-print study, Labouesse and colleagues use 2D polyacrylamide gels, spanning a wide range of substrate stiffness and adhesion-sides, to elucidate how soft substrates act in 'boosting' pluripotency by supressing ERK, and promoting STAT3 signalling (Labouesse et al., 2019). Yet, all the studies above focus on S+LIF cultured ESCs, which appear to show more pronounced phenotypes regarding mechano-signalling, and do not investigate the microenvironmental effects on naïve/ground state pluripotency. This approach makes sense, in particular due to the ERK inhibition under 2i+LIF conditions, but also means, that one might miss potentially small albeit meaningful differences.

In vivo, at the state of naïve epiblast formation, the embryo undergoes repetitive changes in blastocoelic pressure, leading to mechanosensitive tight junction formation in the trophectoderm (Chan et al., 2019). Although this study did not investigate the effects of luminal-pressure changes on the nascent naïve epiblast, it certainly allows us to contemplate a potential role of mechano-signalling in the establishment of pluripotency. Consistent with the previously mentioned studies, I also have observed a 'boost' in pluripotency, upon microgel encapsulation of S+LIF cultured ESCs. These cells showed an increase of naïve-state associated

transcription factors and acquired the round and stress fibre-free phenotype of naïve cells. Remarkably, even under naïve culture conditions (2i+LIF), microgel-encapsulated cells exhibited an upregulation across the naïve gene regulatory network as measure by whole-transcriptome analysis. What this observation means, in particular with regard to 2i+LIF cells already being transcriptionally very close to their in vivo counterpart, the epiblast, needs further investigation. Besides changes in pluripotency associated transcription factors, genes regulating epigenetic plasticity and genome structure appeared to be differentially regulated when cultivating cells in agarose microgels. This finding is consistent with the hypothesis, that soft and chemically defined 3D environments can enhance reprogramming of somatic cells to iPSCs by promoting epigenetic remodelling (Caiazzo et al., 2016; Downing et al., 2013). Therefore, in the future of this project, it will be interesting to investigate if, and how, microgel culture influences the epigenome of S+LIF and 2i+LIF cultured ESCs.

Consistent with Labouesse's work, I also observe an increase in the LIF/STAT3 and additionally also in the WNT/β-catenin signalling pathways, based on the upregulation of their downstream negative regulators SOCS3 and AXIN2, respectively. Yet, unexpectedly no differences across the expression of the typical signalling components of these pathways were observed. Consequently, I also analysed the extended protein network and found that the β-catenin homologue plakoglobin (γ-catenin) and another armadillo protein, p120 (δ-catenin) were significantly upregulated. The role of p120 in stabilising adherens junctions has been well established (Xiao et al., 2007). Furthermore, p120 has been shown to influence stem cell differentiation (Lee et al., 2014b) and regulate WNT signalling as well as EMT induction during primitive streak formation in the embryo (Hernandez-Martinez et al., 2019). Interestingly, in *Drosophila*, p120 has recently been shown to undergo mechanosensitive re-localisation, which in turn leads to restructuring of the junctional network (Iyer et al., 2019). Plakoglobin's role however, is more ambiguous.

6.2 Plakoglobin, a previously unknown member of the naïve gene regulatory network?

In comparison to β-catenin and δ-catenin, little is known about the β-catenin vertebrate homologue plakoglobin, also known as γ-catenin (Gene name: *Jup*). Originally identified as a member of the desmosomal plaque (Cowin et al., 1986; Franke et al., 1983), it was then mostly studied in the 90's but quickly disregarded due to its less severe knockout phenotype in comparison to β-catenin. β-catenin null embryos fail to undergo gastrulation and cannot establish the AP-axis, whereas plakoglobin null embryos develop until around E10.5 at which point they die due to severe failure in heart and skin formation (Bierkamp et al., 1996; Haegel et al., 1995;

Huelsken et al., 2000b; Ruiz et al., 1996). In mouse ESCs, β-catenin's transcriptional role in the maintenance of pluripotency has been well established (Lyashenko et al., 2011; Wray et al., 2011). Although plakoglobin gets upregulated upon knockout of β-catenin, it cannot compensate for its transcriptional activity (Lyashenko et al., 2011). And still, upon agarose microgel encapsulation of naïve mouse ESCs, typical WNT/β-catenin targets, such as *Axin2*, *Esrrb* and *Sp5*, were upregulated and simultaneously accompanied by an upregulation of plakoglobin expression, but surprisingly not β-catenin. Due to the concomitant 'boost' across the pluripotency network and the significant upregulation of plakoglobin, I hypothesised that these two observations might be connected.

At this point, it is not known what causes the upregulation of plakoglobin in microgel encapsulated ESCs, but one might suspect that mechano-sensing could be involved. To test this idea, several different systems could be tested and plakoglobin levels examined. If it is indeed the stiffness of the substrate orchestrating plakoglobin expression, the 2D polyacrylamide gels designed by Labouesse and colleagues could be used as they cover a broad range of stiffnesses (Labouesse et al., 2019). However, if confinement and pressure rather than stiffness is the underlaying cause of plakoglobin upregulation, 2D surfaces (even with varying stiffnesses) would not be able to deliver the desired physical properties. Hence, future experiments will also include the comparison of microgel and hanging drop cultured ESCs, and the release of ESC colonies after microgel culture followed by culture in the hanging drop format to see if plakoglobin will be immediately degraded upon the release from the microgel-mediated pressure. Additionally, a plakoglobin knockout cell line will be required to confirm that the stabilisation of the pluripotency network upon encapsulation is exclusively mediated through plakoglobin.

To further test the idea, that a causation between increase in plakoglobin and boost in pluripotency exists, I generated a plakoglobin overexpression cell line. Previous work has demonstrated, that stabilisation of plakoglobin in ESCs leads to neuroectodermal differentiation defects due to retention of pluripotency factors, however, this study failed to fully assess the state of pluripotency and did not include any in vivo references (Mahendram et al., 2013). Yet, consistent with this work, my plakoglobin overexpressing cells also failed to upregulate neuroectodermal markers upon differentiation, regardless of their starting condition (2i+LIF or S+LIF). Remarkably, when reaching a critical threshold, plakoglobin overexpressing ESCs in S+LIF, became morphologically indistinguishable, from naïve ESCs in 2i+LIF. Further, these cells exhibited a homogeneous REX1-GFPd2 signal as well as homogeneous expression of the naïve state associated transcription factors such as KLF4 and TFCP2L1. Due to this unexpected shift towards naïve pluripotency upon overexpression of plakoglobin, I decided to fully characterise

the state of pluripotency via extensive transcriptional single-cell profiling. Subsequent analysis, confirmed the re-establishment of a naïve-like pluripotency. Plakoglobin overexpressing cells distinguished themselves from all other S+LIF based ESCs by the strong and homogeneous expression of the naïve gene regulatory network as described by Boroviak and colleagues (Boroviak et al., 2014; Boroviak et al., 2015), and the absence of early differentiation markers such as *Otx2* and *Pou3f1*. Additionally, plakoglobin overexpressing cells differed in their expression of the metabolic enzyme *Thd*, which is known to be downregulated upon differentiation (Kalkan et al., 2017; Wang et al., 2009) and several epigenetic regulators including *Tets* and *Dnmts*. It is well known that ESCs in S+LIF and 2i+LIF have distinct epigenetic signatures regarding histone modifications and DNA methylation state (Marks et al., 2012). Hence, future analysis of the epigenome in plakoglobin overexpressing cells will allow an even more comprehensive understanding of the state of pluripotency. Re-establishment of naïve state-like pluripotency was based on the observation, that plakoglobin overexpressing cells displayed homogeneous expression of the members of the naïve gene regulatory network. However, to doubtlessly confirm the existence of ground state pluripotency, a functional read out in the form of chimera-contribution efficiency was needed. When injecting single S+LIF cultured ESCs into the 8-cell state embryo, contribution efficiency is generally very poor, but improved upon culture in 2i+LIF (Martin Gonzalez et al., 2016; Wang and Jaenisch, 2004). Surprisingly, I did not observe a significant difference in chimera contribution efficiency between the wild type cells, regardless of their culture conditions. However, plakoglobin overexpressing cells in S+LIF displayed a doubling in contribution efficiency, thereby supplying further evidence, that these cells are indeed bona fide naïve-like stem cells.

In ESCs, naïve pluripotency can be maintained by any dual combination of the components of 2i+LIF (Wray et al., 2010). If cultured in LIF, PD or CH alone, pluripotency gets dismantled and ESCs initiate differentiation. In contrast, high plakoglobin overexpressing cells can be maintained self-renewing and pluripotent in the sole presence of LIF or PD. Though, it was still possible, that plakoglobin acted indirectly through β-catenin, by releasing it from the membrane and thereby promoting its transcriptional activity. However, my evidence suggests otherwise, because low plakoglobin overexpressing cells can be maintained by CH alone. This result suggests, that plakoglobin might have transcriptional targets distinct from β-catenin, which remain to be identified via e.g. ChIP-seq. If plakoglobin would have acted indirectly through β-catenin, maintenance in CH alone should have not been possible due to the necessity for dual inhibition/stimulation (Wray et al., 2010). This hypothesis was further supported by the observation that plakoglobin appeared to be unaffected by XAV treatment, a known inhibitor of β-catenin mediated transcription (Zimmerlin et al., 2016). Still, to fully eliminate any remaining

ambiguity regarding the differences in β-catenin and plakoglobin mediated transcription, clonal and homozygous knockouts for both proteins will need to be generated. If plakoglobin overexpressing cells can then be maintained naïve pluripotent in the absence of β-catenin with the sole treatment of either LIF or PD then we could say with certainty that plakoglobin can promote pluripotency independently of β-catenin. To this end, the exact mechanism by which plakoglobin promotes pluripotency remains elusive. Previous studies have shown differential interactions of β-catenin and plakoglobin with the TCF/LEF transcription factors (Shimizu et al., 2008). In particular the abrogation of the repressive function of TCF7L1 on the pluripotency network by β-catenin has been described in detail, however it is believed that plakoglobin cannot substitute in β-catenin knockout cells (Lyashenko et al., 2011; Wray et al., 2011). This observation and my finding that low overexpressing cells can be maintained pluripotent with CH alone, suggest two separately working ways of maintaining pluripotency. However, due to their structural similarity I believe that plakoglobin, just like β-catenin, acts as a transcriptional co-factor in regulating the transcriptional pluripotency network by either promoting the expression of pluripotency supporting transcription factors or alleviating the effects of differentiation initiating transcription factors.

As I had previously observed differentiation defects in the plakoglobin overexpressing cells, I was wondering at what point during differentiation, plakoglobin became inhibitory. Therefore, I transferred the naïve-like plakoglobin overexpressing cells from S+LIF, to primed conditions generating epiblast-like cells (EpiLCs) (Hayashi et al., 2011). I was surprised to find, that although plakoglobin transcription remained stable, protein levels had almost disappeared completely, suggesting post-translational regulation via intrinsic activation of the degradation pathway upon exit from naïve pluripotency. This discovery prompted me to further investigate plakoglobin expression during primed pluripotency in epiblast-derived stem cells (EpiSCs) (Brons et al., 2007; Tesar et al., 2007). Consistent with the observation in EpiLCs, EpiSCs were devoid of plakoglobin, but remained positive for β-catenin. These experiments showed for the first time a hitherto unknown differential expression of plakoglobin during naïve and primed state pluripotency.

Although in developmental biology quickly disregarded as a less important homologue of β-catenin, plakoglobin received special attention in the field of cancer biology. In particular, due to its distinct function from β-catenin in acting as a tumour suppresser rather than having oncogenic potential like β-catenin (Alaee et al., 2018; Kolligs et al., 2000; Korinek et al., 1997). So, is it possible, that there are also more plakoglobin-specific developmental functions, that we might have overlooked? To answer this question, I investigated plakoglobin and β-catenin levels

throughout early embryonic development. Consistent with previous reports, I found β-catenin to be expressed throughout all stages of pre- and post-implantation development, whereas plakoglobin only emerges with the formation of the blastocysts and therefore, simultaneously with the establishment of pluripotency (Boroviak et al., 2014; Ohsugi et al., 1996; Ohsugi et al., 1997). In particular, due to the absence of desmosomes in the pre-implantation epiblast (Fleming et al., 1991; Hardy et al., 1996), the question arises why plakoglobin is suddenly expressed and where exactly it locates to adjunct to the membrane? With regard to its location there are two seemingly obvious options. Option 1: Since binding of β-catenin and plakoglobin to E-cadherin is mutually exclusive (Nathke et al., 1994; Ozawa et al., 1989), plakoglobin might partially replace β-catenin in the adherens junctions of the epiblast resulting in two different types of complexes – one with β-catenin and one with plakoglobin. Option 2: Plakoglobin associates with another and yet to be determined membrane-bound protein. In vitro, plakoglobin as well as β-catenin have been shown to interact with the epidermal growth factor receptor (EGFR) (Lorch et al., 2004; Miravet et al., 2003). Interestingly, EGFR appears to be another mechanosensitive signalling component which might be of interest regarding our findings of mechano-responsive (in particular pressure) upregulation of plakoglobin in embryonic stem cells (Saxena et al., 2017). In future experiments I will therefore address plakoglobin's potential association with the EGFR in vivo. Furthermore, I will try and regulate the pressure within the embryonic blastocoel as described by Chan and colleagues to investigate if the sudden appearance of plakoglobin within the epiblast is caused by the increase in pressure during cavity expansion (Chan et al., 2019).

Just as surprising as plakoglobin's sudden appearance, is its abrupt loss upon implantation, further supporting the hypothesis of a pluripotency-specific role of plakoglobin. Overexpression of β-catenin in the pre-implantation embryo leads to premature EMT and failure in AP-axis formation due to lack of neuroectodermal specification (Kemler et al., 2004). Embryonal overexpression of plakoglobin was only studied in *Xenopus* where it leads to axis duplication, indicating additional plakoglobin functions beyond mediating cell-adhesion (Karnovsky and Klymkowsky, 1995). The question remains: If plakoglobin has indeed a specific role in naïve pluripotency, what happens when plakoglobin is ectopically expressed during primed pluripotency? β-catenin mediated transcription is known to support naïve pluripotency in ESCs (Lyashenko et al., 2011; Wray et al., 2011), but leads to rapid differentiation in primed EpiSCs (Kim et al., 2013; Sumi et al., 2013). Consistent with these studies, stabilisation of β-catenin by CH treatment caused EpiSCs to differentiate. In contrast, forced plakoglobin expression appeared to actually stabilise pluripotency as indicated by an increase in OCT4 reporter signal. Conclusively these data indicate, that β-catenin and plakoglobin's transcriptional function diverge upon transition from naïve to primed pluripotency.

EpiSCs do not spontaneously revert to naïve pluripotency when transferred to 2i+LIF (Brons et al., 2007; Tesar et al., 2007), but require the forced expression of a naïve state-associated transcription factor such as KLF4 (Guo et al., 2009). So far, ectopic plakoglobin expression did not yield naïve induced pluripotent EpiSCs. However, although overexpressed, plakoglobin levels remained low in EpiSCs. Most likely due to the strongly activated, but unidentified, degradation pathway of plakoglobin. Future experiments concerning the short-term proteasomal inhibition with the small molecule inhibitor MG-132 or replacing destabilising phosphorylation sites via mutagenesis, might be beneficial for reprogramming purposes. Additionally, it has been shown, that the cadherin-catenin-complex associates with the epidermal growth factor receptor (EGFR) (Hoschuetzky et al., 1994), and that inhibition of the receptor can stabilise plakoglobin keratinocytes and squamous cell carcinoma cells (Lorch et al., 2004; Yin et al., 2005). Hence, one might try to regulate plakoglobin levels by treating ESCs and EpiSCs with the well-established EGFR inhibitor PKI-166.

Intriguingly, β-catenin's promotion of naïve pluripotency appears to be a mouse ESC-specific feature. Although naïve rat ESCs have been derived in 2i+LIF (Buehr et al., 2008), they remain susceptible to spontaneous differentiation if the amount of β-catenin signalling is not well mediated through correct titration of CH (Chen et al., 2013). The same observation was made during the first resetting experiments of human pluripotent stem cells (PSCs) towards the naïve state (Takashima et al., 2014). Recently, it was shown, that indeed inhibition of β-catenin-mediated transcription with XAV, rather than stabilisation of β-catenin by CH, is beneficial for stabilising pluripotency in human stem cells (Zimmerlin et al., 2016). Since then, the majority of studies involving human PSCs have shifted towards using a combination of PD, XAV, LIF and GÖ (PXLG) to maintain naïve pluripotency (Bredenkamp et al., 2019; Guo et al., 2017). Remarkably, I have observed a strong increase in plakoglobin levels, but not β-catenin when comparing primed against naïve hPSCs. Similar results were obtained when resetting conventional marmoset stem cells towards naïve-like pluripotency. Since my previous results indicate a plakoglobin-specific role in the establishment of naïve pluripotency, it would be of great value to investigate how primate stem cells behave upon forced expression of plakoglobin.

6.3 Microgel co-culture of embryonic and extraembryonic cell lines

After having establishing a microfluidic-based 3D culture system for embryonic stem cells followed by in-depth characterisation of these microgel encapsulated cells, in particular with regard to their state of pluripotency, I was naturally interested in taking the system one step further and investigate ESC differentiation. Hence, the last part of this dissertation was devoted to the

preliminary exploration into the suitability of the microgel-system as a tool for stem cell differentiation. Although well suited for the maintenance of pluripotent cells, agarose turned out to perform poorly in supporting differentiation. This finding was most likely due to the complete absence of any extra cellular matrix which is crucial for integrin binding and subsequent differentiation (Hayashi et al., 2007). In particular, laminin knockout embryos fail to develop past the per-implantation stage due to failure in basal lamina formation (Coucouvanis and Martin, 1995; Smyth et al., 1999). Although basal lamina can be provided by supplementing media with Matrigel (Bedzhov and Zernicka-Goetz, 2014), I intended to keep working under defined conditions. Since in the developing embryo, basal membrane deposition is mainly driven by endodermal precursors (Li et al., 2004; Li et al., 2003; Li et al., 2002), extraembryonic endoderm (XEN) cells appeared to be a promising candidate for aiding ESC differentiation in agarose microgels. Indeed, co-encapsulation of ES and XEN cells led to formation of self-organising aggregates with a phenotype similar to the peri-implantation epiblast (Bedzhov and Zernicka-Goetz, 2014). These aggregates, termed EX-structures, exhibited basal lamina deposition, acquired correct apical-basal polarity, which is followed by central lumen formation and lineage-specific differentiation. Intriguingly, RNA-seq revealed the existence of two XEN cell transcriptional subpopulations when cultured in EX-structure format. To this end, their origin remains elusive and could be caused by several different reasons: 1) XEN cells already exists as two distinct populations in regular maintenance culture – or 2) XEN cells separate into these apparent sub-populations upon co-culture with embryonic stem cells. For the first point the observation speaks that freshly derived, as well as long term cultured, XEN cells appear in two distinct morphologies, either as highly refractile or epithelial-like (Kunath et al., 2005; Niakan et al., 2013). However, paracrine signalling (soluble signalling molecules and direct cell-cell interactions) between the encapsulated ESCs and XEN cells, might also be contributing to the existence of transcriptionally distinct XEN cell clusters. To address this question, XEN cells will need to be single cell sequenced on their own before starting the co-culture with ESCs. Although XEN cells have been described as the in vitro representative for the primitive endoderm, they are transcriptionally distinct from the in vivo primitive endoderm(Zhong and Binas, 2019). XEN cells as well as ESC-derived END2 and PYS2 endoderm-like cells lack the expression of OCT4, however, OCT4 is present in the in vivo primitive endoderm (Brown et al., 2010). Reducing the concentration of serum and the additional supplementation with PDGF in the culture medium eventually allowed the derivation of primitive XEN cell (pXEN) (Zhong et al., 2018). pXEN cells do express OCT4 but still cluster separately from their supposed in vivo counterpart. Alternatively, one could consider the use of expanded potential stem cells (EPSCs) (Yang et al., 2017a; Yang et al., 2017b). EPSCs have the potential to contribute to extraembryonic lineages and thereby bypass the need to maintain endoderm-like cells for prolonged period in culture. In the future, this system could be an addition to the already existing systems for studying

spatiotemporal differentiation events in vitro. Microgels can be used to co-encapsulate any possible combination of cell types into a chemically defined matrix. Already, we are developing new ways of investigating cell-cell communication by co-culturing different cell types, such systems include e.g. the co-culture of:

1) Trophoblast stem cells and endometrial cells to investigate the mechanisms of how the trophectoderm initiates interactions with, and eventually invades the decidua of the maternal uterus.

2) Marmoset ESCs and fibroblasts to elucidate early lineage decision of non-human primate PSCs. To this end we have generated a fully-defined system that enables us to control differentiation towards an amnion-like population or the emergence of an embryonic disc-like structure.

3) Liver organoid progenitor cells and mesenchymal cells to investigate how liver homeostasis is maintained (Cordero-Espinoza et al, 2020 preprint https://doi.org/10.1101/2020.09.21.306258)

7 Conclusion and working hypothesis

Over the course of this dissertation, I have (1) established a microgel culture system for embryonic stem cells, which (2) led to the identification of a hitherto unknown function of plakoglobin in the establishment and maintenance of naïve pluripotency and finally, (3) extended the microgel system for the co-culture of embryonic and extraembryonic cells resulting in aggregate formation with morphological and transcriptional features of the peri-implantation epiblast. Although rather an unsophisticated hydrogel, agarose microgels turned out to be a well-suited system for the culture of embryonic stem cells due to unexpected beneficial effects regarding the pluripotency network. Microenvironmentally-induced upregulation of plakoglobin appeared to be one of the main contributing factors. Overexpression of plakoglobin in S+LIF cultured ESCs was able to re-establish a state of naïve-like pluripotency. Furthermore, I found β-catenin and plakoglobin expression to be distinct from one another during naïve and primed states of pluripotency (**Figure 7.1**). This feature seems to be evolutionary well-conserved as similar observation were made in human and marmoset stem cells. The data suggests, that β-catenins functions in promoting naïve pluripotency switches to inducing differentiation upon the transition into primed pluripotency, whereas plakoglobin expression remains to have beneficial effects on the pluripotency network, regardless of which pluripotent state the cells are in (**Figure 7.1**).

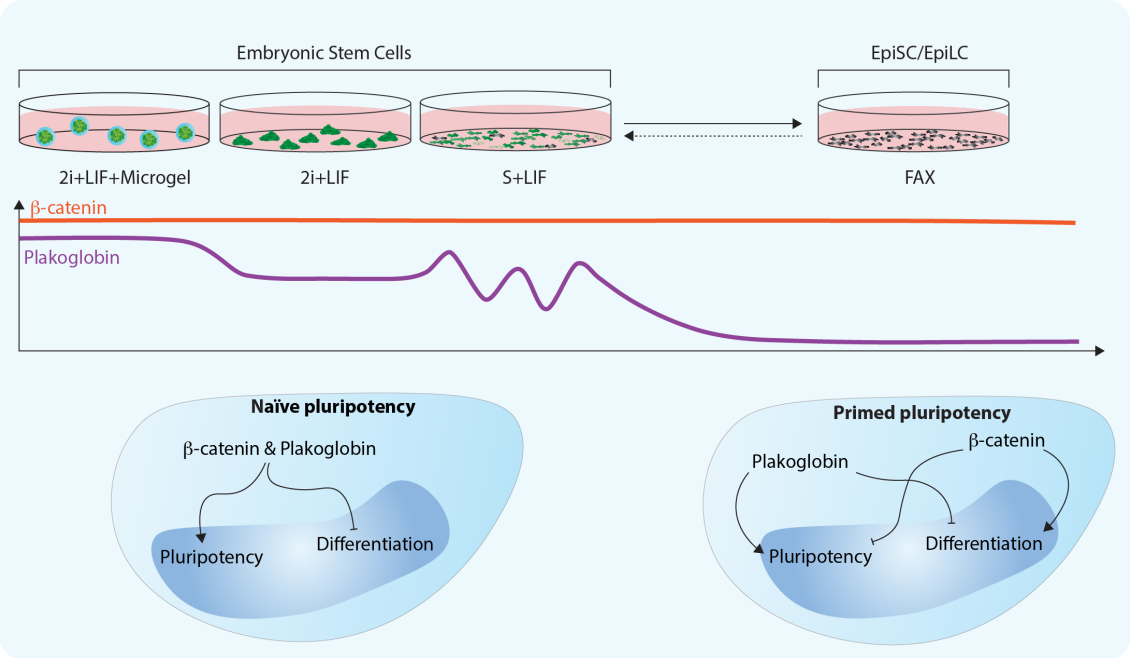

Figure 7.1 | Plakoglobin and β-catenin's function diverge upon transition from naïve to primed pluripotency. Depending on their culture conditions, ESCs express varying levels of plakoglobin. However, plakoglobin abruptly disappears upon differentiation towards primed pluripotency. Current data suggests, that plakoglobin and b-catenin both support maintenance of the naïve pluripotency network in ESCs. Yet, during primed pluripotency, β-catenin's function shifts towards differentiation induction effects whereas ectopic plakoglobin expression remains beneficial to the pluripotency network.

8 References

Ahier, A., and Jarriault, S. (2014). Simultaneous expression of multiple proteins under a single promoter in Caenorhabditis elegans via a versatile 2A-based toolkit. Genetics *196*, 605-613.

Aiken, C.E., Swoboda, P.P., Skepper, J.N., and Johnson, M.H. (2004). The direct measurement of embryogenic volume and nucleo-cytoplasmic ratio during mouse pre-implantation development. Reproduction *128*, 527-535.

Aktary, Z., Alaee, M., and Pasdar, M. (2017). Beyond cell-cell adhesion: Plakoglobin and the regulation of tumorigenesis and metastasis. Oncotarget *8*, 32270-32291.

Alaee, M., Nool, K., and Pasdar, M. (2018). Plakoglobin restores tumor suppressor activity of p53(R175H) mutant by sequestering the oncogenic potential of beta-catenin. Cancer Sci *109*, 1876-1888.

Allazetta, S., Kolb, L., Zerbib, S., Bardy, J., and Lutolf, M.P. (2015). Cell-Instructive Microgels with Tailor-Made Physicochemical Properties. Small *11*, 5647-5656.

Allazetta, S., and Lutolf, M.P. (2015). Stem cell niche engineering through droplet microfluidics. Curr Opin Biotechnol *35*, 86-93.

Anna, S.L., Bontoux, N., and Stone, H.A. (2003). Formation of dispersions using "flow focusing" in microchannels. Applied Physics Letters *82*, 364-366.

Ashburner, M., Ball, C.A., Blake, J.A., Botstein, D., Butler, H., Cherry, J.M., Davis, A.P., Dolinski, K., Dwight, S.S., Eppig, J.T.*, et al.* (2000). Gene ontology: tool for the unification of biology. The Gene Ontology Consortium. Nat Genet *25*, 25-29.

Avilion, A.A., Nicolis, S.K., Pevny, L.H., Perez, L., Vivian, N., and Lovell-Badge, R. (2003). Multipotent cell lineages in early mouse development depend on SOX2 function. Genes Dev *17*, 126-140.

Aziz, M., and Alexandre, H. (1991). The origin of the nascent blastocoele in preimplantation mouse embryos ultrastructural cytochemistry and effect of chloroquine. Roux Arch Dev Biol *200*, 77-85.

Baillie-Johnson, P., van den Brink, S.C., Balayo, T., Turner, D.A., and Martinez Arias, A. (2015). Generation of Aggregates of Mouse Embryonic Stem Cells that Show Symmetry Breaking, Polarization and Emergent Collective Behaviour In Vitro. J Vis Exp.

Barcroft, L.C., Offenberg, H., Thomsen, P., and Watson, A.J. (2003). Aquaporin proteins in murine trophectoderm mediate transepithelial water movements during cavitation. Dev Biol *256*, 342-354.

Beccari, L., Moris, N., Girgin, M., Turner, D.A., Baillie-Johnson, P., Cossy, A.C., Lutolf, M.P., Duboule, D., and Arias, A.M. (2018). Multi-axial self-organization properties of mouse embryonic stem cells into gastruloids. Nature *562*, 272-276.

Beddington, R.S., and Robertson, E.J. (1999). Axis development and early asymmetry in mammals. Cell *96*, 195-209.

Bedzhov, I., and Zernicka-Goetz, M. (2014). Self-organizing properties of mouse pluripotent cells initiate morphogenesis upon implantation. Cell *156*, 1032-1044.

Behrens, J., von Kries, J.P., Kuhl, M., Bruhn, L., Wedlich, D., Grosschedl, R., and Birchmeier, W. (1996). Functional interaction of beta-catenin with the transcription factor LEF-1. Nature *382*, 638-642.

Benos, D.J., Biggers, J.D., Balaban, R.S., Mills, J.W., and Overstrom, E.W. (1985). Developmental aspects of sodium-dependent transport processes of preimplantation rabbit embryos. Soc Gen Physiol Ser *39*, 211-235.

Berryman, M., Franck, Z., and Bretscher, A. (1993). Ezrin is concentrated in the apical microvilli of a wide variety of epithelial cells whereas moesin is found primarily in endothelial cells. J Cell Sci *105 (Pt 4)*, 1025-1043.

Bertocchi, C., Wang, Y., Ravasio, A., Hara, Y., Wu, Y., Sailov, T., Baird, M.A., Davidson, M.W., Zaidel-Bar, R., Toyama, Y.*, et al.* (2017). Nanoscale architecture of cadherin-based cell adhesions. Nature Cell Biology *19*, 28-37.

Biase, F.H., Cao, X., and Zhong, S. (2014). Cell fate inclination within 2-cell and 4-cell mouse embryos revealed by single-cell RNA sequencing. Genome Res *24*, 1787-1796.

Biechele, S., Cockburn, K., Lanner, F., Cox, B.J., and Rossant, J. (2013). Porcn-dependent Wnt signaling is not required prior to mouse gastrulation. Development *140*, 2961-2971.

Bierkamp, C., McLaughlin, K.J., Schwarz, H., Huber, O., and Kemler, R. (1996). Embryonic heart and skin defects in mice lacking plakoglobin. Dev Biol *180*, 780-785.

Blakeley, P., Fogarty, N.M., Del Valle, I., Wamaitha, S.E., Hu, T.X., Elder, K., Snell, P., Christie, L., Robson, P., and Niakan, K.K. (2015). Defining the three cell lineages of the human blastocyst by single-cell RNA-seq. Development *142*, 3613.

Boretto, M., Cox, B., Noben, M., Hendriks, N., Fassbender, A., Roose, H., Amant, F., Timmerman, D., Tomassetti, C., Vanhie, A.*, et al.* (2017). Development of organoids from mouse and human endometrium showing endometrial epithelium physiology and long-term expandability. Development *144*, 1775-1786.

Boroviak, T., Loos, R., Bertone, P., Smith, A., and Nichols, J. (2014). The ability of inner-cell-mass cells to self-renew as embryonic stem cells is acquired following epiblast specification. Nat Cell Biol *16*, 516-528.

Boroviak, T., Loos, R., Lombard, P., Okahara, J., Behr, R., Sasaki, E., Nichols, J., Smith, A., and Bertone, P. (2015). Lineage-Specific Profiling Delineates the Emergence and Progression of Naive Pluripotency in Mammalian Embryogenesis. Dev Cell *35*, 366-382.

Boroviak, T., and Nichols, J. (2017). Primate embryogenesis predicts the hallmarks of human naive pluripotency. Development *144*, 175-186.

Boroviak, T., Stirparo, G.G., Dietmann, S., Hernando-Herraez, I., Mohammed, H., Reik, W., Smith, A., Sasaki, E., Nichols, J., and Bertone, P. (2018). Single cell transcriptome analysis of human, marmoset and mouse embryos reveals common and divergent features of preimplantation development. Development *145*.

Bottenstein, J.E., and Harvey, A.L. (1985). Cell Culture in the Neurosciences. Plenum Press: New York and London, 3.

Boxman, J., Sagy, N., Achanta, S., Vadigepalli, R., and Nachman, I. (2016). Integrated live imaging and molecular profiling of embryoid bodies reveals a synchronized progression of early differentiation. Sci Rep *6*, 31623.

Bradley, A., Evans, M., Kaufman, M.H., and Robertson, E. (1984). Formation of germ-line chimaeras from embryo-derived teratocarcinoma cell lines. Nature *309*, 255-256.

Bredenkamp, N., Stirparo, G.G., Nichols, J., Smith, A., and Guo, G. (2019). The Cell-Surface Marker Sushi Containing Domain 2 Facilitates Establishment of Human Naive Pluripotent Stem Cells. Stem Cell Reports.

Brennan, J., Lu, C.C., Norris, D.P., Rodriguez, T.A., Beddington, R.S., and Robertson, E.J. (2001). Nodal signalling in the epiblast patterns the early mouse embryo. Nature *411*, 965-969.

Brewer, G.J., Torricelli, J.R., Evege, E.K., and Price, P.J. (1993). Optimized survival of hippocampal neurons in B27-supplemented Neurobasal, a new serum-free medium combination. J Neurosci Res *35*, 567-576.

Briggs, J.A., Weinreb, C., Wagner, D.E., Megason, S., Peshkin, L., Kirschner, M.W., and Klein, A.M. (2018). The dynamics of gene expression in vertebrate embryogenesis at single-cell resolution. Science *360*.

Brons, I.G., Smithers, L.E., Trotter, M.W., Rugg-Gunn, P., Sun, B., Chuva de Sousa Lopes, S.M., Howlett, S.K., Clarkson, A., Ahrlund-Richter, L., Pedersen, R.A.*, et al.* (2007). Derivation of pluripotent epiblast stem cells from mammalian embryos. Nature *448*, 191-195.

Brown, K., Legros, S., Artus, J., Doss, M.X., Khanin, R., Hadjantonakis, A.K., and Foley, A. (2010). A comparative analysis of extra-embryonic endoderm cell lines. PLoS One *5*, e12016.

Buehr, M., Meek, S., Blair, K., Yang, J., Ure, J., Silva, J., McLay, R., Hall, J., Ying, Q.L., and Smith, A. (2008). Capture of authentic embryonic stem cells from rat blastocysts. Cell *135*, 1287-1298.

Butz, S., and Kemler, R. (1994). Distinct cadherin-catenin complexes in Ca(2+)-dependent cell-cell adhesion. FEBS Lett *355*, 195-200.

Butz, S., Stappert, J., Weissig, H., and Kemler, R. (1992a). Plakoglobin and Beta-Catenin - Distinct but Closely Related. Science *257*, 1142-1144.

Butz, S., Stappert, J., Weissig, H., and Kemler, R. (1992b). Plakoglobin and beta-catenin: distinct but closely related. Science *257*, 1142-1144.

Cai, L., Ye, Z., Zhou, B.Y., Mali, P., Zhou, C., and Cheng, L. (2007). Promoting human embryonic stem cell renewal or differentiation by modulating Wnt signal and culture conditions. Cell Res *17*, 62-72.

Caiazzo, M., Okawa, Y., Ranga, A., Piersigilli, A., Tabata, Y., and Lutolf, M.P. (2016). Defined three-dimensional microenvironments boost induction of pluripotency. Nat Mater *15*, 344-352.

Camus, A., Perea-Gomez, A., Moreau, A., and Collignon, J. (2006). Absence of Nodal signaling promotes precocious neural differentiation in the mouse embryo. Dev Biol *295*, 743-755.

Cano, A., Perez-Moreno, M.A., Rodrigo, I., Locascio, A., Blanco, M.J., del Barrio, M.G., Portillo, F., and Nieto, M.A. (2000). The transcription factor snail controls epithelial-mesenchymal transitions by repressing E-cadherin expression. Nat Cell Biol *2*, 76-83.

Carey, B.W., Finley, L.W., Cross, J.R., Allis, C.D., and Thompson, C.B. (2015). Intracellular alpha-ketoglutarate maintains the pluripotency of embryonic stem cells. Nature *518*, 413-416.

Carver, E.A., Jiang, R., Lan, Y., Oram, K.F., and Gridley, T. (2001). The mouse snail gene encodes a key regulator of the epithelial-mesenchymal transition. Mol Cell Biol *21*, 8184-8188.

Cassar, P.A., Carpenedo, R.L., Samavarchi-Tehrani, P., Olsen, J.B., Park, C.J., Chang, W.Y., Chen, Z., Choey, C., Delaney, S., Guo, H*., et al.* (2015). Integrative genomics positions MKRN1 as a novel ribonucleoprotein within the embryonic stem cell gene regulatory network. EMBO Rep *16*, 1334-1357.

Casser, E., Israel, S., Witten, A., Schulte, K., Schlatt, S., Nordhoff, V., and Boiani, M. (2017). Totipotency segregates between the sister blastomeres of two-cell stage mouse embryos. Sci Rep *7*, 8299.

Chambers, I., Colby, D., Robertson, M., Nichols, J., Lee, S., Tweedie, S., and Smith, A. (2003). Functional expression cloning of Nanog, a pluripotency sustaining factor in embryonic stem cells. Cell *113*, 643-655.

Chambers, I., Silva, J., Colby, D., Nichols, J., Nijmeijer, B., Robertson, M., Vrana, J., Jones, K., Grotewold, L., and Smith, A. (2007). Nanog safeguards pluripotency and mediates germline development. Nature *450*, 1230-1234.

Chan, C.J., Costanzo, M., Ruiz-Herrero, T., Monke, G., Petrie, R.J., Bergert, M., Diz-Munoz, A., Mahadevan, L., and Hiiragi, T. (2019). Hydraulic control of mammalian embryo size and cell fate. Nature *571*, 112-116.

Charpentier, E., Lavker, R.M., Acquista, E., and Cowin, P. (2000). Plakoglobin suppresses epithelial proliferation and hair growth in vivo. J Cell Biol *149*, 503-520.

Chazaud, C., and Rossant, J. (2006). Disruption of early proximodistal patterning and AVE formation in Apc mutants. Development *133*, 3379-3387.

Chazaud, C., Yamanaka, Y., Pawson, T., and Rossant, J. (2006). Early lineage segregation between epiblast and primitive endoderm in mouse blastocysts through the Grb2-MAPK pathway. Dev Cell *10*, 615-624.

Chen, G., Gulbranson, D.R., Hou, Z., Bolin, J.M., Ruotti, V., Probasco, M.D., Smuga-Otto, K., Howden, S.E., Diol, N.R., Propson, N.E*., et al.* (2011). Chemically defined conditions for human iPSC derivation and culture. Nat Methods *8*, 424-429.

Chen, Q., Shi, J.C., Tao, Y., and Zernicka-Goetz, M. (2018). Tracing the origin of heterogeneity and symmetry breaking in the early mammalian embryo. Nat Commun *9*.

Chen, Y., Blair, K., and Smith, A. (2013). Robust self-renewal of rat embryonic stem cells requires fine-tuning of glycogen synthase kinase-3 inhibition. Stem Cell Reports *1*, 209-217.

Chowdhury, F., Li, Y., Poh, Y.C., Yokohama-Tamaki, T., Wang, N., and Tanaka, T.S. (2010a). Soft substrates promote homogeneous self-renewal of embryonic stem cells via downregulating cell-matrix tractions. PLoS One *5*, e15655.

Chowdhury, F., Na, S., Li, D., Poh, Y.C., Tanaka, T.S., Wang, F., and Wang, N. (2010b). Material properties of the cell dictate stress-induced spreading and differentiation in embryonic stem cells. Nat Mater *9*, 82-88.

Christodoulou, N., Kyprianou, C., Weberling, A., Wang, R., Cui, G., Peng, G., Jing, N., and Zernicka-Goetz, M. (2018). Sequential formation and resolution of multiple rosettes drive embryo remodelling after implantation. Nat Cell Biol *20*, 1278-1289.

Conlon, F.L., Lyons, K.M., Takaesu, N., Barth, K.S., Kispert, A., Herrmann, B., and Robertson, E.J. (1994). A primary requirement for nodal in the formation and maintenance of the primitive streak in the mouse. Development *120*, 1919-1928.

Coucouvanis, E., and Martin, G.R. (1995). Signals for death and survival: a two-step mechanism for cavitation in the vertebrate embryo. Cell *83*, 279-287.

Cowin, P., Kapprell, H.P., Franke, W.W., Tamkun, J., and Hynes, R.O. (1986). Plakoglobin - a Protein Common to Different Kinds of Intercellular Adhering Junctions. Cell *46*, 1063-1073.

Daniel, J.M., and Reynolds, A.B. (1995). The tyrosine kinase substrate p120cas binds directly to E-cadherin but not to the adenomatous polyposis coli protein or alpha-catenin. Mol Cell Biol *15*, 4819-4824.

Daniels, R.W., Rossano, A.J., Macleod, G.T., and Ganetzky, B. (2014). Expression of multiple transgenes from a single construct using viral 2A peptides in Drosophila. PLoS One *9*, e100637.

Davidson, K.C., Adams, A.M., Goodson, J.M., McDonald, C.E., Potter, J.C., Berndt, J.D., Biechele, T.L., Taylor, R.J., and Moon, R.T. (2012). Wnt/beta-catenin signaling promotes differentiation, not self-renewal, of human embryonic stem cells and is repressed by Oct4. Proc Natl Acad Sci U S A *109*, 4485-4490.

Davidson, K.C., Mason, E.A., and Pera, M.F. (2015). The pluripotent state in mouse and human. Development *142*, 3090-3099.

Davis, M.A., Ireton, R.C., and Reynolds, A.B. (2003). A core function for p120-catenin in cadherin turnover. J Cell Biol *163*, 525-534.

del Valle, I., Rudloff, S., Carles, A., Li, Y., Liszewska, E., Vogt, R., and Kemler, R. (2013). E-cadherin is required for the proper activation of the Lifr/Gp130 signaling pathway in mouse embryonic stem cells. Development *140*, 1684-1692.

Di-Gregorio, A., Sancho, M., Stuckey, D.W., Crompton, L.A., Godwin, J., Mishina, Y., and Rodriguez, T.A. (2007). BMP signalling inhibits premature neural differentiation in the mouse embryo. Development *134*, 3359-3369.

Ding, J., Yang, L., Yan, Y.T., Chen, A., Desai, N., Wynshaw-Boris, A., and Shen, M.M. (1998). Cripto is required for correct orientation of the anterior-posterior axis in the mouse embryo. Nature *395*, 702-707.

Discher, D.E., Janmey, P., and Wang, Y.L. (2005). Tissue cells feel and respond to the stiffness of their substrate. Science *310*, 1139-1143.

Doble, B.W., Patel, S., Wood, G.A., Kockeritz, L.K., and Woodgett, J.R. (2007). Functional redundancy of GSK-3alpha and GSK-3beta in Wnt/beta-catenin signaling shown by using an allelic series of embryonic stem cell lines. Dev Cell *12*, 957-971.

Downing, T.L., Soto, J., Morez, C., Houssin, T., Fritz, A., Yuan, F., Chu, J., Patel, S., Schaffer, D.V., and Li, S. (2013). Biophysical regulation of epigenetic state and cell reprogramming. Nat Mater *12*, 1154-1162.

Dravid, G., Ye, Z., Hammond, H., Chen, G., Pyle, A., Donovan, P., Yu, X., and Cheng, L. (2005). Defining the role of Wnt/beta-catenin signaling in the survival, proliferation, and self-renewal of human embryonic stem cells. Stem Cells *23*, 1489-1501.

Dufort, D., Schwartz, L., Harpal, K., and Rossant, J. (1998). The transcription factor HNF3beta is required in visceral endoderm for normal primitive streak morphogenesis. Development *125*, 3015-3025.

Dumont, J.N., and Brummett, A.R. (1985). Egg envelopes in vertebrates. Dev Biol (N Y 1985) *1*, 235-288.

Dunn, N.R., Vincent, S.D., Oxburgh, L., Robertson, E.J., and Bikoff, E.K. (2004). Combinatorial activities of Smad2 and Smad3 regulate mesoderm formation and patterning in the mouse embryo. Development *131*, 1717-1728.

Engler, A.J., Sen, S., Sweeney, H.L., and Discher, D.E. (2006). Matrix elasticity directs stem cell lineage specification. Cell *126*, 677-689.

Evans, M.J., and Kaufman, M.H. (1981). Establishment in culture of pluripotential cells from mouse embryos. Nature *292*, 154-156.

Evans, N.D., Minelli, C., Gentleman, E., LaPointe, V., Patankar, S.N., Kallivretaki, M., Chen, X., Roberts, C.J., and Stevens, M.M. (2009). Substrate stiffness affects early

differentiation events in embryonic stem cells. Eur Cell Mater *18*, 1-13; discussion 13-14.

Fan, R., Kim, Y.S., Wu, J., Chen, R., Zeuschner, D., Mildner, K., Adachi, K., Wu, G., Galatidou, S., Li, J.*, et al.* (2020). Wnt/Beta-catenin/Esrrb signalling controls the tissue-scale reorganization and maintenance of the pluripotent lineage during murine embryonic diapause. Nat Commun *11*, 5499.

Faunes, F., Hayward, P., Descalzo, S.M., Chatterjee, S.S., Balayo, T., Trott, J., Christoforou, A., Ferrer-Vaquer, A., Hadjantonakis, A.K., Dasgupta, R.*, et al.* (2013). A membrane-associated beta-catenin/Oct4 complex correlates with ground-state pluripotency in mouse embryonic stem cells. Development *140*, 1171-1183.

Fierro-Gonzalez, J.C., White, M.D., Silva, J.C., and Plachta, N. (2013). Cadherin-dependent filopodia control preimplantation embryo compaction. Nat Cell Biol *15*, 1424-1433.

Finley, M.F., Devata, S., and Huettner, J.E. (1999). BMP-4 inhibits neural differentiation of murine embryonic stem cells. J Neurobiol *40*, 271-287.

Fleming, T.P., Garrod, D.R., and Elsmore, A.J. (1991). Desmosome biogenesis in the mouse preimplantation embryo. Development *112*, 527-539.

Franke, W.W., Mueller, H., Mittnacht, S., Kapprell, H.P., and Jorcano, J.L. (1983). Significance of 2 Desmosome Plaque-Associated Polypeptides of Molecular-Weights 75000 and 83000. Embo J *2*, 2211-2215.

Fujita, Y., Krause, G., Scheffner, M., Zechner, D., Leddy, H.E.M., Behrens, J., Sommer, T., and Birchmeier, W. (2002). Hakai, a c-Cbl-like protein, ubiquitinates and induces endocytosis of the E-cadherin complex. Nature Cell Biology *4*, 222-231.

Fukunaga, Y., Liu, H.J., Shimizu, M., Komiya, S., Kawasuji, M., and Nagafuchi, A. (2005). Defining the roles of beta-catenin and plakoglobin in cell-cell adhesion: Isolation of beta-catenin/plakoglobin-deficient F9 cells. Cell Struct Funct *30*, 25-34.

Gibson, D.G., Young, L., Chuang, R.Y., Venter, J.C., Hutchison, C.A., 3rd, and Smith, H.O. (2009). Enzymatic assembly of DNA molecules up to several hundred kilobases. Nat Methods *6*, 343-345.

Goh, S.K., Olsen, P., and Banerjee, I. (2013). Extracellular matrix aggregates from differentiating embryoid bodies as a scaffold to support ESC proliferation and differentiation. PLoS One *8*, e61856.

Gumbiner, B., Stevenson, B., and Grimaldi, A. (1988). The role of the cell adhesion molecule uvomorulin in the formation and maintenance of the epithelial junctional complex. J Cell Biol *107*, 1575-1587.

Guo, G., Huss, M., Tong, G.Q., Wang, C., Li Sun, L., Clarke, N.D., and Robson, P. (2010). Resolution of cell fate decisions revealed by single-cell gene expression analysis from zygote to blastocyst. Dev Cell *18*, 675-685.

Guo, G., von Meyenn, F., Rostovskaya, M., Clarke, J., Dietmann, S., Baker, D., Sahakyan, A., Myers, S., Bertone, P., Reik, W.*, et al.* (2017). Epigenetic resetting of human pluripotency. Development *144*, 2748-2763.

Guo, G., von Meyenn, F., Santos, F., Chen, Y., Reik, W., Bertone, P., Smith, A., and Nichols, J. (2016). Naive Pluripotent Stem Cells Derived Directly from Isolated Cells of the Human Inner Cell Mass. Stem Cell Reports *6*, 437-446.

Guo, G., Yang, J., Nichols, J., Hall, J.S., Eyres, I., Mansfield, W., and Smith, A. (2009). Klf4 reverts developmentally programmed restriction of ground state pluripotency. Development *136*, 1063-1069.

Guo, H., Zhu, P., Yan, L., Li, R., Hu, B., Lian, Y., Yan, J., Ren, X., Lin, S., Li, J.*, et al.* (2014). The DNA methylation landscape of human early embryos. Nature *511*, 606-610.

Guzman-Ayala, M., Ben-Haim, N., Beck, S., and Constam, D.B. (2004). Nodal protein processing and fibroblast growth factor 4 synergize to maintain a trophoblast stem cell microenvironment. Proc Natl Acad Sci U S A *101*, 15656-15660.

Haegel, H., Larue, L., Ohsugi, M., Fedorov, L., Herrenknecht, K., and Kemler, R. (1995). Lack of beta-catenin affects mouse development at gastrulation. Development *121*, 3529-3537.

Hailesellasse Sene, K., Porter, C.J., Palidwor, G., Perez-Iratxeta, C., Muro, E.M., Campbell, P.A., Rudnicki, M.A., and Andrade-Navarro, M.A. (2007). Gene function in early mouse embryonic stem cell differentiation. BMC Genomics *8*, 85.

Hall, J., Guo, G., Wray, J., Eyres, I., Nichols, J., Grotewold, L., Morfopoulou, S., Humphreys, P., Mansfield, W., Walker, R.*, et al.* (2009). Oct4 and LIF/Stat3 additively induce Kruppel factors to sustain embryonic stem cell self-renewal. Cell Stem Cell *5*, 597-609.

Hardy, K., Warner, A., Winston, R.M., and Becker, D.L. (1996). Expression of intercellular junctions during preimplantation development of the human embryo. Mol Hum Reprod *2*, 621-632.

Harris, T.J., and Tepass, U. (2010). Adherens junctions: from molecules to morphogenesis. Nat Rev Mol Cell Biol *11*, 502-514.

Harrison, O.J., Jin, X., Hong, S., Bahna, F., Ahlsen, G., Brasch, J., Wu, Y., Vendome, J., Felsovalyi, K., Hampton, C.M.*, et al.* (2011). The extracellular architecture of adherens junctions revealed by crystal structures of type I cadherins. Structure *19*, 244-256.

Harrison, R.G. (1906). Observations on the living developing nerve fiber. Exp

Biol Med.

Harrison, S.E., Sozen, B., Christodoulou, N., Kyprianou, C., and Zernicka-Goetz, M. (2017). Assembly of embryonic and extraembryonic stem cells to mimic embryogenesis in vitro. Science *356*.

Hatzfeld, M. (1999). The armadillo family of structural proteins. Int Rev Cytol *186*, 179-224.

Hayashi, K., Ohta, H., Kurimoto, K., Aramaki, S., and Saitou, M. (2011). Reconstitution of the mouse germ cell specification pathway in culture by pluripotent stem cells. Cell *146*, 519-532.

Hayashi, Y., Furue, M.K., Okamoto, T., Ohnuma, K., Myoishi, Y., Fukuhara, Y., Abe, T., Sato, J.D., Hata, R., and Asashima, M. (2007). Integrins regulate mouse embryonic stem cell self-renewal. Stem Cells *25*, 3005-3015.

Headen, D.M., Garcia, J.R., and Garcia, A.J. (2018). Parallel droplet microfluidics for high throughput cell encapsulation and synthetic microgel generation. Microsyst Nanoeng *4*.

Hernandez-Martinez, R., Ramkumar, N., and Anderson, K.V. (2019). p120-catenin regulates WNT signaling and EMT in the mouse embryo. Proc Natl Acad Sci U S A *116*, 16872-16881.

Herrenknecht, K., Ozawa, M., Eckerskorn, C., Lottspeich, F., Lenter, M., and Kemler, R. (1991). The Uvomorulin-Anchorage Protein Alpha-Catenin Is a Vinculin Homolog. P Natl Acad Sci USA *88*, 9156-9160.

Hinck, L., Nathke, I.S., Papkoff, J., and Nelson, W.J. (1994). Dynamics of cadherin/catenin complex formation: novel protein interactions and pathways of complex assembly. J Cell Biol *125*, 1327-1340.

Hirate, Y., Cockburn, K., Rossant, J., and Sasaki, H. (2012). Tead4 is constitutively nuclear, while nuclear vs. cytoplasmic Yap distribution is regulated in preimplantation mouse embryos. Proc Natl Acad Sci U S A *109*, E3389-3390; author reply E3391-3382.

Hirate, Y., Hirahara, S., Inoue, K., Suzuki, A., Alarcon, V.B., Akimoto, K., Hirai, T., Hara, T., Adachi, M., Chida, K.*, et al.* (2013). Polarity-dependent distribution of angiomotin localizes Hippo signaling in preimplantation embryos. Curr Biol *23*, 1181-1194.

Hooper, M., Hardy, K., Handyside, A., Hunter, S., and Monk, M. (1987). HPRT-deficient (Lesch-Nyhan) mouse embryos derived from germline colonization by cultured cells. Nature *326*, 292-295.

Hoschuetzky, H., Aberle, H., and Kemler, R. (1994). Beta-catenin mediates the interaction of the cadherin-catenin complex with epidermal growth factor receptor. J Cell Biol *127*, 1375-1380.

Huang, S.M., Mishina, Y.M., Liu, S., Cheung, A., Stegmeier, F., Michaud, G.A., Charlat, O., Wiellette, E., Zhang, Y., Wiessner, S.*, et al.* (2009). Tankyrase inhibition stabilizes axin and antagonizes Wnt signalling. Nature *461*, 614-620.

Huang, Y., Osorno, R., Tsakiridis, A., and Wilson, V. (2012). In Vivo differentiation potential of epiblast stem cells revealed by chimeric embryo formation. Cell Rep *2*, 1571-1578.

Huber, O., Krohn, M., and Kemler, R. (1997). A specific domain in alpha-catenin mediates binding to beta-catenin or plakoglobin. J Cell Sci *110 (Pt 15)*, 1759-1765.

Huch, M., and Koo, B.K. (2015). Modeling mouse and human development using organoid cultures. Development *142*, 3113-3125.

Huebner, A., Sharma, S., Srisa-Art, M., Hollfelder, F., Edel, J.B., and Demello, A.J. (2008). Microdroplets: a sea of applications? Lab Chip *8*, 1244-1254.

Huelsken, J., Vogel, R., Brinkmann, V., Erdmann, B., Birchmeier, C., and Birchmeier, W. (2000a). Requirement for beta-catenin in anterior-posterior axis formation in mice. J Cell Biol *148*, 567-578.

Huelsken, J., Vogel, R., Brinkmann, V., Erdmann, B., Birchmeier, C., and Birchmeier, W. (2000b). Requirement for beta-catenin in anterior-posterior axis formation in mice. J Cell Biol *148*, 567-578.

Hyafil, F., Babinet, C., and Jacob, F. (1981). Cell-Cell Interactions in Early Embryogenesis - a Molecular Approach to the Role of Calcium. Cell *26*, 447-454.

Hyafil, F., Morello, D., Babinet, C., and Jacob, F. (1980). A cell surface glycoprotein involved in the compaction of embryonal carcinoma cells and cleavage stage embryos. Cell *21*, 927-934.

Ishiyama, N., Lee, S.H., Liu, S., Li, G.Y., Smith, M.J., Reichardt, L.F., and Ikura, M. (2010). Dynamic and Static Interactions between p120 Catenin and E-Cadherin Regulate the Stability of Cell-Cell Adhesion. Cell *141*, 117-128.

Iyer, K.V., Piscitello-Gomez, R., Paijmans, J., Julicher, F., and Eaton, S. (2019). Epithelial Viscoelasticity Is Regulated by Mechanosensitive E-cadherin Turnover. Curr Biol *29*, 578-591 e575.

Jho, E.H., Zhang, T., Domon, C., Joo, C.K., Freund, J.N., and Costantini, F. (2002). Wnt/beta-catenin/Tcf signaling induces the transcription of Axin2, a negative regulator of the signaling pathway. Mol Cell Biol *22*, 1172-1183.

Johnson, M.H., Maro, B., and Takeichi, M. (1986). The Role of Cell-Adhesion in the Synchronization and Orientation of Polarization in 8-Cell Mouse Blastomeres. J Embryol Exp Morph *93*, 239-255.

Johnson, M.H., and Ziomek, C.A. (1981). Induction of Polarity in Mouse 8-Cell Blastomeres - Specificity, Geometry, and Stability. J Cell Biol *91*, 303-308.

Jou, T.S., Stewart, D.B., Stappert, J., Nelson, W.J., and Marrs, J.A. (1995). Genetic and Biochemical Dissection of Protein Linkages in the Cadherin-Catenin Complex. P Natl Acad Sci USA *92*, 5067-5071.

Kaestner, K.H., Ntambi, J.M., Kelly, T.J., Jr., and Lane, M.D. (1989). Differentiation-induced gene expression in 3T3-L1 preadipocytes. A second differentially expressed gene encoding stearoyl-CoA desaturase. J Biol Chem *264*, 14755-14761.

Kahan, B.W., and Ephrussi, B. (1970). Developmental potentialities of clonal in vitro cultures of mouse testicular teratoma. J Natl Cancer Inst *44*, 1015-1036.

Kalkan, T., Olova, N., Roode, M., Mulas, C., Lee, H.J., Nett, I., Marks, H., Walker, R., Stunnenberg, H.G., Lilley, K.S.*, et al.* (2017). Tracking the embryonic stem cell transition from ground state pluripotency. Development *144*, 1221-1234.

Kanehisa, M., and Goto, S. (2000). KEGG: kyoto encyclopedia of genes and genomes. Nucleic Acids Res *28*, 27-30.

Kang, M., Garg, V., and Hadjantonakis, A.K. (2017). Lineage Establishment and Progression within the Inner Cell Mass of the Mouse Blastocyst Requires FGFR1 and FGFR2. Dev Cell *41*, 496-510 e495.

Karnovsky, A., and Klymkowsky, M.W. (1995). Anterior axis duplication in Xenopus induced by the over-expression of the cadherin-binding protein plakoglobin. Proc Natl Acad Sci U S A *92*, 4522-4526.

Katayama, M., Ellersieck, M.R., and Roberts, R.M. (2010). Development of monozygotic twin mouse embryos from the time of blastomere separation at the two-cell stage to blastocyst. Biol Reprod *82*, 1237-1247.

Keith Ho, H.C., McGrath, K.E., Brodbeck, K.C., Palis, J., and Schick, B.P. (2001). Serglycin proteoglycan synthesis in the murine uterine decidua and early embryo. Biol Reprod *64*, 1667-1676.

Kelly, K.F., Ng, D.Y., Jayakumaran, G., Wood, G.A., Koide, H., and Doble, B.W. (2011). beta-catenin enhances Oct-4 activity and reinforces pluripotency through a TCF-independent mechanism. Cell Stem Cell *8*, 214-227.

Kelly, O.G., Pinson, K.I., and Skarnes, W.C. (2004). The Wnt co-receptors Lrp5 and Lrp6 are essential for gastrulation in mice. Development *131*, 2803-2815.

Kemler, R. (1993). From cadherins to catenins: cytoplasmic protein interactions and regulation of cell adhesion. Trends Genet *9*, 317-321.

Kemler, R., Hierholzer, A., Kanzler, B., Kuppig, S., Hansen, K., Taketo, M.M., de Vries, W.N., Knowles, B.B., and Solter, D. (2004). Stabilization of beta-catenin in the mouse zygote leads to premature epithelial-mesenchymal transition in the epiblast. Development *131*, 5817-5824.

Kemp, C., Willems, E., Abdo, S., Lambiv, L., and Leyns, L. (2005). Expression of all Wnt genes and their secreted antagonists during mouse blastocyst and postimplantation development. Dev Dyn *233*, 1064-1075.

Kim, H., Wu, J., Ye, S., Tai, C.I., Zhou, X., Yan, H., Li, P., Pera, M., and Ying, Q.L. (2013). Modulation of beta-catenin function maintains mouse epiblast stem cell and human embryonic stem cell self-renewal. Nat Commun *4*, 2403.

Kinoshita, M., Barber, M., Mansfield, W., Cui, Y., Spindlow, D., Stirparo, G.G., Dietmann, S., Nichols, J., and Smith, A. (2020). Capture of Mouse and Human Stem Cells with Features of Formative Pluripotency. Cell Stem Cell.

Klein, A.M., Mazutis, L., Akartuna, I., Tallapragada, N., Veres, A., Li, V., Peshkin, L., Weitz, D.A., and Kirschner, M.W. (2015). Droplet barcoding for single-cell transcriptomics applied to embryonic stem cells. Cell *161*, 1187-1201.

Kleine-Bruggeney, H., van Vliet, L.D., Mulas, C., Gielen, F., Agley, C.C., Silva, J.C.R., Smith, A., Chalut, K., and Hollfelder, F. (2019). Long-Term Perfusion Culture of Monoclonal Embryonic Stem Cells in 3D Hydrogel Beads for Continuous Optical Analysis of Differentiation. Small *15*, e1804576.

Kleinsmith, L.J., and Pierce, G.B., Jr. (1964). Multipotentiality of Single Embryonal Carcinoma Cells. Cancer Res *24*, 1544-1551.

Knudsen, K.A., and Wheelock, M.J. (1992). Plakoglobin, or an 83-kD homologue distinct from beta-catenin, interacts with E-cadherin and N-cadherin. J Cell Biol *118*, 671-679.

Kojima, Y., Kaufman-Francis, K., Studdert, J.B., Steiner, K.A., Power, M.D., Loebel, D.A., Jones, V., Hor, A., de Alencastro, G., Logan, G.J.*, et al.* (2014). The transcriptional and functional properties of mouse epiblast stem cells resemble the anterior primitive streak. Cell Stem Cell *14*, 107-120.

Kolligs, F.T., Kolligs, B., Hajra, K.M., Hu, G., Tani, M., Cho, K.R., and Fearon, E.R. (2000). gamma-catenin is regulated by the APC tumor suppressor and its oncogenic activity is distinct from that of beta-catenin. Genes Dev *14*, 1319-1331.

Kolodziejczyk, A.A., Kim, J.K., Tsang, J.C., Ilicic, T., Henriksson, J., Natarajan, K.N., Tuck, A.C., Gao, X., Buhler, M., Liu, P.*, et al.* (2015). Single Cell RNA-Sequencing of Pluripotent States Unlocks Modular Transcriptional Variation. Cell Stem Cell *17*, 471-485.

Korinek, V., Barker, N., Morin, P.J., van Wichen, D., de Weger, R., Kinzler, K.W., Vogelstein, B., and Clevers, H. (1997). Constitutive transcriptional activation by a beta-catenin-Tcf complex in APC-/- colon carcinoma. Science *275*, 1784-1787.

Koutsourakis, M., Langeveld, A., Patient, R., Beddington, R., and Grosveld, F. (1999). The transcription factor GATA6 is essential for early extraembryonic development. Development *126*, 723-732.

Kowalczyk, A.P., Bornslaeger, E.A., Borgwardt, J.E., Palka, H.L., Dhaliwal, A.S., Corcoran, C.M., Denning, M.F., and Green, K.J. (1997). The amino-terminal domain of desmoplakin binds to plakoglobin and clusters desmosomal cadherin-plakoglobin complexes. J Cell Biol *139*, 773-784.

Krawchuk, D., Honma-Yamanaka, N., Anani, S., and Yamanaka, Y. (2013). FGF4 is a limiting factor controlling the proportions of primitive endoderm and epiblast in the ICM of the mouse blastocyst. Dev Biol *384*, 65-71.

Kumachev, A., Greener, J., Tumarkin, E., Eiser, E., Zandstra, P.W., and Kumacheva, E. (2011). High-throughput generation of hydrogel microbeads with varying elasticity for cell encapsulation. Biomaterials *32*, 1477-1483.

Kunath, T., Arnaud, D., Uy, G.D., Okamoto, I., Chureau, C., Yamanaka, Y., Heard, E., Gardner, R.L., Avner, P., and Rossant, J. (2005). Imprinted X-inactivation in extra-embryonic endoderm cell lines from mouse blastocysts. Development *132*, 1649-1661.

Kurek, D., Neagu, A., Tastemel, M., Tuysuz, N., Lehmann, J., van de Werken, H.J.G., Philipsen, S., van der Linden, R., Maas, A., van, I.W.F.J., *et al.* (2015). Endogenous WNT signals mediate BMP-induced and spontaneous differentiation of epiblast stem cells and human embryonic stem cells. Stem Cell Reports *4*, 114-128.

Labouesse, C., Agley, C.C., Tan, B.X., Hofer, M., Winkel, A., Stirparo, G.G., Stuart, H.T., Verstreken, C.M., Mansfield, W., Bertone, P., *et al.* (2019). StemBond hydrogels optimise the mechanical microenvironment for embryonic stem cells. BioRxiv.

Lahaye, M., and Rochas, C. (1991). Chemical-Structure and Physicochemical Properties of Agar. Hydrobiologia *221*, 137-148.

Larue, L., Ohsugi, M., Hirchenhain, J., and Kemler, R. (1994). E-cadherin null mutant embryos fail to form a trophectoderm epithelium. Proc Natl Acad Sci U S A *91*, 8263-8267.

Lawson, K.A. (1999). Fate mapping the mouse embryo. Int J Dev Biol *43*, 773-775.

Lee, M., Ji, H., Furuta, Y., Park, J.I., and McCrea, P.D. (2014a). p120-catenin regulates REST and CoREST, and modulates mouse embryonic stem cell differentiation. Journal of Cell Science *127*, 4037-4051.

Lee, M., Ji, H., Furuta, Y., Park, J.I., and McCrea, P.D. (2014b). p120-catenin regulates REST and CoREST, and modulates mouse embryonic stem cell differentiation. J Cell Sci *127*, 4037-4051.

Leung, C.Y., and Zernicka-Goetz, M. (2013). Angiomotin prevents pluripotent lineage differentiation in mouse embryos via Hippo pathway-dependent and -independent mechanisms. Nat Commun *4*, 2251.

Li, G., Margueron, R., Ku, M., Chambon, P., Bernstein, B.E., and Reinberg, D. (2010). Jarid2 and PRC2, partners in regulating gene expression. Genes Dev *24*, 368-380.

Li, L., Arman, E., Ekblom, P., Edgar, D., Murray, P., and Lonai, P. (2004). Distinct GATA6- and laminin-dependent mechanisms regulate endodermal and ectodermal embryonic stem cell fates. Development *131*, 5277-5286.

Li, R., Zhong, C., Yu, Y., Liu, H., Sakurai, M., Yu, L., Min, Z., Shi, L., Wei, Y., Takahashi, Y., *et al.* (2019). Generation of Blastocyst-like Structures from Mouse Embryonic and Adult Cell Cultures. Cell *179*, 687-702 e618.

Li, S., Edgar, D., Fassler, R., Wadsworth, W., and Yurchenco, P.D. (2003). The role of laminin in embryonic cell polarization and tissue organization. Dev Cell *4*, 613-624.

Li, S., Harrison, D., Carbonetto, S., Fassler, R., Smyth, N., Edgar, D., and Yurchenco, P.D. (2002). Matrix assembly, regulation, and survival functions of laminin and its receptors in embryonic stem cell differentiation. J Cell Biol *157*, 1279-1290.

Li, X., Burnight, E.R., Cooney, A.L., Malani, N., Brady, T., Sander, J.D., Staber, J., Wheelan, S.J., Joung, J.K., McCray, P.B., Jr., *et al.* (2013). piggyBac transposase tools for genome engineering. Proc Natl Acad Sci U S A *110*, E2279-2287.

Liu, P., Wakamiya, M., Shea, M.J., Albrecht, U., Behringer, R.R., and Bradley, A. (1999). Requirement for Wnt3 in vertebrate axis formation. Nat Genet *22*, 361-365.

Lloyd, S., Fleming, T.P., and Collins, J.E. (2003). Expression of Wnt genes during mouse preimplantation development. Gene Expr Patterns *3*, 309-312.

Lorch, J.H., Klessner, J., Park, J.K., Getsios, S., Wu, Y.L., Stack, M.S., and Green, K.J. (2004). Epidermal growth factor receptor inhibition promotes desmosome assembly and strengthens intercellular adhesion in squamous cell carcinoma cells. J Biol Chem *279*, 37191-37200.

Louvet, S., Aghion, J., Santa-Maria, A., Mangeat, P., and Maro, B. (1996). Ezrin becomes restricted to outer cells following asymmetrical division in the preimplantation mouse embryo. Dev Biol *177*, 568-579.

Lowe, L.A., Yamada, S., and Kuehn, M.R. (2001). Genetic dissection of nodal function in patterning the mouse embryo. Development *128*, 1831-1843.

Lu, C.C., Brennan, J., and Robertson, E.J. (2001). From fertilization to gastrulation: axis formation in the mouse embryo. Curr Opin Genet Dev *11*, 384-392.

Lu, D., Luo, C., Zhang, C., Li, Z., and Long, M. (2014). Differential regulation of morphology and stemness of mouse embryonic stem cells by substrate stiffness and topography. Biomaterials *35*, 3945-3955.

Lutolf, M.P., Gilbert, P.M., and Blau, H.M. (2009). Designing materials to direct stem-cell fate. Nature *462*, 433-441.

Lyashenko, N., Winter, M., Migliorini, D., Biechele, T., Moon, R.T., and Hartmann, C. (2011). Differential requirement for the dual functions of beta-catenin in embryonic stem cell self-renewal and germ layer formation. Nat Cell Biol *13*, 753-761.

Lyko, F. (2018). The DNA methyltransferase family: a versatile toolkit for epigenetic regulation. Nat Rev Genet *19*, 81-92.

MacDonald, B.T., Tamai, K., and He, X. (2009). Wnt/beta-Catenin Signaling: Components, Mechanisms, and Diseases. Developmental Cell *17*, 9-26.

Macosko, E.Z., Basu, A., Satija, R., Nemesh, J., Shekhar, K., Goldman, M., Tirosh, I., Bialas, A.R., Kamitaki, N., Martersteck, E.M., *et al.* (2015). Highly Parallel Genome-wide Expression Profiling of Individual Cells Using Nanoliter Droplets. Cell *161*, 1202-1214.

Mahendram, S., Kelly, K.F., Paez-Parent, S., Mahmood, S., Polena, E., Cooney, A.J., and Doble, B.W. (2013). Ectopic gamma-catenin expression partially mimics the effects of stabilized beta-catenin on embryonic stem cell differentiation. PLoS One *8*, e65320.

Maitre, J.L., Berthoumieux, H., Krens, S.F., Salbreux, G., Julicher, F., Paluch, E., and Heisenberg, C.P. (2012). Adhesion functions in cell sorting by mechanically coupling the cortices of adhering cells. Science *338*, 253-256.

Maitre, J.L., Niwayama, R., Turlier, H., Nedelec, F., and Hiiragi, T. (2015). Pulsatile cell-autonomous contractility drives compaction in the mouse embryo. Nat Cell Biol *17*, 849-855.

Marks, H., Kalkan, T., Menafra, R., Denissov, S., Jones, K., Hofemeister, H., Nichols, J., Kranz, A., Stewart, A.F., Smith, A.*, et al.* (2012). The transcriptional and epigenomic foundations of ground state pluripotency. Cell *149*, 590-604.

Martello, G., Bertone, P., and Smith, A. (2013). Identification of the missing pluripotency mediator downstream of leukaemia inhibitory factor. Embo J *32*, 2561-2574.

Martello, G., Sugimoto, T., Diamanti, E., Joshi, A., Hannah, R., Ohtsuka, S., Gottgens, B., Niwa, H., and Smith, A. (2012). Esrrb is a pivotal target of the Gsk3/Tcf3 axis regulating embryonic stem cell self-renewal. Cell Stem Cell *11*, 491-504.

Martin Gonzalez, J., Morgani, S.M., Bone, R.A., Bonderup, K., Abelchian, S., Brakebusch, C., and Brickman, J.M. (2016). Embryonic Stem Cell Culture Conditions Support Distinct States Associated with Different Developmental Stages and Potency. Stem Cell Reports *7*, 177-191.

Martin, G.R. (1981). Isolation of a pluripotent cell line from early mouse embryos cultured in medium conditioned by teratocarcinoma stem cells. Proc Natl Acad Sci U S A *78*, 7634-7638.

McCrea, P.D., Brieher, W.M., and Gumbiner, B.M. (1993). Induction of a secondary body axis in Xenopus by antibodies to beta-catenin. J Cell Biol *123*, 477-484.

McCrea, P.D., Maher, M.T., and Gottardi, C.J. (2015). Nuclear signaling from cadherin adhesion complexes. Curr Top Dev Biol *112*, 129-196.

Mccrea, P.D., Turck, C.W., and Gumbiner, B. (1991a). A Homolog of the Armadillo Protein in Drosophila (Plakoglobin) Associated with E-Cadherin. Science *254*, 1359-1361.

McCrea, P.D., Turck, C.W., and Gumbiner, B. (1991b). A homolog of the armadillo protein in Drosophila (plakoglobin) associated with E-cadherin. Science *254*, 1359-1361.

McMahon, A.P., and Moon, R.T. (1989). Ectopic expression of the proto-oncogene int-1 in Xenopus embryos leads to duplication of the embryonic axis. Cell *58*, 1075-1084.

Meilhac, S.M., Adams, R.J., Morris, S.A., Danckaert, A., Le Garrec, J.F., and Zernicka-Goetz, M. (2009). Active cell movements coupled to positional induction are involved in lineage segregation in the mouse blastocyst. Dev Biol *331*, 210-221.

Mfopou, J.K., Geeraerts, M., Dejene, R., Van Langenhoven, S., Aberkane, A., Van Grunsven, L.A., and Bouwens, L. (2014). Efficient definitive endoderm induction from mouse embryonic stem cell adherent cultures: a rapid screening model for differentiation studies. Stem Cell Res *12*, 166-177.

Miravet, S., Piedra, J., Castano, J., Raurell, I., Franci, C., Dunach, M., and Garcia de Herreros, A. (2003). Tyrosine phosphorylation of plakoglobin causes contrary effects on its association with desmosomes and adherens junction components and modulates beta-catenin-mediated transcription. Mol Cell Biol *23*, 7391-7402.

Mishina, Y., Suzuki, A., Ueno, N., and Behringer, R.R. (1995). Bmpr encodes a type I bone morphogenetic protein receptor that is essential for gastrulation during mouse embryogenesis. Genes Dev *9*, 3027-3037.

Mistri, T.K., Arindrarto, W., Ng, W.P., Wang, C., Lim, L.H., Sun, L., Chambers, I., Wohland, T., and Robson, P. (2018). Dynamic changes in Sox2 spatio-temporal expression promote the second cell fate decision through Fgf4/Fgfr2 signaling in preimplantation mouse embryos. Biochem J *475*, 1075-1089.

Mitsui, K., Tokuzawa, Y., Itoh, H., Segawa, K., Murakami, M., Takahashi, K., Maruyama, M., Maeda, M., and Yamanaka, S. (2003). The homeoprotein Nanog is required for maintenance of pluripotency in mouse epiblast and ES cells. Cell *113*, 631-642.

Molenaar, M., van de Wetering, M., Oosterwegel, M., Peterson-Maduro, J., Godsave, S., Korinek, V., Roose, J., Destree, O., and Clevers, H. (1996). XTcf-3 transcription factor mediates beta-catenin-induced axis formation in Xenopus embryos. Cell *86*, 391-399.

Molotkov, A., Mazot, P., Brewer, J.R., Cinalli, R.M., and Soriano, P. (2017). Distinct Requirements for FGFR1 and FGFR2 in Primitive Endoderm Development and Exit from Pluripotency. Dev Cell *41*, 511-526 e514.

Morris, S.A., Graham, S.J., Jedrusik, A., and Zernicka-Goetz, M. (2013). The differential response to Fgf signalling in cells internalized at different times influences lineage segregation in preimplantation mouse embryos. Open Biol *3*, 130104.

Morrison, S.J., and Spradling, A.C. (2008). Stem cells and niches: mechanisms that promote stem cell maintenance throughout life. Cell *132*, 598-611.

Mulas, C., Kalkan, T., and Smith, A. (2017). NODAL Secures Pluripotency upon Embryonic Stem Cell Progression from the Ground State. Stem Cell Reports *9*, 77-91.

Munoz Descalzo, S., Rue, P., Faunes, F., Hayward, P., Jakt, L.M., Balayo, T., Garcia-Ojalvo, J., and Martinez Arias, A. (2013). A competitive protein interaction network buffers Oct4-mediated differentiation to promote pluripotency in embryonic stem cells. Mol Syst Biol *9*, 694.

Munoz-Descalzo, S., Hadjantonakis, A.K., and Arias, A.M. (2015). Wnt/ss-catenin signalling and the dynamics of fate decisions in early mouse embryos and embryonic stem (ES) cells. Semin Cell Dev Biol *47-48*, 101-109.

Munoz-Sanjuan, I., and Brivanlou, A.H. (2002). Neural induction, the default model and embryonic stem cells. Nat Rev Neurosci *3*, 271-280.

Murakami, K., Gunesdogan, U., Zylicz, J.J., Tang, W.W.C., Sengupta, R., Kobayashi, T., Kim, S., Butler, R., Dietmann, S., and Surani, M.A. (2016). NANOG alone induces germ cells in primed epiblast in vitro by activation of enhancers. Nature *529*, 403-407.

Murayama, H., Masaki, H., Sato, H., Hayama, T., Yamaguchi, T., and Nakauchi, H. (2015). Successful reprogramming of epiblast stem cells by blocking nuclear localization of beta-catenin. Stem Cell Reports *4*, 103-113.

Murphy, W.L., McDevitt, T.C., and Engler, A.J. (2014). Materials as stem cell regulators. Nature Materials *13*, 547-557.

Murray, P., and Edgar, D. (2000). Regulation of programmed cell death by basement membranes in embryonic development. J Cell Biol *150*, 1215-1221.

Nakaki, F., Hayashi, K., Ohta, H., Kurimoto, K., Yabuta, Y., and Saitou, M. (2013). Induction of mouse germ-cell fate by transcription factors in vitro. Nature *501*, 222-226.

Nakamura, T., Okamoto, I., Sasaki, K., Yabuta, Y., Iwatani, C., Tsuchiya, H., Seita, Y., Nakamura, S., Yamamoto, T., and Saitou, M. (2016). A developmental coordinate of pluripotency among mice, monkeys and humans. Nature *537*, 57-62.

Nanes, B.A., Chiasson-MacKenzie, C., Lowery, A.M., Ishiyama, N., Faundez, V., Ikura, M., Vincent, P.A., and Kowalczyk, A.P. (2012). p120-catenin binding masks an endocytic signal conserved in classical cadherins. J Cell Biol *199*, 365-380.

Nathke, I.S., Hinck, L., Swedlow, J.R., Papkoff, J., and Nelson, W.J. (1994). Defining interactions and distributions of cadherin and catenin complexes in polarized epithelial cells. J Cell Biol *125*, 1341-1352.

Neagu, A., van Genderen, E., Escudero, I., Verwegen, L., Kurek, D., Lehmann, J., Stel, J., Dirks, R.A.M., van Mierlo, G., Maas, A.*, et al.* (2020). In vitro capture and characterization of embryonic rosette-stage pluripotency between naive and primed states. Nat Cell Biol *22*, 534-545.

Neri, F., Krepelova, A., Incarnato, D., Maldotti, M., Parlato, C., Galvagni, F., Matarese, F., Stunnenberg, H.G., and Oliviero, S. (2013). Dnmt3L antagonizes DNA methylation at bivalent promoters and favors DNA methylation at gene bodies in ESCs. Cell *155*, 121-134.

Niakan, K.K., Ji, H., Maehr, R., Vokes, S.A., Rodolfa, K.T., Sherwood, R.I., Yamaki, M., Dimos, J.T., Chen, A.E., Melton, D.A.*, et al.* (2010). Sox17 promotes differentiation in mouse embryonic stem cells by directly regulating extraembryonic gene expression and indirectly antagonizing self-renewal. Genes Dev *24*, 312-326.

Niakan, K.K., Schrode, N., Cho, L.T., and Hadjantonakis, A.K. (2013). Derivation of extraembryonic endoderm stem (XEN) cells from mouse embryos and embryonic stem cells. Nat Protoc *8*, 1028-1041.

Nichols, J., Jones, K., Phillips, J.M., Newland, S.A., Roode, M., Mansfield, W., Smith, A., and Cooke, A. (2009a). Validated germline-competent embryonic stem cell lines from nonobese diabetic mice. Nat Med *15*, 814-818.

Nichols, J., Silva, J., Roode, M., and Smith, A. (2009b). Suppression of Erk signalling promotes ground state pluripotency in the mouse embryo. Development *136*, 3215-3222.

Nichols, J., and Smith, A. (2009). Naive and primed pluripotent states. Cell Stem Cell *4*, 487-492.

Nichols, J., Zevnik, B., Anastassiadis, K., Niwa, H., Klewe-Nebenius, D., Chambers, I., Scholer, H., and Smith, A. (1998). Formation of pluripotent stem cells in the mammalian embryo depends on the POU transcription factor Oct4. Cell *95*, 379-391.

Nicholson, S.E., Willson, T.A., Farley, A., Starr, R., Zhang, J.G., Baca, M., Alexander, W.S., Metcalf, D., Hilton, D.J., and Nicola, N.A. (1999). Mutational analyses of the SOCS proteins suggest a dual domain requirement but distinct mechanisms for inhibition of LIF and IL-6 signal transduction. Embo J *18*, 375-385.

Nishioka, N., Inoue, K., Adachi, K., Kiyonari, H., Ota, M., Ralston, A., Yabuta, N., Hirahara, S., Stephenson, R.O., Ogonuki, N.*, et al.* (2009). The Hippo signaling pathway components Lats and Yap pattern Tead4 activity to distinguish mouse trophectoderm from inner cell mass. Dev Cell *16*, 398-410.

Nishioka, N., Yamamoto, S., Kiyonari, H., Sato, H., Sawada, A., Ota, M., Nakao, K., and Sasaki, H. (2008). Tead4 is required for specification of trophectoderm in pre-implantation mouse embryos. Mech Dev *125*, 270-283.

Niwa, H., Burdon, T., Chambers, I., and Smith, A. (1998). Self-renewal of pluripotent embryonic stem cells is mediated via activation of STAT3. Genes Dev *12*, 2048-2060.

Niwa, H., Toyooka, Y., Shimosato, D., Strumpf, D., Takahashi, K., Yagi, R., and Rossant, J. (2005). Interaction between Oct3/4 and Cdx2 determines trophectoderm differentiation. Cell *123*, 917-929.

Niwa, H., Yamamura, K., and Miyazaki, J. (1991). Efficient selection for high-expression transfectants with a novel eukaryotic vector. Gene *108*, 193-199.

Norris, D.P., and Robertson, E.J. (1999). Asymmetric and node-specific nodal expression patterns are controlled by two distinct cis-acting regulatory elements. Genes Dev *13*, 1575-1588.

Ohinata, Y., Ohta, H., Shigeta, M., Yamanaka, K., Wakayama, T., and Saitou, M. (2009). A signaling principle for the specification of the germ cell lineage in mice. Cell *137*, 571-584.

Ohkubo, T., and Ozawa, M. (1999). p120(ctn) binds to the membrane-proximal region of the E-cadherin cytoplasmic domain and is involved in modulation of adhesion activity. J Biol Chem *274*, 21409-21415.

Ohnishi, Y., Huber, W., Tsumura, A., Kang, M., Xenopoulos, P., Kurimoto, K., Oles, A.K., Arauzo-Bravo, M.J., Saitou, M., Hadjantonakis, A.K.*, et al.* (2014). Cell-to-cell expression variability followed by signal reinforcement progressively segregates early mouse lineages. Nat Cell Biol *16*, 27-37.

Ohno, S. (2001). Intercellular junctions and cellular polarity: the PAR-aPKC complex, a conserved core cassette playing fundamental roles in cell polarity. Curr Opin Cell Biol *13*, 641-648.

Ohsugi, M., Hwang, S.Y., Butz, S., Knowles, B.B., Solter, D., and Kemler, R. (1996). Expression and cell membrane localization of catenins during mouse preimplantation development. Dev Dyn *206*, 391-402.

Ohsugi, M., Larue, L., Schwarz, H., and Kemler, R. (1997). Cell-junctional and cytoskeletal organization in mouse blastocysts lacking E-cadherin. Dev Biol *185*, 261-271.

Ohtsuka, S., Nishikawa-Torikai, S., and Niwa, H. (2012). E-cadherin promotes incorporation of mouse epiblast stem cells into normal development. PLoS One *7*, e45220.

Okano, H., Hikishima, K., Iriki, A., and Sasaki, E. (2012). The common marmoset as a novel animal model system for biomedical and neuroscience research applications. Semin Fetal Neonatal Med *17*, 336-340.

Oldberg, A., Hayman, E.G., and Ruoslahti, E. (1981). Isolation of a chondroitin sulfate proteoglycan from a rat yolk sac tumor and immunochemical demonstration of its cell surface localization. J Biol Chem *256*, 10847-10852.

Orive, G., Hernandez, R.M., Rodriguez Gascon, A., Calafiore, R., Chang, T.M., de Vos, P., Hortelano, G., Hunkeler, D., Lacik, I., and Pedraz, J.L. (2004). History, challenges and perspectives of cell microencapsulation. Trends Biotechnol *22*, 87-92.

Ozawa, M. (2002). Lateral dimerization of the E-cadherin extracellular domain is necessary but not sufficient for adhesive activity. J Biol Chem *277*, 19600-19608.

Ozawa, M., Baribault, H., and Kemler, R. (1989). The cytoplasmic domain of the cell adhesion molecule uvomorulin associates with three independent proteins structurally related in different species. Embo J *8*, 1711-1717.

Ozawa, M., Ringwald, M., and Kemler, R. (1990). Uvomorulin-catenin complex formation is regulated by a specific domain in the cytoplasmic region of the cell adhesion molecule. Proc Natl Acad Sci U S A *87*, 4246-4250.

Paramasivam, M., Sarkeshik, A., Yates, J.R., 3rd, Fernandes, M.J., and McCollum, D. (2011). Angiomotin family proteins are novel activators of the LATS2 kinase tumor suppressor. Mol Biol Cell *22*, 3725-3733.

Peifer, M., McCrea, P.D., Green, K.J., Wieschaus, E., and Gumbiner, B.M. (1992a). The vertebrate adhesive junction proteins beta-catenin and plakoglobin and the Drosophila segment polarity gene armadillo form a multigene family with similar properties. J Cell Biol *118*, 681-691.

Peifer, M., Mccrea, P.D., Green, K.J., Wieschaus, E., and Gumbiner, B.M. (1992b). The Vertebrate Adhesive Junction Proteins Beta-Catenin and Plakoglobin and the Drosophila Segment Polarity Gene Armadillo Form a Multigene Family with Similar Properties. J Cell Biol *118*, 681-691.

Pelton, T.A., Sharma, S., Schulz, T.C., Rathjen, J., and Rathjen, P.D. (2002). Transient pluripotent cell populations during primitive ectoderm formation: correlation of in vivo and in vitro pluripotent cell development. J Cell Sci *115*, 329-339.

Perea-Gomez, A., Shawlot, W., Sasaki, H., Behringer, R.R., and Ang, S. (1999). HNF3beta and Lim1 interact in the visceral endoderm to regulate primitive streak formation and anterior-posterior polarity in the mouse embryo. Development *126*, 4499-4511.

Perea-Gomez, A., Vella, F.D., Shawlot, W., Oulad-Abdelghani, M., Chazaud, C., Meno, C., Pfister, V., Chen, L., Robertson, E., Hamada, H.*, et al.* (2002). Nodal antagonists in the anterior visceral endoderm prevent the formation of multiple primitive streaks. Dev Cell *3*, 745-756.

Perona, R.M., and Wassarman, P.M. (1986). Mouse blastocysts hatch in vitro by using a trypsin-like proteinase associated with cells of mural trophectoderm. Dev Biol *114*, 42-52.

Petropoulos, S., Edsgard, D., Reinius, B., Deng, Q., Panula, S.P., Codeluppi, S., Reyes, A.P., Linnarsson, S., Sandberg, R., and Lanner, F. (2016). Single-Cell RNA-Seq Reveals Lineage and X Chromosome Dynamics in Human Preimplantation Embryos. Cell *167*, 285.

Pevny, L.H., Sockanathan, S., Placzek, M., and Lovell-Badge, R. (1998). A role for SOX1 in neural determination. Development *125*, 1967-1978.

Picelli, S., Faridani, O.R., Bjorklund, A.K., Winberg, G., Sagasser, S., and Sandberg, R. (2014). Full-length RNA-seq from single cells using Smart-seq2. Nat Protoc *9*, 171-181.

Pieters, T., Goossens, S., Haenebalcke, L., Andries, V., Stryjewska, A., De Rycke, R., Lemeire, K., Hochepied, T., Huylebroeck, D., Berx, G.*, et al.* (2016). p120 Catenin-Mediated Stabilization of E-Cadherin Is Essential for Primitive Endoderm Specification. Plos Genetics *12*.

Plusa, B., and Hadjantonakis, A.K. (2014). Embryonic stem cell identity grounded in the embryo. Nat Cell Biol *16*, 502-504.

Plusa, B., Piliszek, A., Frankenberg, S., Artus, J., and Hadjantonakis, A.K. (2008). Distinct sequential cell behaviours direct primitive endoderm formation in the mouse blastocyst. Development *135*, 3081-3091.

Pokutta, S., Drees, F., Takai, Y., Nelson, W.J., and Weis, W.I. (2002). Biochemical and structural definition of the l-afadin- and actin-binding sites of alpha-catenin. J Biol Chem *277*, 18868-18874.

Pokutta, S., Drees, F., Yamada, S., Nelson, W.J., and Weis, W.I. (2008). Biochemical and structural analysis of alpha-catenin in cell-cell contacts. Biochem Soc T *36*, 141-147.

Pokutta, S., and Weis, W.I. (2000). Structure of the dimerization and beta-catenin-binding region of alpha-catenin. Mol Cell *5*, 533-543.

Porter, A.G., and Janicke, R.U. (1999). Emerging roles of caspase-3 in apoptosis. Cell Death Differ *6*, 99-104.

Qian, L., Huang, Y., Spencer, C.I., Foley, A., Vedantham, V., Liu, L., Conway, S.J., Fu, J.D., and Srivastava, D. (2012). In vivo reprogramming of murine cardiac fibroblasts into induced cardiomyocytes. Nature *485*, 593-598.

Qiu, D., Ye, S., Ruiz, B., Zhou, X., Liu, D., Zhang, Q., and Ying, Q.L. (2015). Klf2 and Tfcp2l1, Two Wnt/beta-Catenin Targets, Act Synergistically to Induce and Maintain Naive Pluripotency. Stem Cell Reports *5*, 314-322.

Rakeman, A.S., and Anderson, K.V. (2006). Axis specification and morphogenesis in the mouse embryo require Nap1, a regulator of WAVE-mediated actin branching. Development *133*, 3075-3083.

Rasmussen, K.D., and Helin, K. (2016). Role of TET enzymes in DNA methylation, development, and cancer. Genes Dev *30*, 733-750.

Renard, C.A., Labalette, C., Armengol, C., Cougot, D., Wei, Y., Cairo, S., Pineau, P., Neuveut, C., de Reynies, A., Dejean, A.*, et al.* (2007). Tbx3 is a downstream target of the Wnt/beta-catenin pathway and a critical mediator of beta-catenin survival functions in liver cancer. Cancer Res *67*, 901-910.

Renfree, M.B., and Fenelon, J.C. (2017). The enigma of embryonic diapause. Development *144*, 3199-3210.

Riethmacher, D., Brinkmann, V., and Birchmeier, C. (1995). A targeted mutation in the mouse E-cadherin gene results in defective preimplantation development. Proc Natl Acad Sci U S A *92*, 855-859.

Rivron, N.C., Frias-Aldeguer, J., Vrij, E.J., Boisset, J.C., Korving, J., Vivie, J., Truckenmuller, R.K., van Oudenaarden, A., van Blitterswijk, C.A., and Geijsen, N. (2018). Blastocyst-like structures generated solely from stem cells. Nature *557*, 106-111.

Robertson, E.J. (1997). Derivation and maintenance of embryonic stem cell cultures. Methods Mol Biol *75*, 173-184.

Rodriguez, T.A., Srinivas, S., Clements, M.P., Smith, J.C., and Beddington, R.S. (2005). Induction and migration of the anterior visceral endoderm is regulated by the extra-embryonic ectoderm. Development *132*, 2513-2520.

Rossi, G., Manfrin, A., and Lutolf, M.P. (2018). Progress and potential in organoid research. Nat Rev Genet *19*, 671-687.

Rudloff, S., and Kemler, R. (2012). Differential requirements for beta-catenin during mouse development. Development *139*, 3711-3721.

Rugg-Gunn, P.J., Cox, B.J., Ralston, A., and Rossant, J. (2010). Distinct histone modifications in stem cell lines and tissue lineages from the early mouse embryo. Proc Natl Acad Sci U S A *107*, 10783-10790.

Ruiz, P., Brinkmann, V., Ledermann, B., Behrend, M., Grund, C., Thalhammer, C., Vogel, F., Birchmeier, C., Gunthert, U., Franke, W.W.*, et al.* (1996). Targeted mutation of plakoglobin in mice reveals essential functions of desmosomes in the embryonic heart. J Cell Biol *135*, 215-225.

Russ, A.P., Wattler, S., Colledge, W.H., Aparicio, S.A., Carlton, M.B., Pearce, J.J., Barton, S.C., Surani, M.A., Ryan, K., Nehls, M.C., *et al.* (2000). Eomesodermin is required for mouse trophoblast development and mesoderm formation. Nature *404*, 95-99.

Safer, D., Golla, R., and Nachmias, V.T. (1990). Isolation of a 5-kilodalton actin-sequestering peptide from human blood platelets. Proc Natl Acad Sci U S A *87*, 2536-2540.

Salamat, M., Miosge, N., and Herken, R. (1995). Development of Reichert's membrane in the early mouse embryo. Anat Embryol (Berl) *192*, 275-281.

Salomon, D., Sacco, P.A., Roy, S.G., Simcha, I., Johnson, K.R., Wheelock, M.J., and Ben-Ze'ev, A. (1997). Regulation of beta-catenin levels and localization by overexpression of plakoglobin and inhibition of the ubiquitin-proteasome system. J Cell Biol *139*, 1325-1335.

Samarage, C.R., White, M.D., Alvarez, Y.D., Fierro-Gonzalez, J.C., Henon, Y., Jesudason, E.C., Bissiere, S., Fouras, A., and Plachta, N. (2015). Cortical Tension Allocates the First Inner Cells of the Mammalian Embryo. Dev Cell *34*, 435-447.

Saruwatari, L., Aita, H., Butz, F., Nakamura, H.K., Ouyang, J., Yang, Y., Chiou, W.A., and Ogawa, T. (2005). Osteoblasts generate harder, stiffer, and more delamination-resistant mineralized tissue on titanium than on polystyrene, associated with distinct tissue micro- and ultrastructure. J Bone Miner Res *20*, 2002-2016.

Sasaki, E., Hanazawa, K., Kurita, R., Akatsuka, A., Yoshizaki, T., Ishii, H., Tanioka, Y., Ohnishi, Y., Suemizu, H., Sugawara, A., *et al.* (2005a). Establishment of novel embryonic stem cell lines derived from the common marmoset (Callithrix jacchus). Stem Cells *23*, 1304-1313.

Sasaki, E., Hanazawa, K., Kurita, R., Akatsuka, A., Yoshizaki, T., Ishii, H., Tanioka, Y., Ohnishi, Y., Suemizu, H., Sugawara, A., *et al.* (2005b). Establishment of novel embryonic stem cell lines derived from the common marmoset (Callithrix jacchus). Stem Cells *23*, 1304-1313.

Sato, N., Meijer, L., Skaltsounis, L., Greengard, P., and Brivanlou, A.H. (2004). Maintenance of pluripotency in human and mouse embryonic stem cells through activation of Wnt signaling by a pharmacological GSK-3-specific inhibitor. Nat Med *10*, 55-63.

Saxena, M., Liu, S., Yang, B., Hajal, C., Changede, R., Hu, J., Wolfenson, H., Hone, J., and Sheetz, M.P. (2017). EGFR and HER2 activate rigidity sensing only on rigid matrices. Nat Mater *16*, 775-781.

Schindelin, J., Arganda-Carreras, I., Frise, E., Kaynig, V., Longair, M., Pietzsch, T., Preibisch, S., Rueden, C., Saalfeld, S., Schmid, B., *et al.* (2012). Fiji: an open-source platform for biological-image analysis. Nat Methods *9*, 676-682.

Scognamiglio, R., Cabezas-Wallscheid, N., Thier, M.C., Altamura, S., Reyes, A., Prendergast, A.M., Baumgartner, D., Carnevalli, L.S., Atzberger, A., Haas, S., *et al.*

(2016). Myc Depletion Induces a Pluripotent Dormant State Mimicking Diapause. Cell *164*, 668-680.

Sechler, M., Borowicz, S., Van Scoyk, M., Avasarala, S., Zerayesus, S., Edwards, M.G., Kumar Karuppusamy Rathinam, M., Zhao, X., Wu, P.Y., Tang, K.*, et al.* (2015). Novel Role for gamma-Catenin in the Regulation of Cancer Cell Migration via the Induction of Hepatocyte Growth Factor Activator Inhibitor Type 1 (HAI-1). J Biol Chem *290*, 15610-15620.

Shahbazi, M.N., Jedrusik, A., Vuoristo, S., Recher, G., Hupalowska, A., Bolton, V., Fogarty, N.N.M., Campbell, A., Devito, L., Ilic, D.*, et al.* (2016). Self-organization of the human embryo in the absence of maternal tissues. Nat Cell Biol *18*, 700-708.

Shi, Y., Gao, X.H., Chen, L.Q., Zhang, M., Ma, J.Y., Zhang, X.X., and Qin, J.H. (2013). High throughput generation and trapping of individual agarose microgel using microfluidic approach. Microfluid Nanofluid *15*, 467-474.

Shibamoto, S., Hayakawa, M., Takeuchi, K., Hori, T., Miyazawa, K., Kitamura, N., Johnson, K.R., Wheelock, M.J., Matsuyoshi, N., Takeichi, M.*, et al.* (1995). Association of p120, a tyrosine kinase substrate, with E-cadherin/catenin complexes. J Cell Biol *128*, 949-957.

Shimizu, M., Fukunaga, Y., Ikenouchi, J., and Nagafuchi, A. (2008). Defining the roles of beta-catenin and plakoglobin in LEF/T-cell factor-dependent transcription using beta-catenin/plakoglobin-null F9 cells. Mol Cell Biol *28*, 825-835.

Siltanen, C., Yaghoobi, M., Haque, A., You, J., Lowen, J., Soleimani, M., and Revzin, A. (2016). Microfluidic fabrication of bioactive microgels for rapid formation and enhanced differentiation of stem cell spheroids. Acta Biomater *34*, 125-132.

Silva, J., Nichols, J., Theunissen, T.W., Guo, G., van Oosten, A.L., Barrandon, O., Wray, J., Yamanaka, S., Chambers, I., and Smith, A. (2009). Nanog is the gateway to the pluripotent ground state. Cell *138*, 722-737.

Silva, J., and Smith, A. (2008). Capturing pluripotency. Cell *132*, 532-536.

Simcha, I., Geiger, B., Yehuda-Levenberg, S., Salomon, D., and Ben-Ze'ev, A. (1996). Suppression of tumorigenicity by plakoglobin: an augmenting effect of N-cadherin. J Cell Biol *133*, 199-209.

Singh, A.M., Reynolds, D., Cliff, T., Ohtsuka, S., Mattheyses, A.L., Sun, Y., Menendez, L., Kulik, M., and Dalton, S. (2012). Signaling network crosstalk in human pluripotent cells: a Smad2/3-regulated switch that controls the balance between self-renewal and differentiation. Cell Stem Cell *10*, 312-326.

Smith, A. (2017). Formative pluripotency: the executive phase in a developmental continuum. Development *144*, 365-373.

Smith, A.G., Heath, J.K., Donaldson, D.D., Wong, G.G., Moreau, J., Stahl, M., and Rogers, D. (1988). Inhibition of pluripotential embryonic stem cell differentiation by purified polypeptides. Nature *336*, 688-690.

Smyth, N., Vatansever, H.S., Murray, P., Meyer, M., Frie, C., Paulsson, M., and Edgar, D. (1999). Absence of basement membranes after targeting the LAMC1 gene results in embryonic lethality due to failure of endoderm differentiation. J Cell Biol *144*, 151-160.

Sozen, B., Amadei, G., Cox, A., Wang, R., Na, E., Czukiewska, S., Chappell, L., Voet, T., Michel, G., Jing, N.*, et al.* (2018). Self-assembly of embryonic and two extra-embryonic stem cell types into gastrulating embryo-like structures. Nat Cell Biol *20*, 979-989.

Srinivas, S., Rodriguez, T., Clements, M., Smith, J.C., and Beddington, R.S. (2004). Active cell migration drives the unilateral movements of the anterior visceral endoderm. Development *131*, 1157-1164.

Stephenson, R.O., Yamanaka, Y., and Rossant, J. (2010). Disorganized epithelial polarity and excess trophectoderm cell fate in preimplantation embryos lacking E-cadherin. Development *137*, 3383-3391.

Stevens, L.C., and Little, C.C. (1954). Spontaneous Testicular Teratomas in an Inbred Strain of Mice. Proc Natl Acad Sci U S A *40*, 1080-1087.

Stirparo, G.G., Boroviak, T., Guo, G., Nichols, J., Smith, A., and Bertone, P. (2018). Integrated analysis of single-cell embryo data yields a unified transcriptome signature for the human pre-implantation epiblast. Development *145*.

Strumpf, D., Mao, C.A., Yamanaka, Y., Ralston, A., Chawengsaksophak, K., Beck, F., and Rossant, J. (2005). Cdx2 is required for correct cell fate specification and differentiation of trophectoderm in the mouse blastocyst. Development *132*, 2093-2102.

Stuart, H.T., Stirparo, G.G., Lohoff, T., Bates, L.E., Kinoshita, M., Lim, C.Y., Sousa, E.J., Maskalenka, K., Radzisheuskaya, A., Malcolm, A.A.*, et al.* (2019). Distinct Molecular Trajectories Converge to Induce Naive Pluripotency. Cell Stem Cell.

Sumi, T., Oki, S., Kitajima, K., and Meno, C. (2013). Epiblast ground state is controlled by canonical Wnt/beta-catenin signaling in the postimplantation mouse embryo and epiblast stem cells. PLoS One *8*, e63378.

Sun, H., Wang, X., Liu, K., Guo, M., Zhang, Y., Ying, Q.L., and Ye, S. (2017). beta-catenin coordinates with Jup and the TCF1/GATA6 axis to regulate human embryonic stem cell fate. Dev Biol *431*, 272-281.

Tabata, Y., Horiguchi, I., Lutolf, M.P., and Sakai, Y. (2014). Development of bioactive hydrogel capsules for the 3D expansion of pluripotent stem cells in bioreactors. Biomater Sci-Uk *2*, 176-183.

Takaoka, K., Yamamoto, M., and Hamada, H. (2011). Origin and role of distal visceral endoderm, a group of cells that determines anterior-posterior polarity of the mouse embryo. Nat Cell Biol *13*, 743-752.

Takashima, Y., Guo, G., Loos, R., Nichols, J., Ficz, G., Krueger, F., Oxley, D., Santos, F., Clarke, J., Mansfield, W.*, et al.* (2014). Resetting transcription factor control circuitry toward ground-state pluripotency in human. Cell *158*, 1254-1269.

Takeichi, M. (1991). Cadherin cell adhesion receptors as a morphogenetic regulator. Science *251*, 1451-1455.

Tanaka, S., Kunath, T., Hadjantonakis, A.K., Nagy, A., and Rossant, J. (1998). Promotion of trophoblast stem cell proliferation by FGF4. Science *282*, 2072-2075.

ten Berge, D., Koole, W., Fuerer, C., Fish, M., Eroglu, E., and Nusse, R. (2008). Wnt signaling mediates self-organization and axis formation in embryoid bodies. Cell Stem Cell *3*, 508-518.

ten Berge, D., Kurek, D., Blauwkamp, T., Koole, W., Maas, A., Eroglu, E., Siu, R.K., and Nusse, R. (2011). Embryonic stem cells require Wnt proteins to prevent differentiation to epiblast stem cells. Nat Cell Biol *13*, 1070-1075.

Tesar, P.J., Chenoweth, J.G., Brook, F.A., Davies, T.J., Evans, E.P., Mack, D.L., Gardner, R.L., and McKay, R.D. (2007). New cell lines from mouse epiblast share defining features with human embryonic stem cells. Nature *448*, 196-199.

Theberge, A.B., Courtois, F., Schaerli, Y., Fischlechner, M., Abell, C., Hollfelder, F., and Huck, W.T. (2010). Microdroplets in microfluidics: an evolving platform for discoveries in chemistry and biology. Angew Chem Int Ed Engl *49*, 5846-5868.

Theunissen, T.W., Powell, B.E., Wang, H., Mitalipova, M., Faddah, D.A., Reddy, J., Fan, Z.P., Maetzel, D., Ganz, K., Shi, L.*, et al.* (2014). Systematic Identification of Culture Conditions for Induction and Maintenance of Naive Human Pluripotency. Cell Stem Cell *15*, 524-526.

Thomas, F.C., Sheth, B., Eckert, J.J., Bazzoni, G., Dejana, E., and Fleming, T.P. (2004). Contribution of JAM-1 to epithelial differentiation and tight-junction biogenesis in the mouse preimplantation embryo. J Cell Sci *117*, 5599-5608.

Thomas, P., and Beddington, R. (1996). Anterior primitive endoderm may be responsible for patterning the anterior neural plate in the mouse embryo. Curr Biol *6*, 1487-1496.

Thomson, J.A., Itskovitz-Eldor, J., Shapiro, S.S., Waknitz, M.A., Swiergiel, J.J., Marshall, V.S., and Jones, J.M. (1998). Embryonic stem cell lines derived from human blastocysts. Science *282*, 1145-1147.

Thomson, J.A., Kalishman, J., Golos, T.G., Durning, M., Harris, C.P., Becker, R.A., and Hearn, J.P. (1995). Isolation of a primate embryonic stem cell line. Proc Natl Acad Sci U S A *92*, 7844-7848.

Thomson, J.A., Kalishman, J., Golos, T.G., Durning, M., Harris, C.P., and Hearn, J.P. (1996). Pluripotent cell lines derived from common marmoset (Callithrix jacchus) blastocysts. Biol Reprod *55*, 254-259.

Thomson, M., Liu, S.J., Zou, L.N., Smith, Z., Meissner, A., and Ramanathan, S. (2011). Pluripotency factors in embryonic stem cells regulate differentiation into germ layers. Cell *145*, 875-889.

Torres, M., Stoykova, A., Huber, O., Chowdhury, K., Bonaldo, P., Mansouri, A., Butz, S., Kemler, R., and Gruss, P. (1997). An alpha-E-catenin gene trap mutation defines its function in preimplantation development. Proc Natl Acad Sci U S A *94*, 901-906.

Toyooka, Y., Shimosato, D., Murakami, K., Takahashi, K., and Niwa, H. (2008). Identification and characterization of subpopulations in undifferentiated ES cell culture. Development *135*, 909-918.

Troyanovsky, S.M., Troyanovsky, R.B., Eshkind, L.G., Krutovskikh, V.A., Leube, R.E., and Franke, W.W. (1994a). Identification of the plakoglobin-binding domain in desmoglein and its role in plaque assembly and intermediate filament anchorage. J Cell Biol *127*, 151-160.

Troyanovsky, S.M., Troyanovsky, R.B., Eshkind, L.G., Leube, R.E., and Franke, W.W. (1994b). Identification of amino acid sequence motifs in desmocollin, a desmosomal glycoprotein, that are required for plakoglobin binding and plaque formation. Proc Natl Acad Sci U S A *91*, 10790-10794.

Tsakiridis, A., Huang, Y., Blin, G., Skylaki, S., Wymeersch, F., Osorno, R., Economou, C., Karagianni, E., Zhao, S., Lowell, S.*, et al.* (2014). Distinct Wnt-driven primitive streak-like populations reflect in vivo lineage precursors. Development *141*, 1209-1221.

Turco, M.Y., Gardner, L., Hughes, J., Cindrova-Davies, T., Gomez, M.J., Farrell, L., Hollinshead, M., Marsh, S.G.E., Brosens, J.J., Critchley, H.O.*, et al.* (2017). Long-term, hormone-responsive organoid cultures of human endometrium in a chemically defined medium. Nat Cell Biol *19*, 568-577.

Turco, M.Y., Gardner, L., Kay, R.G., Hamilton, R.S., Prater, M., Hollinshead, M.S., McWhinnie, A., Esposito, L., Fernando, R., Skelton, H.*, et al.* (2018). Trophoblast organoids as a model for maternal-fetal interactions during human placentation. Nature *564*, 263-267.

Turner, D.A., Girgin, M., Alonso-Crisostomo, L., Trivedi, V., Baillie-Johnson, P., Glodowski, C.R., Hayward, P.C., Collignon, J., Gustavsen, C., Serup, P.*, et al.* (2017). Anteroposterior polarity and elongation in the absence of extra-embryonic tissues and of spatially localised signalling in gastruloids: mammalian embryonic organoids. Development *144*, 3894-3906.

Turner, D.A., Rue, P., Mackenzie, J.P., Davies, E., and Martinez Arias, A. (2014). Brachyury cooperates with Wnt/beta-catenin signalling to elicit primitive-streak-like behaviour in differentiating mouse embryonic stem cells. BMC Biol *12*, 63.

Umehara, H., Kimura, T., Ohtsuka, S., Nakamura, T., Kitajima, K., Ikawa, M., Okabe, M., Niwa, H., and Nakano, T. (2007). Efficient derivation of embryonic stem cells by inhibition of glycogen synthase kinase-3. Stem Cells *25*, 2705-2711.

van Amerongen, R., and Berns, A. (2006). Knockout mouse models to study Wnt signal transduction. Trends Genet *22*, 678-689.

van de Wetering, M., Cavallo, R., Dooijes, D., van Beest, M., van Es, J., Loureiro, J., Ypma, A., Hursh, D., Jones, T., Bejsovec, A.*, et al.* (1997). Armadillo coactivates

transcription driven by the product of the Drosophila segment polarity gene dTCF. Cell *88*, 789-799.

van den Brink, S.C., Baillie-Johnson, P., Balayo, T., Hadjantonakis, A.K., Nowotschin, S., Turner, D.A., and Martinez Arias, A. (2014). Symmetry breaking, germ layer specification and axial organisation in aggregates of mouse embryonic stem cells. Development *141*, 4231-4242.

van der Maaten, L., and Hinton, G. (2008). Visualizing Data using t-SNE. J Mach Learn Res *9*, 2579-2605.

Verstreken, C.M., Labouesse, C., Agley, C.C., and Chalut, K.J. (2019). Embryonic stem cells become mechanoresponsive upon exit from ground state of pluripotency. Open Biol *9*, 180203.

Vestweber, D., Gossler, A., Boller, K., and Kemler, R. (1987). Expression and distribution of cell adhesion molecule uvomorulin in mouse preimplantation embryos. Dev Biol *124*, 451-456.

Vianello, S., and Lutolf, M.P. (2019). Understanding the Mechanobiology of Early Mammalian Development through Bioengineered Models. Developmental Cell *48*, 751-763.

Vinot, S., Le, T., Ohno, S., Pawson, T., Maro, B., and Louvet-Vallee, S. (2005). Asymmetric distribution of PAR proteins in the mouse embryo begins at the 8-cell stage during compaction. Dev Biol *282*, 307-319.

von Mering, C., Jensen, L.J., Snel, B., Hooper, S.D., Krupp, M., Foglierini, M., Jouffre, N., Huynen, M.A., and Bork, P. (2005). STRING: known and predicted protein-protein associations, integrated and transferred across organisms. Nucleic Acids Res *33*, D433-437.

Waldrip, W.R., Bikoff, E.K., Hoodless, P.A., Wrana, J.L., and Robertson, E.J. (1998). Smad2 signaling in extraembryonic tissues determines anterior-posterior polarity of the early mouse embryo. Cell *92*, 797-808.

Wales, R.G. (1970). Effects of Ions on Development of Pre-Implantation Mouse Embryo in-Vitro. Aust J Biol Sci *23*, 421-&.

Walker, E., Ohishi, M., Davey, R.E., Zhang, W., Cassar, P.A., Tanaka, T.S., Der, S.D., Morris, Q., Hughes, T.R., Zandstra, P.W.*, et al.* (2007). Prediction and testing of novel transcriptional networks regulating embryonic stem cell self-renewal and commitment. Cell Stem Cell *1*, 71-86.

Wang, H., Ding, T., Brown, N., Yamamoto, Y., Prince, L.S., Reese, J., and Paria, B.C. (2008). Zonula occludens-1 (ZO-1) is involved in morula to blastocyst transformation in the mouse. Dev Biol *318*, 112-125.

Wang, J., Alexander, P., Wu, L., Hammer, R., Cleaver, O., and McKnight, S.L. (2009). Dependence of mouse embryonic stem cells on threonine catabolism. Science *325*, 435-439.

Wang, Z., and Jaenisch, R. (2004). At most three ES cells contribute to the somatic lineages of chimeric mice and of mice produced by ES-tetraploid complementation. Dev Biol *275*, 192-201.

White, M.D., and Plachta, N. (2015). How Adhesion Forms the Early Mammalian Embryo. Curr Top Dev Biol *112*, 1-17.

White, M.D., Zenker, J., Bissiere, S., and Plachta, N. (2018). Instructions for Assembling the Early Mammalian Embryo. Dev Cell *45*, 667-679.

Whitten, W.K., and Biggers, J.D. (1968). Complete development in vitro of the pre-implantation stages of the mouse in a simple chemically defined medium. J Reprod Fertil *17*, 399-401.

Wilder, P.J., Kelly, D., Brigman, K., Peterson, C.L., Nowling, T., Gao, Q.S., McComb, R.D., Capecchi, M.R., and Rizzino, A. (1997). Inactivation of the FGF-4 gene in embryonic stem cells alters the growth and/or the survival of their early differentiated progeny. Dev Biol *192*, 614-629.

Wilkinson, D.G., Bhatt, S., and Herrmann, B.G. (1990). Expression pattern of the mouse T gene and its role in mesoderm formation. Nature *343*, 657-659.

Williams, M., Burdsal, C., Periasamy, A., Lewandoski, M., and Sutherland, A. (2012). Mouse primitive streak forms in situ by initiation of epithelial to mesenchymal transition without migration of a cell population. Dev Dyn *241*, 270-283.

Williams, R.L., Hilton, D.J., Pease, S., Willson, T.A., Stewart, C.L., Gearing, D.P., Wagner, E.F., Metcalf, D., Nicola, N.A., and Gough, N.M. (1988). Myeloid leukaemia inhibitory factor maintains the developmental potential of embryonic stem cells. Nature *336*, 684-687.

Wilson, J.L., Najia, M.A., Saeed, R., and McDevitt, T.C. (2014). Alginate encapsulation parameters influence the differentiation of microencapsulated embryonic stem cell aggregates. Biotechnol Bioeng *111*, 618-631.

Wood, H.B., and Episkopou, V. (1999). Comparative expression of the mouse Sox1, Sox2 and Sox3 genes from pre-gastrulation to early somite stages. Mech Dev *86*, 197-201.

Wray, J., Kalkan, T., Gomez-Lopez, S., Eckardt, D., Cook, A., Kemler, R., and Smith, A. (2011). Inhibition of glycogen synthase kinase-3 alleviates Tcf3 repression of the pluripotency network and increases embryonic stem cell resistance to differentiation. Nat Cell Biol *13*, 838-845.

Wray, J., Kalkan, T., and Smith, A.G. (2010). The ground state of pluripotency. Biochem Soc Trans *38*, 1027-1032.

Wu, J., Okamura, D., Li, M., Suzuki, K., Luo, C., Ma, L., He, Y., Li, Z., Benner, C., Tamura, I.*, et al.* (2015). An alternative pluripotent state confers interspecies chimaeric competency. Nature *521*, 316-321.

Xia, Y.N., and Whitesides, G.M. (1998). Soft lithography. Angewandte Chemie-International Edition *37*, 550-575.

Xiao, K., Oas, R.G., Chiasson, C.M., and Kowalczyk, A.P. (2007). Role of p120-catenin in cadherin trafficking. Biochim Biophys Acta *1773*, 8-16.

Xiao, K.Y., Allison, D.F., Buckley, K.M., Kottke, M.D., Vincent, P.A., Faundez, V., and Kowalczyk, A.P. (2003). Cellular levels of p120 catenin function as a set point for cadherin expression levels in microvascular endothelial cells. J Cell Biol *163*, 535-545.

Xu, Z., Robitaille, A.M., Berndt, J.D., Davidson, K.C., Fischer, K.A., Mathieu, J., Potter, J.C., Ruohola-Baker, H., and Moon, R.T. (2016). Wnt/beta-catenin signaling promotes self-renewal and inhibits the primed state transition in naive human embryonic stem cells. Proc Natl Acad Sci U S A *113*, E6382-E6390.

Yagi, R., Kohn, M.J., Karavanova, I., Kaneko, K.J., Vullhorst, D., DePamphilis, M.L., and Buonanno, A. (2007). Transcription factor TEAD4 specifies the trophectoderm lineage at the beginning of mammalian development. Development *134*, 3827-3836.

Yamamoto, M., Saijoh, Y., Perea-Gomez, A., Shawlot, W., Behringer, R.R., Ang, S.L., Hamada, H., and Meno, C. (2004). Nodal antagonists regulate formation of the anteroposterior axis of the mouse embryo. Nature *428*, 387-392.

Yan, L., Yang, M., Guo, H., Yang, L., Wu, J., Li, R., Liu, P., Lian, Y., Zheng, X., Yan, J.*, et al.* (2013). Single-cell RNA-Seq profiling of human preimplantation embryos and embryonic stem cells. Nat Struct Mol Biol *20*, 1131-1139.

Yang, J., Ryan, D.J., Wang, W., Tsang, J.C., Lan, G., Masaki, H., Gao, X., Antunes, L., Yu, Y., Zhu, Z.*, et al.* (2017a). Establishment of mouse expanded potential stem cells. Nature *550*, 393-397.

Yang, Y., Liu, B., Xu, J., Wang, J., Wu, J., Shi, C., Xu, Y., Dong, J., Wang, C., Lai, W.*, et al.* (2017b). Derivation of Pluripotent Stem Cells with In Vivo Embryonic and Extraembryonic Potency. Cell *169*, 243-257 e225.

Yaphe, W. (1957). The Use of Agarase from Pseudomonas-Atlantica in the Identification of Agar in Marine Algae (Rhodophyceae). Can J Microbiol *3*, 987-993.

Ye, S., Zhang, D., Cheng, F., Wilson, D., Mackay, J., He, K., Ban, Q., Lv, F., Huang, S., Liu, D.*, et al.* (2016). Wnt/beta-catenin and LIF-Stat3 signaling pathways converge on Sp5 to promote mouse embryonic stem cell self-renewal. J Cell Sci *129*, 269-276.

Yin, T., Getsios, S., Caldelari, R., Godsel, L.M., Kowalczyk, A.P., Muller, E.J., and Green, K.J. (2005). Mechanisms of plakoglobin-dependent adhesion: desmosome-specific functions in assembly and regulation by epidermal growth factor receptor. J Biol Chem *280*, 40355-40363.

Ying, Q.L., Nichols, J., Chambers, I., and Smith, A. (2003a). BMP induction of Id proteins suppresses differentiation and sustains embryonic stem cell self-renewal in collaboration with STAT3. Cell *115*, 281-292.

Ying, Q.L., Nichols, J., Evans, E.P., and Smith, A.G. (2002). Changing potency by spontaneous fusion. Nature *416*, 545-548.

Ying, Q.L., Stavridis, M., Griffiths, D., Li, M., and Smith, A. (2003b). Conversion of embryonic stem cells into neuroectodermal precursors in adherent monoculture. Nat Biotechnol *21*, 183-186.

Ying, Q.L., Wray, J., Nichols, J., Batlle-Morera, L., Doble, B., Woodgett, J., Cohen, P., and Smith, A. (2008). The ground state of embryonic stem cell self-renewal. Nature *453*, 519-523.

Zaidel-Bar, R. (2013). Cadherin adhesome at a glance. J Cell Sci *126*, 373-378.

Zeng, L., Fagotto, F., Zhang, T., Hsu, W., Vasicek, T.J., Perry, W.L., 3rd, Lee, J.J., Tilghman, S.M., Gumbiner, B.M., and Costantini, F. (1997). The mouse Fused locus encodes Axin, an inhibitor of the Wnt signaling pathway that regulates embryonic axis formation. Cell *90*, 181-192.

Zhang, J., Nuebel, E., Daley, G.Q., Koehler, C.M., and Teitell, M.A. (2012). Metabolic regulation in pluripotent stem cells during reprogramming and self-renewal. Cell Stem Cell *11*, 589-595.

Zhang, M., Lai, Y., Krupalnik, V., Guo, P., Guo, X., Zhou, J., Xu, Y., Yu, Z., Liu, L., Jiang, A.*, et al.* (2020). beta-Catenin safeguards the ground state of mousepluripotency by strengthening the robustness of the transcriptional apparatus. Sci Adv *6*, eaba1593.

Zhang, S., Chen, T., Chen, N., Gao, D., Shi, B., Kong, S., West, R.C., Yuan, Y., Zhi, M., Wei, Q.*, et al.* (2019). Implantation initiation of self-assembled embryo-like structures generated using three types of mouse blastocyst-derived stem cells. Nat Commun *10*, 496.

Zheng, Y., Xue, X., Shao, Y., Wang, S., Esfahani, S.N., Li, Z., Muncie, J.M., Lakins, J.N., Weaver, V.M., Gumucio, D.L.*, et al.* (2019). Controlled modelling of human epiblast and amnion development using stem cells. Nature *573*, 421-425.

Zhong, Y., and Binas, B. (2019). Transcriptome analysis shows ambiguous phenotypes of murine primitive endoderm-related stem cell lines. Genes Cells *24*, 324-331.

Zhong, Y., Choi, T., Kim, M., Jung, K.H., Chai, Y.G., and Binas, B. (2018). Isolation of primitive mouse extraembryonic endoderm (pXEN) stem cell lines. Stem Cell Res *30*, 100-112.

Zhu, M., Leung, C.Y., Shahbazi, M.N., and Zernicka-Goetz, M. (2017). Actomyosin polarisation through PLC-PKC triggers symmetry breaking of the mouse embryo. Nat Commun *8*, 921.

Zilionis, R., Nainys, J., Veres, A., Savova, V., Zemmour, D., Klein, A.M., and Mazutis, L. (2017). Single-cell barcoding and sequencing using droplet microfluidics. Nat Protoc *12*, 44-73.

Zimmerlin, L., Park, T.S., Huo, J.S., Verma, K., Pather, S.R., Talbot, C.C., Jr., Agarwal, J., Steppan, D., Zhang, Y.W., Considine, M.*, et al.* (2016). Tankyrase inhibition promotes

a stable human naive pluripotent state with improved functionality. Development *143*, 4368-4380.

Ziomek, C.A., and Johnson, M.H. (1980). Cell surface interaction induces polarization of mouse 8-cell blastomeres at compaction. Cell *21*, 935-942.

9 List of abbreviation

AJ	Adherens junction
AVE	Anterior visceral endoderm
bFGF	Basic fibroblast growth factor
BMP	Bone morphogenetic protein
CBD	Catenin binding domain
CCC	Cadherin-catenin-complex
CH	CHIR99021 (GSK3 inhibitor)
cmESC	Common marmoset embryonic stem cell
DMSO	Dimethyl sulfoxide
DVE	Distal visceral endoderm
EC	Embryonic carcinoma
ECM	Extracellular matrix
EGF	Epidermal growth factor
EGFR	Epithelial growth factor receptor
EPI	Epiblast
EpiLC	Epiblast-like cells
EpiSC	Epiblast-derived stem cell
ESC	Embryonic stem cell
ExE	Extraembryonic ectoderm
FACS	Fluorescence-activated cell sorting
FBS	Foetal bovine serum
FFD	Flow focusing device
FGFR	Fibroblast growth factor receptor
GFP	Green fluorescent protein
GSK3	Glycogen synthase kinase-3
hPSC	Human pluripotent stem cell
ICM	Inner cell mass
iMEF	Inactivated mouse embryonic fibroblast
JMD	Juxta membrane domain
KEGG	Kyoto Encyclopaedia of Genes and Genomes
KSR	KnockOut serum replacement
LIF	Leukaemia inhibitory factor
NEAA	Non-essential amino acids
NGS	Next-generation sequencing
PBS	Phosphate buffered saline

PD	PD0325901 (ERK inhibitor)
PDGFRα	Platelet-derived growth factor receptor alpha
PEG	Polyethylene glycol
PFA	Paraformaldehyde
PFO	1H,1H,2H,2H-perfluoro-1-octanol
PG	Plakoglobin
PMDS	Polydimethylsiloxane
PODXL	Podocalyxin
PrE	Primitive endoderm
PVP	Polyvinylpyrrolidone
RCF	Relative centrifugal force
RFP	Red fluorescent protein
TCP	Tissue culture plastic
TE	Trophectoderm
TGFβ	Transforming growth factor β
VE	Visceral endoderm
XEN	Extraembryonic endoderm
ZGA	Zygotic genome activation
ZP	Zona pellucida

10 List of figures

Figure 1.1 | Development from zygote to the compacted morula..... 3
Figure 1.2 | E-cadherin dependent filopodia formation during blastomere compaction..... 4
Figure 1.3 | Compaction via cadherin-mediated adhesion and pulsatile actomyosin contractility.. 4
Figure 1.4 | Schematic illustration of the composition of adherens junctions. 6
Figure 1.5 | Polarity-mediated localisation of YAP to the nucleus initiates trophec. differentiation.. 7
Figure 1.6 | Hallmark events during blastocyst formation..... 9
Figure 1.7 | Polarised rosette formation of the epiblast during implantation.. 10
Figure 1.8 | Signalling in the pre-gastrulating embryo.. 12
Figure 1.9 | The gastrulating embryo. 13
Figure 2.1 | Chemical structures of (a) Trichloro(1H,1H,2H,2H-perfluorooctyl)silane and (b) HFE-7500. 24
Figure 3.1 | Microfluidic encapsulation of mouse embryonic stem cells into agarose micro gels with subsequent in-gel suspension culture. 37
Figure 3.2 | The Rex1::GFPd2 reporter system. 39
Figure 3.3 | RNA-seq anlysis of microgel encapsulated ESC vs conventionally cultured ESC in 2i+LIF.. ... 41
Figure 3.4 | In-gel cultured embryonic stem cells readily integrate into the developing epiblast after injection into 8-cell embryos..... 43
Figure 3.5 Microgel cultured embryonic stem cells display adjustments across their pluripotency gene regulatory network..... 43
Figure 3.6 | Microgel culture does not inhibit the exit from naive pluripotency. 45
Figure 3.7 | Microgel encapsulated ESCs display enhanced activation of WNT/β-catenin and LIF/STAT3 targets under naïve culture conditions..... 46
Figure 3.8 | Microgel encapsulated embryonic stem cells upregulate plakoglobin under naïve culture conditions. 47
Figure 3.9 | Microgel suspension culture of embryonic stem cells leads to structural reorganisation of adherens junctions in S+LIF medium. 48
Figure 4.1| Generation and characterisation of a mouse embryonic stem cell line overexpressing plakoglobin..... 56
Figure 4.2 | Plakoglobin overexpression promotes naïve pluripotency and slows differentiation kinetics of embryonic stem cells. 57
Figure 4.3| Plakoglobin acts in a concentration-dependent manner to promote naïve pluripotency. 60
Figure 4.4 | Single-cell sequencing confirms re-establishment of naïve pluripotency. 62
Figure 4.5 | Strong plakoglobin expression is concomitant with a distinct transcriptomic signature. 63
Figure 4.6 | Plakoglobin overexpressing cells display changes in the transcription of epigenetic regulators..... 64
Figure 4.7 | Single plakoglobin overexpressing cells contribute twice as efficiently to the epiblast when injected into 8-cell embryos in comparison to wild type cells.. 65

Figure 4.8 | Plakoglobin impedes the exit from pluripotency in the presence of serum..... 67
Figure 4.9 | Plakoglobin and β-catenin display differential protein levels upon differentiation..... 68
Figure 4.10 | Plakoglobin overexpressing cells display severe differentiation defects in the presence of serum..... 69
Figure 4.11 | Plakoglobin overexpressing cells maintain naïve pluripotency when supplemented with LIF or PD but not CH..... 71
Figure 4.12 | CRISPR mediated knockout of Ctnnb1 (β-catenin) in RGd2 and PG^{HIGH}#5 cells. 72
Figure 4.13 | Plakoglobin overexpression suppresses neuroectodermal but not mesendodermal differentiation of ESC..... 74
Figure 4.14 | EpiLC differentiation of ESC..... 76
Figure 4.15 | Differential expression of β-catenin and plakoglobin during naïve and primed pluripotency. 78
Figure 4.16 | Generation of plakoglobin overexpressing epiblast-derived stem cells (EpiSCs)..... 80
Figure 4.17 | Plakoglobin expression in EpiSCs does not upregulate the naïve-state associated transcription factors KLF4 and TFCP2L1..... 82
Figure 4.18 | Plakoglobin overexpression does not mitigate the reprogramming barrier from primed to naïve pluripotency..... 83
Figure 4.19 | Forced plakoglobin expression does not inhibit the exit from primed pluripotency in EpiSC. 84
Figure 4.20 | Plakoglobin, unlike β-catenin, does not promote differentiation of EpiSCs..... 85
Figure 4.21 | Human naïve embryonic stem cells as well as the pre-implantation epiblast express plakoglobin..... 88
Figure 4.22 | Resetting of conventional cmESCs towards naïve-like pluripotency is accompanied by upregulation of plakoglobin.. 90
Figure 4.23 | Microgel culture of conventional and naïve-like cmESCs in different media conditions. ... 91
Figure 5.1 | Microgel co culture of embryonic stem cells (ESC) and extraembryonic endoderm (XEN) cells..... 101
Figure 5.2 | EX-structure formation is orchestrated by highly dynamic XEN cell membrane protrusions.. 101
Figure 5.3 | Characterisation of EX-structures via single-cell transcriptomics..... 104
Figure 5.4 | XEN cells deposit the basal membrane component laminin, thereby supporting polarisation of ESCs. 104
Figure 5.5 | XEN cells support the transition from naïve to primed pluripotency and subsequent lineage specification in EX-structures..... 105
Figure 7.1 | Plakoglobin and β-catenin's function diverge upon transition from naïve to primed pluripotency..... 120

11 Appendix

11.1 List of antibodies

Table 3 | List of primary antibodies.

Prim. Antibody	Clone	Host	IF	Company	Source/Cat. #
aPKC	C-20	Rabbit	1:200	Santa Cruz Biotec	sc-216
Cleaved caspase 3	5A1E	Rabbit	1:400	CST	9663
Connexin 31	Polyclonal	rabbit	1:100	Thermo Fisher	36-5100
E-cadherin	ECCD-2	Rat	1:100	Thermo Fisher	TF/13-1900
Esrrb	H6705	Mouse	1:300	R&D Systems	PP-H6705-00
FoxA2	D56D6	Rabbit	1:400	CST	8186
Ki-67	D3B5	Rabbit	1:400	CST	9129
Klf4	Polyclonal	Goat	1:400	R&D Systems	AF3158
LaminB1	Polyclonal	Rabbit	1:1000	abcam	ab16048
Laminin	Polyclonal	Rabbit	1:500	Sigma Aldrich/Merck	L9393
Nanog	eBioMLC-51	Rat	1:200	eBioscience/Thermo Fisher	14-5761-80
Oct3/4	C-10	Mouse	1:200	Santa Cruz Biotec	SC/5279
p120-catenin	D7S2M	Rabbit	1:800	CST	CST/59854
Plakoglobin	Polyclonal	Rabbit	1:400	CST	CST/2309
SOCS3	1B2	Mouse	1:200	Thermo Fisher	37-7200
Sox1	Polyclonal	Rabbit	1:200	CST	4194
Sox17	Polyclonal	Goat	1:400	R&D Systems	AF1924
Sox2	245610	Mouse	1:100	R&D Systems	MAB2018
T(Brachyury)	Polyclonal	Goat	1:200	R&D Systems	AF2085
Tfcp2l1	Polyclonal	Goat	1:300	R&D Systems	AF7526
Vinculin	SPM227	Mouse	1:200	abcam	ab18058
β-catenin	D10A8	Rabbit	1:200	CST	8480